EPFL

Revisiting Detailing Rules for Bending Bars, Anchorage and Minimum Shear Reinforcement in Concrete Structures

Frédéric MONNEY

École
polytechnique
fédérale
de Lausanne

2022

Foreword

Not every old question in structural engineering, even if investigated previously by a number of clever and dedicated colleagues, has a clear and widely accepted answer nowadays. This is particularly the case of detailing rules in structural concrete. These rules allow for the applicability of design models, but also contribute to other aspects such as enhanced structural robustness or avoiding explicit verifications. Within this frame, many of the detailing rules used nowadays have been developed on the basis of empirical observations (dated in several cases from several decades ago) or are rules of good practice that may vary upon country or design tradition. In many cases, they lack of mechanical models supporting them, and thus hide the influence of relevant aspects. In addition, the fact that many detailing rules are simply inherited from old standards is inconsistent, as the materials used in construction and their performance have significantly evolved in the last years.

This situation requires a revision of several of these rules. In this thesis, a number of relevant issues are investigated, namely the cover spalling near to bent reinforcement, the performance of anchorages of bent bars and hooks and the minimum amount of shear reinforcement in beams and slabs. The aim of this work is to provide a new look on the detailing rules by conducting new systematic tests with refined measurement such as Digital Image Correlation or Distributed Fibre Optic Sensing. Such refined measurements allow for the first time to understand the mechanics ruling the response of the details and thus to make a consistent step forward in developing new provisions on the basis of mechanical models. The work of Frédéric Monney shows a number of complex interactions. For the bent details, both regions dominated by plastic strains in compressions and by a brittle response in tension may govern the response. With respect to minimum shear reinforcement, it is shown how it allows shifting the failure mode from strain localization to multiple cracking. On the basis of the experiments, it is clearly identified the mechanical parameters ruling the response of the details and members. Thanks to this detailed analysis, tailored mechanical approaches are proposed to predict their behaviour, allowing eventually to develop consistent code provisions for design.

This work presents both a significant experimental programme and theoretical work. Its results have found practical application and have been incorporated in the discussions and provisions of the current stable draft for the 2nd generation of the Eurocode 2.

Lausanne, April 2022

Prof. Aurelio Muttoni   Prof. Miguel Fernández Ruiz

Acknowledgments

the translations of the abstract. Also a special thanks to Oliver Burdet, Miguel Fernández Ruiz and Enrique Corres Sojo for their proofreading of the introduction or conclusion.

My friends, who gave me their support and allowed me to take my mind off work.

My family, and in particular my parents Françoise and Patrick Monney as well as my sister Caroline Monney. Their support, their love and their education were the greatest gifts they could give me.

My wife, Julia Monney-Veuillet for her unconditional support and love. Without her, nothing would have happened, it is thanks to her that I actually started this thesis and it is also thanks to her incredible support that I could finish it.

Lausanne, June 2022

Frédéric Monney

iv

Abstract

Reinforcement detailing rules describe the shape, geometrical dimensions and amount of steel to be placed in reinforced concrete structures. These rules allow for simple and fast designs, account for several effects neglected in the design, ensure a satisfactory behaviour under serviceability conditions, a sufficient robustness and an adequate behaviour in case of unexpected actions. Over the past decades, most detailing rules provided in codes of practice have not been updated to correspond to current manufacturing processes (automatization of the bending of bars), material performances (increasing steel and concrete strengths) and scientific knowledge. They are often based on "rules of good practice" which, while deemed satisfactory, lack a sound scientific basis and may not be needed. This is one reason why detailing rules may significantly differ amongst countries and design codes. Some of these rules are in many cases overly conservative, in particular when evaluating existing structures, while others may neglect significant effects. Even though these rules play a major role in the economy and safety of concrete structures, little research has been performed in this domain in recent years.

Several detailing rules have been identified needing additional investigations to verify their adequacy to current practical needs and recent technological evolutions. This thesis presents a comprehensive research programme on three main detailing rules: bend detailing and required mandrel diameter, anchorage of shear reinforcement with bends and hooks and minimum amount of shear reinforcement. This research aims developing mechanical models, simplified formulas and detailing provisions and is supported by experimental results. These were obtained using state-of-the-art measurement techniques such as Digital Image Correlation measurement or Fibre-Optic Measurements and lead to a better understanding of the structural response.

Bends and hooks of steel reinforcing bars are usually obtained by plastic bending of the bars against mandrels. Codes specify minimum mandrel diameters to ensure a safe transfer of forces and to avoid splitting or spalling failures that may potentially limit the resistance of the detail. The thesis includes a comprehensive research programme on the detailing of bends and the required mandrel diameter to avoid local concrete failures leading to spalling of the concrete cover. A mechanical model for the design of bent reinforcement was developed, together with corresponding detailing rules. A simplifying standard bending procedures is proposed, in which details formerly requiring various bend diameters can be obtained by using a single mandrel, allowing for faster automated manufacturing of bent reinforcement.

Bends and hooks at the end of the bars are simple and cost-efficient solutions for the anchorage of reinforcement. However, these details are relatively sensitive to the cracking state of the surrounding concrete. For shear reinforcement, brittle failures can also occur due to spalling of the concrete cover for bars close to the concrete surface. The thesis includes an investigation on the mechanical response and performance of bend and hook anchorages. On that basis, a mechanical model as well as practical considerations on the activation of shear reinforcement in beams are presented to update current detailing rules.

The required minimum amount of shear reinforcement in beams and slabs has been discussed for decades. It is crucial to ensure economic and safe new structures and to accurately assess existing ones. The results of an experimental investigation shows that the shear behaviour is strongly dependent on the amount of shear reinforcement and the post-yield response of the reinforcement (ductility class of the shear reinforcement).

For all investigated detailing rules, the implementation of these findings into codes of practice is discussed, highlighting the consistency of the recent changes, particularly with reference to the new generation of Eurocode 2.

Keywords: reinforced concrete structures, detailing rules, mandrel diameter, anchorage, spalling, splitting, bond, hooks, bends, shear reinforcement, minimum shear reinforcement, Fibre-Optic measurements, Digital Image Correlation.

Résumé

Les dispositions constructives liées à l'armature décrivent la forme, les dimensions et la quantité de barres à placer dans les structures en béton armé. Ces règles permettent un dimensionnement simple et rapide, tiennent compte de certains effets négligés dans le calcul, assurent un comportement satisfaisant en service et à la rupture ainsi qu'un comportement adéquat en cas d'actions imprévues. Au cours des dernières décennies, la plupart des dispositions constructives indiquées dans les normes de construction n'ont pas été actualisées et ne suivent par conséquent ni les procédés de production actuels (automatisation du pliage des barres), ni les performances des matériaux (augmentation de la résistance de l'acier et du béton), ni les connaissances scientifiques. Elles sont souvent basées sur des "règles de bonne pratique" qui, bien que jugées satisfaisantes, manquent de base scientifique solide et peuvent s'avérer superflues. C'est l'une des raisons pour lesquelles certaines dispositions constructives diffèrent considérablement selon les pays et les normes de construction. Certaines de ces règles sont trop conservatrices, en particulier lors de l'évaluation de structures existantes, tandis que d'autres peuvent négliger des effets importants. Bien que ces règles jouent un rôle majeur dans l'économie et la sécurité des ouvrages en béton armé, peu de recherches ont été menées dans ce domaine ces dernières années.

Un certain nombre de dispositions constructives a été identifié comme nécessitant une recherche approfondie permettant de tenir compte des besoins pratiques actuels et des évolutions technologiques récentes. Cette thèse présente un programme de recherche complet sur trois dispositions constructives importantes : le détail des pliages et le diamètre requis des mandrins, l'ancrage des armatures à l'effort tranchant composé de crochets et la quantité minimale d'armatures à l'effort tranchant. A travers de modèles mécaniques, de formules simplifiées et de dispositions constructives, cette recherche est étayée par des résultats expérimentaux obtenus à l'aide de techniques de mesures avancées telles que la mesure par corrélation d'images numériques ou la mesure par fibre optique, permettant ainsi de mieux comprendre la réponse structurelle.

Le pliage des armatures en acier est généralement obtenu par flexion plastique de barres contre des mandrins. Les normes spécifient les diamètres minimaux de mandrins afin d'assurer un transfert adéquat des forces et d'éviter les ruptures par fendage ou éclatement de l'enrobage qui peuvent limiter la résistance du détail. Cette thèse comprend un programme de recherche complet sur les dispositions liées aux pliages et le diamètre requis des mandrins afin d'éviter les défaillances locales du béton conduisant à l'éclatement de l'enrobage. Un modèle mécanique a été développé pour le dimensionnement des armatures pliées, accompagné des dispositions constructives correspondantes. Une procédure de pliage standard simplifiée est proposée. Ainsi, les détails nécessitant différents diamètres de pliage peuvent être obtenus par l'utilisation d'un seul diamètre de mandrin, ce qui permet une fabrication automatisée plus rapide des armatures pliées.

La mise en place de crochets à l'extrémité des barres est une solution simple et efficace lors de l'ancrage des armatures. Ce détail est relativement sensible à l'état de fissuration du béton adjacent. Pour les armatures d'effort tranchant, des ruptures fragiles peuvent se produire en raison de l'éclatement de l'enrobage du béton pour les barres proches d'un bord. Cette thèse comporte une étude de la réponse mécanique et des performances d'ancrage des armatures avec crochet. Sur cette base, un modèle mécanique et des considérations pratiques sur l'activation des armatures d'effort tranchant dans les poutres sont présentés pour actualiser les règles constructives actuelles.

La quantité minimale requise d'armature d'effort tranchant dans les poutres et les dalles a été débattue pendant des décennies. Elle est nécessaire pour garantir l'efficience et la sécurité des nouvelles structures et pour la vérification des structures existantes. Cette thèse présente les résultats d'une étude expérimentale montrant que le comportement dépend fortement de la quantité minimale d'armature d'effort tranchant et de la réponse après écoulement de l'armature (classe de ductilité de l'armature à l'effort tranchant).

Vu leur pertinence, l'ensemble des dispositions constructives étudiées fait actuellement l'objet de discussions en vue de leur introduction dans les normes de construction, en particulier dans la nouvelle génération de l'Eurocode 2.

Mots-clefs : béton armé structural, dispositions constructives, diamètre du mandrin, ancrage, éclatement de l'enrobage, fendage, crochets, pliage, armature à l'effort tranchant, taux minimal d'armature à l'effort tranchant, mesures par fibres optiques, corrélation d'images numériques.

Zusammenfassung

Normen und Regeln für die konstruktive Durchbildung in Stahlbetonbauwerken helfen bei der Bestimmung der Form, Abmessungen und Anzahl an Bewehrungsstäben. Sie ermöglichen eine einfache und schnelle Bemessung und berücksichtigen Effekte die in Berechnungen üblicherweise vernachlässigt werden. Ausserdem garantieren solche Regeln ein gutes Verhalten im Grenzzustand der Gebrauchstauglichkeit sowie eine ausreichende Robustheit bei unvorhersehbaren Einwirkungen. In den vergangenen Jahrzehnten wurden die meisten Regeln für die konstruktive Durchbildung kaum aktualisiert, obwohl es zahlreiche Änderungen bezüglich Herstellungsmethoden (automatisches biegen der Stäbe) Materialeigenschaften und neue wissenschaftliche Erkenntnissen gab. Sie basieren grösstenteils auf anerkannte Verfahren die zwar zufriedenstellende Ergebnisse liefern aber oftmals keine eindeutige wissenschaftliche Basis haben. Entsprechend gibt es grosse Unterschiede in verschiedenen Ländern und Normwerken. Einige der Regeln liegen weit auf der sicheren Seite (was bei der Betrachtung bestehender Bauwerke problematisch sein kann), während andere, signifikante Effekte vernachlässigen. Obwohl die Bewehrungsführung eine wichtige Rolle in der Wirtschaftlichkeit und Sicherheit von Bauwerken spielt, wurde in den letzten Jahren kaum Forschung in diesem Gebiet betrieben.

Die vorliegende Dissertation beschäftigt sich mit einigen Regeln für die konstruktive Durchbildung, welche den aktuellen Bedürfnissen angepasst werden sollten. Es wird ein umfangreiches Forschungsprogramm präsentiert, welches auf drei wichtige Themen fokussiert: das Biegen von Stäben und der hierfür erforderliche Biegerollendurchmesser; die Verankerung der Querkraft-Bewehrung mittels Abbiegungen und Endhaken; und die Mindestquerkraftbewehrung. Ziel des Forschungsprogramms ist die Entwicklung mechanischer Modelle, vereinfachter Formeln und Regeln für die Bewehrungsführung die auf experimentellen Erkenntnissen basieren. Für ein besseres Verständnis des mechanischen Verhaltens werden moderne Messmethoden angewendet, wie die Digitale Bilderkorrelation oder Messungen mit Glasfasern.

Abbiegungen und Endhaken in Bewehrungsstäbe werden üblicherweise durch Biegen mittels Biegerollen hergestellt. Der minimale Durchmesser dieser Biegerollen ist normiert, sodass eine sichere Kräfteübertragung gewährleistet wird und ein Versagen des Betons infolge Abplatzen der Betonüberdeckung vermieden wird. In der vorliegenden Dissertation wird ein entsprechendes mechanisches Modell entwickelt, sowie Regeln für die Bewehrungsführung vorgeschlagen. Es wird eine vereinfachte, standardisierte Prozedur für das Abbiegen beschrieben, mit welcher Stäbe mit unterschiedlichen Abbiegungs-Radien mit einer einzigen Biegerolle durchgeführt werden können. Dies ermöglicht einen effizienteren automatischen Herstellungsprozess.

Das Vorsehen von Haken oder Abbiegungen an den Enden ist eine einfache Lösung für die Verankerung der Bewehrungsstäbe. Solche Details können aber mit Bezug zur Rissbildung im

Beton problematisch sein. Zum Beispiel kann das Abspalten der Betonüberdeckung im Bereich der Verankerung der Querkraftbewehrung zu einem fragilen Querkraft-Versagen führen. Die vorliegende Dissertation beinhaltet eine Untersuchung des mechanischen Verhaltens und der Wirkung von Verankerungen mit Abbiegungen und Endhaken. Es wird ein entsprechendes mechanisches Modell präsentiert welches die Aktivierung der Querkraftbewehrung beschreibt, sodass die existierenden Regeln für die Bewehrungsführung aktualisiert werden können.

Die erforderliche Mindestbewehrung in Trägern und Platten wird sein mehreren Jahrzehnten diskutiert, da sie sowohl für den Bau von wirtschaftlichen und sicheren Neubauten als auf für die Analyse von bestehenden Bauten eine wichtige Rolle spielt. Es werden die Ergebnisse verschiedener Versuche präsentiert, welche zeigen, dass das Verhalten solcher Bauteile stark von der Bewehrungsmenge und der Duktilitätsklasse der Bewehrung abhängt. Schlussendlich werden die Implikationen der vorliegenden Forschungsergebnisse für Regelwerke diskutiert. Dabei wird gezeigt, dass die Ergebnisse mit den Änderungen in der neusten Generation des Eurocode 2 (insbesondere mit Bezug zu den Duktilitätsklassen) übereinstimmen.

Stichwörter: Stahlbeton Bauwerk, konstruktive Details, Bewehrungsführung, Biegerollendurchmesser, Abplatzen, Verankerung, Verbund, Endhaken, Abbiegungen, Querkraftbewehrung, minimale Querkraftbewehrung, Messungen mit Glasfasern, Digitale Bilderkorrelation.

Riassunto

I dettagli costruttivi delle barre di armatura descrivono la forma, le dimensioni geometriche e la quantità di acciaio da disporre nelle strutture in calcestruzzo armato. Queste regole permettono una progettazione semplice e veloce, tengono conto di alcuni effetti trascurati nei calcoli, assicurano una sufficiente robustezza e un comportamento soddisfacente in condizioni di esercizio e riguardo ad azioni imprevedibili. Negli ultimi decenni, la maggior parte delle regole di dettaglio fornite nei codici non sono state aggiornate considerando i metodi di produzione attuali (automatizzazione della piegatura delle barre), le prestazioni dei materiali (aumento della resistenza dell'acciaio e del calcestruzzo) e le conoscenze scientifiche. I dettagli costruttivi, si basano spesso su "regole di buona pratica" che, anche se ritenute soddisfacenti, mancano di una forte base scientifica e potrebbero non essere necessarie. Questo è uno dei motivi per cui alcune regole di dettaglio differiscono significativamente a seconda del paese e la norma considerata. Di conseguenza, alcune di queste regole costruttive risultano eccessivamente conservative, in particolare nella valutazione delle strutture esistenti, mentre altre possono trascurare effetti significativi. Anche se queste regole giocano un ruolo importante nell'economia e nella sicurezza delle opere civili, la ricerca svolta negli ultimi anni è lacunosa.

Diverse regole costruttive che si trovano in letteratura necessitano di essere analizzate per tenere conto delle attuali esigenze pratiche e delle recenti evoluzioni tecnologiche. Questa tesi presenta un programma di ricerca completo focalizzato su tre regole di dettagli prioritari: dettaglio delle piegature delle barre d'armatura e diametro del mandrino, ancoraggio dell'armatura a taglio con piegature e ganci, e rapporto minimo di armatura a taglio. Questa ricerca ha lo scopo di sviluppare modelli meccanici, formule semplificate e dettagli costruttivi con il supporto di risultati sperimentali. Tali risultati sperimentali sono stati ottenuti utilizzando tecniche di misura all'avanguardia (*Digital Image Correlation* e *Fibre Optical Measurements*) grazie alle quali si può ottenere una migliore comprensione della risposta strutturale.

Le piegature e i ganci delle barre d'armatura in acciaio sono solitamente ottenuti mediante deformazione plastica delle barre contro i mandrini. Le norme specificano i diametri minimi dei mandrini per garantire un trasferimento sicuro delle forze e per evitare rotture per "splitting" o "spalling" che possono potenzialmente limitare la resistenza del dettaglio. Questa tesi include un programma di ricerca completo sui dettagli costruttivi delle piegature e sul diametro del mandrino necessario per evitare rotture locali del calcestruzzo che porterebbero all'espulsione del copriferro (spalling).

Su tale base, un modello meccanico è stato sviluppato per la progettazione delle armature piegate, insieme ai corrispondenti dettagli costruttivi. Quindi, una procedura di piegatura standard semplificata viene proposta grazie alla quale i dettagli che richiedono vari diametri di piegatura possono essere ottenuti utilizzando un singolo diametro del mandrino, consentendo una produzione automatizzata e più rapida delle armature piegate.

La disposizione dei ganci o delle piegature all'estremità delle barre è una soluzione semplice e conveniente per l'ancoraggio dell'armatura stessa. Questi dettagli sono relativamente sensibili allo stato fessurativo del calcestruzzo circostante. Per l'armatura a taglio, le rotture fragili possono verificarsi anche a causa dell'espulsione del copriferro (spalling), specialmente per le barre in prossimità di una superficie libera. Sulla base di indagini sperimentali, un modello meccanico, nonché delle considerazioni pratiche sull'attivazione dell'armatura a taglio vengono presentate allo scopo di aggiornare le norme e regole attualmente in vigore.

L'armatura minima a taglio in travi e solette è stata discussa per decenni. Tale armatura è necessaria per garantire nuove strutture economiche e sicure e per valutare accuratamente quelle esistenti. I risultati di un'indagine sperimentale mostrano che il comportamento dipende fortemente dalla quantità di armatura a taglio e dalla risposta post-snervamento dell'armatura (classe di duttilità). Infine, una discussione dell'implementazione di questi risultati nella nuova generazione di norme è presentata, evidenziando la coerenza delle recenti modifiche, in particolare per quanto riguarda le classi di duttilità, introdotte nella nuova generazione dell'Eurocodice 2.

Parole chiave: strutture in calcestruzzo armato, dettagli costruttivi, diametro del mandrino, ancoraggio, spalling, fessurazione, aderenza, ganci, barre piegate, armatura a taglio, armatura minima a taglio, misurazioni con fibre ottiche, correlazione digitale di immagini.

摘要

钢筋细部设计涉及其形状、几何尺寸及其在钢筋混凝土中的用量等细则。这些细则能够考虑既往设计中被忽视的因素，便于简化设计并提高效率，且能满足正常使用状态与预期作用之外的性能需求，保证结构鲁棒性。近几十年来，钢筋混凝土结构的制造工艺不断更新（如钢筋弯起工艺自动化）、材料性能逐步提升（钢筋和混凝土强度提高）、相关理论日渐深化，然而设计规范中的大部分设计细则未能与之变化相适应。现有设计细则往往基于工程实践经验提出，虽然能够满足工程应用需要，但缺乏可靠理论基础，这也是导致不同国家、不同规范中钢筋细部设计准则差异显著的原因之一。其中一些准则在很多工况下偏于保守，尤其是在评估现有结构时，而另外一些准则可能忽视了一些重要效应的影响。钢筋细部设计准则对钢筋混凝土结构的经济性与安全性影响重大，然而近年来这一领域的研究十分有限。

目前，一些关键细部构造设计亟需开展进一步研究，以便验证其是否满足当前设计实践需求，符合技术变革需要。为此，本文针对三个重要的钢筋细部构造，开展了详尽研究，包括：钢筋弯曲细部构造及其弯曲直径、带末端弯钩抗剪钢筋的锚固以及抗剪钢筋的最小配筋率。本研究旨在利用数字图像相关与光纤传感测量等前沿测试技术，开展相关试验，深入了解结构力学响应。基于试验结果，建立相应的力学模型，提出简化设计公式以及细部设计准则。

钢筋末端弯钩一般通过将钢筋沿芯筒弯曲实现加工制作。规范规定了其最小弯曲直径以确保传力可靠并且避免发生劈裂与剥落等破坏模态。此类破坏模态有制约细部构造承载力的潜在风险。为避免局部混凝土剥落失效，本文针对钢筋弯曲细部构造及其弯曲直径开展了系统试验研究，提出了相应的力学模型与细部设计准则。鉴于既往钢筋弯曲构造需经由多种直径芯筒制造，提出了一套简化标准弯曲流程，通过单一直径芯筒可实现钢筋弯曲，便于实现弯筋制造自动化。

设置末端弯钩是实现钢筋可靠锚固的便捷构造措施，然而该细部构造对周围混凝土的开裂状态较为敏感。靠近结构表面钢筋的混凝土保护层可能发生剥落，导致抗剪钢筋脆性失效。为此，本文研究了末端弯钩锚固构造的力学响应与性能。在此基础上，建立了相应力学模型，提出了充分发挥梁内抗剪钢筋作用的实用构造要求，为修正当前设计细则提供理论依据。

混凝土梁与板中所需的最小抗剪配筋率对于确保新结构的经济性、安全性以及准确评估现有结构至关重要，关于这一问题业界已持续争论多年。本文试验研究结果表明，抗剪钢筋用量与钢筋屈服后响应即钢筋的延性等级显著影响钢筋混凝土的抗剪行为。

针对上述细部设计准则，进一步讨论了本研究成果在行业规范中的应用，着重阐述了与新近规范特别是新一代 Eurocode 2 规范变化的一致性。

关键词：钢筋混凝土结构，细部构造准则，弯曲直径，锚固，剥落，劈裂，粘结，末端弯钩，抗剪钢筋，最小抗剪配筋，光纤测量技术，数字图像相关技术。

Contents

Chapter 2 Design against splitting failures in reinforced concrete due to concentrated forces and minimum bend diameter of reinforcement 11

Chapter 3   Anchorage of shear reinforcement in beams and slabs   61

Chapter 4 Influence of amount and post-yield response of shear reinforcement on the shear strength of reinforced concrete beams 113

Chapter 1

Introduction

1.1   Context and motivation

The aim of this research is to contribute to updating the detailing rules for concrete structures, with high relevance for both reinforced concrete bridges (Figure 1.1a) and buildings (Figure 1.1b). An update of these rules is necessary to optimise the economy of structures, to avoid unnecessary repairs, but also to simplify the construction of new structures, to make the level of safety more homogeneous and to allow a convergence of the detailing rules at the international level.

(a)   (b)
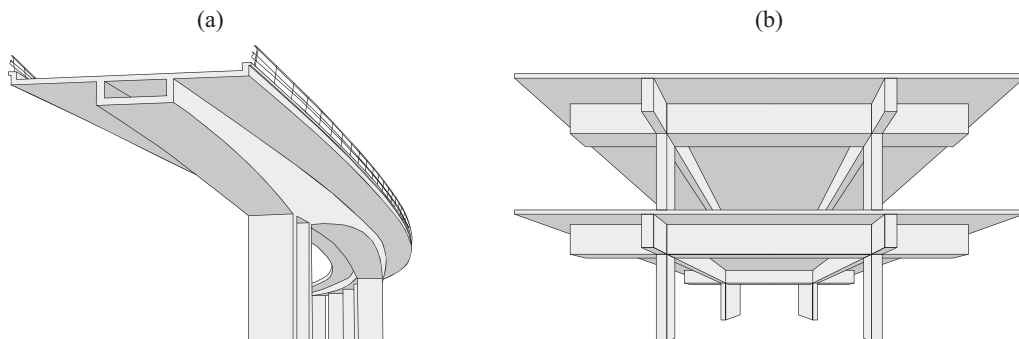
Figure 1.1:   Structural members requiring the application of detailing rules in the case of: (a) bridges; and (b) buildings

From a historical perspective, detailing rules were established since the first concrete works. Indeed, through patents, the constructive systems specified how to assemble reinforcement in a concrete member. Figure 1.2a show the state-of-the-art of the main patents of the constructive systems in 1899 published in the Belgium journal of Hennebique *Le Béton Armé* [Sys99]. For instance, the first patents of Monier in 1878, Hennebique in 1893 (Figure 1.2b) and Wayss & Koenen in 1892 used bent-up bars with detailed provisions of the geometry [Mon78, Hen93, Koe92]. First open stirrups with simple bends were incorporated in the early patents by Hennebique in 1892-1893 [Hen92, Hen93] (under the name of "staple" composed by a flat steel plate, later renamed as stirrup in 1893 [Hen93], refer to Figure 1.2c) followed by Coignet in the

1

same year [Coi92]. The 90° bends at the end of the beams in the patents of Hyatt in [Hya77] or 180° hooks in the patents of Considère in 1907 [Con07] and Mörsch in 1908 [Mör08] are examples of early detailing rules provided to engineers.

(a)

(b)

(c)
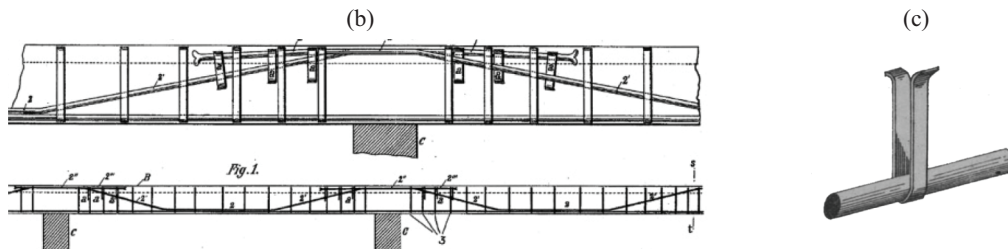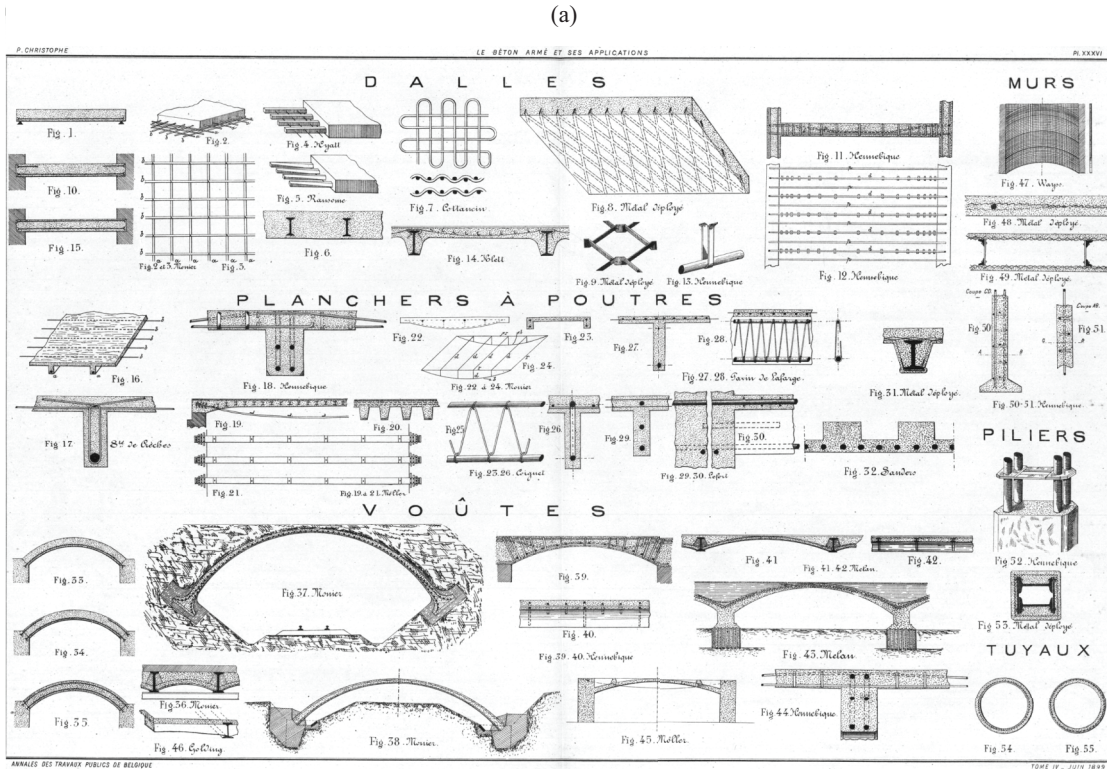
Figure 1.2:   (a) State-of-the-art of the main patents of constructive systems for reinforced concrete in 1899 [Sys99]; (b) system Hennebique for beams [Hen93]; and (c) first stirrup developed by Hennebique [Hen92, Hen93]

In concrete structures, detailing rules and some minimum geometrical dimensions and minimum amount of reinforcement are defined in Codes [Eur04, Eur21, FIB13, SIA13, ACI19, AAS20], in Guidelines (see for example the Guidelines for Bridge Construction Details of the Swiss Federal Roads Authority [OFR10]), in books, or can be provisioned in memoranda. In codes, the detailing rules concern among others [Eur04, SIA13]:

- minimum and maximum spacing of reinforcement;

- minimum mandrel diameter for bent reinforcement;

- anchorage length and lap splice of reinforcement;

- minimum amount of reinforcement as well as maximum spacing of shear and flexural reinforcement for various structural members.

Some of these rules are necessary to:

- allow for simple and rapid design without explicit verification of Serviceability and Ultimate Limit States (SLS and ULS);

- allow neglecting some effects in the design or to ensure suitable behaviour in the event of unpredictable actions;

- ensure sufficient robustness of structural members (deformation capacity and residual strength);

- comply with the limits of applicability of design models.

These rules are therefore justified for the design of new structures but may be too restrictive and even problematic in the context of the assessment of existing structures that do not meet the provisions of current codes. In the latter case, when the verification is critical, it is more reasonable to check explicitly the limit states (SLS, ULS and fatigue) or the risk of progressive collapse in case of insufficient robustness. This means that, in theory, for the assessment of existing structures, only the detailing rules defining the limits of applicability of design models should be considered and, where appropriate, the use of more refined models (allowing the limits of applicability to be extended) may make respecting specific detailing rules unnecessary.

In addition, codes contain other rules defined on the basis of so-called "rules of good practice" without a particular scientific basis and which may not be necessarily justified. Some of these rules were defined in the past when the strength of concrete and reinforcement was significantly different from current practice and should be adapted in current Codes. It is also part of the reasons why some detailing rules significantly differ between standards [Eur04, Eur21, FIB13, SIA13, ACI19, AAS20] and this topic is the focus of significant efforts in the revision of the new generation of Eurocode 2.

The priority topics of the thesis are presented in the following and in Figure 1.3.

Bend detailing and required mandrel diameter (Figure 1.3b)

Bending of steel reinforcement bars has been performed since the beginning of reinforced concrete construction to provide anchorage, lapping and detailing. For beams and slabs, a common application of bent reinforcement was for bent-up bars or stirrups for the shear reinforcement of beams. The research in this field dates a long way back (1930s-'70s). Most of the experimental results [Gra33, Wäs34, Wäs35, Wäs36, Gra40, Öst63, Ber66, Leo73] refer to very different concrete strengths and bar types (smooth bars with low yield strength) than those currently used in practice.

Based on previous research, codes of practice normally define a variety of bend diameters depending on the bar diameter and on the structural application. For example, *fib*'s Model Code 2010 (MC2010) [FIB13] or SIA262:2013 [SIA13] require the use of different mandrel diameter for hooks, loops, stirrups and general bends. EC2:2004 [Eur04] includes a design equation to verify the mandrel diameter according to the concrete compressive strength, the steel tensile stress, the bar diameter and the concrete cover. This large number of possibilities, complicates the manufacturing process of reinforcement and, as already reported by Bernardi et al. [Ber66], is a potential source of execution errors.

Anchorage of shear reinforcement with bends and hooks (Figure 1.3c)

Since the beginning of reinforced concrete construction, mechanical anchorage of reinforcement in tension by means of bends and hooks has been extensively used in beams, walls and slabs.

The shear reinforcement of reinforced concrete bridges built in the second half of the 20th century usually consists of open stirrups in the upper part at the intersection of the web with the deck slab (Figure 1.3c). Closed stirrups, more frequently used in buildings for beams with rectangular cross-section, lead to a greater difficulty in the placement of the longitudinal reinforcement and prestressing tendons. It should be noted that some Codes allow the use of open stirrups [Eur04, ACI19] while others prohibit them or allow them only under certain conditions [Eur04, FIB13, SIA13].

From the 1970s onwards, the design of shear in beams was explicitly based on the assumption of the formation of an inclined compression field linked to the tensile and compression chord (see for example approaches based on the Variable Truss Model [Rit99, Mör08, Kup69, Dru61, Gro76, Nie78, Thü79]). As a result of this model, the stirrups must be fully activated up to their yielding strength over their entire height between the tensile and the compression chord forces. If stirrups must be closed, 90° bends (Figures 1.3c) or L-shaped reinforcement bars must be added. This implies a large amount of reinforcement in the upper part of the web, causing difficulties in the casting of these regions because of reinforcement congestion. In the presence of a slab at the top of the web, its reinforcement further increases the difficulty of construction.

Some researchers have tried to verify the influence of anchorage details on the SLS and ULS behaviour of beams only on the basis of shear beam tests (see for example [Reg04, Var11, Rup13, Leq18, For19]). The results of this research have influenced the design provisions defined in Codes such as EC2:2004 [Eur04].

Current provisions of the European Standard for concrete structures [Eur04] define both bends (bend between 90° and 135°) and hooks (with a bend angle ≥ 135°) as details to enhance the anchorage of reinforcement bars. In the case of one-leg links, both bends and hooks are typically used (see Figure 1.3c) and according to EC2:2004 [Eur04], only transverse welded bars or headed bars (prEN 2021 [Eur21]) are accepted as alternatives.

Finally, some beams and bridges built in the past (until the 1980s) have insufficient shear anchorage according to the current provisions due to the updating of the Codes.

Minimum amount of shear reinforcement (Figure 1.3a)

Since the early works in reinforced concrete, shear reinforcement has been used in a wide variety of constructions (Figure 1.1). The first applications of shear reinforcement can be traced to patents by Hennebique [Hen92, Hen93] and Coignet [Coi92] (Figure 1.2), and was soon acknowledged as an efficient solution to increase the shear resistance.

A number of physical tests were performed to better understand the mechanical response and to develop tools for design of beams with sufficient shear reinforcement [Rit99, Mör08, Kup69, Dru61, Gro76, Nie78, Thü79, Sch87, Nie11, Mut97]. This led to a number of consistent methods for shear design based on limit analysis [Nie78, Thü79] accounting for the smeared nature of shear cracking (right side of the beam in Figure 1.3a).

In addition, several research efforts have been performed to better understand the response of members without shear reinforcement [ASC98, Cha87, Fen68, Kan64, Tay69, Vec86, Tay70, Wal80, Baz84, Mut08, Cam13, Fer15, Cav15, Cav17, Cav18]. These members are characterized by a brittle failure in shear due to the localization of the strains in a Critical Shear Crack (CSC) [Mut08, Fer15, Cav15] (left side of the beam in Figure 1.3a).

The minimum amount of shear reinforcement has been traditionally adopted as a limit to consider if approaches for members with shear reinforcement can be applied or if, conversely, models for members without shear reinforcement must be used. In addition, this detailing rule has also been used to ensure sufficient robustness, development of distributed cracking and cover effects neglected in design.

The minimum amount of shear reinforcement to be provided in webs of girders and slabs has been a topic of debate and research for decades without reaching a consensus. Although limited, several research efforts have been performed to better understand the response of members with low amounts of shear reinforcement [Ang99, Aut21, Tue19, Bre63, Cam13, Cla05, Hub16, Piy02, Rup13, Vec04, Yoo96, Yos00, Bac80]. Models have also been developed to describe the transition between these the case with and without shear reinforcement (see for example [Ben06] implemented in MC2010 [FIB13] or [Cav18, Tun20]).

The minimum shear reinforcement ratio defined in the Codes [SIA13, Eur04, FIB13, ACI19, AAS20, CSA14] was developed essentially empirically, without using rigorous considerations. A systematic and consistent study of the minimum shear reinforcement required to ensure crack distribution in the web of beams (and thus allow the applicability of models such as stress field) is not available in the scientific literature.

Defining this value is however needed to build in an economic manner and to safely ensure the applicability of the design or assessment methods (considering the contribution of the web reinforcement or neglecting it). The latter is justified by the fact that the minimum shear reinforcement ratio defined in older codes was very low (or even not mentioned, e.g. Switzerland).
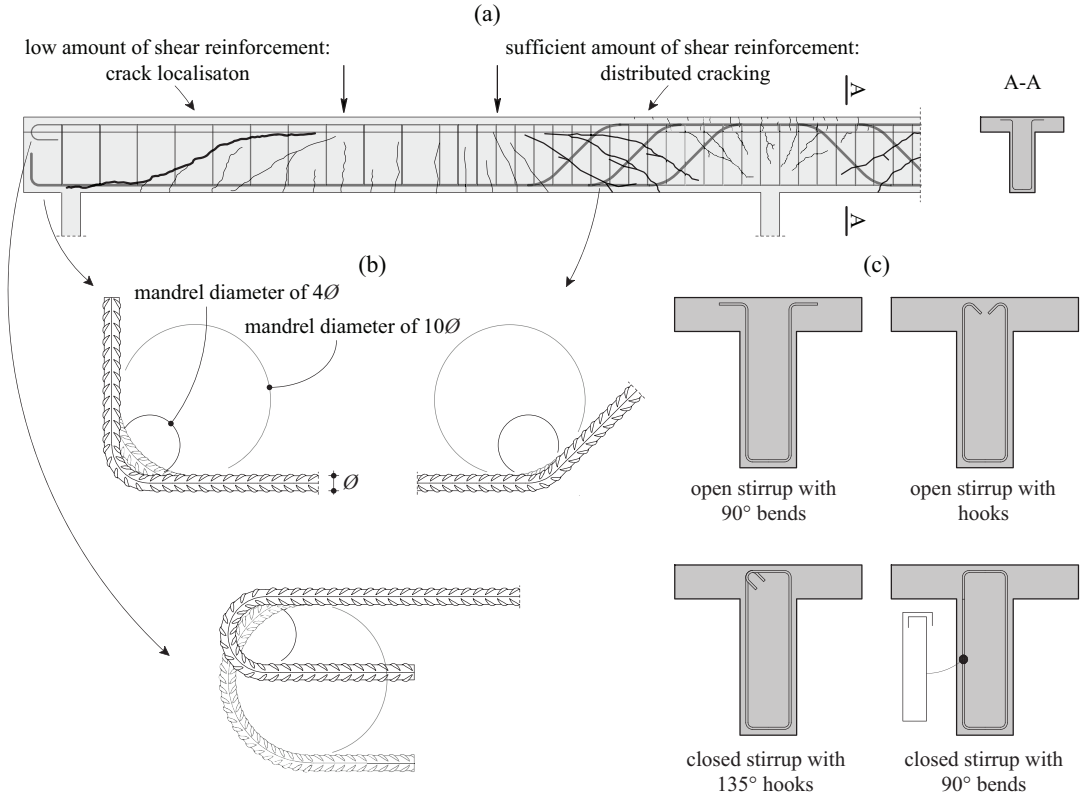
Figure 1.3:   Some detailing rules concerning reinforcement: (a) minimum shear reinforcement ratio; (b) bend detailing and required mandrel diameter; and (c) anchorage of shear reinforcement with bends and hooks

This thesis presents a detailed investigation on the three detailing rules: bend detailing and required mandrel diameter, anchorage of shear reinforcement with bends and hooks and minimal amount of shear reinforcement. For each topic, theoretical considerations and new experimental programmes with current detailing and material properties were performed. All series were instrumented using state-of-the-art measurement techniques such as Digital Image Correlation measurement (DIC) [Cor10] or Fibre-Optic Measurements (FOM) [Lun13] helping to understand the structural response.

1.2   Objectives

The main objectives of this research are to:

- Contribute with new experimental data on the behaviour of bent bars and particularly the implications of spalling failures on the strength of such details.

- Investigate the mechanism of concrete cover spalling induced by a concentrated force and the influence of the bend diameter of the reinforcement.

- Investigate in a detailed manner the influence of the mandrel diameter, bend angle, concrete cover, distance between multiple bends, bar diameter and casting position on spalling.

- Develop a mechanical model for the design of bent reinforcement.

- Propose and simplify the existing detailing/design rules for bent reinforcement.

- Contribute with new experimental data on bond and spalling resistance in case of bend and hook anchorages close to the concrete surface.

- Investigate the response of bends and hooks focusing on the bond and spalling of the concrete cover mechanism.

- Investigate in a detailed manner the influence the concrete cover, tail length, crack opening in the plane of the bend and presence of a longitudinal bar within the bend on the spalling and bond resistance.

- Develop a mechanical model for the design of the anchorage of bends and hooks.

- Contribute with new experimental data on shear failure in beams with low amounts of shear reinforcement.

- Investigate in a detailed manner the influence of the shear reinforcement ratio, ductility class and anchorage of the shear reinforcement on the shear response and failure.

- Investigate the variable Shear Transfer Action of beam with low amount of shear reinforcement by means of detail measurements of cracks kinematics as well as strains in the stirrups and the flexural reinforcement.

- Evaluate the shear design model of the present [Eur04] and the new generation [Eur21] of Eurocode 2 in case of low amount of shear reinforcement.

1.3   Scientific contributions

The main scientific contributions of the research are listed below:

- Comprehensive literature review including research and design codes on detailing of mandrel diameters in case of bent reinforcement.

- Experimental programme comprising loops tests of 41 specimens on the influence of the mandrel diameter, bend angle, concrete cover, distance between multiple bends, size effect and casting position on the spalling response.

- Experimental programme comprising 24 prisms tests on the influence of the concrete cover, concrete compressive strength, size effect on the splitting response.

- Detailed measurements of the out-of-plane displacements to understand spalling failures.

- Consistent mechanical modelling assessing spalling resistance of bent reinforcement with a code-like formulation introduced in the current draft for the new generation of Eurocode 2 [Eur21].

- Database of 135 tests with variable test configurations used to assess the mechanical model.

- Innovative design recommendations for bent reinforcement, multiple bends, hook and presence of transverse bars within the bend.

- Comprehensive literature review including research and design codes on hooks and bends with a focus on the anchorage of shear reinforcement.

- Experimental programme comprising pull-out tests of 24 specimens on the influence of the concrete cover, tail length, crack opening in the plane of the bend and presence of longitudinal bar within the bend on the spalling and bond resistance.

- Detailed measurements of the out-of-plane displacements to understand the mechanics of spalling and bond failures.

- Rebar strain measurements to understand the bond stresses and the deviation forces leading to spalling and bond failures.

- Consistent mechanical model and design recommendations, including a code-like formulation, assessing the resistance of bends and hooks which applies also to the anchorage of shear reinforcement.

- Database of 40 tests (hooks and bends) including crack opening in the plane of the bend used to assess the mechanical model.

- Comprehensive literature review including research and design codes on beam with low amount of shear reinforcement.

- Experimental programme comprising 10 beam tests with variable shear reinforcement ratio, ductility class of the shear reinforcement and shear anchorage detail on the shear response.

- Detailed measurements of the shape and the kinematics of cracks to understand the response of beam with low shear reinforcement ratio.

- Detailed measurements of the strains in the stirrups and flexural reinforcement to evaluate their activation.

- Evaluation of the Shear Transfer Action based on the detailed measurements.

- Evaluation of the shear design equation of the actual [Eur04] and the new generation [Eur21] of Eurocode 2 in case of low amount of shear reinforcement.

1.4   Structure of the thesis

This thesis is a composed by an introduction, a compilation of three journal articles and a conclusion. The following topics are treated:

- **Chapter 1**: *Introduction*

  Context and motivation, objectives, scientific contributions and list of publications.

- **Chapter 2**: *Design against splitting failures in reinforced concrete due to concentrated forces and minimum bend diameter of reinforcement*

  Results of a comprehensive research programme on bend detailing and required mandrel diameter to avoid local concrete failures leading to spalling of the concrete cover.

- **Chapter 3**: *Anchorage of shear reinforcement in beams and slabs*

  Results of an investigation addressed at understanding the mechanical response and performance of bend and hook anchorages.

- **Chapter 4**: *Influence of amount of shear reinforcement and its post-yield response on the shear resistance of reinforced concrete members*

  Results of an investigation addressed at the activation and contribution to the resistance of shear reinforcement, particularly when low amounts are provided.

- **Chapter 5**: *Conclusion and Outlook*

  Conclusion of this research and provides an outlook on potential future research.

It must be noted that chapters 2 to 4 include their own introduction, state-of-the art (literature review), conclusions, appendixes and notations as the present thesis is a compilation of journal articles (paper-based thesis). The full bibliography is given at the end of the thesis.

1.5   List of publications

The research was conducted at the Stuctural Concrete Laboratory (IBETON) of the Swiss Institute of Technology of Lausanne (Ecole polytechnique Fédérale de Lausanne, EPFL) resulting in the following publications:

- **Monney F., Fernández Ruiz M., Muttoni A.**, *Design against splitting failures in reinforced concrete due to concentrated forces and minimum bend diameter of reinforcement*, Engineering Structures, Vol. 245, 112902, 2021.
  DOI: https://doi.org/10.1016/j.engstruct.2021.112902

- **Muttoni A., Fernández Ruiz M., Monney F.**, *Permissible mandrel diameters for bent bars*, Background document 11.3 to prEN 1992-1-1:2018, European Committee for Standardization (CEN), Brussels, Belgium, 2021.

- **Monney F., Yu Q., Fernández Ruiz M., Muttoni A.**, *Anchorage of shear reinforcement in beams and slabs*, Engineering Structures. [accepted, May 2022]

- **Monney F., Fernández Ruiz M., Muttoni A.**, *Influence of amount of shear reinforcement and its post-yield response on the shear resistance of reinforced concrete members*, Structural Concrete. [submitted for review, April 2022]

Chapter 2

Design against splitting failures in reinforced concrete due to concentrated forces and minimum bend diameter of reinforcement

This chapter is the post-print version of the article mentioned below, published in Engineering Structures Journal. The authors of the article are Frédéric Monney (PhD Candidate), Prof. Miguel Fernández Ruiz (thesis co-director) and Prof. Aurelio Muttoni (thesis director). The reference is the following:

Monney F., Fernández Ruiz M., Muttoni A., *Design against splitting failures in reinforced concrete due to concentrated forces and minimum bend diameter of reinforcement*, Engineering Structures, Vol. 245, 112902, 2021. (DOI: https://doi.org/10.1016/j.engstruct.2021.112902)

The work presented in this publication was performed by Frédéric Monney under the supervision of Prof. Miguel Fernández Ruiz and Prof. Aurelio Muttoni who provided constant and valuable feedbacks, proofreadings and revisions of the manuscript. It has to be noted that Figure 2.22 and 2.24 with the associated text as well as Section 2.6.3 are not in the article but are part of the Background document 11.3 of the prEN 1992-1-1:2018 for the new generation of Eurocode 2. The reference is the following:

Muttoni A., Fernández Ruiz M., Monney F., *Permissible mandrel diameters for bent bars*, Background document 11.3 to prEN 1992-1-1:2018, European Committee for Standardization (CEN), Brussels, Belgium, 2021.

Section 2.6.4 is also not in the article and have been added to this chapter.

The main contributions of Frédéric Monney to this article and chapter are the following:

- Comprehensive literature review including research and design codes on detailing of bent reinforcement focusing on spalling failure.

- Preparation, casting and testing of 41 loop tests (loops) as well as 24 prism tests with variable bend angle, mandrel diameter, concrete cover, distance between multiple bends, size effect, casting position and concrete compressive strength.

- Detailed measurements on the out-of-plane displacements, using Digital Image Correlation, to understand spalling failures.

- Implementation of Fibre-Optical measurements on steel reinforcement of two loops for an evaluation of the strain profile.

- Post-processing of the experimental data.

- Interpretation, analysis and discussion of the tests results.

- Proposition of a consistent mechanical model assessing spalling resistance of bent reinforcement; it considers the concrete compressive strength, concrete cover, mandrel diameter, bend angle and size effect.

- Proposition of innovative design recommendations for bent reinforcement, multiple bends and hooks.

- Collection of a database with 135 tests with variable test configurations used to validate the mechanical model.

- Development of a code-like formulation of the mechanical model; this formulation is included in the current draft for the new generation of Eurocode 2 (prEN 1992-1-1:2021).

- Elaboration of the figures and tables included in the article.

- Writing of the manuscript of the article.

Abstract

Plastic bending of reinforcement bars against mandrels is the usual procedure to provide bends and hooks for steel reinforcement bars. Minimum mandrel diameters are usually given in to codes of practice, depending on the type of detail and diameter of the bar. These recommendations for the bend diameter ensure a safe transfer of forces, avoiding splitting failures that may potentially limit the resistance of the detail. In most cases, these recommendations are largely based on a number of experimental works performed several decades ago. At that time, these investigations were performed on reinforcement and concrete with lower strengths than currently used. This chapter presents the results of a comprehensive research programme on bend detailing and required mandrel diameter to avoid local concrete failures leading to spalling of the concrete cover. The results of an experimental programme are presented, showing the influence of different parameters such as the mandrel diameter, the bending angle and the concrete cover. The tests were instrumented with advanced measurement techniques (Fibre-Optic Measurements and Digital Image Correlation), showing that consistent modelling of the transfer of forces can be performed on the basis of the geometrical and mechanical parameters of the details.

Keywords: reinforced concrete, mandrel diameter, concentrated forces, testing, detailing rules, spalling, splitting, Fibre-Optic Measurements, Digital Image Correlation

2.1 Introduction

Bending of steel reinforcement bars has been performed since the beginning of reinforced concrete construction to provide anchorage, lapping and detailing (Figures 2.1a-d) by plastic deformation of the bars against mandrels. Originally, bending of the reinforcement was needed for anchorage of plain bars due to their poor bond performance. Hooks were generally bent at 180° with a straight segment at their end. This detailing was extensively used in the initial developments of reinforced concrete (Considère [Con07]) and validated by testing (Wayss and Freytag [Mör08]). Hooks with a 90° bend were at that time not recommended for smooth bars due to their lower anchorage performance and due to the fact that the straight segment of the anchorage could be located too close to the surface of the beams, leading potentially to a concrete cover failure [Mör08]. Based on experimental observations [Con07], it was further advised that hooks were to be bent with a minimum mandrel diameter equal to 4 times the bar diameter $\varnothing$ to avoid a concrete crushing failure.

For beams and slabs, a common application of bent reinforcement was that of bent-up bars (Figure 2.1a), as incorporated in the early patents by Monier in 1878 [Mon78], Hennebique in 1893 [Hen93] and Wayss & Koenen in 1892 [Koe92] (see [Mör08]). This detailing contributed simultaneously to the anchorage of the flexural reinforcement and to the shear resistance, also avoiding congestion of anchorage hooks at support (which could potentially create splitting cracks and lead to cover spalling [Mör06]). Bent reinforcement was also adopted for the shear reinforcement of beams in the form of stirrups (Figure 2.1d). The introduction of this latter element is attributed to Hennebique in 1892 [Hen92] (under the name of "staple" composed by a flat steel plate, later renamed to stirrup in 1893 [Hen93]), followed by Coignet in the same year [Coi92]. During the 1960s (see for instance [SIA68]), specific provisions were developed for bending of the stirrups, generally associated to smaller required mandrel diameter ($\emptyset_{mand}$) than for other elements. Applications of bent reinforcement were also developed for lapping of reinforcement of smooth bars [Mes08] (Figure 2.1b), where it was experimentally observed that larger mandrel diameters than for stirrups were required in order to avoid concrete failures (following also the results of early tests [Con07]).
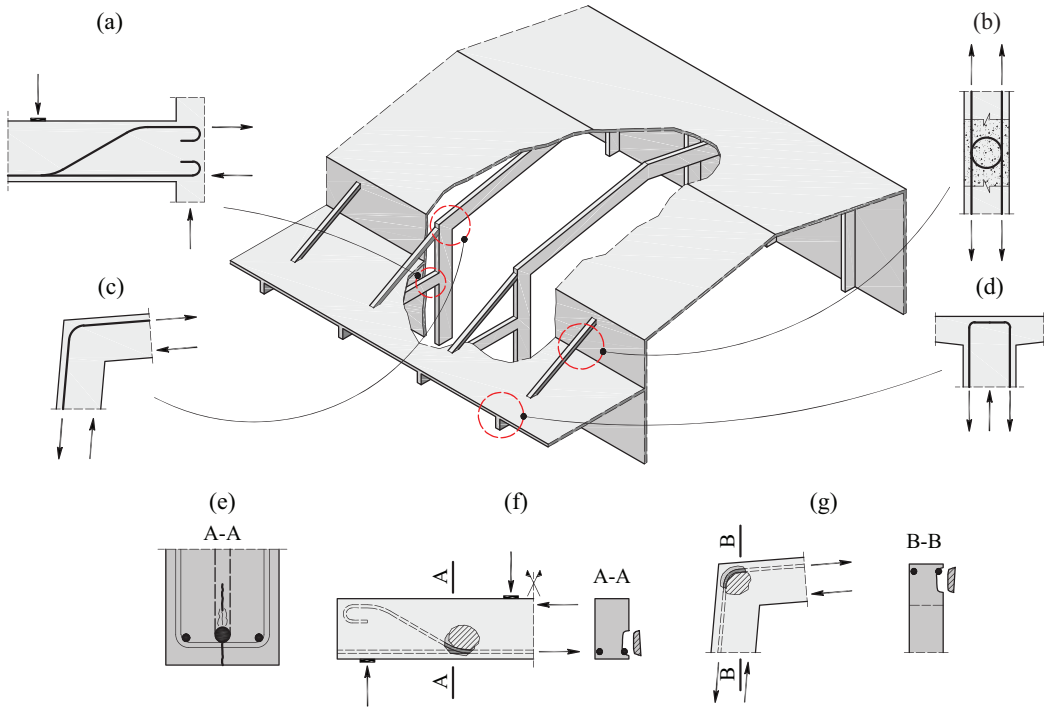
Figure 2.1:   Applications of bent bars (a)-(d) and type of concrete failures (e)-(g): (a) beams; (b) joints; (c) corners; (d) stirrups; (e) splitting cracks with local concrete crushing in case of large cover; and (f)-(g) spalling of concrete cover.

As early shown by researches on the performance of bent bars, the diameter of the mandrel is a parameter governing the response of reinforcement details and potentially limiting their strength according to the following failure modes:

- bending cracks in the bars during their plastic deformation against the mandrel [Gra40a, Ber66];

- concrete failures [Mes08, Dra75, Joe13] due to splitting cracks and local concrete crushing in case of large cover, Figure 2.1e;

- concrete failures due to spalling of the concrete cover [Ber66, Gra33, Wäs34, Gra40, Öst63, Leo73, Gra99], Figure 2.1f-g.

Based on previous research, codes of practice normally define various bend diameters requirements depending on the bar diameter and on the structural application. This situation complicates the manufacturing process of the reinforcement and, as reported by Bernardi et al. [Ber66], is a potential source of execution errors. The difficulties associated to varying the diameter of bends lie in the process followed to bend the reinforcement. The classical manufacturing process consists of clamping the bar and applying a force to deform it around a mandrel (Figure 2.2a). This technique is typically used for small mandrel diameters ($\varnothing_{mand} \leq 10\varnothing$), whereas for larger bending diameters, a three-roller mechanism is preferred (Figure 2.2b-c). The use of efficient industrial procedures for bending of reinforcement requires to use a single machine and to minimize the amount of changes of mandrel diameters in the machine. This is however in contradiction with the varying values of bend diameter prescribed by codes (details are later given in Section 2.2.2).
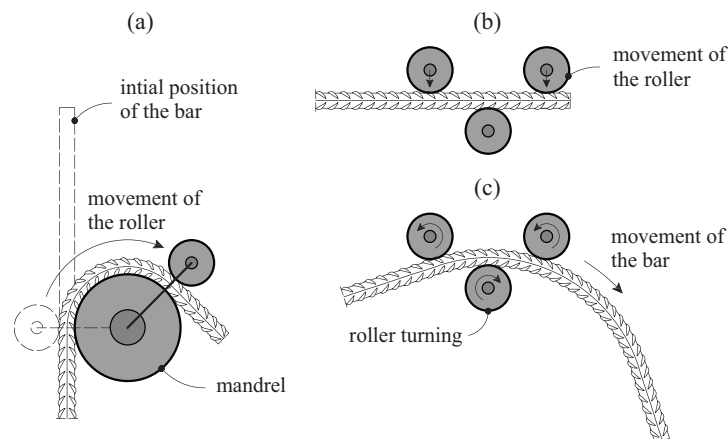
Figure 2.2:   Bending machines: (a) classical bending machine using mandrels; (b) three-roller bending machine with its initial position; and (c) three-roller bending machine during the process of bending.

This chapter presents a detailed investigation on the response of bent reinforcement, focusing on the spalling resistance of such details. It introduces the results of a comprehensive testing programme performed by the authors on specimens with current detailing and material properties. These tests are aimed at completing previous experimental evidences performed earlier with lower strength materials. They were instrumented with advanced measurement techniques (Digital Image Correlation or Fibre-Optic Measurements), helping to understand the mechanics of spalling failures. On that basis, a rational model for design of bent reinforcement is proposed. Its results are compared to the performed tests as well as to a database of experimental tests collected from the literature. The results show a consistent agreement, significantly improving the design equations in current codes of practice. Based on these findings, a rational approach for new detailing rules for the bending of reinforcement is outlined, showing how details requiring different bend diameter can obtained by using a single mandrel diameter. This latter proposal is aimed at simplifying standard bending procedures, allowing for automated manufacturing of bent reinforcement.

2.2 Consideration of cover spalling for bent reinforcement: background, current code provisions and limitations

2.2.1 Research on spalling of concrete cover

A number of research efforts were devoted in the past to understanding the anchorage performance of bent reinforcement. Some of their recommendations, as those of Considère [Con07] ($Ø_{mand} = 4Ø$), are still partly found in current codes of practice (EN 1992-1-1:2004 [Eur04] or *fib*'s Model Code 2010 [FIB11]). It is however interesting to note that such recommendations were proposed a long time ago for very different concrete strengths and bar types (smooth bars with low yield strength) than those currently used in practice.

The majority of the research programmes on spalling failures of bent bars were performed several decades ago. These investigations were mostly focused on lapping in tensile members (Leonhardt et al. [Leo73] Figure 2.3a), bent-up bars in beams (Graf [Gra33, Gra40] and Bernardi et al. [Ber66], Figure 2.3b), frame corners with closing/opening bending moments (Östlund [Öst63] and Wästlund [Wäs34], Figure 2.3c), lapping in bending members (Grassl [Gra99] and Wästlund [Wäs34], Figure 2.3d) and loops (Wästlund [Wäs34], Figure 2.3e). Other authors have also investigated spalling failures within more general testing programmes on frame corners [Wäs34, Wäs35, Cra65, Swa69, Bal72, Nil73, Str81, Str83, Ske84, Stu90, Luo94, Joh01] and lapping in beams [Wäs34, Wäs36, Tim69, Kor72].
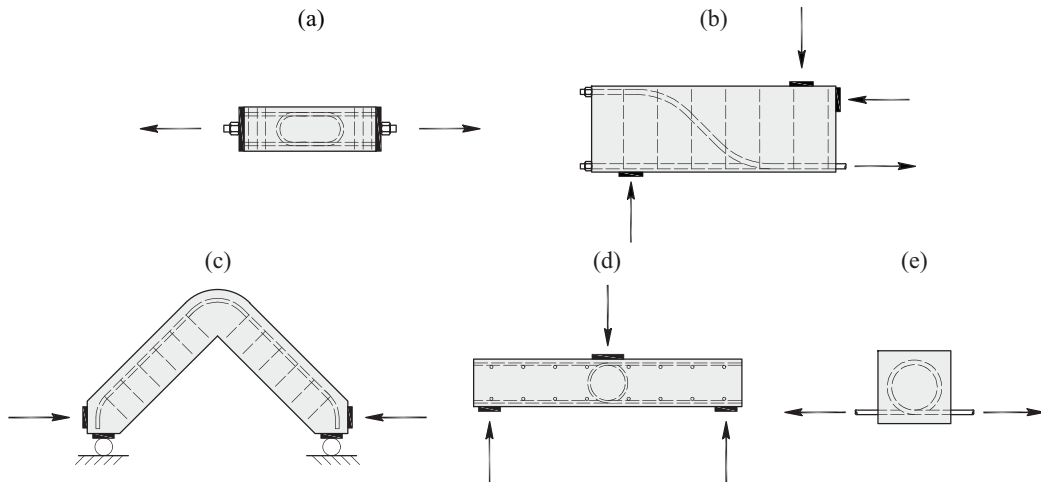
Figure 2.3: Experimental programmes on bent reinforcement: (a) lapping in tensile members; (b) bent-up bars in beam specimens; (c) corner frame members; (d) lapping in bending members: and (e) spalling/splitting specimens.

The results of these experimental programmes led to relatively different detailing rules. One of the first systematic testing series was performed in the 1930s-1940s by Graf [Gra33, Gra40] on bent-up bars in beams. It comprised specimens with 45° bends, a concrete compressive strength between 10 and 25 MPa and smooth bars with a yield strength of about 400 MPa. Graf concluded that minimum mandrel diameters of at least 5 times the bar diameter were required to avoid spalling of the concrete cover. Similar tests were also performed by Bernardi et al. [Ber66] with higher concrete strengths and deformed bars, concluding that the concrete cover c plays a significant role and that cover spalling can be avoided when the concrete cover is larger than 2 times the bar diameter plus 20 mm and a mandrel diameter larger than 4 times the bar diameter.

One of the most comprehensive experimental programmes was performed by Wästlund [Wäs34, Wäs35, Wäs36] on three type of specimens: spalling/splitting specimens, frame corners and laps in beams. Based on the results of these tests, the author concluded that the spalling strength (reinforcement stress at failure) can be assumed to be proportional to (i) the concrete compressive strength with an exponent of 2/3; (ii) the ratio $\emptyset_{mand}/\emptyset$ with an exponent of 4/5 and (iii) the bar diameter $\emptyset$ with an exponent of -0.3 (size effect). The spalling strength can also be assumed to be linearly dependent on the concrete cover c, with an upper limit for $c = 3.25\emptyset$. For typical investigated details and for $f_c \approx 16$ MPa, the yield strength in the reinforcement ($f_y = 263$ MPa) was reached without spalling for mandrel diameters $\emptyset_{mand}$ larger than $12\emptyset$.

Another work that significantly influenced the development of code provisions [Nil73] was performed by Östlund [Öst63] on frame corners where the influence of the mandrel diameter and of the concrete cover has been investigated. The yield strength of the bars ranged between 390 and 590 MPa and the concrete compressive strength ranged between 10 and 25 MPa. The results showed that spalling can occur when the bars are close to the concrete surface and the yield strength of the reinforcement is larger than 400 MPa. On this basis, Östlund proposed an equation to calculate the tensile force in the bent reinforcement as a function of the mandrel diameter, the bar diameter and the concrete tensile strength (assumed to be proportional to the square root of the concrete compressive strength).

Finally, the works of Leonhardt et al. [Leo73] conducted on U-bars laps (180° bends) shall also be acknowledged. These tests performed with higher concrete strength and with deformed bars, showed that, in absence of transverse reinforcement, cover spalling can only be avoided by significantly increasing the mandrel diameter ($\varnothing_{mand} \geq 15\varnothing$). As can be noted, this condition is significantly more restrictive than those of previous recommendations.

In addition to these researches, a number of works can be found on selected topics, such as frame corners [Cra65, Swa69, Bal72, Nil73, Str81, Str83, Ske84, Stu90, Luo94, Joh01, Joh00], loops [Gra99, Wäs36, Tim69, Kor72] and more recently on laps using U-bar loops [Joe13] and headed bars [Vel18].

2.2.2 Code provisions and detailing rules

Codes of practice include a number of provisions both in terms of minimum mandrel diameters ($\varnothing_{mand}$) and concrete cover requirements to avoid spalling failures. The code provisions have significantly evolved with this respect, reflecting the changes in the state-of-the-art. As an example, Figure 2.4b shows the evolution of the mandrel diameter for the Swiss code from 1903 (first version) to 2013 (current version) [SIA03a, SIA09, SIA35, SIA56, SIA68, SIA93, SIA03, SIA13]. As can be noted, starting with earlier versions of the code, a difference was made between general bends, hooks and loops, with less restrictive provisions for the latter. A significant increase of the required bend diameter was introduced in the 1950s following the introduction of reinforcement with higher yield strength. At the same time, specific provisions for stirrups were also introduced that increasingly replaced bent-up bars.
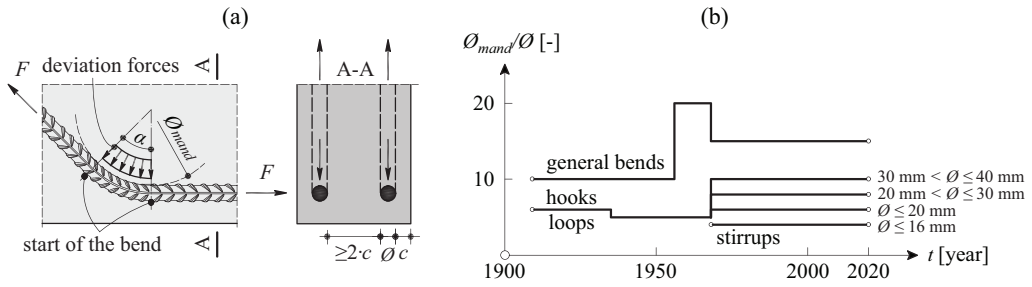
Figure 2.4:   Codes provisions: (a) bent bar detail and deviation forces; and (b) mandrel diameter evolution in Swiss codes (case without transverse reinforcement).

Amongst codes of practice (EN 1992-1-1:2004 [Eur04], MC2010 [FIB11], ACI 318-19 [ACI19] and SIA 262:2013 [SIA13]), there are currently significant discrepancies with respect to bend diameters, as shown in Table 2.1. Some of these differences are found in the parameters governing the mandrel diameters. For instance, the European standard EN 1992-1-1:2004 [Eur04] provides an expression to calculate the minimum mandrel diameter as a function of the steel stress σ_s, the concrete compressive strength f_c, the bar diameter $\emptyset$ and the concrete cover c (see Figure 2.4a):

$$\frac{\emptyset_{mand}}{\emptyset} = \frac{\sigma_s}{f_c} \cdot \frac{\pi}{4}\left(\frac{1}{\dfrac{c}{\emptyset}+\dfrac{1}{2}}+\frac{1}{2}\right) \tag{2.1}$$

This equation presents some analogies with the previous recommendations from the literature, but accounts for some additional parameters (as the concrete strength and the cover of the reinforcement).

The CEB-fib Model Code 1990 [CEB93] also proposes a similar equation:

$$\frac{\emptyset_{mand}}{\emptyset} = \frac{\sigma_s}{f_c} \cdot \frac{k_\alpha}{\sqrt{1+2\dfrac{c}{\emptyset}}} \tag{2.2}$$

Where coefficient k_α accounts for the bending angle ($k_\alpha = 1.8$ for $\alpha = 180°$ bends and $k_\alpha = 1.6$ for $\alpha = 90°$ bends).

19

Table 2.1: Comparison of code provisions for a 16-mm bar and without transverse reinforcement.

Type	EN 1992:1-1:2004	MC2010 and SIA262:2013	ACI-318-19
General bends	$15.4\varnothing$[1]	$15\varnothing$	$6\varnothing$
Hooks/Loops	$15.4\varnothing$[1]	$6\varnothing$	$6\varnothing$
Standard Hooks/Loops	$4\varnothing$	$6\varnothing$	$4\varnothing$[2]
Stirrups	$4\varnothing$	$4\varnothing$	$4\varnothing$[2]

[1] $f_{yd} = 435$ MPa; $f_{cd} = 20$ MPa; $c = 2\varnothing$

[2] used as transverse reinforcement and standard hooks for bars used to anchor

The previous Swedish code [Bov04] also provided a similar equation (adapted from an empirical equation according to [Joh00]):

$$\frac{\varnothing_{mand}}{\varnothing} = 2 \cdot \left(0.028 \cdot \frac{\sigma_s}{f_{ct}} - 0.5 - \frac{1}{\sin(\alpha / 2)}\left(\frac{c}{\varnothing} + \frac{1}{2}\right) \right) \quad \text{where} \quad \frac{c}{\varnothing} \leq 3.5 \tag{2.3}$$

Where f_{ct} is the concrete tensile strength. Unlike EN 1992-1-1:2004 (Eq. 2.1), this equation explicitly accounts for the bending angle α (which was also accounted for by means of coefficient k_α in Eq. 2.2).

2.3 Experimental programme

An experimental programme has been conducted in the Structural Concrete Laboratory of École Polytechnique Fédérale de Lausanne (Switzerland) to investigate the behaviour of bent bars and particularly the implications of spalling failures on the strength of such details. This programme is described in this Section.

2.3.1 Specimens

Two test series were performed. The first, named "TM", consisted of 41 specimens and looked at the performance of different bent reinforcement details. Figure 2.5a-c presents the geometry of the specimens (details are given in Table 2.2). The influence of following parameters was investigated:

- mandrel diameter $\varnothing_{mand}$ ($4\varnothing \leq \varnothing_{mand} \leq 25\varnothing$);
- concrete cover c ($0 \leq c \leq 2.5\varnothing$);

- bend angle α ($\alpha = 45°$, $90°$ and $180°$);

- distance l_{mand} between multiple bends ($0 \leq l_{mand} \leq 20Ø$);

- bar diameter $Ø$ ($Ø = 14$ and 20 mm); and

- position of the bar with respect to the casting direction (top and bottom bars).
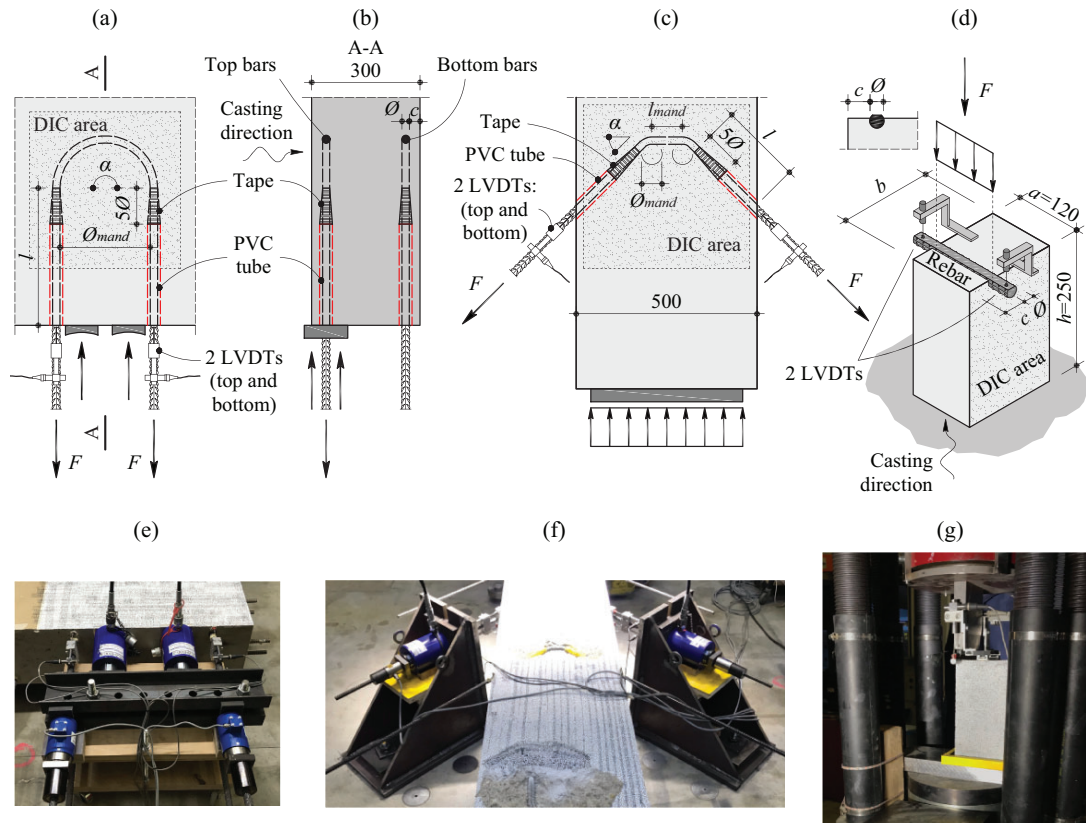
Figure 2.5: Geometry of specimens and test set-up: (a) loops with a bending angle of 180°; (b) cross section; (c) loops with a bending angle of 90° or 45°; (d) series CM, prisms with straight bars; (e) test for loops with a bending angle of 180°; (f) test for loops with a bending angle of 90° or 45°; and (g) test for series CM. Dimensions in [mm].

The second test series, named "CM", consisted of 24 specimens and was aimed at investigating the splitting resistance of concrete prisms subjected to a concentrated force transferred by a reinforcement bar (which could represent the deviation forces in a bent), see Figure 2.5d and Table 2.3. The following parameters were investigated in this series:

- concrete compressive strength f_c ($f_c \approx 34$ MPa and $f_c \approx 77$ MPa);

- concrete cover c ($0.5 \leq c \leq 3Ø$); and

- bar diameter $Ø$ ($Ø = 14$ and 20 mm).

Table 2.2:   Series TM: main parameters and experimental results (F_{max} refers to the maximum force in the reinforcement just before failure, σ_{sR} is the associated average steel stress and w_{max} is the associated maximum out-of-plane displacement measured at the free surface, for meaning of other parameters refer to Section Notation).

Spec.	α [°]	$\varnothing$ [mm]	Casting position	$\varnothing_{mand}/\varnothing$ [-]	$c/\varnothing$ [-]	$l_{mand}/\varnothing$ [-]	l [-]	f_c [MPa]	f_{ct} [MPa]	f_y [MPa]	F_{max} [kN]	σ_{sR}[1] [MPa]	w_{max} [mm]	Fail-ure[2]
TM01	180	20	Top	25	1.50	0	380	41.9	2.3	526	>172	>546	>0.09	-
TM02	180	20	Top	20	1.50	0	290	42.1	2.4	526	>176	>560	>0.11	-
TM03	180	20	Top	15	1.50	0	290	42.1	2.4	526	164	522	0.28	Sy
TM04	180	20	Top	10	1.50	0	280	42.1	2.4	526	144	457	0.36	S
TM05	180	20	Top	7	1.50	0	280	42.1	2.4	526	108	343	0.45	S
TM06	180	20	Top	4	1.50	0	280	42.1	2.4	526	87.7	279	0.42	S
TM11	180	20	Bottom	25	1.50	0	380	42.2	2.4	526	>172	>547	>0.09	-
TM12	180	20	Bottom	20	1.50	0	290	42.2	2.4	526	>165	>525	>0.08	-
TM13	180	20	Bottom	15	1.50	0	290	42.2	2.4	526	>172	>548	>0.17	-
TM14	180	20	Bottom	10	1.50	0	280	42.2	2.4	526	135	429	0.56	S
TM15	180	20	Bottom	7	1.50	0	280	42.2	2.4	526	111	353	0.13	S
TM16	180	20	Bottom	4	1.50	0	280	42.2	2.4	526	88.8	283	0.33	S
TM21	180	14	Top	25	2.36	0	380	42.5	2.5	522	>87.4	>568	>0.02	-
TM22	180	14	Top	20	2.36	0	380	42.5	2.5	522	>85.6	>556	>0.02	-
TM23	180	14	Top	15	2.36	0	380	42.5	2.5	522	>85.5	>555	>0.04	-
TM24	180	14	Top	10	2.36	0	280	42.5	2.5	522	>83.8	>544	>0.32	-
TM25	180	14	Top	7	2.36	0	280	42.5	2.5	522	68.9	448.0	0.40	S
TM26	180	14	Top	4	2.36	0	280	42.5	2.5	522	61.9	402.0	0.35	S
TM34	180	14	Bottom	10	2.36	0	280	42.5	2.5	522	>87.7	>570	>0.16	-
TM35	180	14	Bottom	7	2.36	0	280	42.5	2.5	522	76.2	495	0.20	S
TM36	180	14	Bottom	4	2.36	0	280	42.5	2.5	522	60.1	390	0.21	S
TM43	180	14	Top	15	1.50	0	230	35.9	2.3	522	>85.3	>554	>0.05	-
TM44	180	14	Top	10	1.50	0	230	36.1	2.3	522	67.8	440	0.21	S
TM45	180	14	Top	7	1.50	0	230	35.9	2.3	522	59.7	388	0.19	S
TM46	180	14	Top	4	1.50	0	230	36.1	2.3	522	41.6	270	0.26	S
TM51	180	14	Bottom	7	0.00	0	230	36.2	2.3	522	28.4	184	0.42	S
TM52	180	14	Bottom	7	0.50	0	230	36.2	2.3	522	44.9	292	0.33	S
TM53	180	14	Bottom	7	1.00	0	230	36.2	2.3	522	53.9	350	0.15	S
TM54	180	14	Bottom	7	2.00	0	230	36.1	2.3	522	67.9	441	0.34	S
TM55	180	14	Bottom	7	2.50	0	230	36.1	2.3	522	80.5	523	0.24	Sy
TM64	90	14	Top	10	1.50	0	270	34.1	2.1	522	85.5	555	0.28	Sy
TM65	90	14	Top	7	1.50	0	291	34.2	2.1	522	67.1	436	0.22	S
TM66	90	14	Top	4	1.50	0	312	34.6	2.1	522	50.7	329	0.22	S
TM71	45	14	Top	4	1.50	20	114	35.0	2.2	522	78.1	507	0.97	Sy
TM72	45	14	Top	4	1.50	12	193	34.7	2.2	522	80.6	524	0.24	Sy
TM73	45	14	Bottom	4	1.50	8	232	35.6	2.2	522	>87.7	>570	>0.46	-
TM74	45	14	Bottom	4	1.50	6	251	35.6	2.2	522	78.3	509	0.30	Sy
TM75	45	14	Bottom	4	1.50	4	272	35.6	2.2	522	86.4	561	0.39	Sy
TM76	45	14	Bottom	4	1.50	2	292	35.5	2.2	522	77	500	0.30	S
TM81	180	20	Top	4	1.50	0	280	38.4	2.5	526	82.9	264	0.26	S
TM82	180	20	Bottom	4	1.50	0	280	38.4	2.5	526	84.6	269	0.25	S

[1] $\sigma_{sR} = F_{max}/(\pi \cdot \varnothing^2/4)$

[2] Type of failure mode was determined based on the load-displacement curve

S = spalling before yielding of the reinforcement

Sy = spalling after yielding

- = refers to tests stopped after extensive yielding without spalling

Table 2.3:   Series CM: main parameters and experimental results (F_{max} refers to the maximum force in the reinforcement just before failure, $\sigma_{c,nomR} = F_{max}/(\varnothing \cdot a)$, for meaning of other parameters refer to Section Notation).

Specimen	$\varnothing$ [mm]	$c/\varnothing$ [-]	b [mm]	f_c [MPa]	f_{ct} [MPa]	F_{max} [kN]	$\sigma_{c,nomR}$ [MPa]
CM212	14	0.5	130	76.5	2.8	124	74.1
CM213	14	1	130	76.5	2.8	132	78.5
CM214	14	1.5	130	76.5	2.8	140	83.4
CM215	14	2	130	76.5	2.8	161	95.9
CM216	14	2.5	130	76.5	2.8	138	82.2
CM217	14	3	130	76.4	2.8	146	86.7
CM232	20	0.5	170	76.6	2.8	123	51.3
CM233	20	1	170	76.6	2.8	159	66.4
CM234	20	1.5	170	76.6	2.8	177	73.8
CM235	20	2	170	76.6	2.8	201	83.8
CM236	20	2.5	170	76.6	2.8	212	88.4
CM237	20	3	170	76.6	2.8	222	92.3
CM313	14	1	130	33.5	2.1	88.9	52.9
CM314	14	1.5	130	33.6	2.2	104	61.9
CM315	14	2	130	33.6	2.2	118	70.0
CM316	14	2.5	130	33.6	2.2	123	73.5
CM317	14	3	130	33.6	2.2	127	75.6
CM331	20	0	170	33.7	2.2	83.5	34.8
CM332	20	0.5	170	33.7	2.2	97.7	40.7
CM334	20	1.5	170	33.8	2.3	124	51.7
CM335	20	2	170	33.8	2.3	143	59.6
CM336	20	2.5	170	33.8	2.3	177	73.9
CM337	20	3	170	33.8	2.3	160	66.8

2.3.2   Material properties

For series TM, the specimens were cast from two batches with normal strength concrete (water-to-cement ratio of 0.65 and a cement content of 308 kg/m^3) and a maximum aggregate size of 16 mm (crushed aggregate). The cylinder compressive strength f_c at the time of testing (measured on $\varnothing$160×320 mm specimens) was 42 MPa on average for tests TM00-TM30 and

36 MPa on average for tests TM40-80, details in Table 2.2. For series CM, the specimens were cast from two batches with normal and high strength concrete with a maximum aggregate size of 16 mm (crushed aggregate). The compressive strength f_c at the time of testing was about 34 MPa for the normal concrete strength (series CM300, same concrete as for series TM) and 77 MPa for the high strength concrete (series CM200, water-to-cement ratio of 0.4 and a cement content of 375 kg/m^3), details in Table 2.3. Direct tension tests on cylinders 160×320 mm were also performed (f_{ct} values are reported in Tables 2.2 and 2.3).

Figure 2.6 shows the stress-strain curves for the two bar diameters used for both test series: 14 mm and 20 mm. The 14 mm bars (Figure 2.6a) were cold-worked with a yield strength of 522 MPa (determined at 0.2% residual strain), while the 20 mm bars (Figure 2.6b) were hot-rolled with a well-defined yield plateau and a yield strength f_y equal to 526 MPa. Figure 2.6c-e show the shape of the 14 mm bars and of the 20 mm bars. Figure 2.6c shows the rib position and the number of lugs (4 lugs for the 14 mm-diameter bar and 2 lugs for the 20 mm-diameter bar). For all tests, lugs have been positioned in the arrangement shown in Figure 2.6c (refer to bend detail).
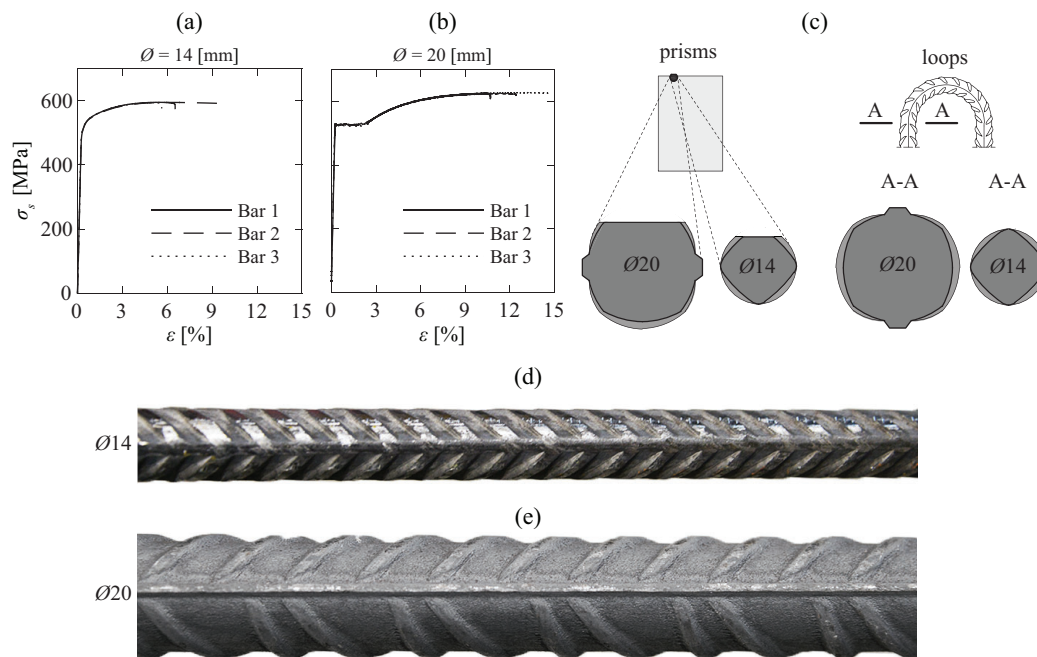
Figure 2.6:   Bar charateristics: (a) stress-strain curves for bars diameter 14 mm; (b) stress-strain curves for bars diameter 20 mm; (c) position of the lugs for series CM and TM; (d) picture of the bars diameter 14 mm; and (e) picture of the bars diameter 20 mm.

2.3.3   Test set-up

Three test set-ups were used:

- *TM series on U-loop bars with a bending angle of 180°* (Figures 2.5a and b). Two forces were applied at the ends of the bars by means of two synchronised jacks, whose reaction was applied to the concrete specimen. Bond between the straight segments of the bars and the concrete was prevented by means of PVC tubes and a tape allowing contact between the bar and the concrete to occur only along the bent part of the bars.

- *TM series on bars with a bending angle of 90° and 45°* (Figures 2.5b and c). The forces were applied at the ends of the reinforcement by means of two synchronised jacks clamped, together with the concrete block, to the strong floor of the laboratory. The introduction of the load in the reinforcement was performed by means of hinges, ensuring that no bending moments was transferred to the bar. Bond was again prevented in the outer straight parts of the bars, but not in the straight segment between inner bends in case of multiple bends (see Figure 2.5c).

- *CM series on prisms specimens* (Figure 2.5d). A Schenck Hydroplus servo-hydraulic testing machine was used to perform these tests. The force was introduced directly in the bars, whose top part was mechanically flattened to obtain a plane surface.

2.3.4   Measurements

For series TM, in addition to the forces measured with load cells and the relative slip measured between the bars and the concrete surface using LVDTs (Figure 2.5a-c), Digital Image Correlation (DIC) measurements were performed on the concrete surface. They allowed tracking the cracking pattern and the displacement field [Cav15, Cav17, Can20, Mat20], with a special focus on out-of-plane displacements. Two digital cameras Manta G504B (5 megapixels) were used. The speckles painted on the surface varied between 1 and 2 mm; the size of the pixels was between 0.152 mm and 0.255 mm. The acquisition rate of the cameras was 0.5 Hz in the initial steps of loading, increased to 5 Hz near failure. The VIC3D software was used to analyse the images [Cor10]. Pictures were taken before running the tests (at displacement equal to zero) and a measured noise (average between the maximum and minimum displacement values) was around 1/75 of a pixel for in-plane displacements and about 1/25 of a pixel for out-of-plane displacements. More details on the treatment of noise in DIC measurements can be found in [Mat20, Hae17].

For specimens TM81 and TM82, also Fibre-Optical Measurement (FOM) of the strains based on Rayleigh scattering was performed. The results have been post-processed using the software Odisi-B version by Luna Innovations [Lun13] based on Optical Frequency Domain Reflectometry. This technique allows obtaining a measurement of the strain profiles along the

bars with a high frequency and a low spatial resolution [Bra19, Bad21] (a gage pitch of 2.6 mm was chosen for specimen TM81 and of 0.65 mm for specimen TM82). Two optical fibres were glued on each bar: one inside, and one outside of the bend (blue and red lines respectively in Figure 2.7a). The 125-µm polyimide optical fibres were installed into two grooves of 1 mm depth along the bar (see Figure 2.7b, same fibre as [Can20, Mat20, Hae17]) and were fixed to the reinforcement with a bi-component glue (Figure 2.7b and c). More details on the technique (installation of fibres, acquisition and processing of data) are given in [Can20].
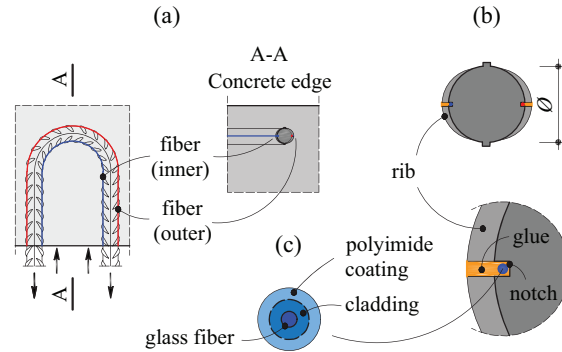
Figure 2.7:   Fibre-Optical Measurement: (a) position of the optical fibres on the bar; (b) detail of the position of the optical fibre glued to the reinforcement; and (c) optical fibre detail.

For series CM, the forces were also measured using load cells and the relative displacement between reinforcement bars and concrete was tracked using LVDTs (Figure 2.5d). DIC measurements were performed for this series on the concrete surface in a similar manner as for series TM (similar dimension of the pixels, image acquisition rate between 0.2 and 0.5 Hz).

2.3.5   Failure modes

The specimens of series TM failed in general by spalling of the concrete cover, see Figure 2.8a-e. This occurred either before yielding of the reinforcement (Failure mode "S" in Table 2.2) or after yielding (Failure mode "Sy"). Some tests however were stopped after extensive plastic deformations of the reinforcement without any visible spalling signs. For the tests failing by spalling, the extent of the spalled region seemed to be influenced by: (i) the concrete cover (Figure 2.8a), (ii) the mandrel diameter (Figure 2.8b), (iii) the bending angle (Figure 2.8c), (iv) the distance between bends (Figure 2.8d) and (v) the diameter of the bar (Figure 2.8e). According to the investigated tests, an increase of the concrete cover, of the bending angle and of the bar diameter led to an increase on the extent of the failure area. For series CM, all specimens failed by splitting, see Figure 2.8f.
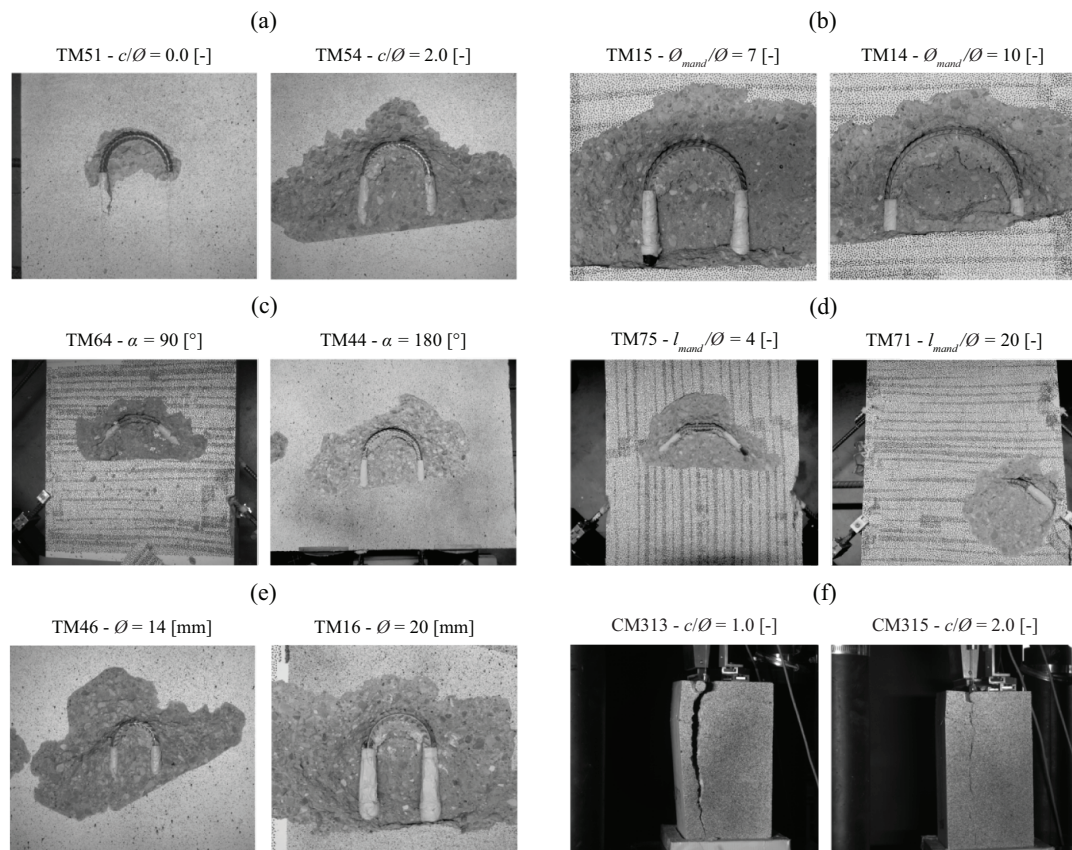
Figure 2.8: Pictures after failure and removal of loose concrete for selected specimens of series TM with varying: (a) concrete cover; (b) mandrel diameter; (c) bending angle; (d) distance between multiple bend; (e) bar diameter; and of series CM with varying (f) concrete cover.

2.3.6 Main experimental results of series TM

The main results for this series are shown in Figure 2.9 in terms of load-slip relationship, maximum steel stress and maximum out-of-plane displacement as a function of the main parameters (defined in Figure 2.10). The following observations can be made:

- *Influence of concrete cover c* (case of U-loops, $\emptyset = 14$ mm, $\emptyset_{mand} = 7\emptyset$ and $\alpha = 180°$, Figure 2.9a): an increase of the concrete cover led to an increase on the spalling strength. For the investigated parameters, only the specimen with a concrete cover equal to $2.5\emptyset$ showed a spalling failure after reinforcement yielding (during the hardening phase of the steel). In general, an increase of the concrete cover led to a decrease of the maximum out-of-plane displacement before failure (w_{max}).

- *Influence of mandrel diameter $\varnothing_{mand}$* (case of U-loops, $\varnothing = 14\text{-}20$ mm, $c = 1.5\varnothing$ and $\alpha = 180°$, Figure 2.9b): an increase of the mandrel diameter led to an increase of the spalling strength for a constant bar diameter. For the investigated parameters, specimens with a mandrel diameter $\varnothing_{mand} > 10\varnothing$ did not exhibit spalling failures before reinforcement yielding. An increase of the mandrel diameter led to a notable decrease of w_{max}. Figure 2.9b also shows the influence of the bar diameter for constant ratios $c/\varnothing$ and $\varnothing_{mand}/\varnothing$. In general, a moderate size effect can be observed with respect to the spalling resistance (slightly higher steel stresses for smaller bar diameters) but with a clear influence on the maximum out-of-plane displacement.

- *Influence of bending angle α* (case with $\varnothing = 14$ mm, $c = 1.5\varnothing$ and $\varnothing_{mand} = 4\varnothing$, Figure 2.9c): an increase of the bending angle α led to a significant reduction of the spalling strength, but had almost no influence on w_{max}.

- *Influence of the distance between multiple bends l_{mand}* (case with $\varnothing = 14$ mm, $c = 1.5\varnothing$, $\varnothing_{mand} = 4\varnothing$ and $\alpha = 45°$, Figure 2.9d): even a small distance between multiple bends is sufficient to increase the spalling strength (yielding of the bars was attained for values of l_{mand} larger than 2 diameters, compared to a ratio $\sigma_{sR}/f_y = 0.63$ for a specimen with $l_{mand} = 0$).

- *Influence of the casting direction* (case of U-loops, $\varnothing = 14\text{-}20$ mm, $c = 1.5\varnothing\text{-}2.36\varnothing$, $\varnothing_{mand} = 4\varnothing$ to $25\varnothing$ and $\alpha = 180°$, Table 2.2): the casting direction (perpendicular to the bending plane, refer to Figure 2.5) had no influence on the spalling strength. The observed response is different from the bond behaviour of straight deformed reinforcement and spalling due to internal pressure, where cracks due to settlement of fresh concrete and the increase in porosity due to bleeding can lead to a reduction of the spalling strength for straight top bars [Moc21, Moc21a]. With respect to the out-of-plane displacement before failure w_{max}, the bottom bars exhibited in general a lower maximum value particularly for larger concrete covers (Table 2.2).
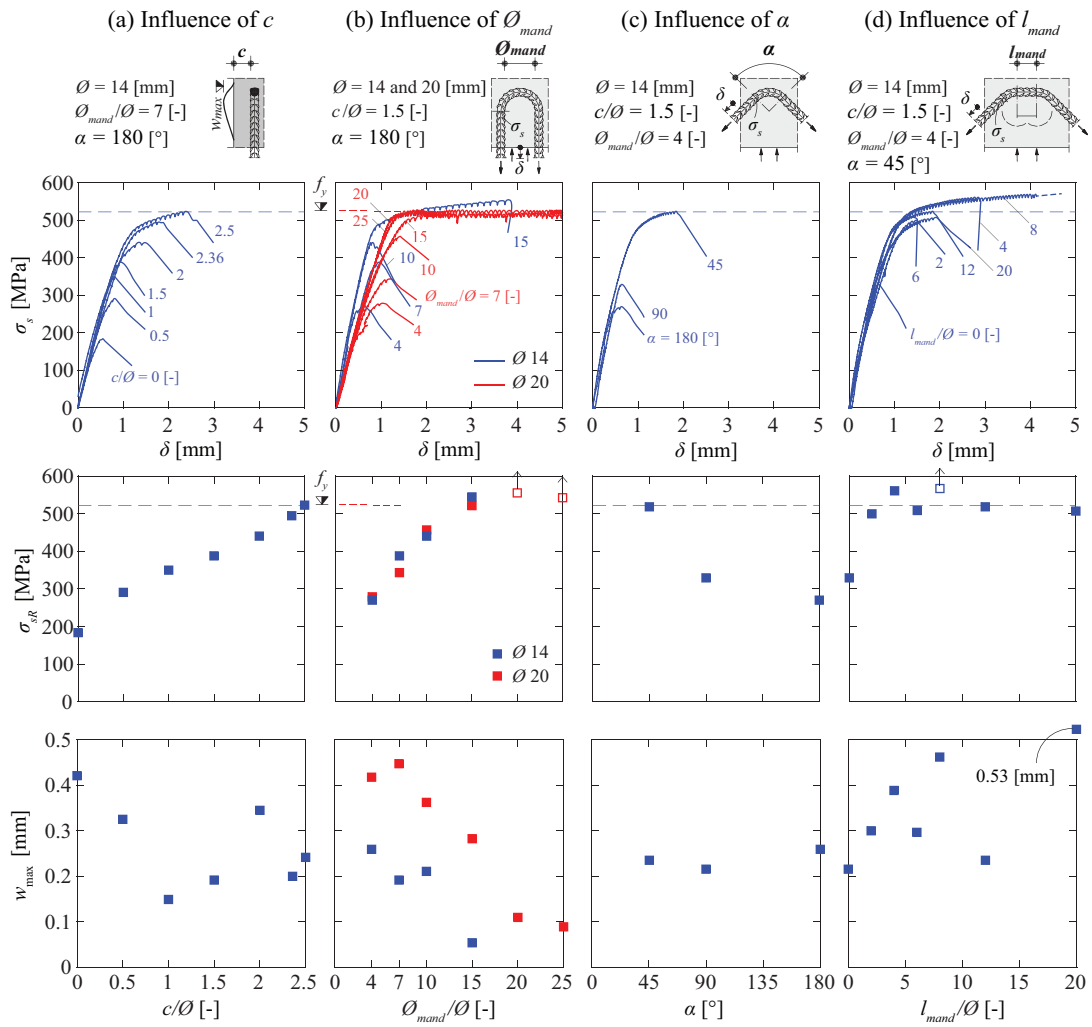
Figure 2.9: Reinforcement stress-slip relationships and influence of the main parameters on the reinforcement stress σ_s as well as the maximum out-of-plane displacement w_{max}: (a) concrete cover; (b) mandrel diameter; (c) bending angle; and (d) distance between multiple bends (empty markers with arrows indicate tests stopped after yielding without spalling; δ is the displacement of the point P defined in Figure 2.10 measured in the direction of the bar with respect to the concrete surface).
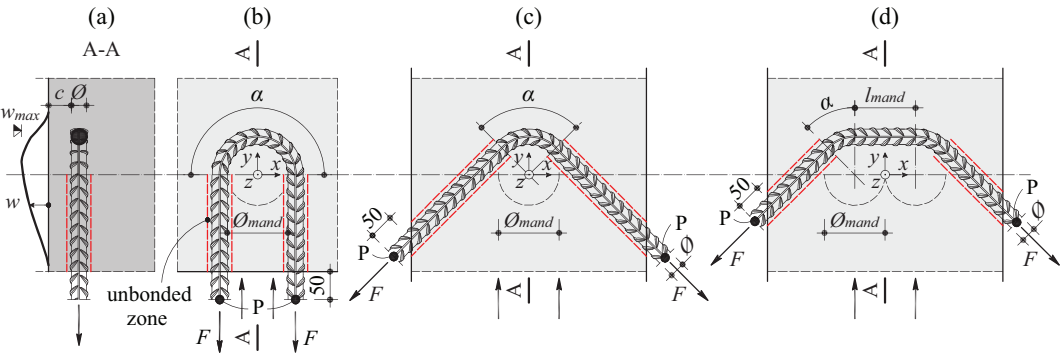
Figure 2.10:   Main parameters: (a) concrete cover; (b) mandrel diameter; (c) bending angle; and (d) distance between multiple bends (points P refers to the location where the displacement δ represented in Figure 2.9 is measured, dimensions in [mm]).

Figure 2.11 gives details on the out-of-plane displacements (w at failure, see Figure 2.10 for definitions) where all dimensions of the plots are normalized to the mandrel diameter. As already observed in Figure 2.8, the area influenced by spalling increases for larger concrete covers, for smaller mandrel diameters, for larger bending angles and for increasing distance between multiple bends. It is also interesting to note that the area influenced by spalling mainly develops on the inner side of the bend.

With respect to multiple bends, Figure 2.11d shows that two cases can govern the response. In the first case, when the distance between two bends is small ($l_{mand} < 6\emptyset$), the out-of-plane displacements w are comparable to those of a single bend with an angle of 90° (spalling region extending between the two bends). In the second case, when the distance between bends is larger, the out-of-plane displacements develop independently near to the bends.

Cross sections showing the distribution of out-of-plane deformations (w) for selected load levels (60, 80, 90, 95, 98 and 100% of the maximum load) are also shown in Figure 2.11. Before 60% of maximum load, almost no out-of-plane deformation occurred. The deformations develop thereafter rapidly, and more than half of the final out-of-plane displacement developed between 90 and 100% of maximum load.
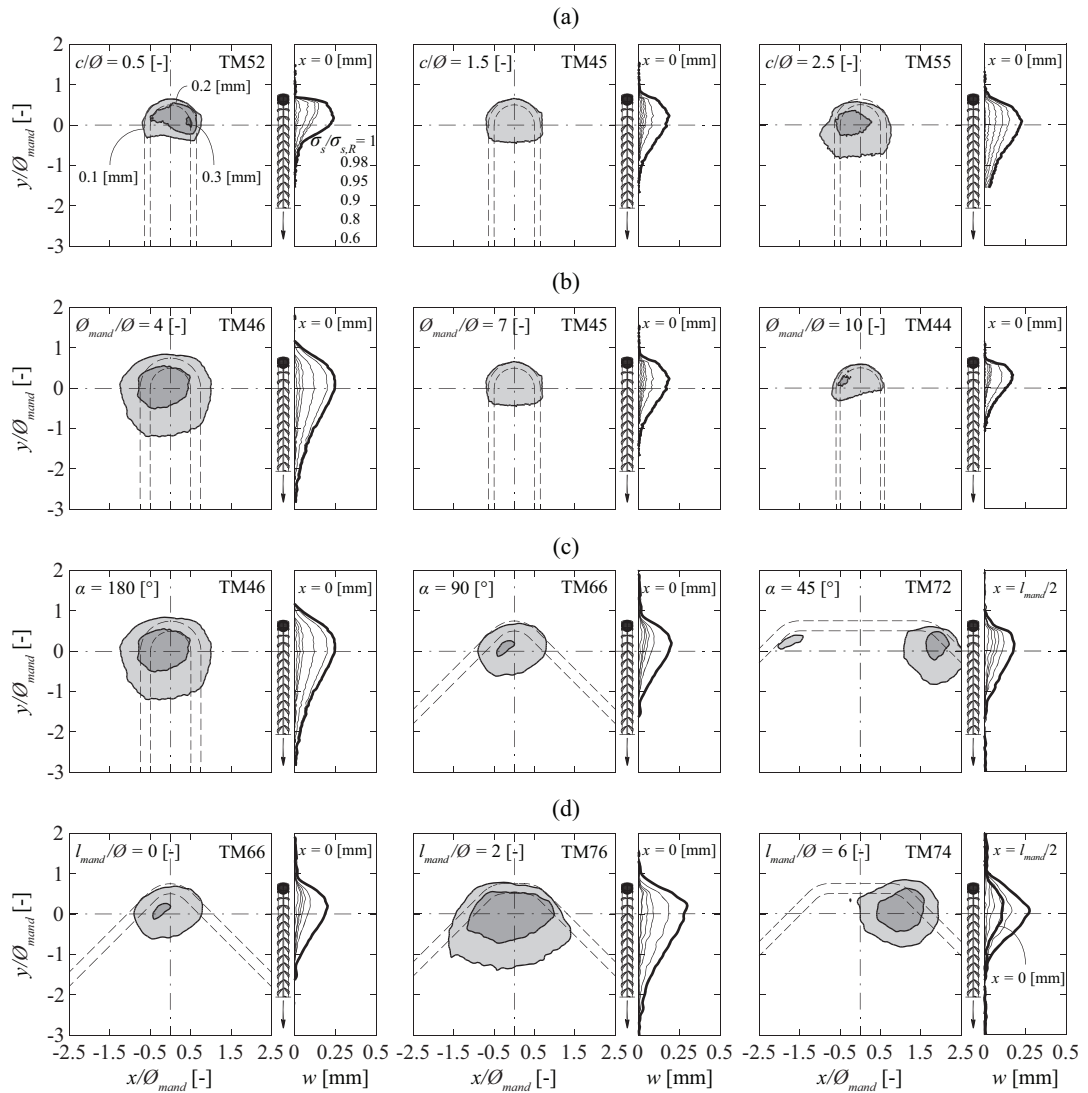
Figure 2.11:   Contour lines of the out-of-plane displacement just before maximum load
and sections with out-of-plane displacement at the mandrel axis for
different load levels: (a) influence of concrete cover (cases with $\alpha = 180°$,
$\varnothing_{mand} = 7\varnothing$ and $\varnothing = 14$ mm); (b) influence of the mandrel diameter (cases
with $\alpha = 180°$, $c = 1.5\varnothing$ and $\varnothing = 14$ mm); (c) influence of the bending angle
(cases with $c = 1.5\varnothing$, $\varnothing_{mand} = 4\varnothing$ and $\varnothing = 14$ mm); and (d) influence of the
distance between multiple bends (cases with $\alpha = 45°$, $c = 1.5\varnothing$, $\varnothing_{mand} = 4\varnothing$
and $\varnothing = 14$ mm).

Figure 2.12 shows the results of the strain measurements using fibre optics for test TM82 (selected load levels: 60, 70, 80, 90 and 100% of the maximum load). An identical test (TM81, not represented) provided comparable strain measurements.
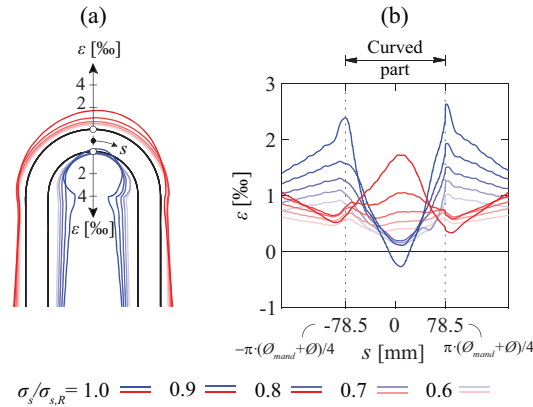
Figure 2.12:   Bar strain profiles at different load levels for test TM82: (a) plan view; and (b) strain profiles along the bar axis (outer fibres in red, inner fibres in blue).

The response shows a difference between the outer and inner strains in the bent region and significant variations along the curved part which indicate potential bending of the bar. This is clearly confirmed by the measurements on the inner fibre of specimen TM82, when compressive strains are present at mid-bend despite the fact that the bar was subjected to a tensile force. At the ends of the bend, small peaks of strain can also be observed, which can be attributed to the local change of geometry of the bar (peaks increasing for increasing levels of load). In the straight parts of the bar, the deformations are slightly different between the outer and the inner fibre, indicating that this region is subjected to some level of bending.

2.3.7   Main experimental results of series CM

The main results of series CM are presented in Figure 2.13, where the nominal stress $\sigma_{c,nom}$ (obtained by dividing the applied force F by the bar diameter $\varnothing$ and the contact length a, Figures 2.5d and 2.13), is normalized by the compressive strength of concrete f_c and is represented as a function of the penetration of the bar in the concrete u and of the splitting crack opening w (measured at a distance $2\varnothing$ from the bottom surface of the reinforcement bar).

An increase of the concrete cover leads to an increase of the strength, but to a decrease of the bar penetration (u) and out-of-plane displacement (associated to the splitting crack opening w) at maximum load. With respect to the influence of the concrete strength, the comparisons of Figures 2.13e and f show that the strength does not increase proportionally with the concrete compressive strength (lower normalized resistances for increased concrete strength). This effect can be due to the larger brittleness of higher strength concrete and to the fact that the resistance in case of splitting failures is also related to the concrete tensile strength (see also [Moc20]).

Finally, with respect to the size effect, an increase of the bar diameter clearly leads to a reduction of the splitting resistance, but it is associated to an increase of the penetration u and of the crack opening w just before failure, refer to Figures 2.13e-f for the resistance and to Figures 2.13a-d for the penetration and crack opening. Concerning the load-penetration curves (Figures 2.13a-d), a stiff initial response is observed until the peak load, with a penetration u at maximum load ranging generally between 0.05 mm and 0.15 mm. After reaching the peak load, a small plateau can be observed in most cases, followed by a softening response (decreasing force with increasing penetration).
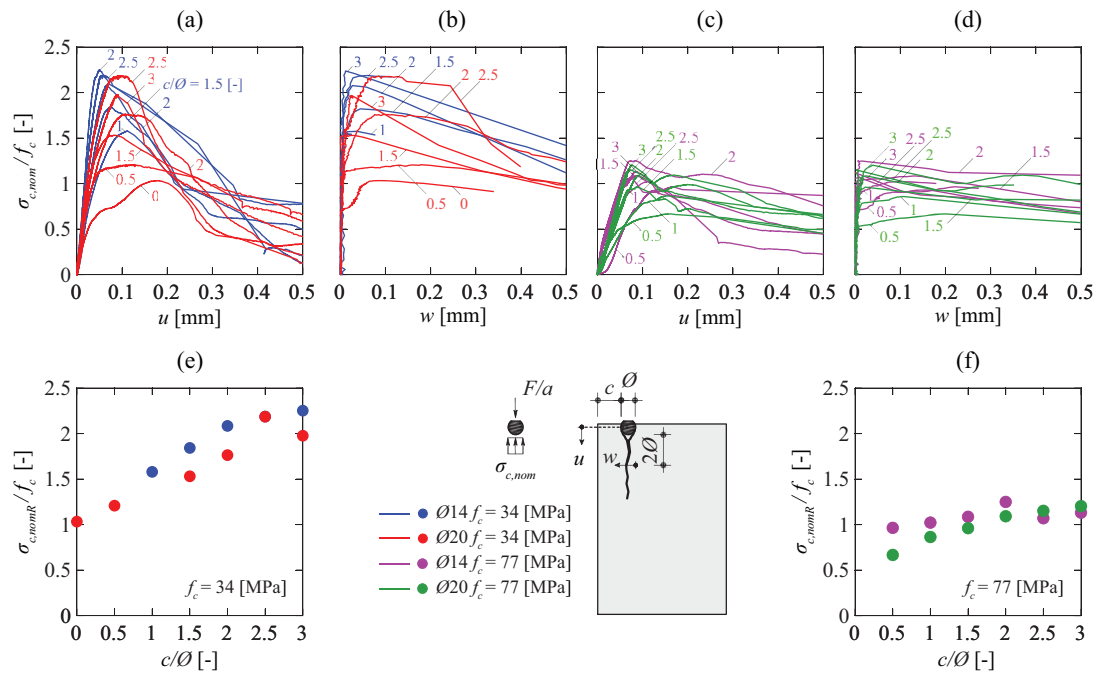
Figure 2.13: Normalized resistance as a function of the penetration u of the reinforcement and of the crack opening w: (a, b and e) normal strength concrete f_c = 34 MPa; and (c, d and f) high-strength concrete f_c = 77 MPa.

2.4 Analysis of test results

Traditionally, the mechanical response of bent details (Figure 2.1a-d) has been approached in a simplified manner, by assuming a constant force in the reinforcement whose deviation forces are in equilibrium with a uniform pressure developed in the concrete (Figure 2.14a):

$$p_{nom} = \frac{2F}{\varnothing_{mand}}$$

(2.4)

However, this does not entirely correspond to the observations performed with FOM for series TM, which show a more complex interaction between the bar and the surrounding concrete. According to strain measurement presented in Figure 2.12, the bar is also subjected to bending and transfer of forces by bond in its curved part.

2.4.1   Contact forces between reinforcement and concrete

Based on the strain measurements performed by FOM, it is possible to estimate the internal forces in the reinforcement as well as the concrete pressure on the bar surface. To that aim, it should be noted that the assumption that plane sections remain plane leads to a nonlinear distribution of strains. This fact was acknowledged by Winkler [Win58] and Bach [Bac89] and its effects are particularly relevant for small mandrel diameters. Detailed consideration of the curvature of the bar and its effect on the calculation of the strain and stress profiles and internal forces of the bar are given in Appendix 2.A. Based on equilibrium conditions, deviation and bond forces can also be calculated. The results of this methodology are shown in Figure 2.14 for specimen TM82.

The resultant of forces considering contact pressures (distribution shown in Figure 2.14h, normalized by the concrete compressive strength f_c and considering the brittleness of concrete by the factor $\eta_{fc} = (30/f_c \text{ [MPa]})^{1/3} \leq 1$ [FIB11, Moc20, Mut90]) and bond stresses (distribution shown in Figure 2.14f) are shown in Figure 2.14c (integrated over 30° sections). As shown in Figure 2.14g, the angle between the resultant and the bar axis varies between roughly 45° close to the beginning of the bend and 90° in the middle. This response, somewhat different to the one traditionally assumed to study this detail (with forces normal to the bar axis, see Figure 2.14a) is due to a significant mobilisation of bond stresses. During the loading process, the variation of the angle (which becomes increasingly more perpendicular to the bar axis) is explained due to the fact that bond stresses increase less than the contact pressure (Figure 2.14f compared to 2.14h). Simultaneously, significant bending moments develop in the bar, increasing the strains and stresses in the outer fibre of the bent (refer to Figure 2.12).

Figure 2.14d shows the deflections of the bar at failure calculated on the basis of measured strains by the FOM and the corresponding slip of the bar. The displacement is mainly in the *y*-direction with a bar penetration of about 0.4 mm at maximum load.

For larger mandrel diameters, the activation of bond stresses leads to a reduction of the force in the middle region of the bend. As a consequence, failure should occur close to the ends of the bends, which is consistent with the experimental results, see Figure 2.14i-j.
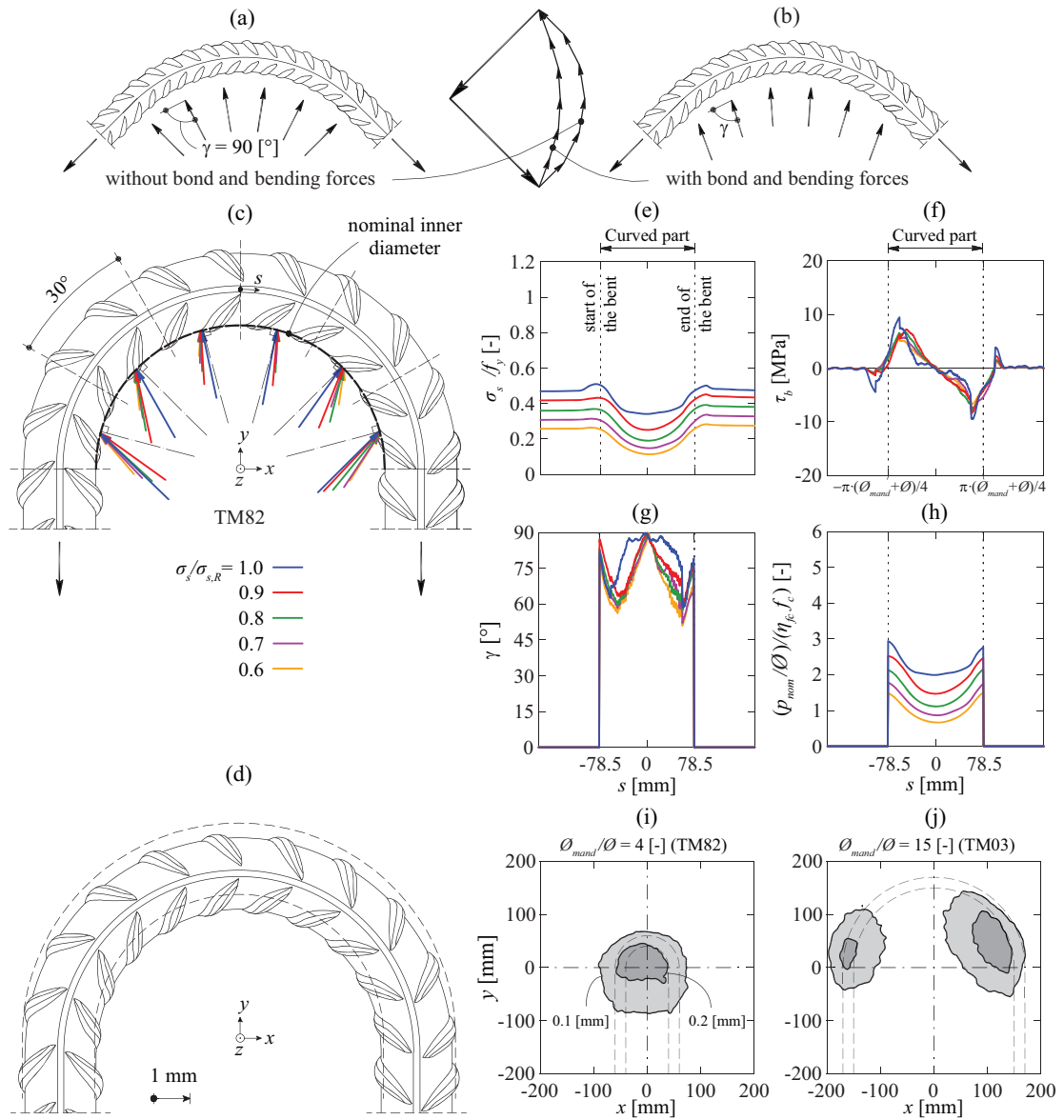
Figure 2.14:   Mechanical response of bent detail: (a) ideal response assuming no bond; (b) actual response assuming bond transfer; (c) calculated forces for test TM82 at different load steps (60, 70, 80, 90 and 100% of the maximum load, sketch of ribs corresponding to their actual arrangement); (d) calculated deformation of the bar; (e) calculated average axial stresses; (f) calculated bond stress; (g) angle of the contact forces with respect to the bar axis; (h) nominal contact concrete stress along the curvilinear abscissa at different load steps (60, 70 80, 90 and 100% of the maximum load); contour lines of the out-of-plane deformation at failure; (i) for small mandrel diameter (test TM82 with $Ø_{mand} = 4Ø$); and (j) for large mandrel diameter (test TM03 with $Ø_{mand} = 15Ø$).

2.4.2   Spalling strength

The development of contact forces due to the geometry of the bend can lead to the development of a splitting crack leading eventually to spalling when the bar is close to a free surface. In the following, a nominal concrete contact stress ($\sigma_{c,nom}$) is adopted to investigate the conditions to develop such failures. This contact stress is calculated as the pressure required to equilibrate over a bar diameter the deviation forces according to Figure 2.15a (nominal contact pressure not accounting for bond transfer and for flexure in the bar):

$$\sigma_{c,nom} = \frac{p_{nom}}{\varnothing} = \frac{\pi}{4} \cdot \varnothing^2 \cdot \sigma_s \cdot \frac{2}{\varnothing \cdot \varnothing_{mand}} = \frac{\pi}{2} \cdot \frac{\varnothing}{\varnothing_{mand}} \cdot \sigma_s \tag{2.5}$$

where σ_s is the tensile stress in the bar at the ends/starts of the bend.
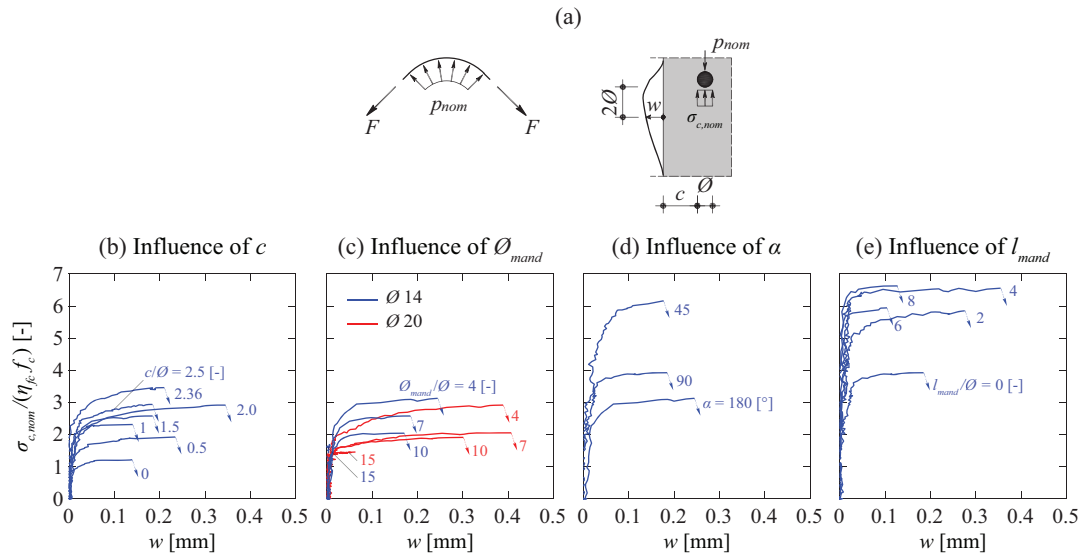
Figure 2.15:   Nominal concrete contact pressure versus out-of-plane displacement: (a) definitions and notation; (b) influence of concrete cover (cases with $\alpha = 180°$, $\varnothing_{mand} = 7\varnothing$ and $\varnothing = 14$ mm); (c) influence of mandrel diameter (cases with $\alpha = 180°$, $c = 1.5\varnothing$ and $\varnothing = 14$ mm); (d) influence of bending angle (cases with $c = 1.5\varnothing$, $\varnothing_{mand} = 4\varnothing$ and $\varnothing = 14$ mm, for test with $\alpha = 45°$ the measure of w is determined at $x = l_{mand}/2$); and (e) influence of distance between multiple bends (cases with $\alpha = 45°$, $c = 1.5\varnothing$, $\varnothing_{mand} = 4\varnothing$ and $\varnothing = 14$ mm).

The concrete stress for $\sigma_{c,nom}$ normalized by the concrete compressive strength f_c and considering the brittleness of concrete by the factor η_{fc} is shown in Figure 2.15 as a function of the out-of-plane displacement measured at the axis of symmetry of the bend at a distance equal to $2\emptyset$ from the inner side of the bar (Figures 2.10 and 2.15a). These plots show consistently two regimes of behaviour: the first one is characterized by almost no out-of-plane displacement whereas the second presents a significant increase of the out-of-plane displacement, indicating the initiation of spalling of the concrete cover.

As shown in Figure 2.15b-e, the maximum nominal contact stress can be significantly larger than the uniaxial concrete compressive strength $f_c \cdot \eta_{fc}$, which is in agreement with experimental evidences and conclusions of other authors for comparable situations [Swa69, Bal72, Tay76, Sco94]. This effect is particularly relevant for lower values of the bending angle α [Str81, Str83, Joh01, Joh00]. The maximum out-of-plane displacement w just before failure remains generally between 0.1 and 0.4 mm, with larger values generally observed for decreasing $\emptyset_{mand}/\emptyset$ and increasing $c/\emptyset$.
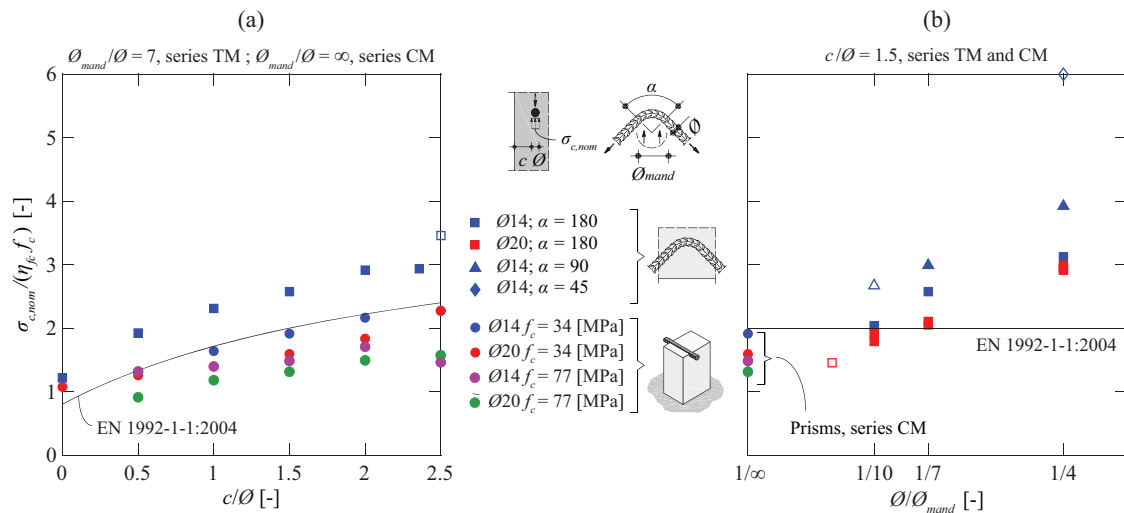
Figure 2.16:   Maximum nominal concrete contact pressure as a function of: (a) the concrete cover; and (b) the mandrel diameter and the bending angle (empty markers indicate tests stopped after yielding without spalling).

Figure 2.15 can be compared to the results of the CM series for normal strength concrete (Figure 2.13b). While the CM series represents a lower bound of the spalling/splitting strength because no redistribution of stresses is possible, series CM reproduces the situation without concrete at the outer side of the bend (observed to contribute to the spalling phenomenon as shown by the contour lines in Figure 2.11). This can be clearly appreciated in Figure 2.16, where the nominal concrete compressive stress is plotted as a function of the concrete cover, mandrel diameter and bending angle for series TM and CM (assumed to correspond to the case of an infinite mandrel diameter, $\emptyset/\emptyset_{mand} = 1/\infty = 0$ in Figure 2.16b). The results show a clear correlation between the concrete cover and the maximum developed contact stress, both for series TM and CM, with increasing values of $\sigma_{c,nom}$ for increasing values of the cover. This is due to the fact that an increase in the cover allows for an enhanced confinement of the region in contact with the bar (when the cover is null, the strength is approximately equal to $f_c \eta_{fc}$). A size effect can also be observed both for bent and straight bars, leading to a decrease of $\sigma_{c,nom}$ for increasing bar sizes. This observation is in agreement with other experimental evidences [Wäs34, Wäs35, Wäs36, Mar51, Sor87]. The concrete strength also plays a role in series CM when the splitting strength of the element is normalized by the compressive strength of concrete (as already shown in Section 2.3.7, Figures 2.13e and f).

The prediction of the EN 1992-1-1:2004 (Eq. 2.5 where σ_s is calculated according to Eq. 2.1) [Eur04] is also shown in Figure 2.16. The influence of the concrete cover is fairly well captured by EN 1992- 1-1:2004, while the influence of the mandrel diameter and especially the bending angle are not suitably accounted for.

2.4.3   Failure mechanism in spalling failures

The mechanism governing spalling failures of bent reinforcement is presented in the following. This mechanism is sketched in Figure 2.17a, where the spalling failure is assumed to be related to the penetration of a concrete wedge developing inside of the bend [Stu90, Sor87, Bac11], see Figure 2.17b, f and Figure 2.14d. This wedge is confined by the tensile resistance of the surrounding concrete (see Figure 2.17c-d) and can thus develop stresses larger than the uniaxial compressive strength [Nie11]. When the wedge penetrates into the concrete, it creates a splitting crack, with an opening which can be assumed to be equal to the out-of-plane displacement w measured on the surface, see Figure 2.17a.
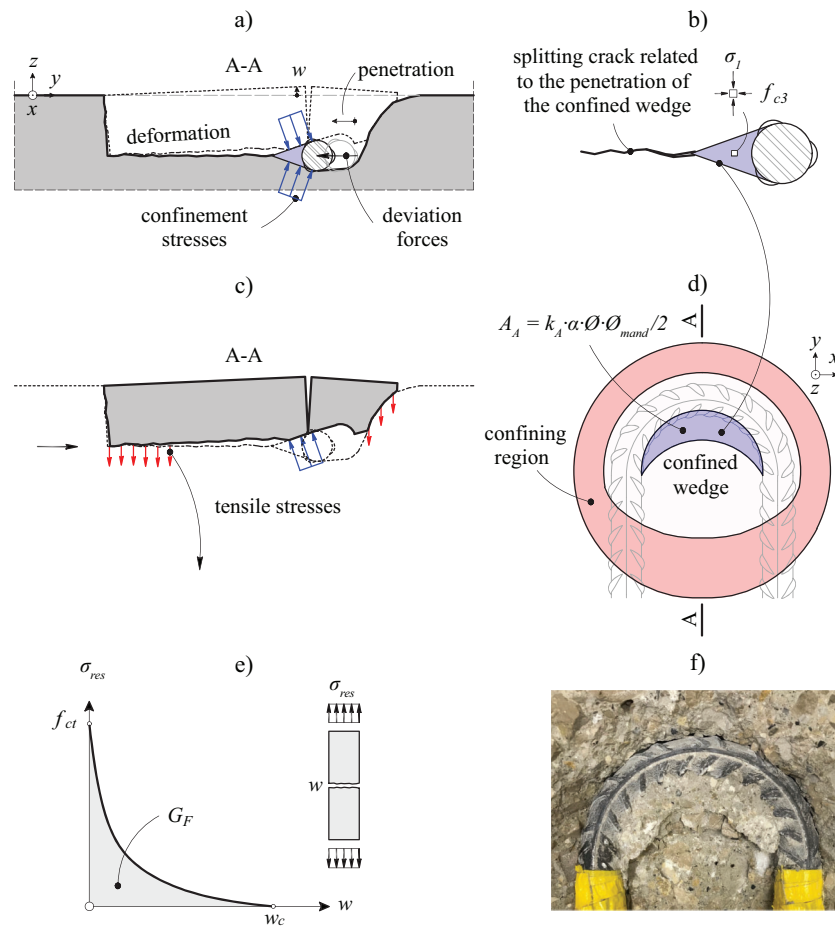
Figure 2.17:   Mechanism of spalling failure: (a) concrete wedge, cover and kinematics; (b) concrete wedge shape; (c) equilibrium of forces; (d) confined wedge and confining region; (e) softening behaviour of cracked concrete; and (f) picture of the concrete wedge observed in test TM16 after cover removal.

As shown in Figure 2.17c-d, the confinement pressure is in equilibrium with the tensile stresses of the concrete in the confining region. These tensile stresses (σ_{res}) are generally lower than the tensile strength of concrete (f_{ct}) and depend upon the local opening of the splitting crack in the fracture process zone (see Figure 2.17e) [Hil83]. A detailed analysis of the tensile stresses calculated according to the formulation of Hordijk [Hor92] (σ_{res} as a function of the crack opening) is presented in Appendix 2.B. Its results, calculated on the basis of the out-of-plane displacements measured during the tests are presented in Figure 2.18, with the distribution of σ_{res} on the axes of symmetry ($x = 0$) at maximum load. In these figures, the value of σ_{res} is normalized by the tensile concrete strength f_{ct} and the dimensions (x and y) are normalized by the mandrel diameter. The following observations can be performed:

- *Influence of concrete cover c* (case of U-loops, $\varnothing$ = 14 mm, $\varnothing_{mand}$ = 7$\varnothing$ and α = 180°, Figure 2.18a): The concrete cover plays a significant role on the extent of the spalled region and thus on the confining region where the residual tensile stresses potentially develop. Larger concrete covers are associated with larger areas subjected to spalling. For larger covers, larger and more uniform residual tensile stresses develop at failure. This influences contribute to the level of confinement of the wedge and the resistance to spalling.

- *Influence of mandrel diameter $\varnothing_{mand}$* (case of U-loops, $\varnothing$ = 14-20 mm, c = 1.5$\varnothing$ and α = 180°, Figure 2.18b): Again, the bending diameter significantly influences the extent of the confining region. In relative terms, larger areas can be observed for smaller bending diameters and, consequently, larger confinement stresses can be attained.

- *Influence of bar diameter* (case of U-loops, $\varnothing$ = 14-20 mm, c = 1.5$\varnothing$ and α = 180°, Figure 2.18b-e): An increase of the bar diameter leads to an increase of the width of the splitting crack and thus to a decrease of the average value of σ_{res}. For the performed tests, some regions around the centre of the mandrel show no residual tensile strength for 20-mm diameter bars (white region in Figure 2.18e). This is due to the larger crack openings for larger bar diameters (Figures 2.9 and 2.15) and justifies the observed size effect of bars, with lower confinement forces (and thus spalling resistance) for larger bar diameters.

- *Influence of bending angle α* (case with $\varnothing$ = 14 mm, c = 1.5$\varnothing$ and $\varnothing_{mand}$ = 4$\varnothing$, Figure 2.18c): The confining area shows some level of dependency on the bending angle, with larger bending angles associated to larger confining regions.

- *Influence of the distance between multiple bends l_{mand}* (case with $\varnothing$ = 14 mm, c = 1.5$\varnothing$, $\varnothing_{mand}$ = 4$\varnothing$ and α = 45°, Figure 2.18d): An increase of the distance between multiple bends seems to increase the extent of the confining region. For small distances, the straight segment between bends also contributes to develop out-of-plane confinement forces, and thus enhances the spalling resistance. When the bends are sufficiently spaced, the size of confining does not increase with the distance l_{mand}.
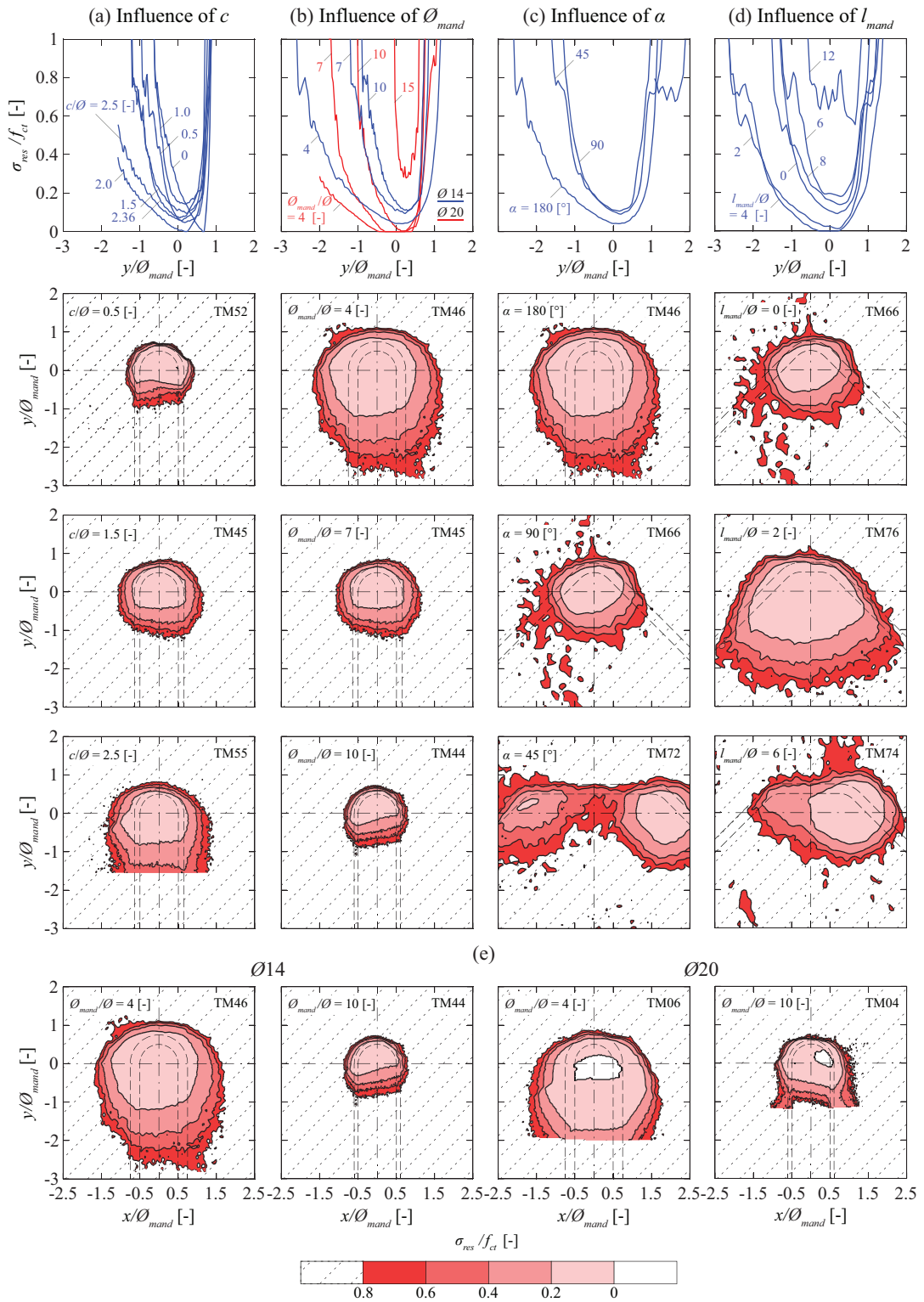
Figure 2.18:   Distribution of residual stresses along the axes of symmetry and contour
                lines of the residual tensile stress at maximum load: (a) influence of the

concrete cover; (b) influence of the mandrel diameter; (c) influence of the bending angle; (d) influence of the distance between multiple bends; and (e) influence of the bar diameter (size effect) (where the crack opening used to calculate the residual stresses is assumed to be equal to the out-of-plane displacement w measured on the surface).

On the basis of the out-of-plane forces calculated by integration of the residual tensile stresses (F_{res}, Eq. 2.B.4 in Appendix 2.B), the confinement stresses of the wedge σ_1 can be estimated as:

$$\sigma_1 = \frac{F_{res}}{A_A} = \frac{F_{res}}{k_A \cdot \alpha / 2 \cdot \varnothing \cdot \varnothing_{mand}} \tag{2.6}$$

where A_A is the projected area of the wedge (plane of splitting crack, see Figure 2.17d) and k_A is a factor accounting for the shape of the wedge. In this expression, the potential forces at the boundaries of the region affected by the splitting crack are neglected. The shape of the confined wedge is complex to define. In the following, it will be considered that the length of the wedge area is related to the mandrel diameter times the angle of the bend, while its average width is proportional to the diameter of the bar. The tri-axial compressive strength of the wedge f_{c3} can be calculated as [Ric28]:

$$f_{c3} = \eta_{fc} \cdot f_c + 4\sigma_1 \tag{2.7}$$

where η_{fc} is the material brittleness factor [Moc20] and the coefficient 4 corresponds to the enhancement of the compressive strength due to confinement stresses considering an internal friction angle for the concrete $\varphi = 37°$ ($4 \approx (1 + \sin\varphi)/(1 - \sin\varphi)$) [Nie11]. The results of this analysis (assuming a simplified value $k_A = 1$), are shown in Figure 2.19 for the tests where the DIC measurements allow calculating the confining stress in the complete area affected by the splitting crack (where out-of-plane displacement have been measured on the surface). This Figure can be compared to the results of Figure 2.16, where the contact pressure at the wedge was derived on the basis of stresses in the reinforcement. The plots show a fine agreement, both in terms of trends and absolute values, confirming the consistency of the failure mechanism shown in Figure 2.17.

The governing parameters of the confining force (F_{res}) can be identified from the calculated confinement stress (σ_1) and the resulting tri-axial strength (f_{c3}). As shown in Figure 2.19, this force is shown to be dependent on some geometrical parameters as the concrete cover, the mandrel diameter and the bending angle (in addition to other effects previously discussed). Consequently, the confining area (see Figures 2.17d and 2.18) also depends on these geometrical parameters.
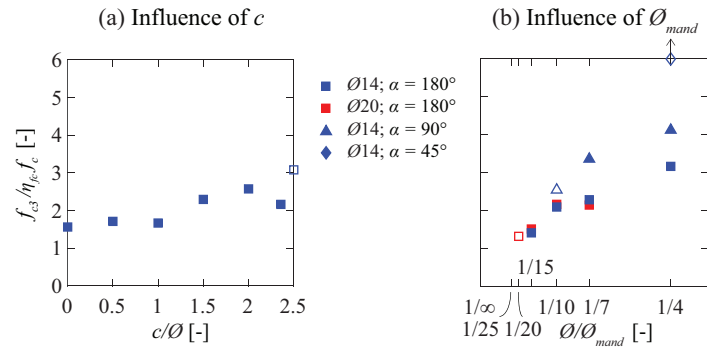
Figure 2.19:   Tri-axial concrete compressive strength calculated on the basis of the out-of-plane displacement by integration of the residual tensile stresses at maximum load: (a) influence of the concrete cover and (b) influence of the mandrel diameter (empty markers refer to tests stopped after yielding without spalling).

2.5   A mechanical model for the resistance of bent reinforcement in case of spalling failures

2.5.1   Assumed mechanism at failure and spalling resistance

On the basis of the observations from the experimental programme, a mechanical model to predict the spalling resistance of bent reinforcement was developed. It will be discussed in the following, considering a simplified geometry of the confining area and including the tri-axial strength increase in the wedge described previously, see Figure 2.20.

As previously discussed, the deviation forces induced by the reinforcement force F are equilibrated by the stresses developing in a confined wedge (Figure 2.20a and b). The strength of the wedge is a function of the confining stresses related to residual tensile strength in the area affected by the splitting crack (refer to Figure 2.20c and to Eq. 2.7).

As a simplification for a design model (consistently with the test observations), the area developing confining stresses is considered as subject to a constant tensile stress acting on a reduced area depending on the width of the splitting crack. The following geometrical parameters are needed (see Figure 2.20a and b):

- Confined area (A_A), where the confinement stresses (σ_1) apply uniformly;

- Confining area (composed of areas A_B and A_C). In this area, the tensile stresses are also assumed to develop in a uniform manner (with an effective tensile strength $f_{ct,eff}$).
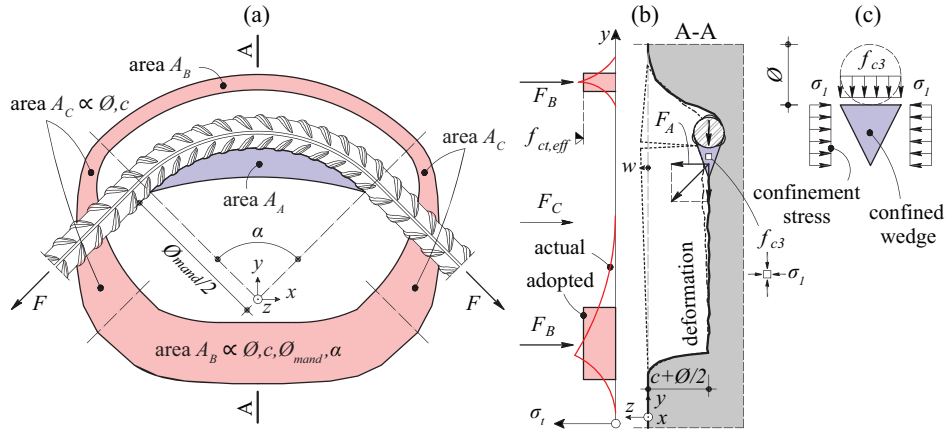
Figure 2.20: Mechanical model: (a) plan view with spalled areas and considered areas in tension; (b) detail of stresses and forces; and (c) detail of the concrete wedge with the confinement stresses.

The confined area is defined in Eq. (2.6) ($A_A = k_A \cdot \alpha \cdot \varnothing_{mand} \cdot \varnothing/2$). With respect to the confining area, it is assumed to be composed of two different regions. The region B in front and behind the bend (A_B, Figure 2.20a) depends on the geometry of the bend (mandrel diameter and angle, associated to the length of the region) as well as on the concrete cover and bar diameter (associated to the width of the region). The lateral region C (A_C) roughly depends on the diameter of the bar and concrete cover (Figure 2.20a). In a simplified manner, these areas can be evaluated according as follows:

$$A_B = k_B \cdot \varnothing^2 \cdot \frac{\alpha}{2} \cdot \frac{\varnothing_{mand}}{\varnothing} \cdot \left(\frac{c}{\varnothing} + \frac{1}{2} \right)$$

$$A_C = k_C \cdot \varnothing^2 \cdot \left(\frac{c}{\varnothing} + \frac{1}{2} \right)$$

(2.8)

The equilibrium of the out-of-plane forces leads to:

$$\sigma_1 = \frac{f_{ct,eff} \cdot (A_B + A_C)}{A_A}$$

(2.9)

By introducing the pertinent values of the areas, the confinement pressure is given:

$$\sigma_1 = f_{ct,eff} \cdot \left(\frac{c}{\varnothing} + \frac{1}{2} \right) \cdot \left(\frac{k_B}{k_A} + \frac{k_C}{k_A} \frac{2}{\alpha} \frac{\varnothing}{\varnothing_{mand}} \right)$$

(2.10)

and thus, the confined resistance of concrete can be determined from Eq. (2.7) as:

$$f_{c3} = \eta_{fc} \cdot f_c + 4 f_{ct,eff} \cdot \left(\frac{c}{\varnothing} + \frac{1}{2} \right) \cdot \left(\frac{k_B}{k_A} + \frac{k_C}{k_A} \frac{2}{\alpha} \frac{\varnothing}{\varnothing_{mand}} \right)$$

(2.11)

The stress in the bar can finally be determined by substituting Eq. (2.11) into Eq. (2.5) and considering that, at failure, $\sigma_{c,nom} = f_{c3}$:

$$\sigma_s = \frac{2}{\pi} \cdot \frac{\varnothing_{mand}}{\varnothing} \cdot \left[\eta_{fc} \cdot f_c + 4 f_{ct,eff} \cdot \left(\frac{c}{\varnothing} + \frac{1}{2} \right) \cdot \left(\frac{k_B}{k_A} + \frac{k_C}{k_A} \frac{2}{\alpha} \frac{\varnothing}{\varnothing_{mand}} \right) \right] \qquad (2.12)$$

In this equation, the effective tensile stress ($f_{ct,eff}$) is evaluated on the basis of the uniaxial tensile strength of concrete, $f_{ct,eff} = 0.7 \cdot f_{ct} = 0.37 f_c^{0.5}$, similarly to the value adopted by Fernández Ruiz et al. [Fer10] for spalling failures of curved reinforcement, modified by a size effect factor $(d_{dg}/\varnothing)^{1/3}$. This expression for the size effect is in accordance to the one proposed in the prEN 1992-1-1:2021 [Eur21] for similar cases and in agreement with experimental evidences [Mar51, Sor87] and with the equation proposed by Wästlund [Wäs34] to calculate the spalling strength. Parameter d_{dg} accounts for the maximum aggregate size (d_g) [Eur21], [Cav18] and can be calculated as $d_{dg} = \min(40, 16 + d_g \text{ mm})$ for $f_c \leq 60$ MPa and $d_{dg} = \min(40, 16 + d_g (60/f_c)^4 \text{ mm})$ for $f_c > 60$ MPa.

Hereafter, the following constant values will be adopted: $k_A = 1$, $k_B = 0.75$ and $k_C = 13.2$. The validity of that simplification will be verified by comparison with the test results. On that basis, Eq. (2.12) can be reformulated as follows:

$$\sigma_s = \frac{2}{\pi} \cdot \frac{\varnothing_{mand}}{\varnothing} \cdot \eta_{fc} \cdot f_c + \sqrt{f_c} \cdot \left(\frac{d_{dg}}{\varnothing} \right)^{1/3} \left(\frac{c}{\varnothing} + \frac{1}{2} \right) \cdot \left(32 \cdot \frac{45°}{\alpha°} + 0.7 \cdot \frac{\varnothing_{mand}}{\varnothing} \right) \leq f_y \qquad (2.13)$$

2.5.2 Comparison of proposed approach, EN 1992-1-1:2004 and Swedish Building Code (BBK 2004) with experimental evidence

In this section, a database of 136 tests is used to assess the suitability and performance of Eq. (2.13) for spalling failures of bent reinforcement. The database includes the experiments presented in this chapter as well as others gathered from the literature [Ber66, Gra33, Gra40, Leo73, Öst63, Wäs35, Swa69, Nil73, Str81, Str83, Stu90, Joh01, Wäs36, Kor72].

The main results are shown in Figure 2.21a, where the predictions of the failure load of Eq. (2.13) are compared to the test results as a function of the ratio $\varnothing_{mand}/\varnothing$. For tests of loops in tension with straight overlapping distances lower than $1.5\varnothing_{mand}$ [Leo73], the value k_B is halved and k_C set to zero to consider the geometric interference of the confining areas. Further comparisons with the provisions of EN 1992-1-1:2004 (Eq. 2.1) and BBK 2004 (Eq. 2.3) are also given in Figures 2.21b and c respectively. Tests where both experimental and calculated tensile stresses are larger than f_y are not considered. The plots on the top consider the tests from this study while those on the bottom consider other tests from the literature.

The proposed approach (Eq. 2.13) shows consistent results with low scatter (average measured-to-calculated strength equal to 0.99 with a Coefficient of Variation of 0.13). Such good agreement is obtained despite the varying mechanical and geometrical conditions. The EN 1992-1-1:2004 approach shows globally unsatisfactory results, significantly underestimating the strength when the mandrel diameter and the bending angle are small, and overestimating the strength when the mandrel diameter and the bending angle are large. The BBK 2004 approach shows better results than EN 1992-1-1:2004 as it accounts for the effect of the bending angle α. However, the results for the BBK 2004 are unsafe on average, particularly for 180° bends.

In addition to the previous comparisons, it shall also be noted that Eq. (2.13) also provides sound results for tests where the yield strength has been reached (average = 0.96 and CoV = 0.12 for 22 tests including 1 test of the experiments presented in this chapter and 21 tests from the literature [Ber66, Öst63, Wäs35, Str83, Stu90]). Notable deviations of Eq. (2.13) from experimental results have only been observed for some old tests as those of Graf 1940 [Gra40], where specific considerations would be required to extend the applicability of the proposed approach.
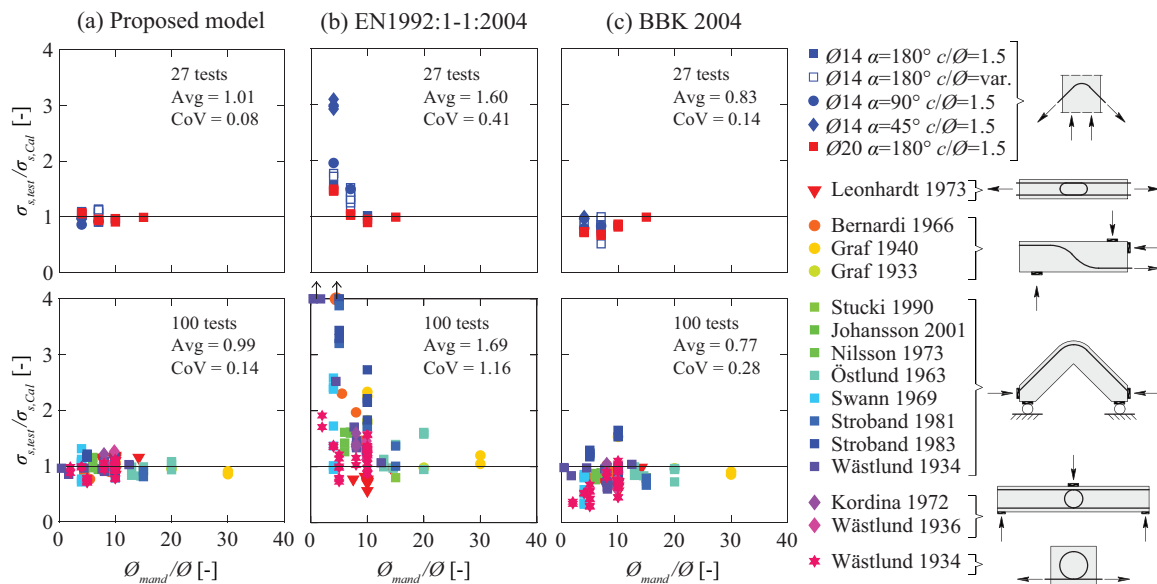
Figure 2.21: Comparison of measured-to-predicted values ($\sigma_{s,test}/\sigma_{s,cal}$): (a) according to Eq. (2.13); (b) according to EN 1992:1-1:2004, Eq. (2.1); and (c) according to BBK 2004, Eq. (2.3). (tests where both experimental and calculated tensile stresses are larger than f_y are not considered).

2.6 Practical detailing rules

2.6.1 Code like formulation

For a practical application, Eq. (2.13) needs to be modified to account for a safety format including material, model and geometric uncertainties. This can be performed by introducing a suitable partial safety factor and considering the characteristic compressive strength of concrete. Eq. (2.13) then becomes:

$$\sigma_{sd} = 0.65 \cdot f_{cd} \cdot \frac{\mathcal{O}_{mand}}{\mathcal{O}} + \frac{\sqrt{f_{ck}}}{\gamma_C}\left(\frac{d_{dg}}{\mathcal{O}}\right)^{1/3}\left(\frac{c_d}{\mathcal{O}}+\frac{1}{2}\right)\cdot\left(32\cdot\frac{45°}{\alpha°}+0.7\cdot\frac{\mathcal{O}_{mand}}{\mathcal{O}}\right) \le f_{yd} \qquad (2.14)$$

where $f_{cd} = \eta_{fc} \cdot f_{ck}/\gamma_C$ and γ_C is the partial safety factor for concrete. Since Eq. (2.13) has been derived accounting for the concrete resistance outside of the bend, the definition of the design cover c_d should consider not only the net cover to the free surface parallel to the bending plane (c_z in Figure 2.23a), but also the cover to a possible free surface outside the bend (c_x, c_y, and c_{xy} in Figure 2.23a). For practical purposes, this can be accounted for by considering the design cover c_d defined as:

$$c_d = \min(c_z; c_x; c_y; c_{xy}) \qquad (2.15)$$

In addition to the previous requirement to prevent spalling, the minimum mandrel diameter should also be selected to prevent damage to the reinforcement while bending of the bar (according to EN 1992-1-1:2004, this is fulfilled with $\mathcal{O}_{mand} \ge 4\mathcal{O}$ for $\mathcal{O} \le 16$ mm and $\mathcal{O}_{mand} \ge 7\mathcal{O}$ for $\mathcal{O} > 16$ mm).
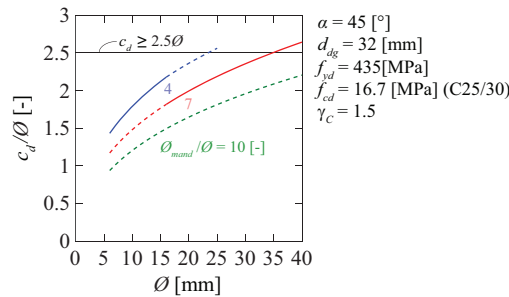
Figure 2.22:   Results of Eq. (2.14) for common compared to the simplified detailing rule $c_z \ge 2.5\mathcal{O}$ in case of normal concrete and steel.

To enhance ease of use, simplified detailing rules can be given for the cases where $f_{yd} \le 28 \cdot f_{cd}$, covering most practical cases. The verification of the concrete inside the bend may be omitted for all bends with an angle $\alpha° \le 45°$ at a clear distance $c_z \ge 2.5\mathcal{O}$ from a free edge parallel to the bending. As shown in Figure 2.22 shows on the basis of Eq. (2.14) the concrete cover limit

$c_z \geq 2.5\varnothing$ covers all practical cases. For diameter not larger than 20 mm, this limit could even be reduced to $c_z \geq 2\varnothing$.

Eq. (2.14) is simple enough for use in practical applications and it has been introduced in the current draft for new generation of Eurocode 2 [Eur21].

2.6.2 Multiple bends using a constant mandrel diameter

Eq. (2.14) allows determining the minimum mandrel diameter as a function of the steel stress σ_s, of the concrete compressive strength f_{ck}, of the aggregate size (considered in d_{dg}), of the bar diameter $\varnothing$, of the net cover c_d and of the bending angle α. For practical applications, the resulting minimum mandrel diameter is often larger than the diameter required to prevent steel damage during bending. If the required mandrel diameter is too large, it requires the use of special machines (Figures 2.2b and c), or, if different mandrels are required to bend a single bar, the bending process can become time-consuming. To avoid these shortcomings and to simplify the bending of reinforcement bars, the required bend can be replaced by a series of bends using always the same mandrel diameter (e.g. the minimum diameter required to prevent steel damage) with smaller bending angles separated by straight segments allowing to use smaller mandrel diameters (e.g. two 45° bends or three 30° bends instead of a single 90° bend), see Figure 2.23b.

The rules described above and the proposed model can also be applied in the case of multiple bends (kinks). In this case, as shown in Figure 2.11d, two different failure modes are possible and should be verified separately. For the case of bends separated by sufficiently long straight segments (right graph in Figure 2.11d), the spalling failures at the bends do not interact and this case can be verified according to previous considerations. For the other case referring to short straight segments (centre graph in the Figure 2.11d), the spalling at single bends can interact leading to a failure affecting the whole area of multiple bends. This failure mode can be studied on the basis of an equivalent mandrel diameter developing inside the reinforcement. As shown in Figure 2.23b, the equivalent mandrel diameter $\varnothing^*_{mand}$ can be calculated on the basis of the mandrel diameter of the single bend $\varnothing_{mand}$, the length of the straight segment between kinks l_{mand} and the bending angle of one kink α (expression valid for any number of identical kinks at regular spacing):

$$\varnothing^*_{mand} = \varnothing_{mand} + l_{mand} \cdot \cot\left(\frac{\alpha}{2}\right) \tag{2.16}$$

The suitability of this approach is shown in Figure 2.23c, where the resistance of the test series on multiple bends (with constant mandrel diameter and variable distance l_{mand}) is compared to the tests on single bends with variable mandrel diameter. Both series perform in a comparable manner, due to the fact that the extent of the confining areas is similar, providing thus analogous confinement forces and resistance to spalling.
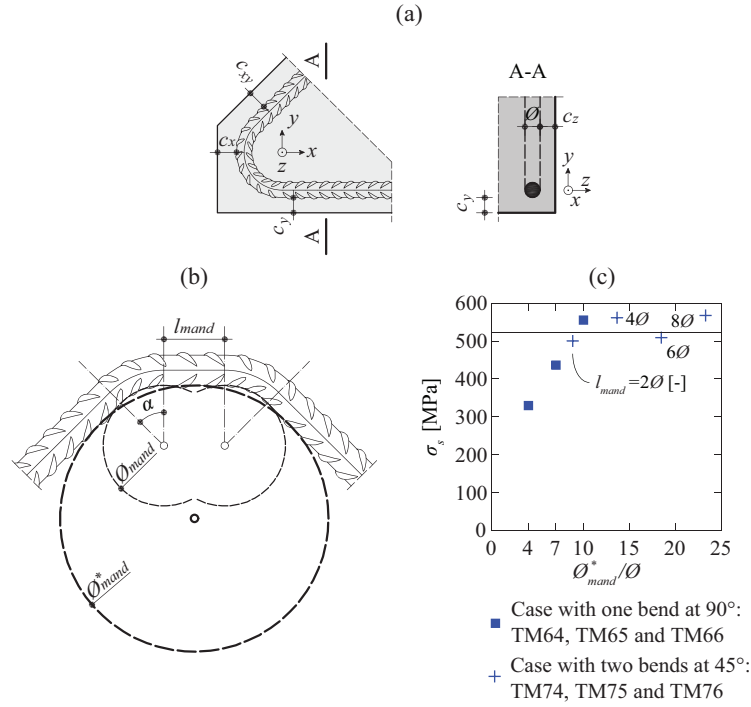
Figure 2.23:   Detailing rules: (a) definition of minimum concrete cover; (b) definition of
the equivalent mandrel diameter in case of multiple bends; and
(c) comparison of tests with variable mandrel diameter and single bend with
tests with multiple bend using a smaller mandrel.

As it can be noted, if the distance l_{mand} is sufficiently long, local spalling becomes governing
and, for practical cases, the verification of global spalling is not required. The limit value for
l_{mand} shifting the failure mode can be determined from the equivalence of the spalling resistance
according to Eq. (2.14) for local failure (using $\varnothing_{mand}$ and angle α) and the resistance for the case
of global spalling (calculated with $\varnothing^*_{mand}$ and angle $2\cdot\alpha$). This limit is thus:

$$\frac{l_{mand}}{\varnothing} \geq \frac{16\cdot\dfrac{45°}{\alpha°}\cdot\tan\dfrac{\alpha}{2}}{0.7+\dfrac{0.65\cdot f_{cd}}{\dfrac{\sqrt{f_{ck}}}{\gamma_C}\left(\dfrac{d_{dg}}{\varnothing}\right)^{1/3}\left(\dfrac{c_d}{\varnothing}+\dfrac{1}{2}\right)}} \approx \frac{10}{1+\dfrac{\eta_{fc}\cdot\sqrt{f_{ck}}\cdot\left(\dfrac{\varnothing}{d_{dg}}\right)^{1/3}}{\dfrac{c_d}{\varnothing}+\dfrac{1}{2}}} \qquad (2.17)$$

Eq. (2.17) is plotted in Figure 2.24 for variable bending angle α, bar diameter and concrete cover
for the cases where $f_{yd} \leq 28\cdot f_{cd}$, covering most practical situations. Such expression can be
simplified to the distance between the bends equal to $4\varnothing$ (black straight line in Figure 2.24b).
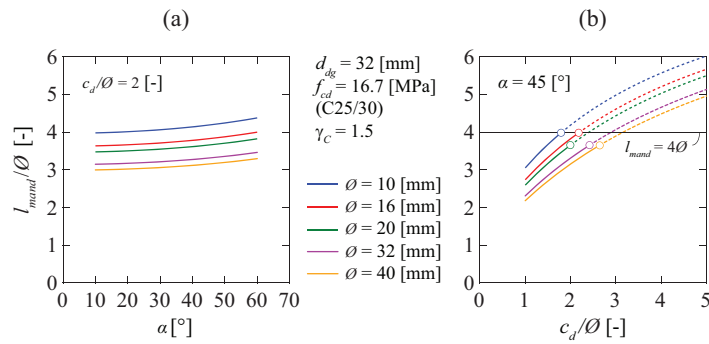
Figure 2.24:   Minimum distance between bends l_{mand} as a function of: (a) the bending angle; and (b) the concrete cover (dashed lines means that there is no spalling failure, refer to Figure 2.22).

2.6.3   Simplified rules for standard hook and bend anchorages

According to EN 1992-1-1:2004 [Eur04], the verification of the concrete strength inside the bend of hook and bend anchorages may be omitted if (i) the anchorage of the bar does not require a length more than 5Ø after the end of the bend; (ii) the bar is not positioned at the edge (plane of bend close to concrete face) and (iii) there is a cross bar with a diameter ≥ Ø inside the bend. Based on theoretical considerations using Eq. (2.14) confirmed by tests (see Figure 2.25), these requirements can be mitigated by defining a minimum clear distance $c_z \geq 1.5$Ø between the bar and a free edge parallel to the bend. The reduction of c_z compared to normal bends can be explained theoretically by the fact that the tensile stress is lower at the start of the bent because a part of the tensile force is transferred by bond.
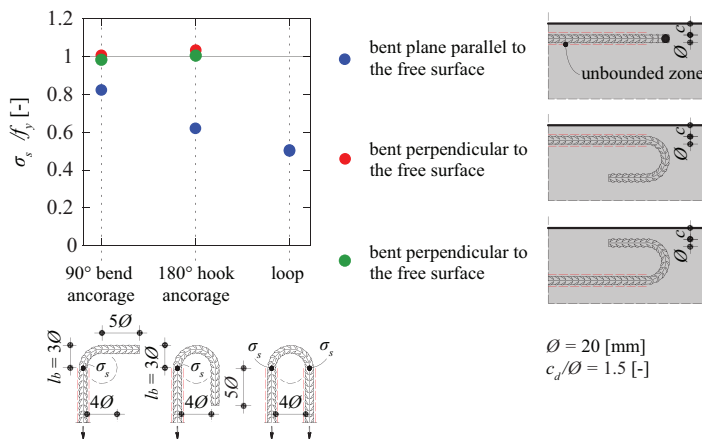
Figure 2.25:   Maximum tensile stress at failure for different hook and bend anchorages (tensile stress measured at the start of the bent, see definition of l_b).

2.6.4   Influence of transverse bars within the bend

The presence of transverse bars within the bend (Figure 2.26a) influences the response of the detail and particularly the assumption on a uniform pressure developed in the concrete due to the deviation forces p_{nom}. A fraction of the deviation forces can be carried by the transverse bar (Figure 2.26a) allowing to reduce the nominal concrete contact stress ($\sigma_{c,nom}$) under the bent reinforcement. This additional contact stress allows increasing the spalling strength. Based on the assumption that the additional contact stress can be developed on a length equal to the transverse bar diameter $\varnothing_{trans}$ (refer to cross section A-A in Figure 2.26a), Eq. (2.5) can be reformulated as:

$$\sigma_{c,nom} = \frac{p_{nom}}{\left(\varnothing + \dfrac{4 \cdot n}{\alpha_{bend}} \dfrac{\varnothing_{trans}^2}{\varnothing_{mand}}\right)} = \frac{\pi}{2} \frac{\varnothing}{\varnothing_{mand}} \frac{1}{\left(1 + \dfrac{\varnothing}{\varnothing_{mand}} \dfrac{4 \cdot n}{\alpha_{bend}} \left(\dfrac{\varnothing_{trans}}{\varnothing}\right)^2\right)} \sigma_s \qquad (2.18)$$

where $\varnothing_{trans}$ is the bar diameter and n is the number of the transverse reinforcement bars within the bend. The stress in the bar can finally be determined by substituting Eq. (2.11) into Eq. (2.18) and considering that, at failure, $\sigma_{c,nom} = f_{c3}$:

$$\sigma_{sd} = k_{trans} \left[0.65 \cdot f_{cd} \cdot \frac{\varnothing_{mand}}{\varnothing} + \frac{\sqrt{f_{ck}}}{\gamma_C} \left(\frac{d_{dg}}{\varnothing}\right)^{1/3} \left(\frac{c_d}{\varnothing} + \frac{1}{2}\right)\left(k_{bend} + 0.7 \cdot \frac{\varnothing_{mand}}{\varnothing}\right)\right] \le f_y \qquad (2.19)$$

where

$$k_{trans} = 1 + \frac{\varnothing}{\varnothing_{mand}} \frac{4 \cdot n}{\alpha_{bend}} \left(\frac{\varnothing_{trans}}{\varnothing}\right)^2 \approx 1 + 5 \cdot n \frac{\varnothing}{\varnothing_{mand}} \left(\frac{\varnothing_{trans}}{\varnothing}\right)^2 \frac{45°}{\alpha_{bend}°} \qquad (2.20)$$
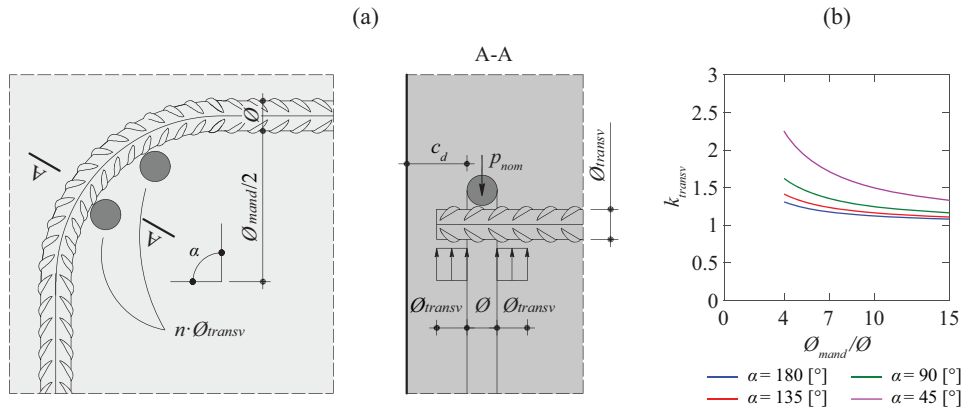
Figure 2.26:   Presence of transverses within the bend: (a) definiton of the mechanical model; and (b) factor k_{transv} in function of the mandrel diameter for variable bending angle in the case of $\varnothing_{trans} = \varnothing$ and for $n = 1$.

Figure 2.26b shows the enhancement factor k_{transv} as a function of the mandrel diameter for various bending angle in the case of $\emptyset_{trans} = \emptyset$ and for one transverse bar ($n = 1$). The Eq. (2.20) shows that an increase of the number of bars or of their diameter lead to an increase on the spalling strength. The enhancement of the stress in the bar remains for the presented cases between 1 and 2.25. These results are derived from the theoretical model but, since no experimental data is available on such detailing, they cannot be confirmed. As future work, additional experimental evidences addressed at this case should be performed to validate the proposed extension of the mechanical model.

2.7   Conclusions

This chapter presents the results of an experimental programme and analytical investigation of the influence of the detailing of bent reinforcement on the spalling resistance. A comprehensive experimental programme is presented as well as a mechanical model for the design of such regions. The main conclusions are listed below:

1. The behaviour of bent reinforcement is a complex phenomenon where both normal and bond stresses act simultaneously. This was confirmed by means of detailed Fibre-Optic measurements.

2. Spalling failures governing the strength of bent reinforcement are initiated by the development of a crack in the plane of the bend. This crack results from the penetration of the bend of the bar, pushing a wedge-shaped volume of the concrete. This phenomenon is analogous to the introduction of a linear concentrated force near an edge.

3. The wedge-shaped volume of concrete can develop contact pressures larger than the uniaxial compressive strength of concrete. These large contact stresses are possible as this region is confined by the tensile forces developing out-of-plane in the spalling region.

4. The casting direction had no marked influence on the spalling strength. This differs from the bond response of straight deformed reinforcement, where cracks due to settlement of fresh concrete and the increase porosity due to bleeding generally lead to a reduction of the bond strength for top bars.

5. A simple mechanical model was developed based on the equilibrium of deviation forces and the strength of the confined wedge-shape volume (accounting for the residual tensile strength of concrete in the splitting crack area confining it). Simple and physically-consistent design expression were derived.

6. The proposed model shows fine agreement with the 41 tests of this study as well as with 100 tests from the literature. This approach leads to consistent results for a variety of geometrical and mechanical parameters, performing better than the current design formulas as the current European Standard EN 1992-1-1:2004.

7. New detailing approaches can be derived on the basis of the mechanical model. For instance, bending with large mandrel diameters can easily be replaced by multiple bends using a smaller mandrel. This solution allows simplifying the manufacturing processes of the reinforcement.

Appendix 2.A: Internal forces inside a curve beam derived from strain measurements

On the basis of the strain measurement of the fibres, it is possible to estimate the complete profile of strains in the bar and the resulting internal forces and pressures on the bar surface. To that aim, plane sections are assumed to remain plane, which results in a nonlinear profile of strains for a curved bar, as demonstrated by Winkler [Win58] and Bach [Bac89].

For derivation of the strain profile, a segment of a curved bar will be considered. The segment (see Figure 2.A.1a) is characterised by two sections AB and A_1B_1, whose distance results:

$$s(\xi) = \Delta\alpha \cdot \left(\frac{\emptyset_{mand}}{2} + \frac{\emptyset}{2} + \frac{\xi}{2} \right)$$ (2.A.1)

After the bar is loaded, the elongations in the fibres of the bar ($\Delta s(\xi)$) are assumed to remain in a plane. Thus, the elongations in each fibre can be determined on the basis of those of the outer and inner fibre as:

$$\Delta s(\xi) = \frac{\Delta s_{outer} + \Delta s_{inner}}{2} + \xi \cdot \frac{\Delta s_{outer} - \Delta s_{inner}}{\emptyset}$$ (2.A.2)

where Δs_{outer} refers to $A_1A'_1$ and Δs_{inner} to $B_1B'_1$. Such elongations can be calculated as:

$$\Delta s_{outer} = \Delta\alpha \cdot \left(\frac{\emptyset_{mand}}{2} + \emptyset \right) \cdot \varepsilon_{outer}$$

$$\Delta s_{inner} = \Delta\alpha \cdot \frac{\emptyset_{mand}}{2} \cdot \varepsilon_{inner}$$ (2.A.3)

where ε_{outer} is the strain measurement of the outer fibre and ε_{inner} is the strain measurement of the inner fibre. As a result, the strain at each fibre can be calculated as:

$$\varepsilon(\xi) = \frac{\Delta s(\xi)}{s(\xi)}$$ (2.A.4)

By substituting Eq. (2.A.1) and Eq. (2.A.2) into Eq. (2.A.4), it results:

$$\varepsilon(\xi) = \frac{1}{\Delta\alpha \cdot \left(\frac{\emptyset_{mand}}{2} + \frac{\emptyset}{2} + \frac{\xi}{2} \right)} \cdot \left[\frac{\Delta\alpha \cdot \left(\frac{\emptyset_{mand}}{2} + \emptyset \right) \cdot \varepsilon_{outer} + \Delta\alpha \cdot \frac{\emptyset_{mand}}{2} \cdot \varepsilon_{inner}}{2} + \xi \cdot \frac{\Delta\alpha \cdot \left(\frac{\emptyset_{mand}}{2} + \emptyset \right) \cdot \varepsilon_{outer} - \Delta\alpha \cdot \frac{\emptyset_{mand}}{2} \cdot \varepsilon_{inner}}{\emptyset} \right]$$ (2.A.5)

that, rearranging and simplifying terms, becomes:

$$\varepsilon(\xi) = \frac{\frac{1}{2} \cdot \left[\left(\frac{\emptyset_{mand}}{2\emptyset} + 1 \right) \cdot \varepsilon_{outer} + \frac{\emptyset_{mand}}{2\emptyset} \cdot \varepsilon_{inner} \right] + \frac{\xi}{\emptyset} \cdot \left[\left(\frac{\emptyset_{mand}}{2\emptyset} + 1 \right) \cdot \varepsilon_{outer} - \frac{\emptyset_{mand}}{2\emptyset} \cdot \varepsilon_{inner} \right]}{\frac{\emptyset_{mand}}{2\emptyset} + \frac{1}{2} + \frac{\xi}{\emptyset}} \quad (2.A.6)$$

Eq. (2.A.6) shows that the strain varies non-linearly across the depth of the bar and follows a hyperbolic distribution. As it can be noted, when the mandrel diameter $\emptyset_{mand}$ tends to infinity (straight bar), Eq. (2.A.6) leads to that of the straight beam theory (linear profile of strains).
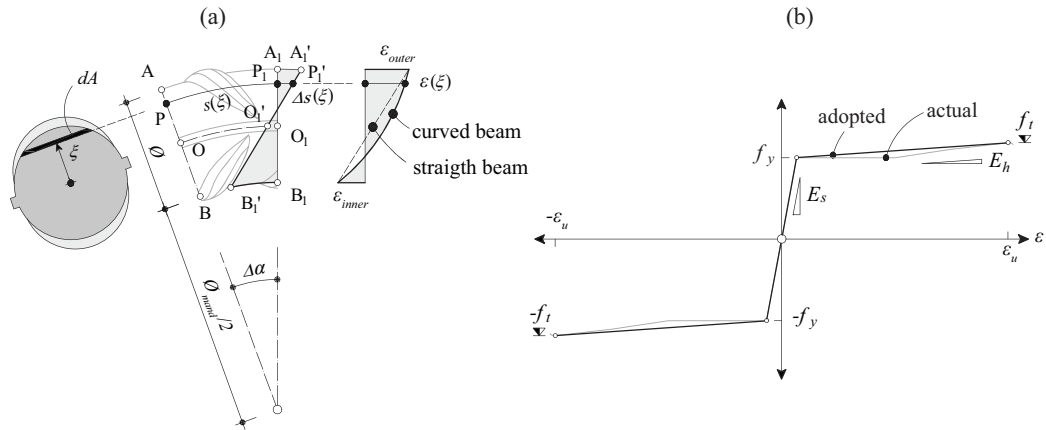
Figure 2.A.1: Determination of the stress at each point of the section: (a) Strains in a curved beam; and (b) behaviour of the steel (where $f_t = 627$ MPa and $\varepsilon_u = 11.3$ %).

On this basis, the stresses σ_s across the depth of the bar can be determined by assuming an elastic-plastic behaviour for the steel, refer to Figure 2.A.1b. The normal forces N and the bending moments M can thus be calculated by integration across the depth of the bar stresses:

$$N = \int_{A(\xi=-\emptyset/2)}^{A(\xi=\emptyset/2)} \sigma_s \cdot dA$$

$$M = \int_{A(\xi=-\emptyset/2)}^{A(\xi=\emptyset/2)} \sigma_s \cdot \xi \cdot dA \quad (2.A.7)$$

And the average stress and the bond stress results:

$$\sigma_s = \frac{N}{\pi \cdot \emptyset^2 / 4}$$

$$\tau_b = \frac{d\sigma_s}{ds} \cdot \frac{\emptyset}{4} \quad (2.A.8)$$

Appendix 2.B: Calculation of residual tensile force of concrete

The softening response of concrete in tension has been investigated by various authors leading to several formulations describing it [FIB11, Hor92]. The relation of Hordijk [Hor92] is used in this chapter to calculate the residual tensile stresses over the surface affected by spalling. The equation describing the residual tensile strength of concrete is thus [Hor92]:

$$\sigma_{res} = f_{ct} \cdot \left[\left(1 + \left(b_1 \cdot \frac{w}{w_c} \right)^3 \right) \cdot e^{-b_2 \cdot \frac{w}{w_c}} - \frac{w}{w_c} \left(1 + b_1^3 \right) \cdot e^{-b_2} \right] \tag{2.B.1}$$

where f_{ct} refers to the tensile concrete strength and $b_1 = 3.0$ and $b_2 = 6.93$ are constants. The parameter G_F refers to the fracture energy defined as [FIB11]:

$$G_F = 73 f_c^{0.18} \ [\text{N/m}] \tag{2.B.2}$$

where f_c is the concrete compressive strength in [MPa]. The parameter w_c refers to the value at which no residual tensile strength is attained, estimated as:

$$w_c = 5.14 \frac{G_F}{f_{ct}} \tag{2.B.3}$$

The Hordijk's model is applied on the basis of the out-of-displacement w resulting from the DIC measurement. The integration of the residual concrete tensile stresses (Eq. 2.B.1) provide the residual concrete tensile force:

$$F_{res} = \int_{A(\sigma_{res}=0.0f_{ct})}^{A(\sigma_{res}=0.8f_{ct})} \sigma_{res} \cdot dA \tag{2.B.4}$$

In this calculation, the integration is limited to a stress up to $0.8f_{ct}$ in order to avoid noise from the measurements. In addition, the area of the concrete under the bar is not considered for calculation of F_{res} (as no residual tensile stress can develop).

Notation

Latin characters: lower case

a	thickness of a prism
b	width of a prism
b_1, b_2	factors for definition of the residual tensile strength of concrete
c	concrete cover
c_d	design value of the concrete cover
c_x	concrete cover in the x-direction
c_y	concrete cover in the y-direction
c_{xy}	concrete cover in the xy-direction
c_z	concrete cover in the z-direction
d_g	maximum aggregate size
d_{dg}	parameter accounting for roughness of surfaces
f_c	concrete compressive strength measured in cylinder
f_{c3}	tri-axial compressive strength
f_{cd}	design value of the concrete compressive strength
f_{ck}	characteristic value of the concrete compressive strength
f_{ct}	concrete tensile strength
$f_{ct,eff}$	concrete effective tensile strength
f_y	yield strength of reinforcement
f_{yd}	design value of the yield strength of reinforcement
h	height of a prism
k_A	factor accounting for the shape of the confined wedge
k_B, k_C	confinement factors
k_α	bending angle coefficient
l	distance between the start of the bend and the concrete edge
l_{mand}	distance between multiple bends
n	number of the transverse reinforcement bars
p_{nom}	deviation forces
s	curvilinear abscissa of a bar
u	penetration of a bar
w	out-of-plane displacement and crack opening

w_c	crack opening leading to no residual tensile strength
w_{max}	maximum out-of-plane displacement
x	in-plane coordinate in the x-direction
y	in-plane coordinate in the y-direction
z	out-of-plane coordinate in the z-direction

Latin characters: upper case

A_A	projected area of the wedge, confined area
A_B, A_C	confining areas
F	applied force
F_A	confinement force
F_B, F_C	confining forces
F_{max}	maximum force applied
F_{res}	out-of-plane force
G_F	fracture energy
N	normal force
M	bending moment
P	point of LVDT measurement

Greek characters: lower case

α	bending angle
δ	displacement of the point P measured in the direction of the bar with respect to the concrete surface
ε	bar strain
ε_{inner}	strain measurement of the inner fibre
ε_{outer}	strain measurement of the outer fibre
γ	angle of the contact forces with respect to the bar axis
γ_C	partial safety factor of concrete
η_{fc}	brittleness factor of concrete
φ	internal friction angle of the concrete
σ_l	confinement stress
$\sigma_{c,nom}$	nominal concrete compressive strength (contact pressure)
$\sigma_{c,nomR}$	maximum nominal concrete compressive strength (contact pressure)

σ_{res}	residual tensile stress of concrete
σ_s	stress in the reinforcement (for characterisation of a bend, referring to the stress at the start of the bend)
σ_{sd}	design stress in the reinforcement at the start of a bend
σ_{sR}	maximum stress in the reinforcement at the start of a bend
σ_t	concrete tensile stress
τ_b	bond stress
ξ	position of the fibre in the cross section of the bar

Greek characters: upper case

Δs	curvilinear abscissa of a segment of a curved bar
Δs_{nner}	curvilinear abscissa of a segment of a curved bar for the inner fibre
Δs_{outer}	curvilinear abscissa of a segment of a curved bar for the outer fibre
$\Delta\alpha$	bending angle of a segment of a curved bar

Others

$\varnothing$	bar diameter
$\varnothing_{mand}$	mandrel diameter
$\varnothing^*_{mand}$	equivalent mandrel diameter
$\varnothing_{trans}$	bar diameter of the transverse reinforcement

Chapter 3

Anchorage of shear reinforcement in beams and slabs

This chapter is the pre-print version of the article mentioned below, accepted in Engineering Structures Journal in May 2022. The authors of the article are Frédéric Monney (PhD Candidate), Qianhui Yu (PhD Candidate), Prof. Miguel Fernández Ruiz (thesis co-director) and Prof. Aurelio Muttoni (thesis director). The provisional reference is the following:

Monney F., Yu Q., Fernández Ruiz M., Muttoni A., *Anchorage of shear reinforcement in beams and slabs*, Engineering Structures. [accepted, May 2022]

The work presented in this publication was performed by Frédéric Monney under the supervision of Prof. Miguel Fernández Ruiz and Prof. Aurelio Muttoni who provided constant and valuable feedbacks, proofreadings and revisions of the manuscript. It should be noted that Qianhui Yu contributed to the article in the section 3.6.8.

The main contributions of Frédéric Monney to this article and chapter are the following:

- Comprehensive literature review including research and design codes on detailing of shear reinforcement focusing on bond and spalling failure.

- Preparation, casting and testing of 24 pull-out tests (23 specimens with 90° bends and one 180° hook) with variable concrete cover, tail length, crack opening in the plane of the bend and presence of longitudinal bar within the bend.

- Detailed measurements on the out-of-plane displacements, using Digital Image Correlation, to understand spalling failures.

- Implementation of Fibre-Optical measurements on steel reinforcement of all 90° bends and 180° hook specimens for an evaluation of the strain profile.

- Post-processing of the experimental data.

- Interpretation, analysis and discussion of the tests results.

- Proposition of a consistent mechanical model assessing bond and spalling resistance of bends and hooks; it considers the concrete compressive strength, yielding strength of reinforcement, concrete cover, mandrel diameter, bend angle, tail length, size effect, bond index, crack opening in the plane of the bend and casting position.

- Proposition of design recommendations for anchorage of shear reinforcement.

- Collection of a database with 40 tests used to validate the mechanical model.

- Development of a code-like formulation based on the mechanical model.

- Elaboration of the figures and tables included in the article.

- Writing of the manuscript of the article (except for section 3.6.8).

Abstract

Anchorage of shear reinforcement, such as links or stirrups, can be performed by providing hooks, bends or heads at their ends, by welding transverse reinforcement or by closing open stirrups with pins. Hooks and bends, also used to enhance the anchorage of flexural reinforcement at the end regions of beams and slabs, have often been preferred because of their simple and cost-effective production. Such anchorages present nevertheless several peculiarities that shall be accounted for. They are relatively sensitive to their detailing (mandrel diameter, length of the tail segment between bar end and bent region) as well as to the cracking state of the surrounding concrete. Also, brittle failures can occur due to spalling of the concrete cover in case of bars near to a free surface.

The anchorage with hooks and bends is currently still widely designed according to old detailing rules, based on the results of tests performed in many cases with materials whose properties are significantly different than those of nowadays. Also, no mechanical models are available for a consistent verification and detailing, acknowledging the different potential failure modes and their interaction with the surrounding concrete. In an effort to provide a consistent approach to its design and verification, this chapter presents an investigation addressed at understanding the mechanical response and performance of bend and hook anchorages. To that aim, the results of an experimental programme performed with state-of-the-art instrumentation are introduced. By means of analysis of Digital Image Correlation and Fibre-Optic Measurements, the complete transfer of forces is analysed under different circumstances. On that basis, a consistent mechanical model is developed and validated, also reproducing a large variety of tests found in the literature. The chapter introduces eventually several practical considerations on the activation of shear reinforcement in beams, and the level of performance required at its anchorages.

Keywords: structural concrete, pull-out tests, spalling, bond, anchorage, hooks, reinforcement bends, development length, mechanical model, design

3.1   Introduction

Since the beginning of reinforced concrete construction, mechanical anchorage of the reinforcement in tension by means of bends and hooks has been extensively used in a large number of applications, such as beams, walls and slabs (Figure 3.1a-f). Arrangement of hooks was first required for the anchorage of plain bars due to their poor bond performance. Such solution was observed to be efficient and was also adopted for the anchorage of various types of shear and punching reinforcement.

The first research works on hooks were performed for the anchorage of flexural reinforcement at the extremity of beams. On the basis of beam tests, Hyatt in 1877 [Hya77] observed that flat reinforcing bars bent at 90° at their ends gave higher performances. As a result of this work, 90° bends became popular in the following years in the USA [Myl28]. In Europe, in 1908 Mörsh [Mör08] encouraged the use of hooks to enhance the performance of anchorages. He also proposed to use higher bend angles than 90°, in contrast to the practice in the USA. The reason for this was that 90°-angle bends caused failure issues in the case of too small concrete cover (as demonstrated by the tests of Wayss and Freytag [Mör06, Bac11a]). It was Considère in 1907 [Con07] who formally proposed a 180° hook bent with a mandrel diameter equal to 4 times the bar diameter to avoid failures due to concrete crushing. In addition to the use of hooks at beam ends, the hook anchorage of shear reinforcement (Figure 3.1a-e) was also used in the early developments of reinforced concrete. First open stirrups with simple bends were incorporated in the early patents by Hennebique in 1892-1893 [Hen92, Hen93] (under the name of "staple" composed by a flat steel plate, later renamed as stirrup in 1893 [Hen93]) followed by Coignet in the same year [Coi92]. The use of open stirrups with bends and hooks at their ends (Figure 3.1b-c) was proposed to simplify the arrangement of the longitudinal reinforcement during construction.
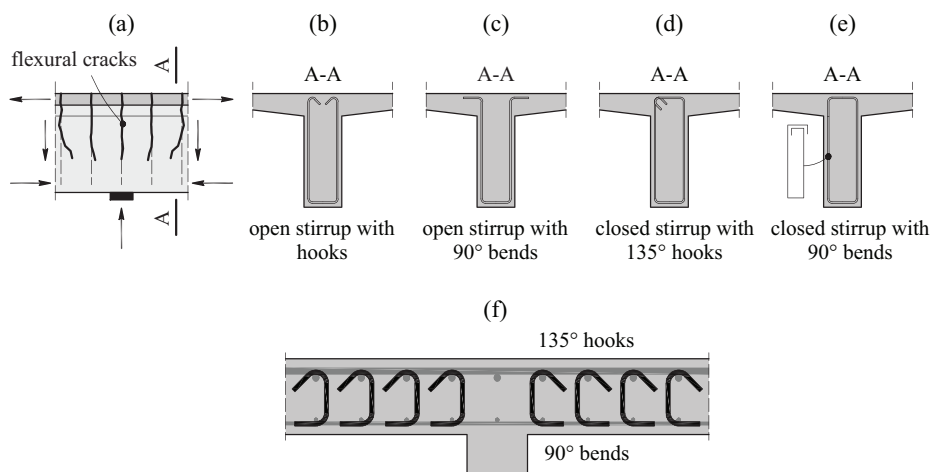
Figure 3.1:   Applications of bends and hooks for: (a) - (e) shear reinforcement in bridges; and (f) for punching or shear reinforcement in slab.

Current provisions of the European Standard for concrete structures [Eur04] define both bends (bend angle < 135°) and hooks (with a bend angle ≥ 135°) as details to enhance the anchorage of reinforcement bars. In the case of one-leg links, both bends and hooks are typically used (see Figure 3.1) and according to EC2:2004 [Eur04], only transverse welded bars or headed bars (prEN:2021 [Eur21]) are accepted as alternatives.

The anchorage of the reinforcement shall ensure satisfactory behaviour at serviceability limit state (cracking development) as well as at ultimate limit state (resistance). Depending on the reinforcement detailing (mandrel diameter of the curved part, length of the straight tail segment which is necessary to bend the bar as well as presence of longitudinal bar inside of the bend, Figure 3.2a) and the cracking conditions of the anchorage (associated to the behaviour of the structural element, refer to Figure 3.1a), the anchorage performance can vary considerably. With this respect, several failure modes have been identified in the literature:

- Failure of the reinforcement;

- Concrete failure due to spalling of the concrete cover perpendicular to the bent, see Figure 3.2b [Bac11a, Reh79, Ram08, Spe17, Spe18, Yas21];

- Concrete failure due to spalling of the concrete cover parallel to the bent, see Figure 3.2d and Chapter 2;

- Bond failure due to pull-out of the bar , see Figure 3.2c [Myl28, Bac11a, Reh79, Ram08, Spe17, Spe18, Yas21, Sal13, Abr13, Kem68, Hri69, Reh68, Reh69, Leo65, Reg80, Shi08, Bra16, Med18, Mar75, Min75, Pin77, Jir79, Joh81, Sor88, Spe15, Cos16, Hwa17, Aja18].

Low values of the concrete cover are usually associated to spalling failures (Figure 3.2b), while higher values of the cover typically lead to pull-out (Figure 3.2c) or failure of the bar.

Despite previous research efforts (described in detail in the next section), design of such details is still performed based on rules directly calibrated on old tests (with reinforcement and concrete with different properties than those used in current practice). Also, no mechanical model (distinguishing between failure modes and the influence of the anchorage conditions) is widely accepted for design, which still relies on empirical formulae in most cases. In an effort to improve this situation, this chapter presents an investigation on the response of bends and hooks focusing on the spalling and bond resistance. It introduces the results of a comprehensive testing programme performed by the authors on specimens with typical current detailing and material properties. To that aim, 24 pull-out tests have been conducted with different parameters investigated: concrete cover, tail length, crack opening in the plane of the bend and presence of longitudinal bar within the bend. These tests are aimed at completing previous experimental evidences. They were instrumented with advanced measurement techniques (Digital Image Correlation and Fibre-Optic Measurements), helping to understand the mechanics of spalling and bond failures. On that basis, a rational model for design of bent reinforcement is proposed. Its results are compared to the performed tests as well as to those of a database of experimental tests collected from the literature showing consistent agreement. The proposed approach, based on a mechanical model and distinguishing between the various potential failure modes, allows to suitably consider the various geometrical and mechanical parameters, overcoming the limitations of current design approaches. Based on these findings, a rational approach for new detailing rules for bends and hooks is outlined.
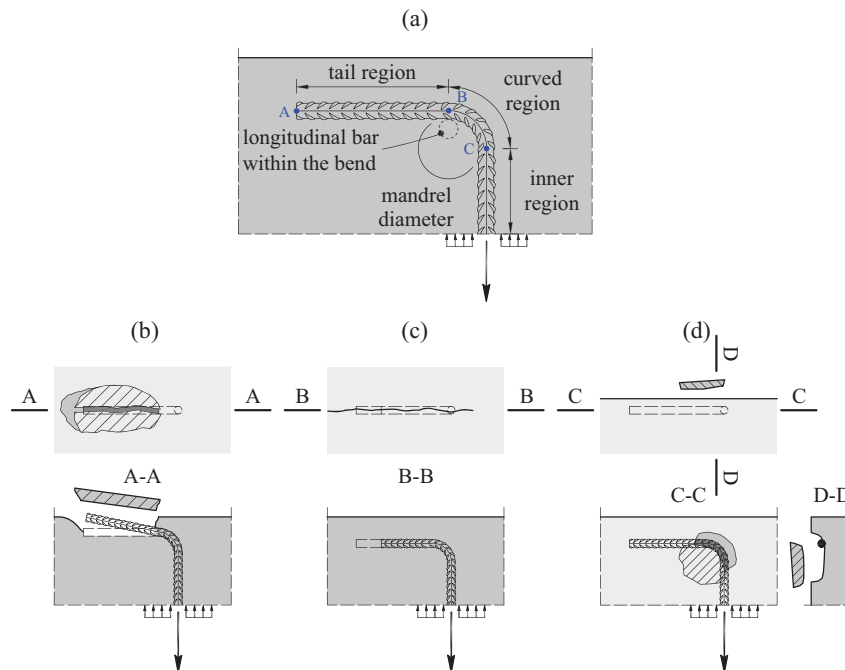
Figure 3.2:   (a) Definition of the a bend anchorage. Type of concrete failures: (b) spalling of concrete cover perpendicular to the bend; (c) pull-out; and (d) lateral spalling failure of concrete cover parallel to the bend.

3.2   State-of-the-art on response and performance of bends and hooks

3.2.1   Experimental research

A significant amount of research has been conducted in the past on the anchorage capacity of bends and hooks. These research programmes have mainly focused on pull-out specimens to characterise the anchorage capacity [Myl28, Reh79, Sal13, Abr13, Kem68, Hri69, Reh68, Reh69, Leo65, Reg80, Shi08, Bra16, Med18], but also on bends and hooks incorporated in structures such as beam-column joints [Ram08, Spe18, Mar75, Min75, Pin77, Jir79, Joh81, Sor88, Spe15, Cos16, Hwa17, Aja18], in beam ends [Bac11a] and shear reinforcement in beams [Reg04, Var11, Rup13, Leq18, For19]. From these research programmes, several phenomena have been acknowledged as playing a significant role:

- Bond properties of the reinforcement: a larger bond index [FIB00] leads generally to higher strength and stiffness of the anchorage [Reg80, Bra16, Med18]. This effect is particularly notable in presence of cracks in the plane of the bend [Bra16].

- Mandrel diameter: with an increase of the strength and stiffness of the anchorage for increasing mandrel diameter [Myl28, Bac11a, Sal13, Abr13, Min75].

- Bending angle: the effect of the bending angle is controversial in the literature. According to some authors, the bending angle has a negligible effect on the resistance [Mar75] whereas for others it does [Bac11a, Reh79, Abr13, Hri69, Bra16, Med18, For19]. This controversy is to a large extent related to the selected parameters in the tests. Authors claiming that the angle has little or no influence have usually performed their tests with a relatively long bonded inner region (Figure 3.2a).

- Tail length (point A to point B in Figure 3.2a): an increase of the tail length leads to an increase of the strength [Myl28, Hri69, Reg80]. Only Marques and Jirsa [Mar75] claimed that increasing this length has no effect because, as for the effect of the bending angle, their tests had a significant inner bonded length.

- Confinement reinforcement: such a reinforcement enhances the strength of the anchorage [Myl28, Sal13, Abr13, Sor88].

- Longitudinal bar within the bend: whose presence increases the strength of the anchorage, as shown by [Reh79, Ram08, Leo65, Reg80, Pin77].

- Bar diameter (size effect): when the bar diameter increases, the normalised strength decreases [Yas21, Hri69, Med18, Sor88].

- Position of the tail region with respect to the concrete surface: potentially leading to spalling failures under different configurations [Bac11a, Reh79, Ram08, Spe17, Spe18, Yas21].

- Casting direction: as shown by [Reh68], this effect can be significant (see also bond in straight bars [Moc21, Moc21a]).

- Influence of cracking: an increase of the width of longitudinal cracks leads to a decrease of the strength and the stiffness of bends and hooks [Reh79, Reg80, Bra16, Med18]. This is particularly the case when cracking is in the plane of the bend [Bra16].

- Spacing between bends/hooks: a decrease of the spacing between parallel bends/hooks leads to a decrease of the strength [Sor88, Aja18].

Most of previous researches focused only on the overall strength and failure mode. In most cases, tests were performed with a bonded straight part before the bend (inner region in Figure 3.2a), whereas some researchers carried out tests where bond was disabled in the straight part [Myl28, Reh79, Hri69, Leo65, Reg80, Shi08, Bra16, Med18, Min75, Sor88]. Such tests do not address typical practical cases, but allow for a clearer interpretation of the phenomena implied.

3.2.2   Physical understanding and code provisions

With respect to theoretical approaches, Minor and Jirsa [Min75, Min71] were probably amongst the first to establish a qualitative, but detailed description of the acting deviation and bond forces in the curved and tail regions of a bend anchorage. According to their findings, large transversal forces can act in the tail region, generating high bending moments in the reinforcement and potentially leading to yielding of the bar and/or to spalling of the reinforcement cover. Such observation was also validated on the basis of several tests with short bends and hooks. Continuing these works, Shima [Shi08] proposed similar considerations and interpretation of the load transfer actions based on detailed measurements over the length of the bar.

Some researchers developed also design equations for bends and hooks including the contribution of the different regions (straight, curved and tail length, [Mar75, Jir79, Joh81, Spe15]). In most cases, the contribution of the curved and tail region was considered as a factor enhancing the development capacity with respect to straight anchorages (similarly to the approach of codes of practice). Some researchers [Sor88, Cos16, Hwa17] also proposed spring models to provide a more detailed insight of the anchorage response. In addition, the Finite Element Method has also been used in the past to have a detailed insight of the bond response [Fer07a, Ino11, Lun05, Lun15, Lur15, Sal04] including related phenomena as spalling [Dao13, Hay13, Lag16] and its application for bent details to structural members [Beu02, Heg04, Sag11a, Sha09].

With respect to code provisions, Model Code 2010 [FIB13], ACI 318-18 [ACI19] and EN 1992-1-1:2004 (Eurocode 2 [Eur04]) define the required development length of bends and hooks complying with several detailing rules according to different parameters, such as the bar diameter, its yield strength or the bond strength. Some additional parameters are also accounted for in some cases, such as the concrete cover [Eur04, FIB13, ACI19], the presence of a longitudinal bar within the bend [Eur04, FIB13, ACI19], the shape of the anchorage [Eur04] and the bar spacing [ACI19]. However, when compared to test results, it appears that the influences of other relevant parameters (as the crack opening in the anchorage region) are not accounted for and several trends can be clearly identified. This is for instance shown in Figure 3.3 for EN 1992-1-1:2004 (Eurocode 2 [Eur04]) when compared to a number of relevant test programmes [Reh79, Bra16, Med18, Min75].
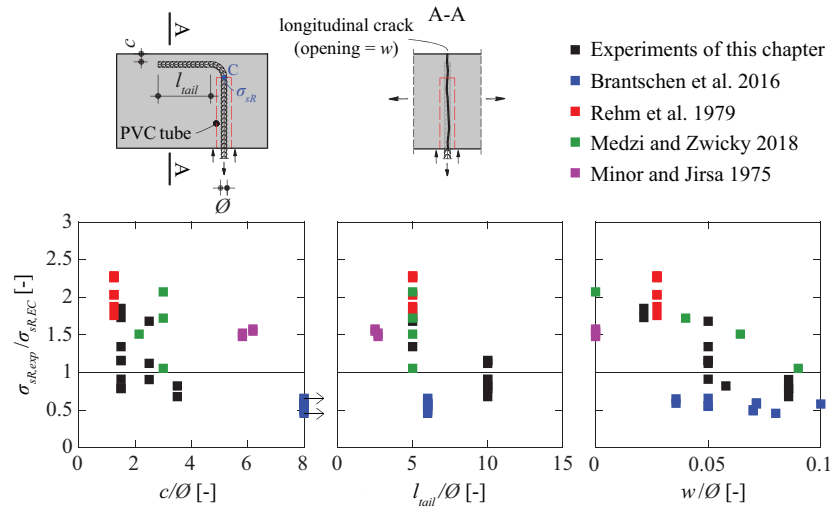
Figure 3.3:   Comparison of measured-to-predicted values ($\sigma_{sR,exp}/\sigma_{sR,EC}$) according to EN 1992-1-1:2004 (Eurocode 2 [Eur04]).

3.3   Experimental programme

In order to propose a rational design model based on detailed measurements, an experimental programme was conducted by the Structural Concrete Laboratory at École Polytechnique Fédérale de Lausanne (Switzerland). This programme was addressed mainly to anchorages with 90° bends with the tail length parallel to the free surface. The choice of this detail was made to reproduce the case of the upper anchorage of open stirrups in beams (Figure 3.1a) with a T cross section as well as the bottom anchorage of one-leg links in slab (Figure 3.1f). Only one 180° hook was tested in this work because Brantschen et al. [Bra16] have already systematically studied this type of detail in a similar experimental programme. The investigation to assess the performance of bends and hooks described in this work was performed under cracked or uncracked concrete conditions (with controlled crack width conditions) to represent regions with hogging and sagging moments in beams (Figure 3.1a) and slabs. The geometry of the specimens as well as the set-up were similar to those adopted previously by Brantschen et al. [Bra16].

The tests were instrumented with Digital Image Correlation (DIC) on the concrete surface and with Fibre-Optic Measurements (FOM) on the bar. The aim was to provide detailed readings of the local and global response of the anchorage, in an effort to understand its mechanical response and the failure mechanisms.

3.3.1 Specimens

Six concrete specimens (250×400×1250 mm) with 4 anchorages each (total of 24 tests) were tested investigating the following parameters (Figure 3.4a):

- in-plane crack opening w ($0 \leq w \leq 1.2$ mm);

- tail length l_{tail} ($l_{tail} = 5\emptyset$ and $10\emptyset$);

- concrete cover c ($0 \leq c \leq 3.5\emptyset$); and

- presence of longitudinal bars within the bend (18 mm diameter bar for series PM41-PM44).

One test was also performed on a 180° hook anchorage (PM54) to obtain strain measurements with FOM (not used in the Brantschen et al. [Bra16] investigation). The mandrel diameters $\emptyset_{mand}$ was equal to $4\emptyset$ for all tests. Additional details and values of the parameters investigated are given in Table 3.1. Figure 3.4b shows the nomenclature used.
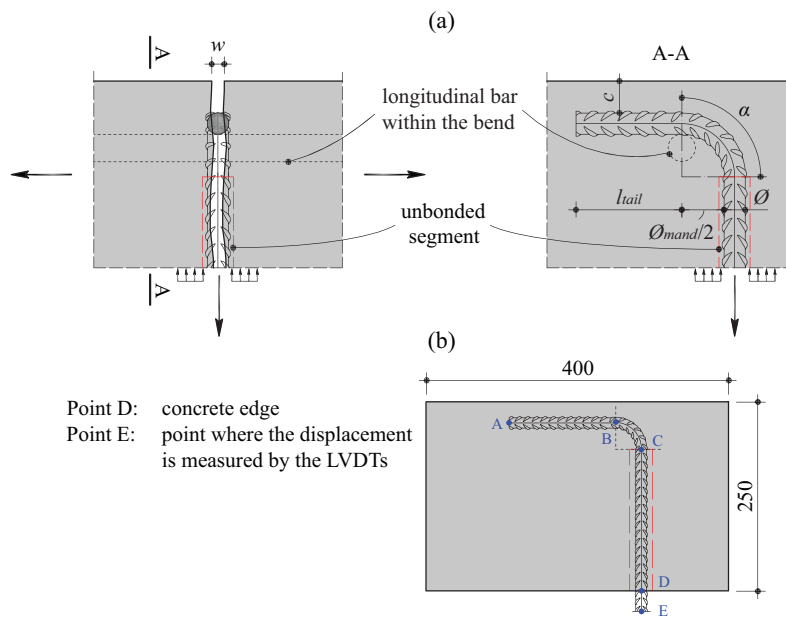
Figure 3.4: (a) Parameters investigated in present experimental programme: in-plane crack opening w; tail length l_{tail}; concrete cover c; presence of longitudinal bar within the bend; and bending angle α; and (b) nomenclature.

Table 3.1: Main parameters and experimental results (F_{max} refers to the maximum force in the reinforcement just before failure, $\sigma_{sR,exp}$ to the associated average steel stress and l_b to the bonded length, l_{DE} to the distance between the concrete edge and position of the LVDTs (Figure 3.4b), for meaning of other parameters refer to section Notation).

Spec.	α [°]	$l_{tail}/\varnothing$ [-]	$l_b/\varnothing$ [-]	l_{CD} [mm]	l_{DE} [mm]	w [mm]	$c/\varnothing$ [-]	f_c [MPa]	f_{ct} [MPa]	F_{max} [kN]	$\sigma_{sR,exp}$[1] [MPa]	f_b[2] [MPa]	Failure mode[3]
PM11	90	10	13.9	201	50	0	0.5	46.9	3	>85.9	>558	>10	-
PM12	90	10	13.9	187	43	0	1.5	46.9	3	>86	>558.7	>10	-
PM13	90	10	13.9	173	50	0	2.5	46.9	3	>87.3	>567.1	>10.2	-
PM14	90	10	13.9	159	50	0	3.5	46.9	3	>90.2	>586	>10.5	-
PM21	90	10	13.9	201	50	0.3	0.5	47.2	3	71.8	466	8.4	S
PM22	90	10	13.9	187	50	0.3	1.5	47.2	3	>86.3	>560.6	>10.1	-
PM23	90	10	13.9	173	50	0.3	2.5	47.2	3	>86.4	>561.3	>10.1	-
PM24	90	10	13.9	159	50	1.2	3.5	47.2	3	55.8	363	6.5	P
PM31	90	10	13.9	201	50	0.7	0.5	47.2	3	34.8	226	4.1	S
PM32	90	10	13.9	187	50	0.7	1.5	47.2	3	61.7	401	7.2	P
PM33	90	10	13.9	173	50	0.7	2.5	47.2	3	59.6	387	6.9	P
PM34	90	10	13.9	159	50	0.81	3.5	47.2	3	67.4	438	7.9	P
PM41	90	10	13.9	187	50	0.3	1.5	47.3	3	>86.6	>562.6	>10.1	-
PM42	90	10	13.9	187	47	1.2	1.5	47.3	3	49.1	319	5.7	P
PM43	90	10	13.9	187	47	0.7	1.5	47.3	3	71.7	466	8.4	P
PM44	90	5	8.9	187	50	0.3	1.5	47.3	3	73.5	478	13.4	P
PM51	90	5	8.9	187	47	0	1.5	47.3	3	>85.8	>557.4	>15.6	-
PM52	90	5	8.9	187	50	0.3	1.5	47.3	3	59	383	10.7	S
PM53	90	5	8.9	173	50	0.7	2.5	47.3	3	57.4	373	10.4	P
PM54	180	5	12.9	187	47	0.3	1.5	47.3	3	>86.7	>563.2	>11	-
PM61	90	10	13.9	187	50	0.7	1.5	47.4	3	48.6	316	5.7	S/P
PM62	90	5	8.9	187	50	0.7	1.5	47.4	3	45.9	298	8.4	S
PM63	90	10	13.9	173	47	1.2	2.5	47.4	3	48.3	314	5.6	P
PM64	90	10	13.9	187	50	1.2	1.5	47.4	3	41.9	272	4.9	P

[1] $\sigma_{sR,exp} = F_{max}/(\pi \cdot \varnothing^2/4)$

[2] $f_b = F_{max}/(\pi \cdot \varnothing \cdot l_b)$

[3] Note: type of failure mode was determined based on the load-displacement curve

S = spalling failure

P = pull-out failure

- = refers to the maximum values attained in tests stopped after extensive yielding without spalling or pull-out failure
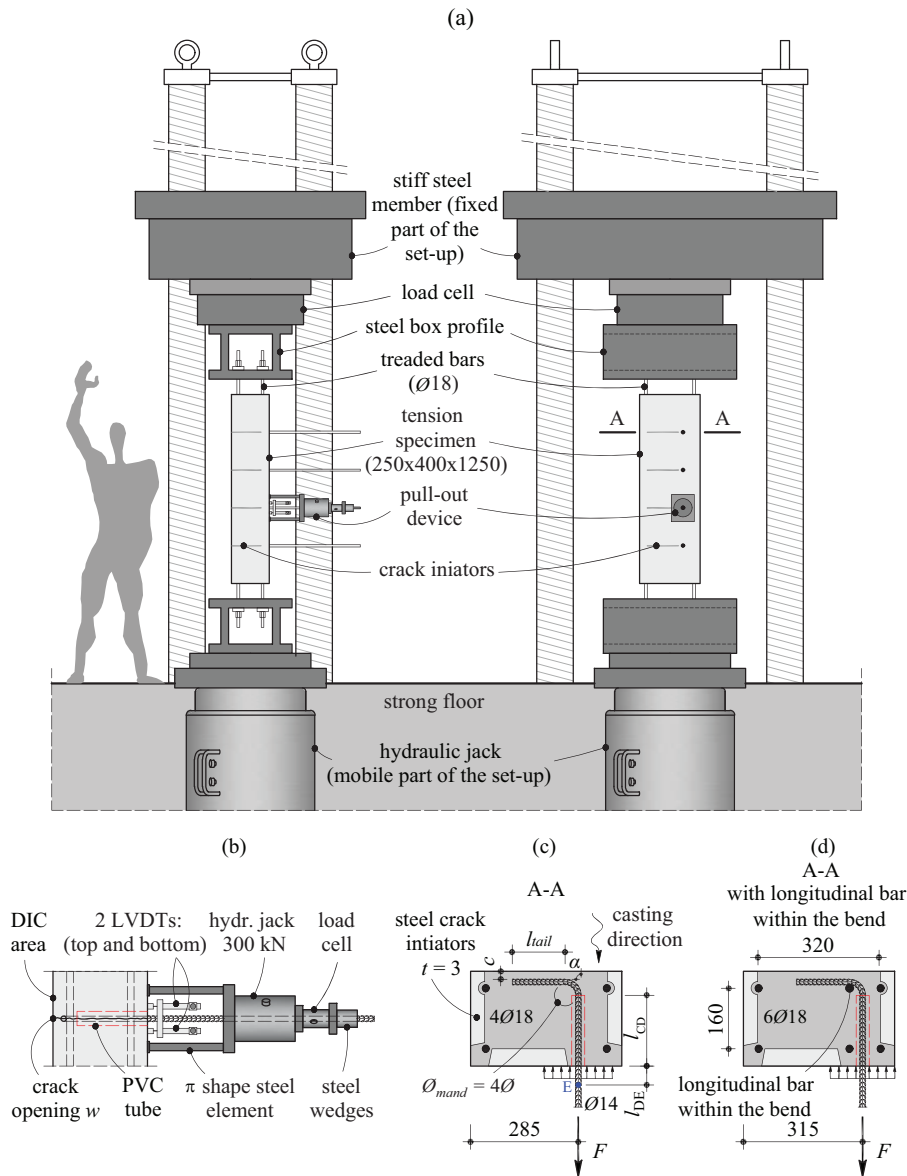
Figure 3.5:   Geometry of specimens and test set-up for the anchorages tested under cracked conditions: (a) test setup; (b) pull-out device; and (c) cross sections of the specimens; and (d) cross sections of the specimens with longitudinal bar within the bend. (points E refers to the points where the displacement δ_E represented in Figure 3.9 is measured, dimensions in [mm]).

3.3.2 Material properties

All specimens were cast from one batch of normal strength concrete (water-to-cement ratio of 0.5; cement content of 300 kg/m^3) and a maximum aggregate size of 16 mm (crushed aggregate). The compressive strength f_c measured on cylinders (height×diameter = 320×160 mm) at the time of testing was 47 MPa on average. Direct tension tests on cylinders 320×160 mm were also performed. For detailed values, refer to Table 3.1.

All specimens were longitudinally reinforced with four or six bars diameter 18 mm (four bars adopted when the detail had no bars within the bend, Figure 3.5c, and six otherwise, see Figure 3.5d). Such longitudinal bars were cold-worked high-strength steel. They had no clear yield plateau to allow for a more progressive cracking after yielding, with a nominal yield strength (0.2 % residual strain) equal to 731 MPa and a tensile strength of 839 MPa. The tested anchorages consisting of 14 mm diameter bars are shown in Figure 3.5c. The cold-worked steel had a yield strength (determined at 0.2 % residual strain) of 513 MPa and a tensile strength of 585 MPa (the stress-strain diagram is shown in Figure 3.6a). Figure 3.6b and c show the rib geometry and the lug arrangement (4 lugs) of the deformed bars. The surface of the 14 mm bar has been laser-scanned to obtain the surface proprieties (according to [FIB00]) such as: bond index f_R (equal to 0.069), average high of the ribs (h_R equal to 0.67 mm), maximum height of the ribs ($h_{R,max}$ equal to 0.86 mm) and spacing between ribs (s_R equal to 7.7 mm in average).
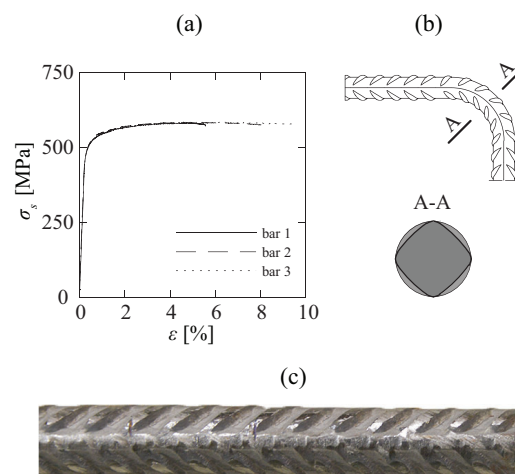
Figure 3.6:   Bar diameter 14 mm for tested anchorages: (a) stress-strain curves for bars diameter 14 mm; (b) position of the lugs; and (c) picture of the bar.

3.3.3 Test set-up and test development

All tests were performed according to the following procedure (for specimens without cracks, step number 2 was skipped):

1. The specimen was arranged in a Schenck-Trebel testing machine (Figure 3.5a);

2. An axial force was applied under displacement control at 0.02 mm/s and 0.01 mm/s until the target crack opening was attained (duration of loading process between 30 and 60 seconds). Four cracks originated at the location of the crack initiators, whose width was tracked by means of Linear Variable Displacement Transformers (LVDTs);

3. When the target crack opening was reached ($w = 0.3$, 0.7 or 1.2 mm), the displacement of the jack was stopped and kept constant. The bars of the anchorages to be tested were then pulled out with an additional jack at a loading rate of 0.5 kN/s (refer to Figure 3.5b).

The crack openings corresponded to stresses in the longitudinal bars of approximatively 300 MPa for $w = 0.3$ mm; 700 MPa for $w = 0.7$ mm and 740 MPa for $w = 1.2$ mm (hardening response). Bond between the straight segments of the tested anchorages and concrete (distance l_{CD} in Figure 3.4) was disabled by means of PVC tubes (allowing contact between the bar and the concrete to occur only along the bent part and the tail region), refer to Figures 3.4 and 3.5b-d.

3.3.4   Measurements

In addition to the LVDTs for tracking crack widths and the axial force measurement, the force of the pull-out jack was measured with a specific load cell and the relative slip between the bars and the concrete surface was measured by means of a LVDTs (refer to Figure 3.5c). As previously stated, Digital Image Correlation (DIC) was also performed on the concrete surface (refer to Figure 3.5b) as well as Fibre-Optical Measurement (FOM) on the rebar surface.

For the DIC, two digital cameras evo4070 (4 megapixels) were used. The size of the speckles painted on the surface varied between 1 and 2 mm and the size of the pixels was 0.27 mm. The image acquisition rate of the cameras was 1 Hz at first loading stages, increased to 10 Hz near to failure. VIC3D software was used to analyse the images [Cor10]. Pictures were taken before running the tests and the measured noise (average between the maximum and minimal displacement values) was around 1/100 of a pixel of the in-plane displacements and about 1/40 of a pixel for the out-of-plane displacements.

Fibre-Optical Measurement (FOM) of the strains based on Rayleigh scattering was performed. The results have been post-processed using the software Odisi-B version by Luna Innovations [Lun13] based on Optical Frequency Domain Reflectometry. This technique allows obtaining a measurement of the strain profiles (up to a strain of approximately 1 %) along the bars with high frequency and low spatial resolution [Bad21, Bra19] (a gage pitch of 0.65 mm was selected). One fibre was glued inside and outside of the bend and tail length allowing to measure both bar elongation and bar flexure (blue and red lines respectively in Figure 3.7a). The 125-µm polyimide optical fibres were installed into two grooves of 2 mm depth along the bar (see Figure 3.7b, same fibre as Chapter 2 and [Mon21, Can20, Mat20]) and were glued to the reinforcement (Figure 3.7c). More details on the technique (installation of fibres, acquisition and processing of data) can be consulted in [Can20].
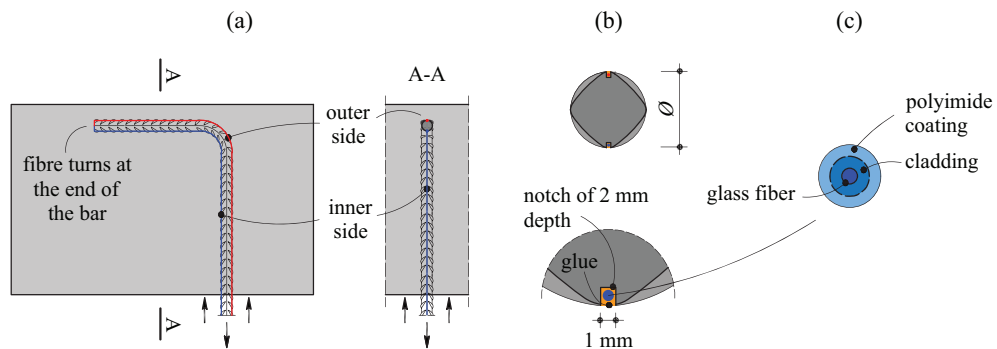
Figure 3.7:   Fibre-Optical Measurement: (a) position of the optical fibres on the bar;
(b) detail of the position of the optical fibre glued to the reinforcement; and
(c) optical fibre detail.

3.3.5   Failure modes

The specimens failed by pull-out (failure mode "P" in Table 3.1) or by spalling of the concrete cover (failure mode "S" in Table 3.1, see Figure 3.8). Some tests were however stopped after extensive plastic/yielding deformations of the reinforcement without any visible spalling signs or pull-out failure ("Y" in Table 3.1). Also, test PM61 failed in a peculiar manner, with spalling of the concrete cover but without any visible out-of-plane movement of the tail region (indicated as "S/P" failure mode in Table 3.1). Figure 3.8 shows the extent of the spalled region after failure generated by the outwards transversal forces applied by the bar.

Figure 3.8:   Picture after failure of specimen PM31 with spalling failure of the concrete cover.

3.3.6   Main experimental results

The main results for this series are shown in Figure 3.9 in terms of load-slip relationship and out-of-plane displacement at peak load as a function of the investigated parameters. The following observations can be made:

- *Influence of concrete cover c*: an increase of the concrete cover led to an increase on the spalling strength. When the crack opening is equal to 0 mm, no spalling failure occurred even for a concrete cover equal to $0.5\varnothing$ for $l_{tail} = 10\varnothing$. For comparable cracked concrete conditions, when the concrete cover is equal or larger than $1.5\varnothing$ for $l_{tail} = 10\varnothing$, an increase of the concrete cover led to an increase on the pull-out strength. The concrete cover had no marked influence on the slip δ_E at the maximum load for spalling failure and pull-out failure. An increase of the concrete cover led to a decrease of the out-of-plane displacement u_{max} at peak load

- *Influence of crack opening w*: an increase of the crack opening led to a decrease of the spalling strength and of the pull-out strength. Specimens with $l_{tail} = 5\varnothing$ failed due to spalling for a concrete cover of $1.5\varnothing$ which show that they were more sensitive to this phenomenon than specimens with $l_{tail} = 10\varnothing$. An increase of the crack opening led to an increase of the slip δ_E and of the out-of-plane displacement u_{max} at peak load for both spalling and pull-out failures

- *Influence of tail length l_{tail}*: an increase of the tail length led to an increase of the spalling strength. In terms of pull-out strength, the comparison between the small and large tail lengths (for a concrete cover equal to $2.5\varnothing$) showed similar performance. No spalling and pull-out occurred in the initially uncracked specimens (blue line in Figure 3.9). An increase of the tail length led to a slight increase of the slip δ_E at peak load for both spalling and pull-out failures, but no marked influence on the out-of-plane displacement u_{max} at peak load.

- *Influence of a longitudinal bar within the bend*: specimens (PM41-PM44) with a longitudinal bar within the bend showed higher resistances (varying between 16 % for $l_{tail} = 10\varnothing$ and 25 % for $l_{tail} = 5\varnothing$) and smaller slips δ_E at peak load, without any marked influence on the out-of-plane displacement u_{max} at peak load.

- *Difference between 90° bends and 180° hooks*: the test with a 180° hook and the comparison test with a 90° bend reached both the yield strength of the bar. At yielding, 90° bends showed less slip δ_E than the 180° hook. No out-of-plane displacement u_{max} was observed for the 180° hook, but about 0.2 mm was measured for the 90° bend at yielding.

Figure 3.9 also shows the post-peak response. After the peak load, all tests exhibited a relatively mild softening response in the case of pull-out failure, whereas for spalling tests, the response was more brittle and a sudden load drop was observed. For the specimens with spalling failures, the residual strength is similar for the different tests because only the curved region contributes to the resistance once the tail region is not active anymore. For the tests with a pull-out failure, the residual strength is also similar for the different tests.
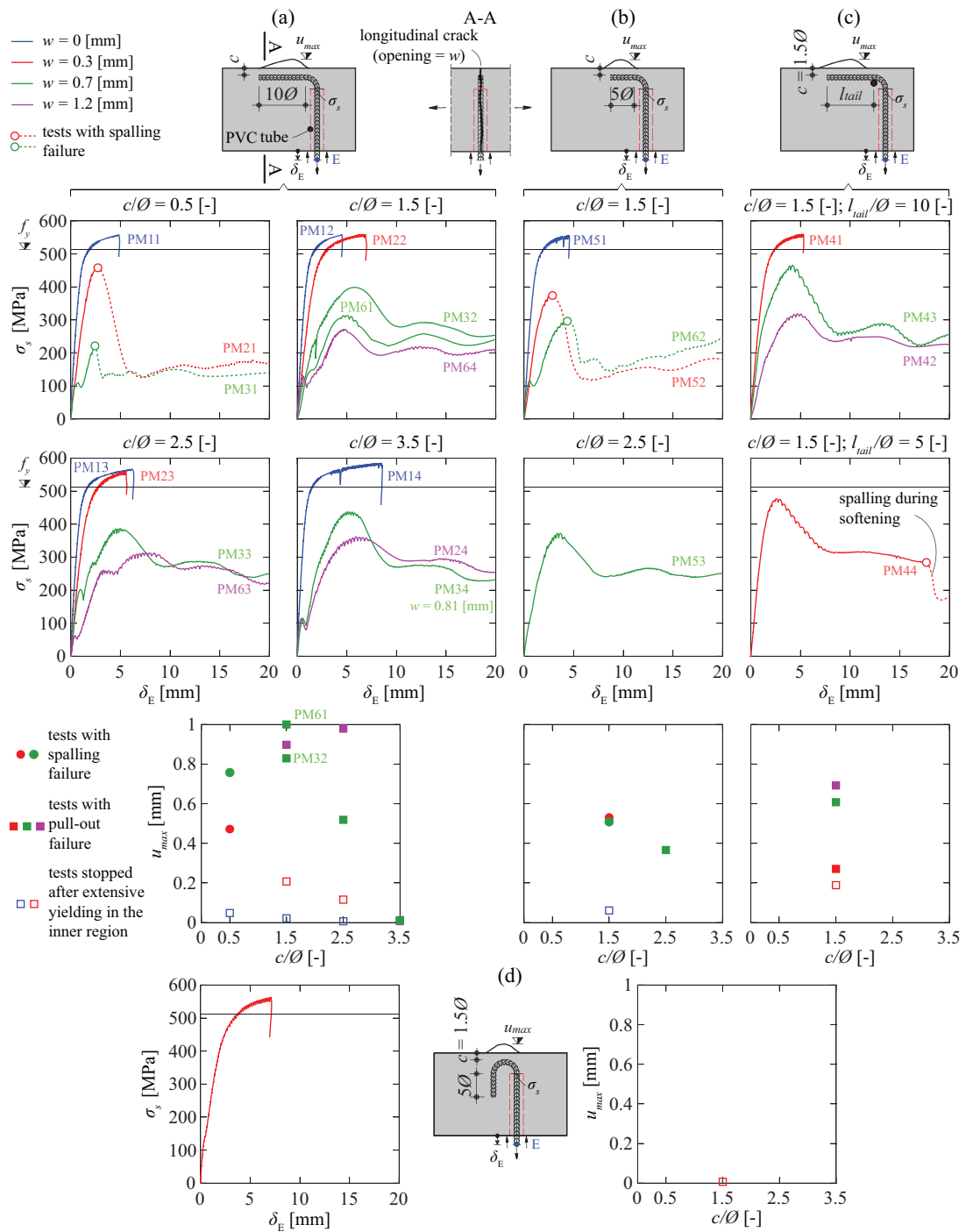
Figure 3.9: Reinforcement stress-slip relationships and influence of the main parameters on the the maximum out-of-plane displacement u_{max}: (a) 90° bends with $l_{tail} = 10Ø$; (b) 90° bends with $l_{tail} = 5Ø$; (c) 90° bends with longitudinal bar within the bend; and (d) 180° hook (δ_E is the displacement of the point E defined in Figure 3.5c measured in the direction of the bar with respect to the concrete surface).

77
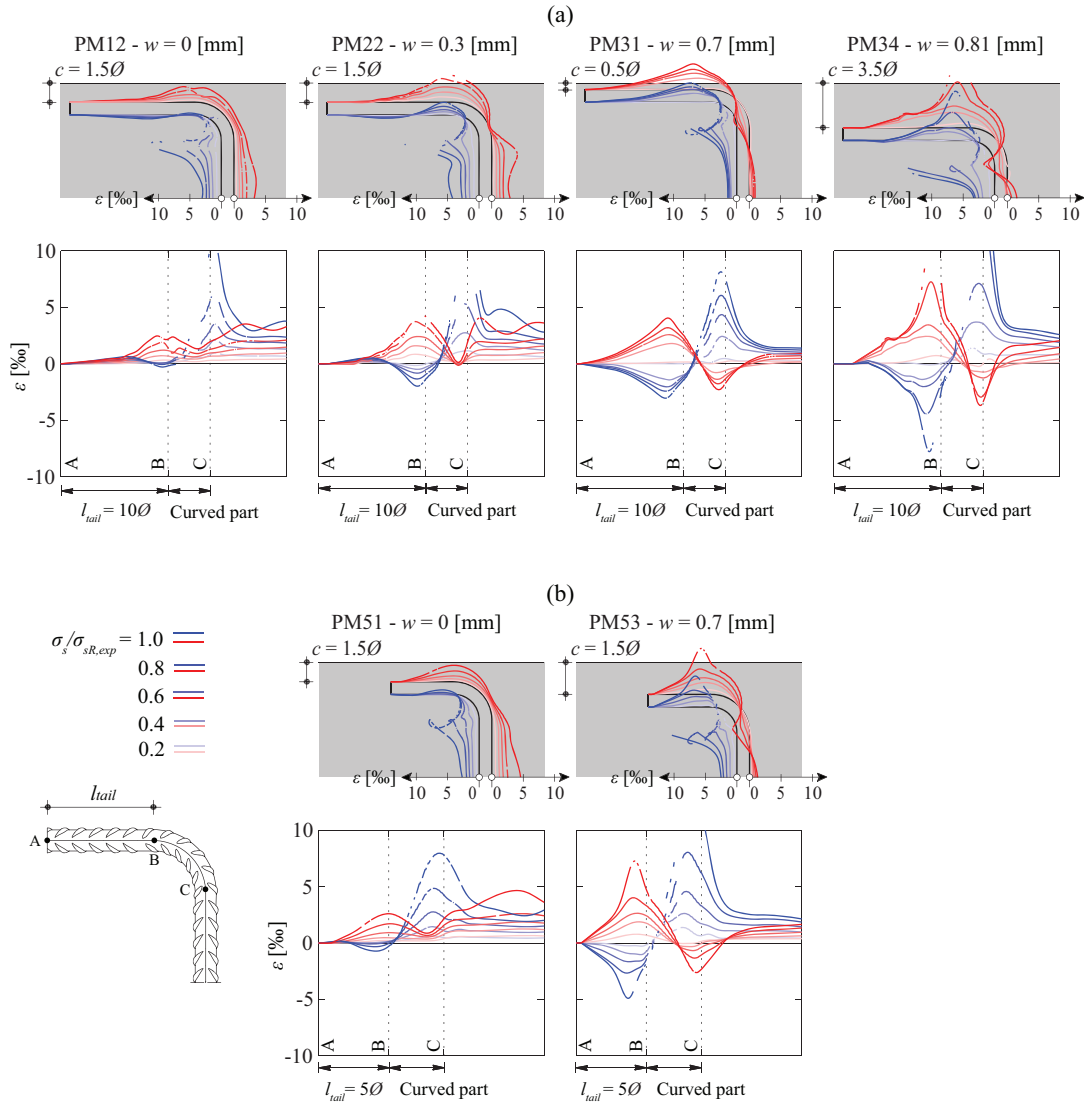
Figure 3.10: Bar strain profiles at different load levels in lateral view and along the bar axis (outer fibres in red, inner fibres in blue) : (a) 90° bend anchorage with $l_{tail} = 10Ø$; and (b) 90° bend anchorage with $l_{tail} = 5Ø$.

Figure 3.10 shows the results of the strain measurements using FOM at selected load levels (20, 40, 60, 80 and 100 % of the peak load) for various specimens. The following observations can be made according to the different regions of the anchorages:

- *tail region:* the measurements show a difference between the strains in the outer and inner fibres of the bar, indicating bending of the bar (a fact already pointed out by Shima [Shi08]). This is clearly confirmed by the measurement of compressive strains in the inner fibre of the bar near to the point B (clamping of the tail, refer to Figure 3.4b for location), despite the fact that the bar is subjected to a tensile force. An increase of the crack opening (refer to PM12 and PM22 as well as to PM51 and PM53) led to an

78

increase of bar strains. A decrease of the tail length (refer to PM12 and PM51) had no clear influence on the strains at the beginning of the tail length. An increase of the concrete cover (refer to PM31 and PM34) led to an increase of bar strains.

- *curved region:* the response shows a difference between the outer and inner strains also in the bend region and variations along the bar which indicate potential bending of the bar. This is clearly confirmed by the measurements where compressive outer strains are present at the point C (refer to Figure 3.4b for location) despite the fact that the bar was subjected to a tensile force. At point C, localized peaks of strain can also be observed, which can be attributed to the local change of geometry of the bar (peaks increasing for increasing levels of load). An increase of the crack opening (PM12 compared to PM22 and PM51 compared to PM53) as well as an increase of the concrete cover (difference between PM31 and PM34) led to an increase of bar strains.

- *inner region (unbonded region):* the deformations are also different between the outer and the inner fibre, indicating that this region is subjected to some level of bending near to the curved region (this effect can be explained by the slip of the curved region which is associated to a restrained rotation of the inner region).

The consequences of a spalling failure on the strain profiles are shown in Figure 3.11 with respect to test PM31, where the profiles of strains are plotted at peak load and after spalling ($\sigma_s/\sigma_{sR,exp} = 0.56$). As it can be noted, after the concrete cover spalls, the tail region experiences almost no strains anymore since the contact with the surrounding concrete is lost. However, in the curved part, the strains increase showing an additional flexure of the bar near to point C. In addition, also the increased bending at point C due to the additional bar sliding after spalling can be clearly observed.
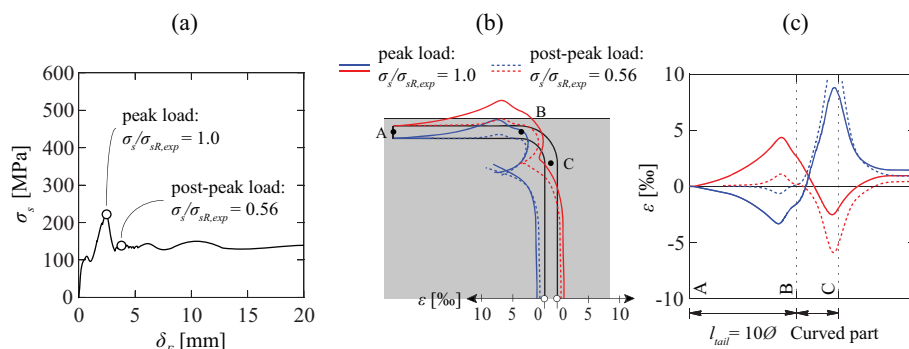
Figure 3.11:   Response of test PM31: (a) load level at failure and post-peak level investigated; and (b,c) strain profiles along the bar axis (outer fibres in red, inner fibres in blue).
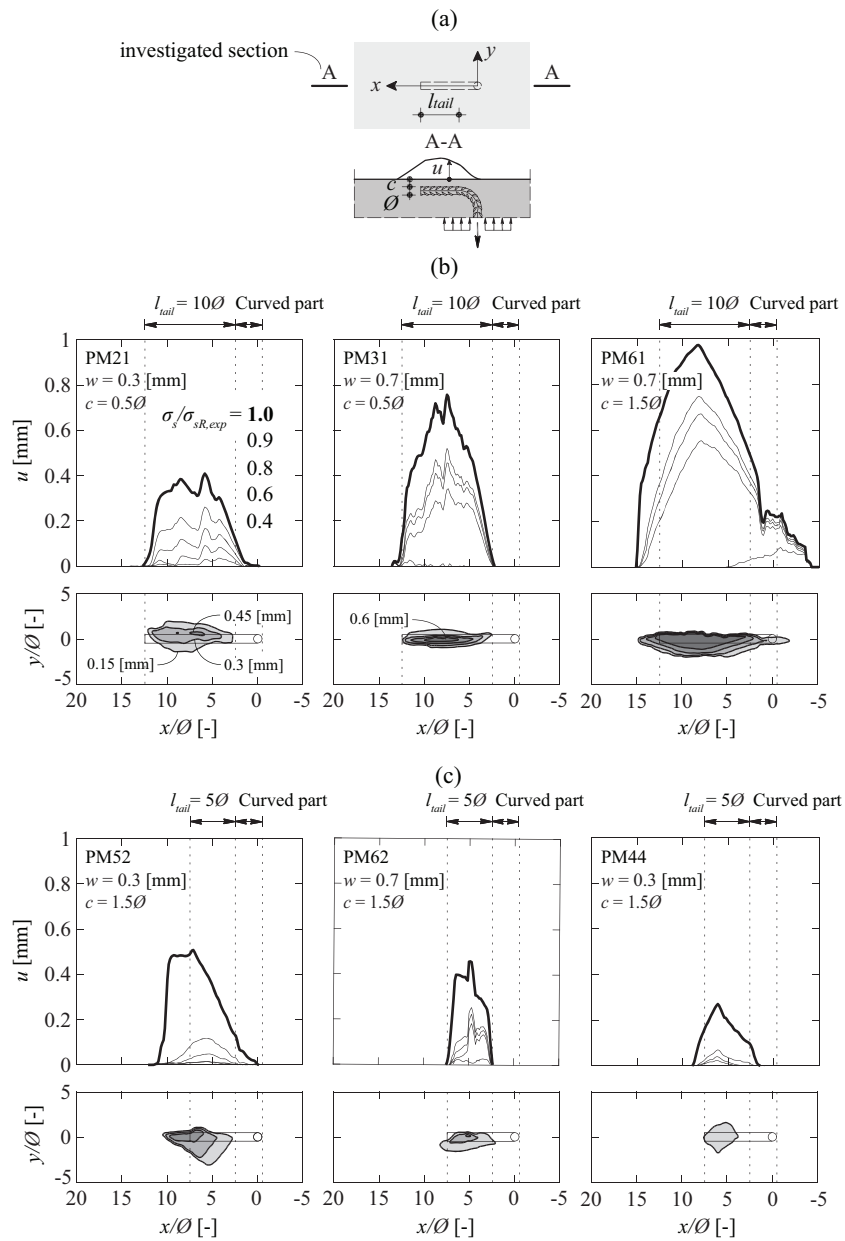
Figure 3.12:   Out-of-plane displacements along the longitudinal axis of the bar for different load levels: (a) definitions and notation; (b) 90° bend hook anchorage with $l_{tail} = 10\varnothing$; and (b) 90° bend hook anchorage with $l_{tail} = 5\varnothing$.

Figure 3.12 provides details on the out-of-plane displacements u (see Figure 3.12a for definitions) for specimens with spalling failure at selected load levels (40, 60, 80, 90 and 100 % of the peak load). As it can be noted, the area influenced by out-of-plane displacements (associated to spalling of the cover) increases for larger values of the concrete cover. The imposed crack opening (crack in the bending plane) seems on the other hand to have a limited influence on size of this area. The area influenced by spalling mainly develops along the bar, but for specimens with smaller tail length ($l_{tail} = 5\varnothing$, Figure 3.12c), the development in transversal direction is more pronounced. It is also interesting to note that the maximum out-of-plane displacement occurs in all cases at a distance about $2\varnothing$ to $5\varnothing$ from point B (somewhat higher values for larger tail lengths). Also, the distribution of out-of-plane deformations show that before 40 % of peak load, almost no out-of-plane deformation could be observed. The deformations develop thereafter rapidly, and for cases with $l_{tail} = 5\varnothing$, more than half of the final out-of-plane displacement developed between 90 and 100 % of peak load.

3.4   Discussion of test results

Based on the strain measurements performed by FOM, it is possible to estimate the internal forces in the reinforcement and the contact forces between the reinforcement and the surrounding concrete. To that aim, it should be noted that, in the curved region, the assumption that plane sections remain plane leads to a nonlinear distribution of strains. This fact, with relevant effects for small mandrel diameters, was acknowledged by Winkler [Win58] and Bach [Bac89]. Detailed consideration of the curvature of the bar and its effect on the calculation of the strain and stress profiles and internal forces of the bar are given in Chapter 2, Appendix 2.A. Based on equilibrium conditions, average axial stresses and bond stresses can also be calculated.

Figure 3.13 and 14 show the results of such analysis at selected load levels (20, 40, 60, 80 and 100 % of the maximum load). To that aim, the average bond stresses over the bar perimeter can be calculated by derivative of the average axial stresses (axial force divided by bar area) based on equilibrium condition:

$$\tau_b = \frac{d\sigma_s}{ds} \frac{\varnothing}{4} \tag{3.1}$$
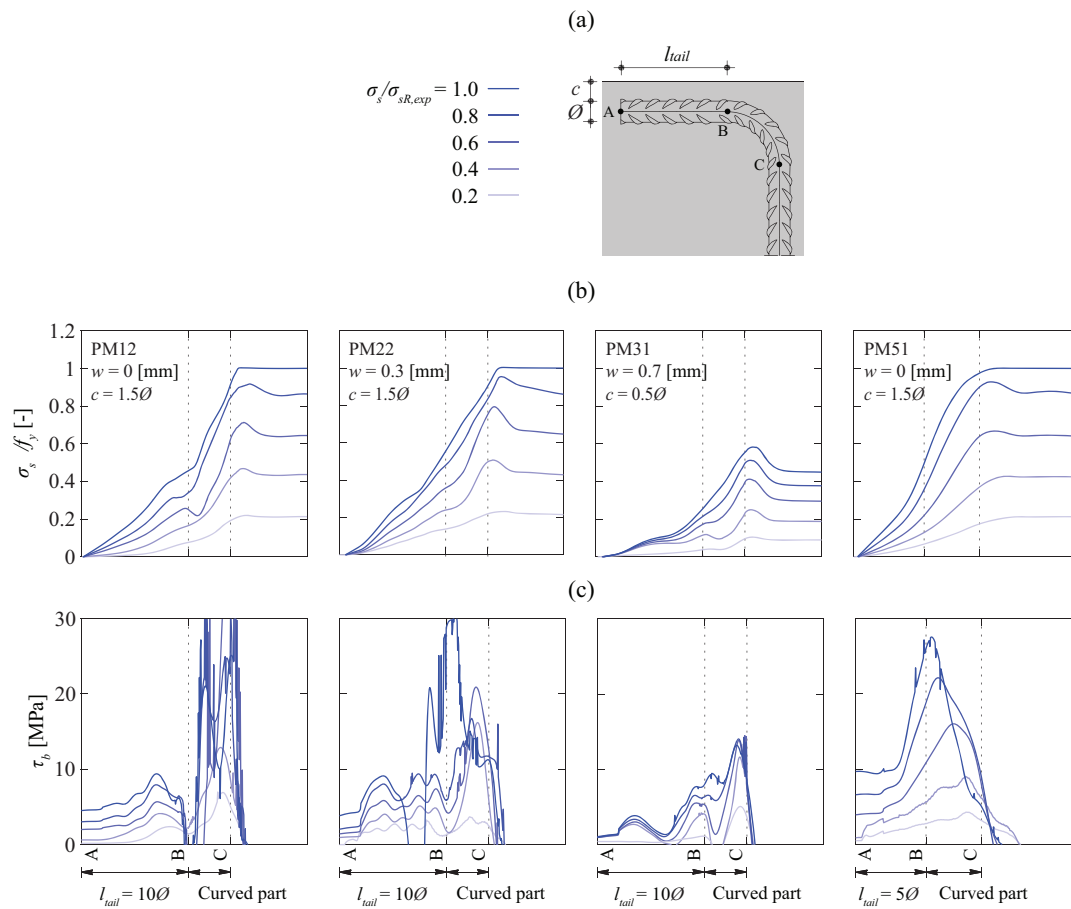
Figure 3.13:   Bond response of the bent detail: (a) definitions and notation; (b) calculated average axial stresses; and (c) calculated bond stress.

Figure 3.13b shows the calculated average axial tensile stresses and Figure 3.13c shows the corresponding average bond stresses along the bar axis. As it can be noted, (i) the average axial stress is higher in the curved region than in the tail region (consistently with the results of Shima [Shi08]); (ii) in the tail region, the average bond stress is higher for smaller tail lengths (refer to Figure 3.13c) and (iii) the distribution of bond stresses is relatively constant in each region.

In fact, the tail region behaves similarly to a cantilever beam, with a parabolic shape of the bending moments for $l_{tail} = 10Ø$ and a more linear shape for $l_{tail} = 5Ø$. The latter response is associated to the application of a significant point force acting at the beginning of the tail length (point A) and the former to a more distributed load. Both cases lead interestingly to a similar location of the resultant of forces acting perpendicular to the bar.
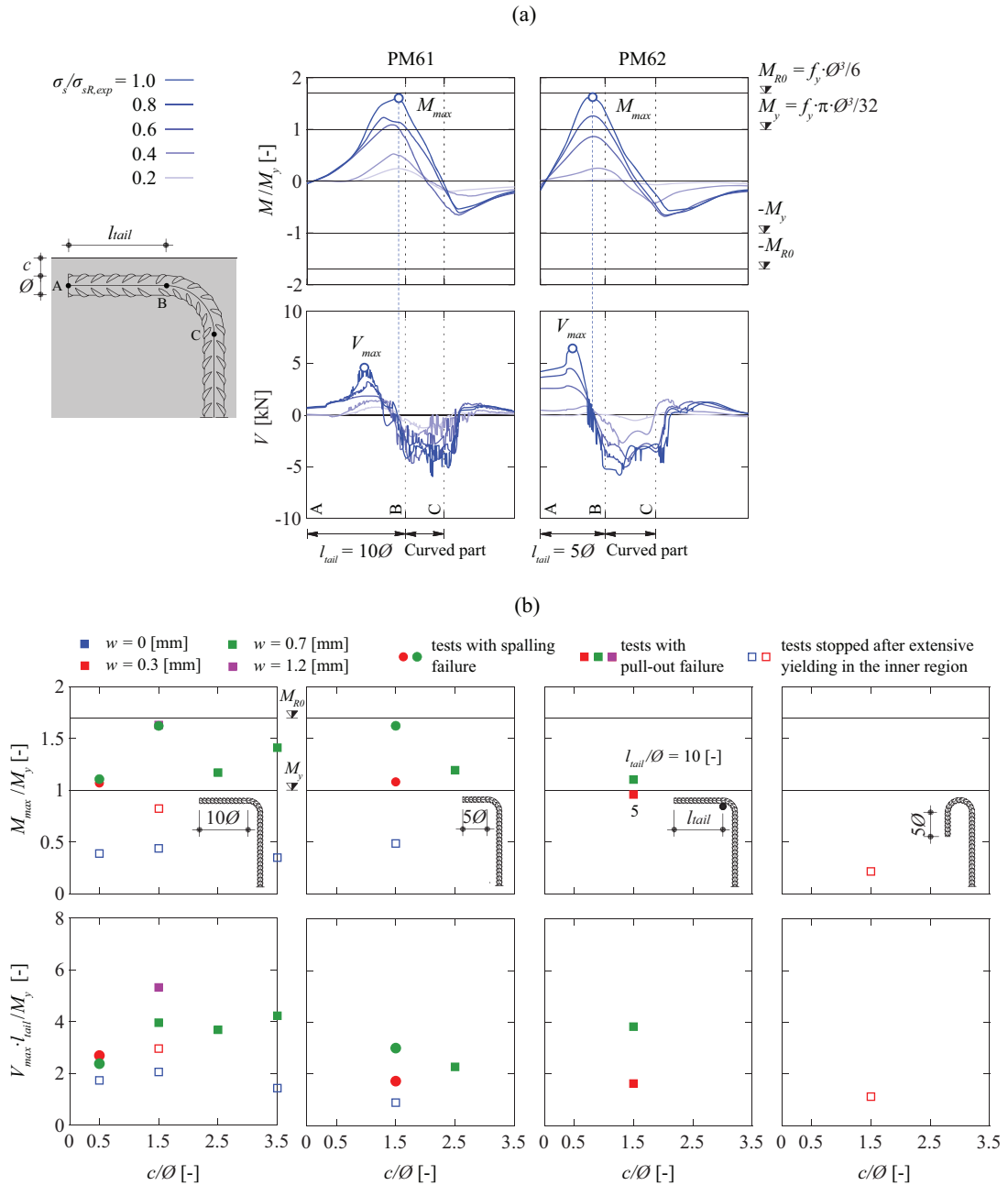
Figure 3.14:   FOM analysis of the bars: (a) calculated bending moments and shear forces; (b) maximum bending moments and shear forces in the tail region (M_y is is the yield moment calculated assuming elastic behaviour neglecting the influence of the axial force).

Figure 3.14 shows the calculated bending moments and shear forces in the bar (consistently with the methodology detailed in Chapter 2, Appendix 2.A). The results show high values of the bending moments, reaching potentially the yield strength of the bar (as previously considered

by Minor [Min75]), near to the end of the tail region (at a distance between 0 and $\varnothing$ from point B, see Figure 3.14a).

Figure 3.14b shows the maximum bending moment M_{max} and the maximum shear force V_{max} (defined in Figure 3.14a). The yield moment M_y (moment at which one fibre of the bar reaches the yield strength) is exceeded for all tests failing by spalling or bond resistance. The values are in some cases very close to the plastic resistance M_{R0} (calculated for the case without axial force, with half of the cross section yielding in tension and the other half yielding in compression). With respect to V_{max}, it increases with the concrete cover (up to $c/\varnothing \approx 1.5$, approximately constant for higher $c/\varnothing$ ratios).

Bending moments are also observed between the curved and the inner region (near to point C). As described above, this flexure results from the rotation of the curved region (associated to bond slip) constrained by the inner region.

3.5 Influence of deformation capacity of bends and hooks on anchorage performance

Figure 3.15 shows the reinforcement stress-slip relationships for 90° bends (selected specimens presented in this chapter, Figure 3.15a) and also for straight bars between points C and D which are assumed to behave as the straight anchorages with a bond length equal to $10\varnothing$ tested by Brantschen et al. [Bra16] (Figure 3.15b). The slip shown in Figure 3.15a is the one at point C, in order to have a direct comparison with the slip of straight bars (such slip is calculated for bent bars from the measurement of the LVDTs at point E by removing the deformation of the bar in the unbonded area). As it can be noted, the behaviour of straight bars is stiffer and therefore, the peak force is reached at significantly lower slips than for 90° bends.

A consequence of such difference in the required level of slip to activate the maximum force, together with the softening response in the post-peak regime, is that the peak force of both the tail and curved region cannot be directly summed to the resistance provided by the inner (straight) part. Such phenomenon is potentially more relevant for larger crack widths and longer tail lengths (associated to higher displacements at peak load). In these cases, only a fraction of the maximum anchorage capacity of the bend can be summed to the anchorage capacity of the inner region (or a suitable reduction of the bond strength shall be considered [Mar98]). In the cases investigated experimentally (Figure 3.15), this effect seems to play a limited role for crack widths up to 0.2 mm (corresponding typically to crack widths at SLS).
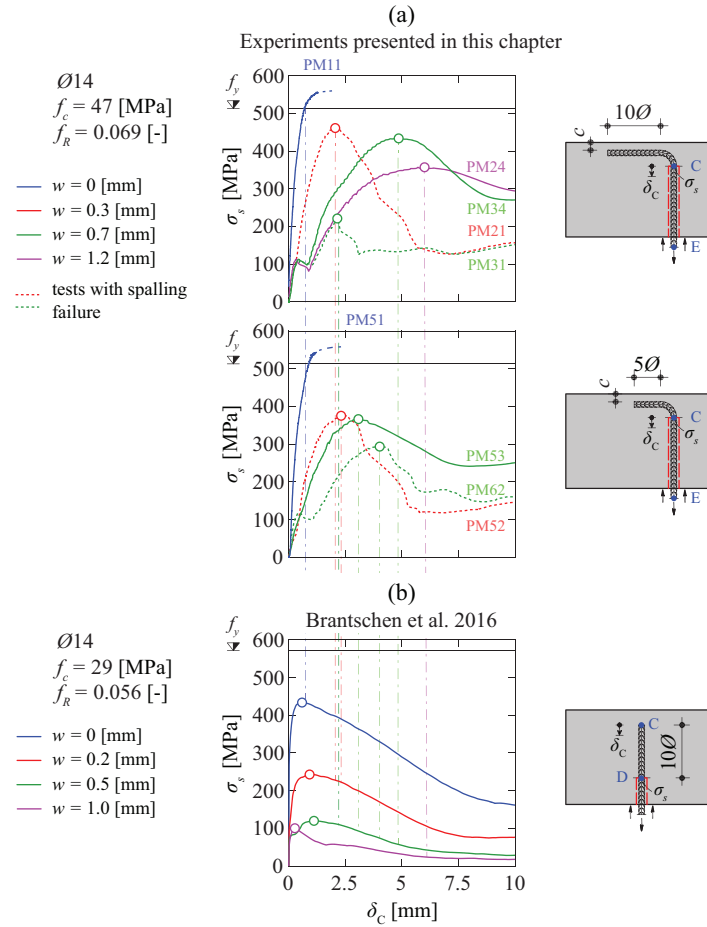
Figure 3.15:   Displacement compatibity between 90° bends and straight bar in term of reinforcement stress-slip relationships for: (a) selected specimens presented in this chapter; and (b) specimens of Brantschen et al. [Bra16].

3.6   A mechanical model and design considerations for the anchorage resistance of bends and hooks

3.6.1   Main assumptions

On the basis of the observations of the experimental programme described above, a number of assumptions will be adopted in order to establish a mechanical model to predict the anchorage resistance of bends and hooks and to account for the interaction between the different regions:

- the response of a bend will be divided into three regions (refer to Figure 3.2a): the tail region between the points A and B, the curved region between the points B and C and

85

the inner region between the points C and D (in the present experimental programme, the contribution of the inner region has been disregarded since the bond was disabled by means of a PVC tube).

- the anchorage resistance is limited by yielding of the reinforcement or by the sum of the pull-out strength of the three regions (tail, curved and straight regions, the latter with a potential reduction to account for its stiffer response followed by a softening phase as previously explained). In addition, the capacity of the tail region can also be limited by a spalling failure when the concrete cover c is small (Figure 3.9). Other potential local failure modes will be discussed later.

- the considered forces acting on the anchorage are presented in Figure 3.16. They comprise bond forces acting in all regions, deviation forces acting on the curved region and uplift forces acting in the tail region. They all contribute to the anchorage capacity F_{sR} (Figure 3.16).

- bond forces arise from the contact between steel and the surrounding concrete associated to bar slip, due to contact of lugs and, additionally, to friction in case of acting transversal forces.

- on the basis of the FOM readings (Figure 3.13c), the distribution of bond stresses is assumed to be constant in the tail and curved regions (τ_{tail} and τ_{curved} in Figure 3.16).

- in the curved and in the tail region, transversal forces are originated by deviation forces (p in Figure 3.16) and by uplift forces (σ_V in Figure 3.16). They can increase bond stresses due to the enhanced friction, that will be considered assuming a friction coefficient equal to $\mu = 0.4$.

- in the tail region, transversal forces originate a lever effect, potentially leading to spalling of the concrete cover. The resultant of these forces (V_{max} and a reaction R_M indicated in Figure 3.16) can be clearly observed in the interpretation of the FOM readings (Figure 3.14a) and can limit the bond strength in that region. These forces can be estimated assuming the development of a plastic hinge at a distance l_M from point B in Figure 3.4b (this assumption is consistent with the strain profiles recorded in Figure 3.10 and the bending moment calculated in Figure 3.14a). The moment in the plastic hinge (assumed to correspond to 95 % of the flexural plastic resistance to account for the interaction with the axial force in the reinforcement) is equilibrated by a force V_{max} applied at a distance l_V and the related reaction R_M distributed over the length l_M ($l_V \approx 3\varnothing$ as well as $l_M \approx 0$ can be assumed for typical properties of structural concrete in accordance with the out-of-plane displacement and the FOM results, see Figures 3.12 and 3.14a, respectively). For the case of large concrete cover with governing pull-out failure (without spalling), the transversal forces associated to the lever effect can enhance the bond strength by friction.

In the following, the different contributions will be described in detail.
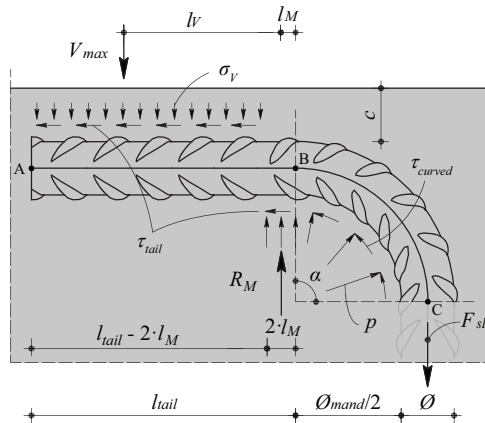
Figure 3.16:   Definition of the geometrical parameters and all forces acting on the anchorage.

3.6.2   Inner region

In this region, the response of the bar is governed by bond conditions, as for conventional straight reinforcement. Figure 3.17a shows the bond stresses in the inner region with the assumed constant distribution. Such bond stress is adapted from the Tension Chord Model [Mar98] (considering a reduced bond strength to account for potential redistributions of stresses, consistently with the observations stated in section 3.5), but accounting for the detrimental influence on bond of longitudinal cracking [Bra16] and of casting effects:

$$\tau_{inner} = \tau_b = \eta_{cp} \cdot k_b \cdot 0.6 \cdot f_c^{2/3} \tag{3.2}$$

Where f_c is the concrete compressive strength, η_{cp} is the coefficient accounting for casting effects on bond conditions ($\eta_{cp} = 1.2$ for good conditions and $\eta_{cp} = 1$ for poor conditions according to its usual definition in codes of practice [Eur04, FIB13] as well as Moccia et al. [Moc21, Moc21a]) and k_b is a coefficient accounting for the influence of cracking parallel to the reinforcement by reducing the contact area [Bra16] (refer to Figure 3.17b).

$$k_b = \cfrac{1}{1 + \cfrac{0.75 \cdot \eta_l}{f_R} \cfrac{w}{\varnothing}} \tag{3.3}$$

Where η_l is the number of lugs per rib [Bra16], f_R is the bond index and w is the crack opening.
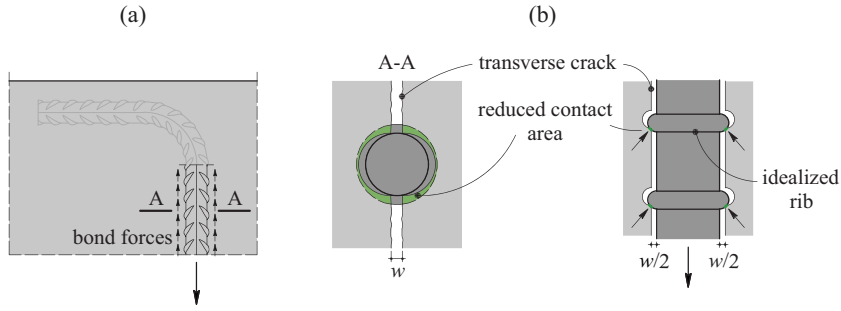
Figure 3.17: Response of the inner part of the bar: (a) bond forces acting in this region; and (b) influence of the transverse crack.

3.6.3 Tail region

The average bond stress in the tail region (τ_{tail}) can be estimated on the basis of the works by [Moc21a] (based on the model by Tepfers [Tep73]) for the activation of bond stresses when a bar is located near to a free surface (τ_b). Such bond stresses might be limited by the spalling failure of the concrete cover ($\tau_b \leq \tau_{tail,spall}$), otherwise (in case of pull-out failures), they are enhanced by the friction between the steel and the concrete upon application of the uplift force ($\tau_{tail,friction}$). A complete derivation of the resulting Equations is presented in Appendix 3.A. Its main expressions are provided below for the bond strength of the tail region τ_{tail}:

$$\tau_{tail} = \min\left(\tau_b; \tau_{tail,spall}\right) + \tau_{tail,friction}$$

$$\tau_{tail} = \min\left(\eta_{cp} \cdot k_b \cdot 0.6 \cdot f_c^{2/3}; \tau_{tail,spall}\right) + \mu \cdot \frac{V_{max} + R_M}{\pi \cdot \varnothing \cdot l_{tail}}$$

(3.4)

where V_{max} and R_M are the transversal forces, determined by equilibrium considerations:

$$V_{max} = \frac{0.95}{6} \cdot \frac{\varnothing}{l_V} f_y \cdot \varnothing^2 \leq 2.65 \cdot f_{ct,eff} \cdot l_{tail} \cdot \varnothing \cdot \left(\frac{c}{\varnothing} + \frac{1}{2}\right)$$

$$\leq 0.8 \cdot \eta_{is} \cdot \eta_{ct} \cdot f_c^{2/3} \cdot l_{tail} \cdot \varnothing \cdot \left(\frac{c}{\varnothing} + \frac{1}{2}\right)$$

(3.5)

$$R_M = V_{max}\left(1 + \sin\alpha \cdot \frac{\dfrac{l_V}{\varnothing}}{\dfrac{1 - \cos\alpha}{2} \cdot \left(\dfrac{\varnothing_{mand}}{\varnothing} + 1\right)}\right)$$

and l_V is the distance of the force V_{max} from the plastic hinge ($l_V \approx 3\varnothing \leq l_{tail}$). The bond spalling strength $\tau_{tail,spall}$ is estimated on the basis of [Moc21a]:

$$\tau_{tail,spall} = 1.04 \cdot \left(\eta_{is} \cdot \eta_{ct} \cdot 0.3 \cdot f_c^{2/3}\left(\frac{c}{\varnothing} + \frac{1}{2}\right) - 0.37\frac{V_{max}}{\varnothing^2}\frac{\varnothing}{l_{tail}}\right)\left(\frac{d_{dg}}{1.6\varnothing}\right)^{1/3} + \eta_{is} \cdot 2.34 \text{ MPa}$$

(3.6)

where $f_{ct,eff}$ is the effective tensile strength ($f_{ct,eff} = \eta_{is} \cdot \eta_{ct} \cdot f_{ct}$), η_{is} is a strength reduction factor to account for the casting position effect ($\eta_{is} = 1$ for good bond conditions and $\eta_{is} = 0.6$ for poor bond conditions according to its usual definition in codes of practice [Eur04, FIB13] as well as Moccia et al. [Moc21, Moc21a]), η_{ct} is a coefficient accounting for the concrete brittleness in tension equal to 0.8 (value valid for concrete strengths up to 50 MPa according to [Fer10]) and f_{ct} is the concrete tensile strength (approximated with $0.3 \cdot f_c^{2/3}$). The parameter d_{dg} accounts for the maximum aggregate size (d_g) [Eur21, Cav18], and can be calculated as $d_{dg} = \min(40 \text{ mm}, 16 \text{ mm} + d_g)$ for $f_c \leq 60$ MPa and $d_{dg} = \min(40 \text{ mm}, 16 \text{ mm} + d_g (60/f_c)^4)$ for $f_c > 60$ MPa.

Figure 3.18 shows the comparison between the bond stresses calculated with Eq. (3.4) and the average values of the bond stress measured in the tail region of the bar during the tests. As it can be noted, a reasonable agreement is found both in terms of trends and average values.
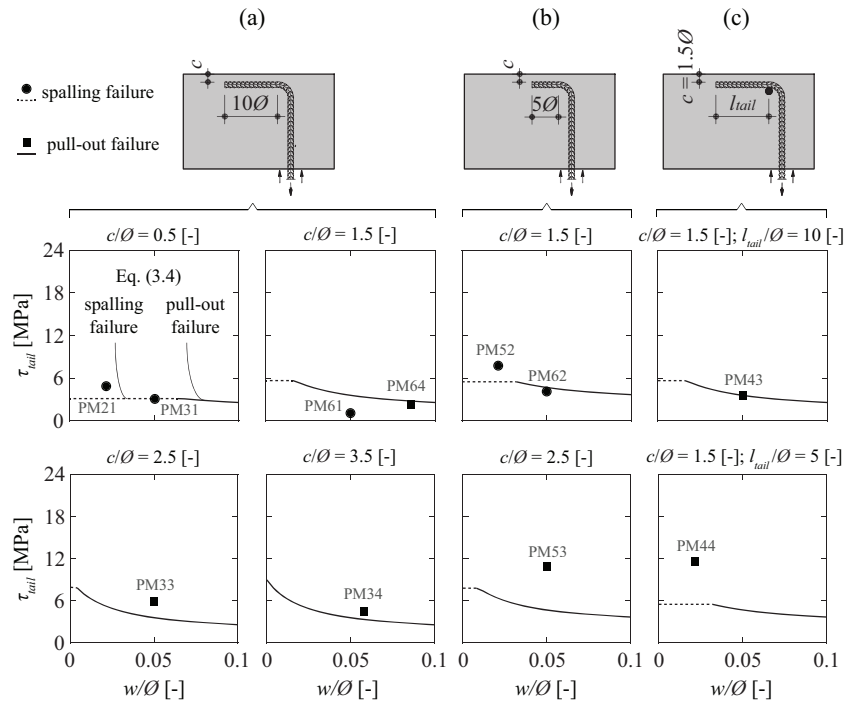
Figure 3.18: Bond stresses in the tail region measured and calculated according to Eq. (3.4): (a) for $l_{tail} = 10\emptyset$; (b) for $l_{tail} = 5\emptyset$; and (c) for tests with longitudinal bar within the bend.

3.6.4 Curved region

As for the curved region, the average bond stress (τ_{curved}) can be calculated on the basis of the rib engagement (τ_b) and additional friction related to the deviation forces ($\tau_{curved,friction}$). The complete derivation of the model is presented in Appendix 3.A, resulting into:

$$\tau_{curved} = \tau_b + \tau_{curved, friction}$$

$$\tau_{curved} = \tau_b + \frac{2 \cdot \tau_{tail} \cdot \dfrac{l_{tail}}{\varnothing_{mand}} + \tau_b \cdot \dfrac{\alpha}{2}}{2.5 - \dfrac{\alpha}{2}} = \eta_{cp} \cdot k_b \cdot 0.6 f_c^{2/3} + \frac{2 \cdot \tau_{tail} \cdot \dfrac{l_{tail}}{\varnothing_{mand}} + \eta_{cp} \cdot k_b \cdot 0.6 f_c^{2/3} \cdot \dfrac{\alpha}{2}}{2.5 - \dfrac{\alpha}{2}} \quad (3.7)$$

For the curved region, it is assumed that sufficient lateral cover is provided (so that spalling failures do not govern, see Chapter 2), but the compressive stress originated by the deviation forces requires to be verified (contact pressure between the bar and concrete lower than the confined strength of concrete):

$$\sigma_c = \frac{p_{avg}}{\varnothing} \le f_{c3} \tag{3.8}$$

where p_{avg} refers to the average deviation forces (see Appendix 3.A) and f_{c3} refers to the confined compressive strength. As shown in Chapter 2, inside reinforcement bends, f_{c3} can reach values up to 3 to 6 times f_c (for $\alpha = 180°$ and $45°$ respectively). Figure 3.19 shows the comparison between the bond stresses calculated with Eq. (3.7) and the average values measured during the tests in the curved region of the bar. Consistent agreement is again found, both in terms of trend and values.
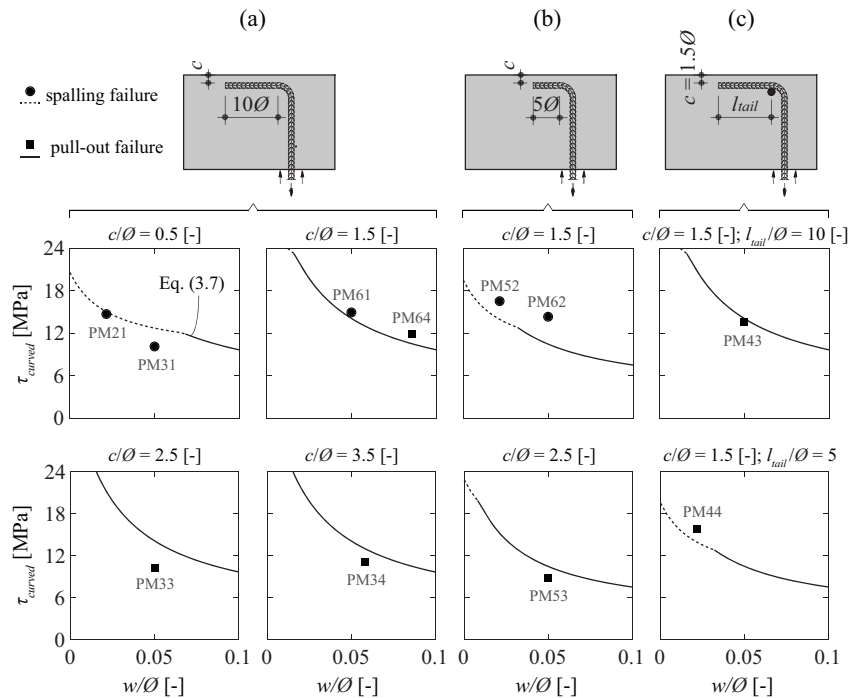
Figure 3.19: Bond stresses in the curved region measured and calculated according to Eq. (3.7): (a) for $l_{tail} = 10\varnothing$; (b) for $l_{tail} = 5\varnothing$; and (c) for tests with longitudinal bar within the bend.

3.6.5   Calculation of anchorage resistance of tail and curved regions

The force that can be developed in the bar at the point C can be determined on the basis of the equilibrium conditions of the tail and curved regions:

$$F_{sR} = F_{s,tail} + F_{s,curved} + F_{s,M} \tag{3.9}$$

where $F_{s,tail}$, $F_{s,curved}$ and $F_{s,M}$ are the different contributions of the anchorage force of the tail region, of the curved region and of the lever effect of the uplift force, respectively. The contribution of the tail region $F_{s,tail}$ can be determined by integration of the bond stress on this region as well as the associated deviation forces for the general case of a bending angle α (refer to Appendix 3.B for development):

$$F_{s,tail} = \pi \cdot \varnothing \cdot \tau_{tail} \cdot l_{tail} \tag{3.10}$$

The contribution of the curved region $F_{s,curved}$ is determined by integration of its bond stress and deviation forces (refer to Appendix 3.B):

$$F_{s,curved} = \pi \cdot \varnothing \cdot \tau_{curved} \cdot \varnothing_{mand} \cdot \left(\sin\alpha - \frac{\alpha}{2} \cdot \cos\alpha \right) \tag{3.11}$$

The contribution of the lever effect of the uplift force $F_{s,M}$ is given in Appendix 3.A, Eq. (3.A.8). Finally, by substituting Eqs. (3.10, 3.11) and (3.A.8) into Eq. (3.9), the following expression results for the anchorage capacity accounting for each contribution (refer to Figure 3.16 for definition of geometric parameters):

$$\sigma_{sR} = \tau_{tail} \frac{4l_{tail}}{\varnothing} + \tau_{curved} \frac{4\varnothing_{mand}}{\varnothing} \left(\sin\alpha - \frac{\alpha}{2}\cos\alpha \right) + \frac{4 \cdot V_{max}}{\pi \cdot \varnothing^2} \frac{\dfrac{l_V}{\varnothing}}{\dfrac{1 - \cos\alpha}{2}\left(\dfrac{\varnothing_{mand}}{\varnothing} + 1 \right)} \tag{3.12}$$

Figure 3.20a shows the results of Eq. (3.12) for typical cases. As it can be noted, the results are fairly sensitive to the length of the tail and its cover, the mandrel diameter of the curved region and, particularly, to the opening of the cracks developing at the plane of the anchorage. The different contribution of σ_{sR} are shown in Figure 3.20b. These diagrams show that the contribution to the anchorage of the uplift forces is significant only for large crack openings and small tail lengths.
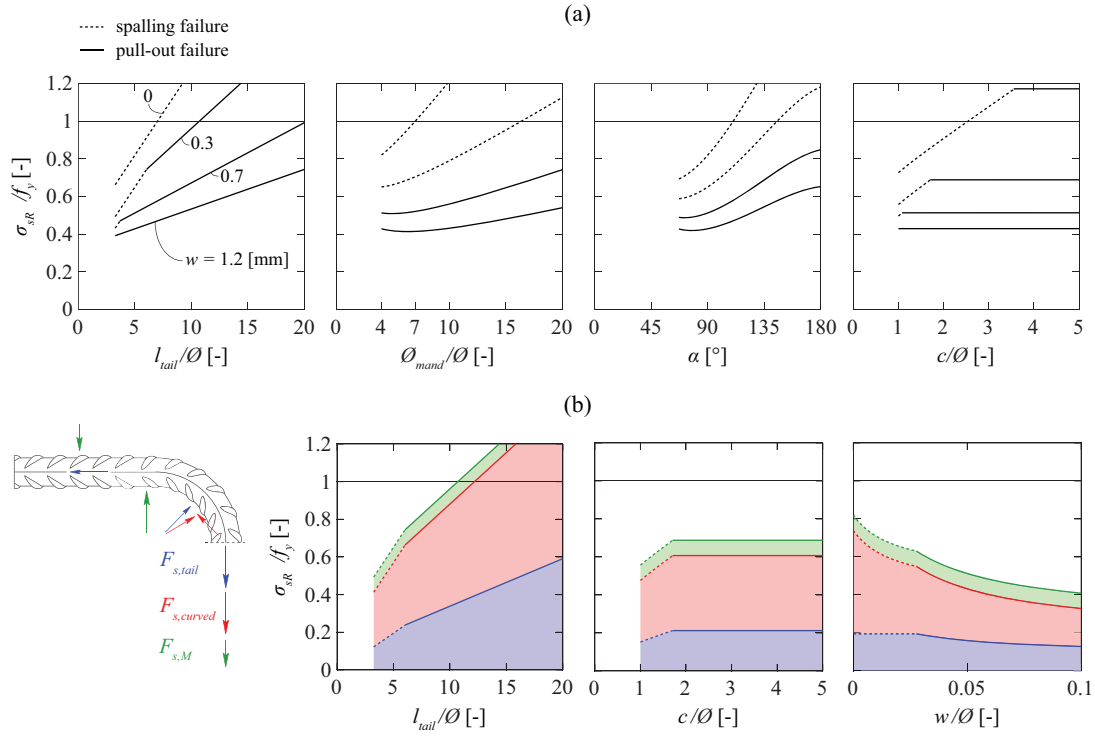
Figure 3.20:   Results of the model: (a) Eq. (3.12) as a function of different parameters; and (b) results of Eq. (3.12) showing the different contributions of the anchorage in case of a crack opening $w = 0.3$ [mm]. (Parameters used: poor bond conditions; $\varnothing14$; $d_g = 16$ [mm]; $\eta_l = 4$; $l_{tail} = 5\varnothing$; $\varnothing_{mand} = 4\varnothing$; $\alpha = 90$ [°]; $c = 1.5\varnothing$; $f_c = 38$ [MPa]; $f_y = 500$ [MPa]; $f_R = 0.056$).

It shall be noted that the potentially beneficial influence of a longitudinal bar within the bend in the anchorage of the detail is not considered in the above expressions. In absence of a refined approach, adopting a constant enhancement factor seems a reasonable consideration. According to the test results of the present experimental programme (refer to tests PM41-PM44 and Figure 3.9c), such a factor can be assumed equal to 1.10 in case the diameter of the bar within the bend is larger than the diameter of the bends/hooks.

Finally, it can be noted that Eq. (3.12) can be rewritten in a compact manner for typical cases, when $l_{tail} \geq l_V$ and $f_y/f_{ct,eff} \leq 75 \cdot l_{tail}/\varnothing$ with $c \geq \varnothing$ (or $f_y/f_{ct,eff} \leq 100 \cdot l_{tail}/\varnothing$ with $c \geq 1.5\varnothing$), resulting into:

$$\sigma_{sR} = 4 \cdot \frac{l_{tail}}{\varnothing} \min(\tau_b ; \tau_{tail,spall})(1 + 2 \cdot k_3 \cdot k_4) + 4 \cdot \frac{\varnothing_{mand}}{\varnothing} \tau_b \cdot k_4 \left(1 + k_3 \cdot \frac{\alpha}{2}\right) +$$
$$4 \cdot f_y \left(k_1 (2 + \sin \alpha \cdot k_2)(1 + 2 \cdot k_3 \cdot k_4) + 0.0168 \cdot k_2\right) \tag{3.13}$$

where the bond stress τ_b (Eq. 3.3 into Eq. 3.2) as well as the spalling stress $\tau_{tail,spall}$ are:

$$\tau_b = \eta_{cp} \cdot \frac{0.6 \cdot f_c^{2/3}}{1 + \dfrac{0.75 \cdot \eta_l}{f_R} \dfrac{w}{\varnothing}} \tag{3.14}$$

$$\tau_{tail,spall} \approx \left(\eta_{is} \cdot \eta_{ct} \cdot 0.3 \cdot f_c^{2/3} \cdot \left(\frac{1}{2} + \frac{c}{\varnothing} \right) - \frac{f_y}{50} \frac{\varnothing}{l_{tail}} \right) \left(\frac{d_{dg}}{1.6\varnothing} \right)^{1/3} + \eta_{is} \cdot 2.4 \text{ MPa}$$

The coefficients k_1 to k_4 of Eq. (3.13) are calculated as:

$$k_1 = 0.00672$$

$$k_2 = \frac{6}{(1 - \cos\alpha) \cdot \left(\dfrac{\varnothing_{mand}}{\varnothing} + 1 \right)}$$

$$k_3 = \frac{1}{2.5 - \dfrac{\alpha}{2}} \tag{3.15}$$

$$k_4 = \sin\alpha - \frac{\alpha}{2}\cos\alpha$$

In case of 90° bends, Eq. (3.13) becomes:

$$\sigma_{sR} = 8.7 \frac{l_{tail}}{\varnothing} \min(\tau_b; \tau_{tail,spall}) + 5.8 \frac{\varnothing_{mand}}{\varnothing} \tau_b + f_y \cdot \left(0.12 + \frac{0.75}{\dfrac{\varnothing_{mand}}{\varnothing} + 1} \right) \tag{3.16}$$

3.6.6   Comparison of proposed approach with experimental evidence

In this section, a database of 40 tests (13 specimens from the experiments presented in this chapter as well as 27 specimens gathered from the literature [Reh79, Bra16, Med18, Min75] using deformed bars, refer to Appendix 3.C for details) is used to assess the suitability and performance of Eq. (3.12) for spalling failures and pull-out of bent reinforcement. For clarity purposes, tests where the bond stresses was not disabled in the inner region in a length larger than 5$\varnothing$ were not considered (for tests with lower lengths of the bonded inner region, this contribution was accounted for by means of Eq. 3.2). Some tests were also disregarded due to lack of information [Hri69, Sor88] or because failures occurred by full yielding of the reinforcement [Leo65, Shi08].

The main results are shown in Figure 3.21, where the predictions of the anchorage resistance according to Eq. (3.12) are compared to the test results as a function of the main parameters for tests where spalling and bond failure occurred. The proposed approach (Eq. 3.12) shows consistent results with low scatter (average value of the measured-to-calculated strength equal to 1.05 with a Coefficient of Variation of 12.9 % for Eq. 3.12). Such good agreement is obtained despite the different mechanical and geometrical conditions as well as different crack openings.

It has to be noted that tests with $c < Ø$ (not fulfilling the requirement of [Eur04]) and $l_{tail} < 2.5Ø$ are not considered. The beneficial influence of a longitudinal bar within the bend in the anchorage of the detail is considered in the comparison in in Figure 3.21 by means of an enhancement factor 1.1 as previously stated. It has to be noted that with the simplified equation (Eq. 3.13), the results are almost the same as for Eq. (3.12) (average value of the measured-to-calculated strength equal to 1.05 with a Coefficient of Variation of 13.0 %).
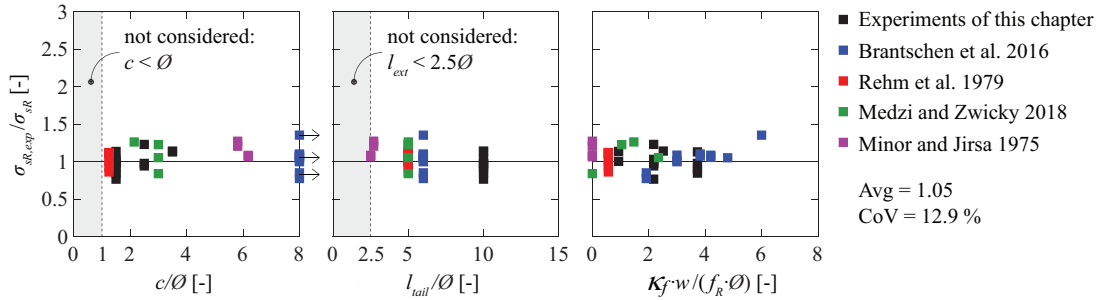
Figure 3.21:   Comparison of measured-to-predicted values $(\sigma_{sR,exp}/\sigma_{sR})$ according to Eq. (3.12), for values $c \geq Ø$ and $l_{tail} \geq 2.5Ø$.

3.6.7   Considerations on group effect

With respect to the group effect (reduction of anchorage performance due to the presence of closely-spaced bars, Figure 3.22a-c), this phenomenon has been reported in the past for anchorage of bent bars [Sor88, Aja18]. Although it has not been a matter of specific investigation in the present research, some considerations can be stated and will be discussed in the following.

In order to estimate the clear distance between bars for which the group effect shall be considered as well as its influence on the anchorage performance, an analogy to the response of straight bars can be established. A comprehensive model for the latter case has been presented by Moccia et al. [Moc21a]. According to this model, the group effect can be governing for a clear spacing between bars up to a value of $c_{s,lim} = 1.33 \cdot (2 \cdot c + Ø)$ (see Moccia et al. [Moc21a]). Figure 3.22d presents for instance the results for the group effect according to the model by Moccia et al. [Moc21a] for several cases on straight bar anchorages (two bars, three bars and a high number of them) as wells as a comparison to experimental data (triangles in Figure 3.22d refer to the case of three bars, closely matching the theoretical prediction). The model by Moccia et al. [Moc21a] describes the influence of the group effect on the basis of a nonlinear equation. For its practical application, however, it is reasonable to assume a simple linear interpolation between the limit situation for group effect and the case of anchorage resistance for side-to-side bars (see Figure 3.22d). The group effect in this latter case (side-to-side bars), can be approximated as $1/n_b$, where n_b refers to the number of bars interacting in the group effect (see Moccia et al. [Moc21a]).

The approach by Moccia et al. [Moc21a] for straight bars can be applied in principle in a safe manner to bend anchorages according to the experimental results presented in this chapter. As it can be observed in Figure 3.12, the distance of the spalled region in bend anchorages did not exceed a distance larger than $c_{s,lim} \approx 1.33 \cdot (c + \emptyset)$, which is lower than the one corresponding to straight bars according to Moccia et al. [Moc21a] ($c_{s,lim} = 1.33 \cdot (2 \cdot c + \emptyset)$ as previously stated). Such approach refers to the case where the bend anchorages are arranged in a parallel manner as bundles, see Figure 3.22e. Other cases can however be found in practice, as the one corresponding to closed stirrups with 90°-bends (see Figure 3.22f). In this case, the previous approach should in principle lead also to safe estimates of the strength, as the overlap length may be lower than the total extent of the tail. Other cases may also be dealt by analogy to straight bars (as replacing bundles of bars by an equivalent bar diameter).

The proposed approach is based on physical considerations and analogies to similar phenomena. Future experimental research is however needed to verify and to refine it.
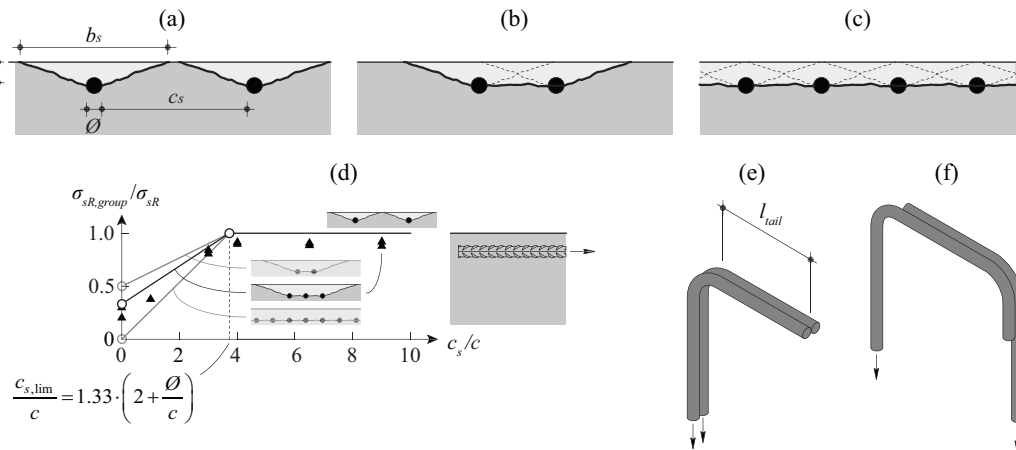
Figure 3.22: Influence of group effect: spalled region when (a) the group effect is not governing; (b) the group effect governs for two bars and (c) the group effect governs for a high number of bars; (d) consideration of group effect for straight bar anchorages according to the experimental results and mechanical model by Moccia et al. [Moc21a] (case with $c/\emptyset = 1.25$); (e) parallel bend anchorages; and (f) opposed bend anchorages in case of closed stirrup with 90°-bends.

3.6.8 Design values based on reliability analysis

The anchorage strength model developed in the previous sections (Eq. 3.12 or its simplified expression Eq. 3.13) is based on the average behaviour of tests. To use the model in practice, the unavoidable uncertainties involved in design need to be accounted for and the design equation (including partial factors) for the developed model needs to be calibrated to fulfil the corresponding reliability requirements.

In this chapter, the target reliability requirement of Eurocode for the ultimate limit state design for structures with medium consequence class and a reference period of 50 years (with a target reliability index of $\beta_{tgt} = 3.8$) is considered and the design equation and the corresponding partial safety factors for the anchorage strength model are calibrated accounting for the material, geometrical and model uncertainties. The probabilistic modelling of the basic uncertainties and the reliability analysis procedures are detailed in [Mon22]. The resulting design equation, based on the simplified expression for the anchorage strength model (Eq. 3.13), is given in Eq. (3.17) accounting for the partial safety factor format (valid for $l_{tail} \geq l_V$ and $f_y / f_{ct,eff} \leq 75 \cdot l_{tail}/\emptyset$ with $c \geq \emptyset$ or $f_y / f_{ct,eff} \leq 100 \cdot l_{tail}/\emptyset$ with $c \geq 1.5\emptyset$):

$$\sigma_{sRd} = \frac{1}{\gamma_R} \left[\begin{array}{l} 4 \cdot \dfrac{l_{tail}}{\emptyset} \min(\tau_b; \tau_{tail,spall})\left(1 + 2 \cdot k_3 \cdot k_4\right) + 4 \cdot \dfrac{\emptyset_{mand}}{\emptyset} \tau_b \cdot k_4 \left(1 + k_3 \cdot \dfrac{\alpha}{2}\right) + \\[2mm] 4 \cdot f_{yk}\left(0.00672 \cdot \left(2 + \sin\alpha \cdot k_2\right)\left(1 + 2 \cdot k_3 \cdot k_4\right) + 0.0168 \cdot k_2\right) \end{array} \right]$$

where

$$\tau_b = \eta_{cp} \frac{0.6 \cdot f_{ck}^{2/3}}{1 + \dfrac{0.75 \cdot \eta_l}{f_R} \dfrac{w}{\emptyset}}$$

$$\tau_{tail,spall} \approx \left(\eta_{is} \cdot \eta_{ct} \cdot 0.3 \cdot f_{ck}^{2/3} \cdot \left(\frac{c_d}{\emptyset} + \frac{1}{2}\right) - \frac{f_{yk}}{50} \frac{\emptyset}{l_{tail}} \right)\left(\frac{d_{dg}}{1.6\emptyset}\right)^{1/3} + \eta_{is} \cdot 2.4 \text{ MPa}$$

(3.17)

Where c is the nominal concrete cover, $\gamma_R = 1.4$, $c_d = c - \Delta c \approx c - 8\text{mm} \geq 0$ and coefficients k_2 to k_4 are given Eq. (3.15). A partial safety factor (γ_R) and a design value of the concrete cover c (c_d) are used in the design Eq. (3.17). This is because the two potential failure modes (spalling failure mode and pull-out failure mode) are verified simultaneously in the anchorage strength model and the dominating uncertainty changes with the shift of failure mode. The values of γ_R and Δ_c are calibrated to achieve a relatively uniform reliability level for representative design cases accounting for this phenomenon. Details related to the influence of multiple failure modes on the safety format calibration of concrete structures can be consulted elsewhere [Yu20].

It should also be noted that the value Δ_c for calculating the design value c_d can potentially be reduced when the concrete cover is updated on the basis of measurements (e.g. in the assessment of existing structures). Under this circumstance, the value of Δ_c can be calculated based upon updated information about the probabilistic model of the concrete cover with the procedure outlined in [Mon22, Yu21].

3.7   Anchorage demand in stirrups

The previous chapters focused on the resistance of bend and hook anchorages in tension with the tail region near to a free surface. A question of practical relevance is however not only related to the resistance of the anchorage, but also to the level of force applied to it (demand). This value is in general difficult to assess, as it depends on the type of structure (beam, wall, slab), on the cross section and on the internal forces (bending and axial forces concurrent with shear).

As previously shown by refined measurements performed with FOM [Pol19, Pol21] in reinforced concrete beams with stirrups (135° bends), the stresses in the shear reinforcement are not constant, but diminish close to the extremities, see Figure 3.23a. This is due to the development of cracking and is consistent with previous experimental observations [Reg04, Leq18].

Similar observations result from the analyses of the experimental programme performed by Rupf et al. [Rup13] on post-tensioned girders with low shear reinforcement and different types of stirrups and link anchorages (Figure 3.23b and c). Based on the Elastic-Plastic Stress Fields method (EPSF) [Fer07, Mut15], the calculated profile of the stress in the shear reinforcement can be obtained at failure (refer to specimen SR21 in Figure 3.23b, as shown by [Rup13]). This approach allows for realistic estimates of the strength and failure mode and location, with an average of measured-to-calculated load-carrying capacity equal to 1.06 with a Coefficient of Variation of 5 % [Rup13]. The same trends as in the beam tested by Poldon et al. [Pol19, Pol21] can be observed also in this investigation, with diminishing stresses close to the anchorage regions. Figure 3.23c provides further details of the stresses in the shear reinforcement at the tension side (green line), mid-high (red line) and compression side (magenta) for different specimens (the lines at the tension and compression sides are located at the beginning of the bent, point C, of the shear reinforcement at both extremities). The following observations can be made:

- Tensile stresses are potentially lower at beginning of the anchorages, but the yield strength is reached for several cases, particularly for non-prestressed members. An increase of the amount of shear reinforcement tends to increase the tensile stresses at the anchorages on the tension side.

- The shear reinforcement stresses are higher in the tension zone of the beam than in the compression zone. This effect is particularly detrimental as in the tension side, the flexural cracks can weaken the capacity of the anchorage as described above.

- In the location of the maximum bending moment (near to supports and to load introductions), the shear reinforcement stresses at the tension side are lower than in the other parts of the beam. This is beneficial, since the maximum demand is not located where the strength is lowest (where the crack openings are largest).

As shown in Figure 3.23c, the maximum steel stresses in the shear reinforcement are very sensitive to various parameters (such as section type, amount of transverse reinforcement or level of prestressing). In addition to these parameters, it has to be noted that, for bridges, a potential increase of the tensile stress at the bent region may also occur due to the transversal bending (partial transfer of the clamping moment from the deck slab to the web). On the basis of these considerations, it is reasonable to assume, as a sound design rule, that the full capacity of the stirrup is required at the end of the bend (point C in Figure 3.4b), but that refined analyses are possible (whenever required) to gain a more detailed insight of the phenomenon.
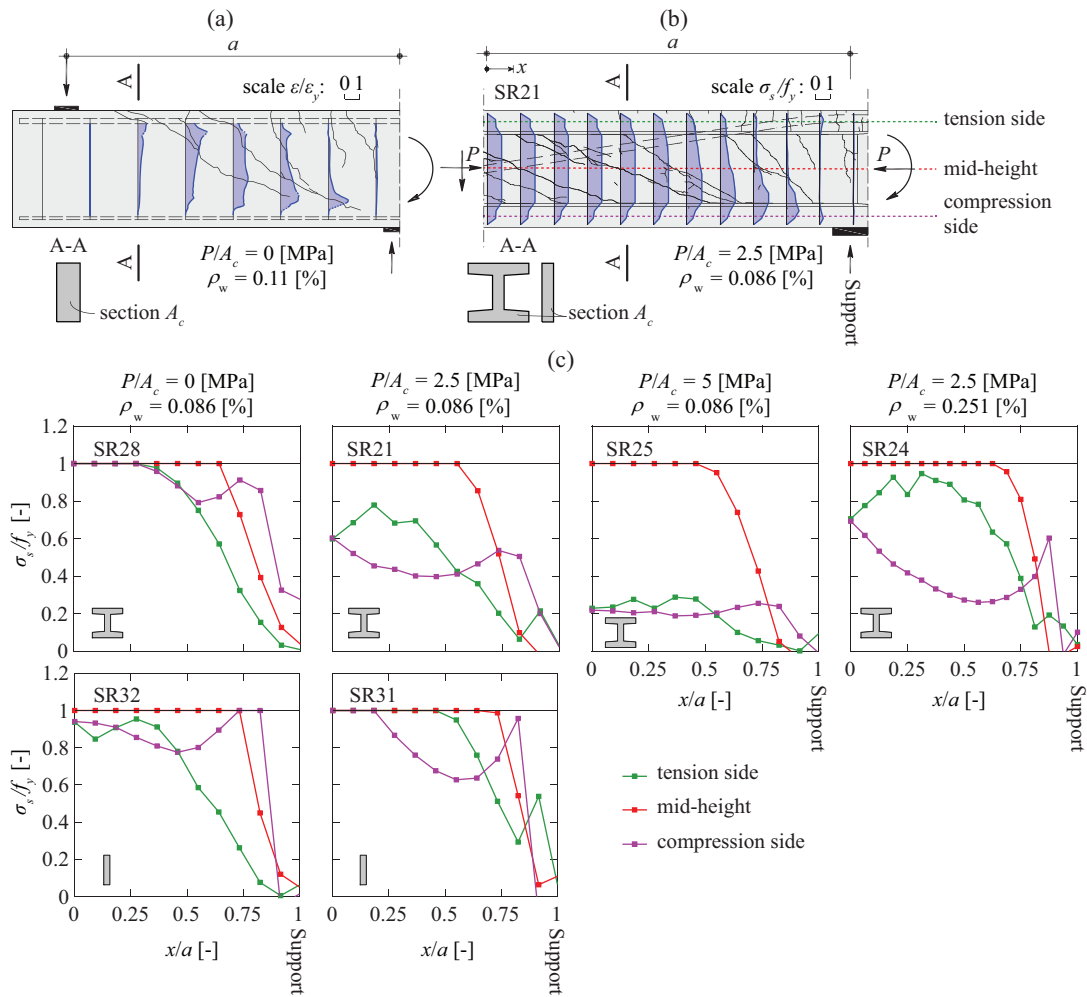
Figure 3.23:   Shear reinforcement strain and stress along the height of the stirrups: (a) shear reinforcement strain measured at 85 % of the failure load for JP-1 [Pol19, Pol21]; (b) shear reinforcement stress calculated based on EPSF for SR21 with cracking pattern [Rup13]; and (c) shear reinforcement stress calculated based on EPSF for selected specimens at tension side (green), mid-hight (red) and compression side (magenta) for various cross sections, shear reinforcement ratios ρ_w and average longitudinal stresses due to prestressing P.

3.8 Conclusions

This chapter presents the results of an experimental programme and a mechanical model allowing to better understand the behaviour and to predict the resistance of bends and hooks in tension. The case of the anchorage of shear reinforcement near to a free surface is investigated. In addition, the influence of bending cracks on the performance of shear reinforcement is also investigated. The main conclusions are listed below:

1. Three failure modes potentially govern the strength of a bend anchorage: (i) spalling of the concrete cover, (ii) pull-out (bond) failure and (iii) reinforcement yielding. The governing failure mode depends upon the size of the concrete cover, the transverse crack opening and the detailing of the region.

2. The mechanical response of bend anchorages is complex, with an interaction between normal, bond stresses and longitudinal steel stresses due to axial forces and bending. Such interaction is confirmed by means of an experimental programme performed with detailed Fibre-Optic Measurements. Also, the experimental results presented in this chapter show a significant influence of the state of cracking, consistently with previous researches on bond.

3. Spalling of the concrete cover is originated by a combination of the tensile stresses associated to bond and the uplift forces in the tail region of bends (lever effect). Such uplift forces allow, by equilibrium conditions, to develop an additional tensile force in the reinforcement at the end of the bend (enhancement of the anchorage capacity in case of pull-out failures).

4. A simple mechanical model based on the response of the different regions of the bend is presented. Consistent agreement to experimental measurements is obtained by considering the bond, frictional and deviation forces developing. The model considers the various potential failure modes and suitably captures the influence of the various implied parameters, improving current design approaches. It allows also accounting for an enhanced performance of bent details provided that some detailing rules related to cover, length of the tail region and mandrel diameter are respected.

5. Design values based on reliability analysis are proposed for the design and assessment of bend and hook anchorages.

6. Although the stresses are potentially variable along the shear reinforcement (with typically higher strains at mid-height of the member and lower stresses at the anchorage regions), it is reasonable to assume that the yield strength can develop at end of the curved region of bends and hooks.

Appendix 3.A: Calculation of the local resistances of bends and hooks

In this appendix, the contributions of the different regions to the anchorage resistance are derived separately.

3.A.1 Tail region

Figure 3.A.1a shows the tail region close to a free concrete surface with a relatively thin concrete cover c. In this region, two set of forces can act: transversal forces acting perpendicular to the free surface on the one hand and bond and friction forces on the other. Both the bond and uplift forces originate tensile stresses in the region of the concrete cover (refer to Figure 3.A.1a,c for uplift forces and to Figure 3.A.1a,b for the bond forces). The concrete cover can be assumed to spall when the tensile stresses generated by these two actions (σ_V for the uplift forces and σ_b for the bond action) equal the effective tensile strength of concrete:

$$\sigma_V + \sigma_b = f_{ct,eff} \tag{3.A.1}$$
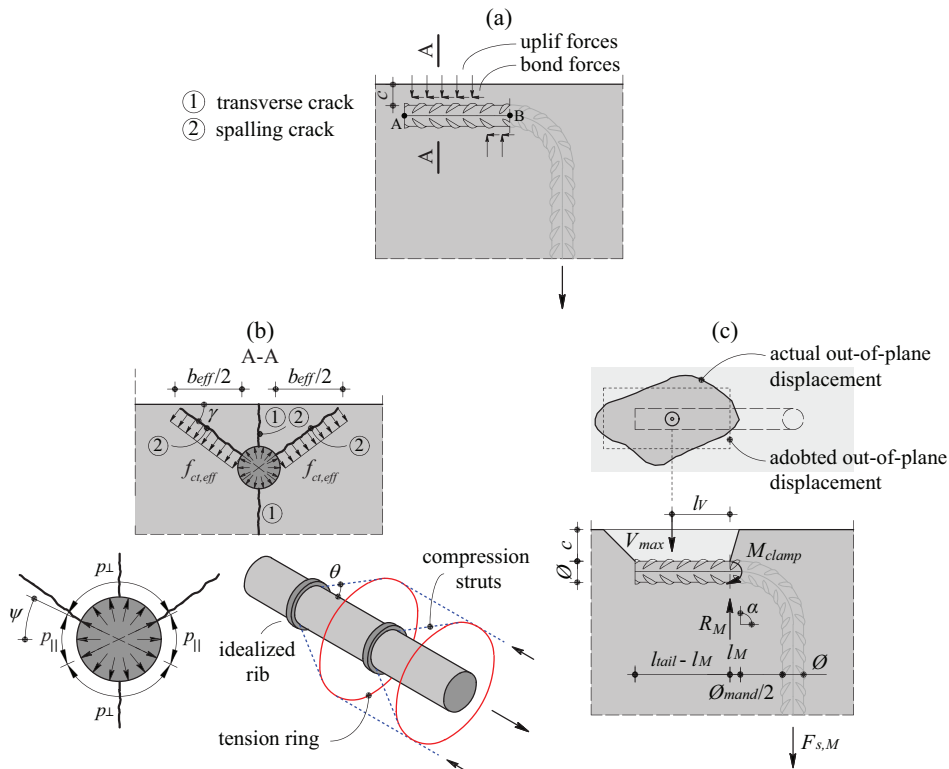
Figure 3.A.1:   Response of the tail region under spalling: (a) bond and uplift forces; (b) forces due to bond engagement; and (c) equilibrium of forces due to uplift.

In order to estimate the forces leading to spalling failures, the simplified model proposed by Moccia et al. [Moc21a] will be used hereafter, considering as the effective tensile strength [Moc21a]:

$$f_{ct,eff} = \eta_{is} \cdot \eta_{ct} \cdot f_{ct} \tag{3.A.2}$$

Where η_{is} is a strength reduction factor to account for the casting position effect ($\eta_{is} = 1$ for good bond conditions and $\eta_{is} = 0.6$ for poor bond conditions according to its usual definition in codes of practice [Eur04, FIB13] as well as Moccia et al. [Moc21, Moc21a]), η_{ct} is a coefficient accounting for the concrete brittleness in tension equal to 0.8 (value valid for concrete strengths up to 50 MPa according to [Fer10]) and where f_{ct} refers to the concrete tensile strength (approximated as $0.3 \cdot f_c^{2/3}$).

3.A.1.1 Uplift forces

The uplift forces (originating a lever effect, see Figure 3.A.1c) are due to the rotation of the curved region (related to bond slip) which is restrained in the tail region by the concrete cover. According to the results of the FOM (refer to Figure 3.14b), yielding of the bar can be assumed at the clamped end of the tail (point B), so that the bending moment can be estimated as follows:

$$M_{clamp} \cong c_p \cdot M_{R0} = c_p \cdot f_y \cdot \frac{\varnothing^3}{6} \tag{3.A.3}$$

where c_p is a coefficient reducing the flexural plastic resistance to account for the presence of the axial force in the reinforcement, whose value will be adopted in the following in a simplified manner as $c_p = 0.95$. It can be noted that the bending moment in the bar is also potentially influenced by the eccentricity of the friction forces (mostly acting on the outer side of the bar), but this effect will be neglected. On that basis, V_{max} can be calculated by equilibrium conditions as (Figure 3.A.1c):

$$V_{max} = \frac{M_{clamp}}{l_V} \tag{3.A.4}$$

V_{max} has to be also limited to the maximal effective tensile strength:

$$V_{max} \leq f_{ct,eff} \cdot (l_{tail} - 2 \cdot l_M) \cdot b_{eff} \tag{3.A.5}$$

Thus, the uplift forces also generate tensile stresses [Moc21a], whose average value (between point A and B, refer to Figure 3.A.1a) will be estimated by equilibrium conditions and limited to the maximum effective tensile strength.

$$\sigma_V = \frac{V_{max}}{(l_{tail} - 2 \cdot l_M) \cdot b_{eff}} \tag{3.A.6}$$

In these expressions, the effective width b_{eff} can be calculated as a function of the geometrical parameters [Moc21a] (see Figure 3.A.1b) resulting into:

$$b_{eff} = 2 \cdot \emptyset \cdot \left(\frac{c}{\emptyset} + \frac{1}{2} \cdot (1 - \sin \psi) \right) \cdot \cot \gamma \cong 2 \cdot \emptyset \cdot \left(\frac{c}{\emptyset} + \frac{1}{2} \right) \cdot \cot \gamma \qquad (3.A.7)$$

Where ψ characterizes the angle at which the crack develops (Figure 3.A.1b) and can be determined by minimization of the failure load [Moc21a] ($\sin(\psi) = 1/(1+2\cdot c/\emptyset)$). Parameter γ is the angle of the spalling crack (which can be approximated as $\gamma = 37°$ according to [Moc21a], see Figure 3.A.1b).

Finally, the contribution of the lever effect in terms of axial force in the bar can be calculated by equilibrium conditions as:

$$F_{s,M} = V_{max} \cdot \frac{\dfrac{l_V}{\emptyset}}{\dfrac{l_M}{\emptyset} \cdot \sin \alpha + \dfrac{1 - \cos \alpha}{2} \cdot \left(\dfrac{\emptyset_{mand}}{\emptyset} + 1 \right)} \qquad (3.A.8)$$

Where l_M and l_V are defined in Figure 3.A.1c and α refers to bending angle (Figure 3.16 and A.1c). The distance l_V is also limited to:

$$l_V \leq l_{tail} - l_M \qquad (3.A.9)$$

With V_{max} and $F_{s,M}$, the reaction R_M can be calculated by equilibrium conditions:

$$R_M = V_{max} + \sin \alpha \cdot F_{s,M} \qquad (3.A.10)$$

3.A.1.2 Bond stresses

The bond strength in the tail region near to the surface can be estimated according to Moccia et al. [Moc21a] for failures induced by spalling. According to this approach, the bond development induces a state of pressures acting perpendicular to the bar (Figure 3.A.1b). Such pressures result from the component perpendicular to the reinforcement of the inclined struts originated by bond and can be divided into (i) the pressure whose resultant acts perpendicular to the free surface $p_\perp$; and (ii) the pressure whose resultant acts parallel to the free surface ($p_\parallel$). Accounting for the fact that a fraction of the effective tensile strength is already required to equilibrate the uplift force (refer to stress σ_V in Eq. 3.A.6), it results according to the approach by Moccia et al. [Moc21a]:

$$p_\perp = \frac{f_{ct,eff} - \sigma_V}{\tan \gamma} \cdot 2 \cdot \sqrt{\frac{c}{\emptyset} + \left(\frac{c}{\emptyset} \right)^2} \cdot \left(\frac{d_{dg}}{1.6\emptyset} \right)^{1/3} \cong \frac{f_{ct,eff} - \sigma_V}{\tan \gamma} \cdot \left(1 + 2\frac{c}{\emptyset} \right) \cdot \left(\frac{d_{dg}}{1.6\emptyset} \right)^{1/3} \qquad (3.A.11)$$

$$p_\parallel = \eta_{is} \cdot p_{\parallel,0} = \eta_{is} \cdot 6 \text{ MPa}$$

The parameter d_{dg} accounts for the maximum aggregate size (d_g) [Eur21, Cav18], and can be calculated as $d_{dg} = \min(40 \text{ mm}, \ 16 \text{ mm} + d_g)$ for $f_c \leq 60$ MPa and $d_{dg} = \min(40 \text{ mm}, 16 \text{ mm} + d_g (60/f_c)^4)$ for $f_c > 60$ MPa.

When spalling is governing, the corresponding average bond stresses can thus be determined by dividing, over the contact area of the bar, the forces acting along the bar axis generated by the engagement of the ribs (according to the model by Moccia et al. [Moc21a]) and those resulting from the friction between the steel and the concrete upon application of the uplift force (V_{max}) and reaction (R_M):

$$\tau_{tail} \leq \tau_{tail,spall} + \tau_{tail,friction}$$

$$\tau_{tail} \leq \left(\lambda \cdot p_\perp + (1-\lambda) \cdot p_\parallel\right) \cdot \cot\theta + \mu \cdot \frac{V_{max} + R_M}{\pi \cdot \varnothing \cdot l_{tail}}$$

(3.A.12)

Where λ is a coefficient denoting the part of the bar perimeter associated to each component $p_\perp$ and $p_\parallel$ (which can be adopted equal to 0.5 according to [Moc21a]). In the following, for calculation of the angle of the struts, θ equal to 52° will be adopted as a simplification of the expressions provided by Moccia et al. [Moc21a] (Figure 3.A.1b).

When spalling is not governing, the bond strength in the tail part is limited by the pull-out bond resistance (as for the inner part [Bra16, Mar98]), but considering the enhancement in the transfer capacity due to friction forces:

$$\tau_{tail} = \tau_b + \tau_{tail,friction}$$

$$\tau_{tail} = \eta_{cp} \cdot k_b \cdot 0.6 f_c^{2/3} + \mu \cdot \frac{V_{max} + R_M}{\pi \cdot \varnothing \cdot l_{tail}}$$

(3.A.13)

In Eq. (3.A.12), $\tau_{tail,spall}$ can be rewritten in a more compact form when $l_{tail} \geq l_V$ and $f_y/f_{ct,eff} \leq 75 \cdot l_{tail}/\varnothing$ with $c \geq \varnothing$ (or $f_y/f_{ct,eff} \leq 100 \cdot l_{tail}/\varnothing$ with $c \geq 1.5\varnothing$) and by substituting l_V, l_M, Eqs. (3.A.11) and (3.A.6) into $\tau_{tail,spall}$ in Eq. (3.A.12):

$$\tau_{tail,spall} = \left(2 \cdot \lambda \cdot \cot\gamma \left(f_{ct,eff} \left(\frac{c}{\varnothing} + \frac{1}{2} \right) - \frac{f_y}{50 \cdot l_{tail}} \frac{\varnothing}{} \right) \left(\frac{d_{dg}}{1.6\varnothing} \right)^{1/3} + (1-\lambda) \cdot \eta_{is} \cdot p_{\parallel,0} \right) \cot\theta$$

(3.A.14)

3.A.2   Curved region

Figure 3.16 shows the curved region whose geometry is characterised by the mandrel diameter $\varnothing_{mand}$. In this region, both deviation forces (perpendicular to the bar axis, Figure 3.A.2a) as well as bond and frictional forces (parallel to the bar axis, Figure 3.A.2a) are acting. The deviation forces are required by equilibrium of a curved bar subjected to an axial force, while the bond and frictional forces result from the engagement of the ribs with the concrete and the friction between the concrete and steel surface.
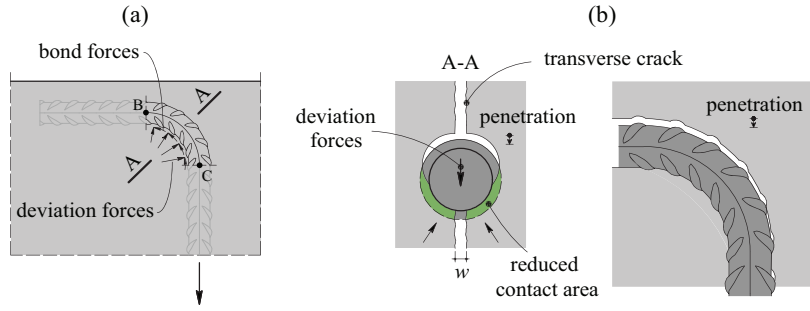
Figure 3.A.2:   Response of the curved part: (a) bond stresses and deviation forces; and (b) influence of the transverse crack.

The bond and friction stresses can, as for the previous regions, be calculated on the basis of the rib engagement and friction of axial forces as:

$$\tau_{curved} = \tau_b + \tau_{curved,friction}$$

$$\tau_{curved} = \eta_{cp} \cdot k_b \cdot 0.6 f_c^{2/3} + \mu \cdot \frac{p_{avg}}{\pi \cdot \varnothing}$$

(3.A.15)

where p_{avg} refers to the deviation forces and μ is the friction coefficient (assumed as previously equal to 0.4), whose average value results:

$$p_{avg} = \frac{(N_B + N_C)/2}{\varnothing_{mand}/2} = \frac{N_B + N_C}{\varnothing_{mand}}$$

(3.A.16)

Where N_B and N_C are respectively the force at the point B and the point C:

$$N_B = \tau_{tail} \cdot l_{tail} \cdot \pi \cdot \varnothing$$

$$N_C = N_B + \tau_{tail} \cdot \alpha \frac{\varnothing_{mand}}{2} \cdot \pi \cdot \varnothing = \left(\tau_{tail} \cdot l_{tail} + \tau_{curved} \cdot \alpha \frac{\varnothing_{mand}}{2} \right) \cdot \pi \cdot \varnothing$$

(3.A.17)

By substituting Eq. (3.A.17) into Eq. (3.A.16):

$$p_{avg} = \left(2 \cdot \tau_{tail} \frac{l_{tail}}{\varnothing_{mand}} + \tau_{curved} \cdot \frac{\alpha}{2} \right) \cdot \pi \cdot \varnothing$$

(3.A.18)

and considering the value of τ_{curved} given in Eq. (3.A.15), it results finally:

$$p_{avg} = \pi \cdot \varnothing \frac{2 \cdot \tau_{tail} \cdot \dfrac{l_{tail}}{\varnothing_{mand}} + \eta_{cp} \cdot k_b \cdot 0.6 f_c^{2/3} \cdot \dfrac{\alpha}{2}}{1 - \mu \cdot \dfrac{\alpha}{2}}$$

(3.A.19)

Appendix 3.B: Detail of the calculation of anchorage resistance of tail and curved regions

The force that can be developed in the bar at the end of the bend (point C) can be calculated on the basis of the equilibrium conditions of the tail and curved regions (see Eq. 3.9). The contribution of the tail region $F_{s,tail}$ can be determined by integration of the bond stress on the tail region as well as the associated deviation forces for the general case of a bending angle α (see Figure 3.B.1a):

$$F_{s,tail} = \int_0^{l_{ext}} \pi \cdot \varnothing \cdot \tau_{tail} \cdot \cos \alpha \cdot ds + \int_0^{\alpha} p_{tail} \cdot \sin \xi \cdot \frac{\varnothing_{mand}}{2} \cdot d\xi = \pi \cdot \varnothing \cdot \tau_{tail} \cdot l_{tail} \qquad (3.B.1)$$

Where ξ is the angular coordinate and p_{tail} to the deviation forces (see Figure 3.B.1a):

$$p_{tail} = \frac{2 \cdot \sigma_s(s) \cdot \pi \cdot \frac{\varnothing^2}{4}}{\varnothing_{mand}} = 2\pi \cdot \frac{\varnothing}{\varnothing_{mand}} \cdot \tau_{tail} \cdot l_{tail} \qquad (3.B.2)$$

Where $\sigma_s(s)$ is the tensile stresses acting in the reinforcement in the curved region along the length. The contribution of the curved region $F_{s,curved}$ is determined by integration of its bond stress and deviation forces (see Figure 3.B.1b):

$$F_{s,curved} = \int_0^{\alpha} \tau_{curved} \cdot \pi \cdot \varnothing \cdot \cos \xi \cdot \frac{\varnothing_{mand}}{2} \cdot d\xi + \int_0^{\alpha} p_{curved} \cdot \sin \xi \cdot \frac{\varnothing_{mand}}{2} \cdot d\xi$$

$$F_{s,curved} = \pi \cdot \varnothing \cdot \tau_{curved} \cdot \varnothing_{mand} \cdot \left(\sin \alpha - \frac{\alpha}{2} \cdot \cos \alpha \right) \qquad (3.B.3)$$

Where p_{curved} refers to the deviation forces (see Figure 3.B.1b):

$$p_{curved} = \frac{2 \cdot \sigma_s(s) \cdot \pi \cdot \frac{\varnothing^2}{4}}{\varnothing_{mand}} = 2\pi \cdot \frac{\varnothing}{\varnothing_{mand}} \cdot \tau_{curved} \cdot s = \pi \cdot \varnothing \cdot \tau_{curved} \cdot \xi \qquad (3.B.4)$$
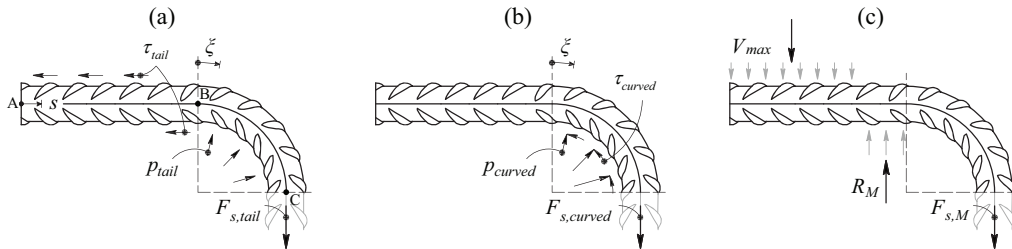
Figure 3.B.1: Distinction of three sets of forces: (a) forces related to bond activated in the tail region; (b) forces related to bond activated in the curved region; and (c) forces related to the lever effect (transverse forces in the tail region).

The contribution of the lever effect of the uplift force $F_{s,M}$ is given in Appendix 3.A, Eq. (3.A.8) (see also Figure 3.B.1c). Finally, by substituting Eqs. (3.B.1, 3.B.3) and (3.A.8) into Eq. (3.9), the following expression results for the anchorage capacity accounting for each contribution (refer to Figure 3.16 for geometric parameters):

$$F_{sR} = \pi \cdot \varnothing \cdot \tau_{tail} \cdot l_{tail} + \pi \cdot \varnothing \cdot \tau_{curved} \cdot \varnothing_{mand} \cdot \left(\sin \alpha - \frac{\alpha}{2} \cdot \cos \alpha \right) +$$

$$V_{max} \frac{\dfrac{l_V}{\varnothing}}{\dfrac{l_M}{\varnothing} \cdot \sin \alpha + \dfrac{1 - \cos \alpha}{2} \cdot \left(\dfrac{\varnothing_{mand}}{\varnothing} + 1 \right)}$$

$$\sigma_{sR} = \tau_{tail} \frac{4 l_{tail}}{\varnothing} + \tau_{curved} \frac{4 \varnothing_{mand}}{\varnothing} \left(\sin \alpha - \frac{\alpha}{2} \cos \alpha \right) +$$

$$\frac{4 \cdot V_{max}}{\pi \cdot \varnothing^2} \frac{\dfrac{l_V}{\varnothing}}{\dfrac{l_M}{\varnothing} \sin \alpha + \dfrac{1 - \cos \alpha}{2} \left(\dfrac{\varnothing_{mand}}{\varnothing} + 1 \right)}$$

(3.B.5)

Appendix 3.C: Comparison of proposed approach with experimental evidence

Table 3.C.1: Test series considered in this study and comparison with the proposed expressions: Eq. (3.12).

Specimens	$\varnothing$ [mm]	$\varnothing_{mand}/\varnothing$ [-]	$\varnothing_l$ [mm]	α [°]	$l_{tail}/\varnothing$ [-]	w [mm]	$c/\varnothing$ [-]	f_R [-]	η_l [-]	f_c [MPa]	f_y [MPa]	Casting cond.	Exp. Fail.[1]	$\sigma_{sR,exp}/\sigma_{sR}$ [-]
Experiments in this research														
PM24	14	4	0	90	10	1.20	3.5	0.069	4	47.5	513	poor	P	1.13
PM32	14	4	0	90	10	0.70	1.5	0.069	4	47.5	513	poor	P	0.98
PM33	14	4	0	90	10	0.70	2.5	0.069	4	47.5	513	poor	P	0.95
PM34	14	4	0	90	10	0.81	3.5	0.069	4	47.5	513	poor	P	1.14
PM42	14	4	18	90	10	1.20	1.5	0.069	4	47.6	513	poor	P	0.91
PM43	14	4	18	90	10	0.70	1.5	0.069	4	47.6	513	poor	P	1.03
PM44	14	4	18	90	5	0.30	1.5	0.069	4	47.6	513	poor	P	1.16
PM52	14	4	0	90	5	0.30	1.5	0.069	4	47.6	513	poor	S	1.02
PM53	14	4	0	90	5	0.70	2.5	0.069	4	47.6	513	poor	P	1.23
PM61	14	4	0	90	10	0.70	1.5	0.069	4	47.7	513	poor	S/P	0.77
PM62	14	4	0	90	5	0.70	1.5	0.069	4	47.7	513	poor	S	0.99
PM63	14	4	0	90	10	1.20	2.5	0.069	4	47.7	513	poor	P	0.98
PM64	14	4	0	90	10	1.20	1.5	0.069	4	47.7	513	poor	P	0.85
													Avg =	1.01
													CoV =	0.130
Brantschen et al. 2016														
SB11-6	10	4	0	180	6	0.50	27	0.050	4	32.4	552	good	P	1.09
SB11-7	10	4	0	180	6	1.00	27	0.050	4	32.4	552	good	P	1.36
SB14-7	10	4	14	180	6	0.50	27	0.050	4	32.6	552	good	P	1.01
SB14-8	10	4	14	180	6	0.50	27	0.050	4	32.6	552	good	P	1.00
SB14-9	10	4	14	180	6	0.70	27	0.050	4	32.6	552	good	P	1.09
SB14-10	10	4	14	180	6	0.70	27	0.050	4	32.6	552	good	P	1.06
SB14-11	10	4	14	180	6	0.80	27	0.050	4	32.6	552	good	P	1.05
SB12-5	14	4	0	180	6	0.50	18	0.056	4	32.5	572	good	P	0.85
SB12-6	14	4	0	180	6	0.50	18	0.056	4	32.5	572	good	P	0.78
SB12-7	14	4	0	180	6	1.00	18	0.056	4	32.5	572	good	P	1.10
SB12-8	14	4	0	180	6	1.00	18	0.056	4	32.5	572	good	P	1.08
													Avg =	1.04
													CoV =	0.141
Rehm et al. 1979														
0h	11	4	0	90	5	0.30	1.25	0.072	2	22.3	546	good	S	0.87
1h	11	4	0	90	5	0.30	1.25	0.072	2	22.3	546	good	S	0.92
2v	11	4	0	90	5	0.30	1.25	0.072	2	22.3	546	good	S	1.00
2h	11	4	0	90	5	0.30	1.25	0.072	2	22.3	546	good	S	1.00
3v	11	4	0	90	5	0.30	1.25	0.072	2	22.3	546	good	S	1.12
3h	11	4	0	90	5	0.30	1.25	0.072	2	22.3	546	good	S	1.12
4v	11	4	0	90	5	0.30	1.25	0.072	2	22.3	546	good	S	1.11
4h	11	4	0	90	5	0.30	1.25	0.072	2	22.3	546	good	S	1.11
													Avg =	1.03
													CoV =	0.098

Medzi and Zwicky 2018															
C1-9	10	6	0	90	5	0.00	3.0	0.058	2	27.1	537	good	P	0.84
9	10	6	0	90	5	0.40	3.0	0.058	2	31.2	537	good	P	1.23
9	10	6	0	90	5	0.90	3.0	0.058	2	33.9	537	good	P	1.06
10	14	6	0	90	5	0.90	2.1	0.066	2	33.9	516	good	P	1.27
													Avg =	1.10
													CoV =	0.176
Minor and Jirsa 1975															
5-3-45-1.5a	15.9	4.8	0	45	2.5	0.00	7.8	-	4	27.6	455	good	P	1.02
5-3-45-1.5b	15.9	4.8	0	45	2.5	0.00	7.8	-	4	27.6	455	good	P	1.00
7-4.3-45-2a	22.3	4.6	0	45	2.7	0.00	7.2	-	4	42.1	434	good	P	1.17
7-4.3-45-2b	22.3	4.6	0	45	2.7	0.00	7.2	-	4	45.5	434	good	P	1.24
													Avg =	1.16
													CoV =	0.086
All tests with spalling failure													**Avg =**	**1.00**
No of specimens = 11													**CoV =**	**0.115**
All tests with bond failure													**Avg =**	**1.06**
No of specimens = 29													**CoV =**	**0.132**
All tests													**Avg =**	**1.05**
No of specimens = 40													**CoV =**	**0.129**

[1] Predicted failure modes of the model are the same as those of the tests except for PM44 and PM62

S = spalling failure ; P = pull-out failure

Notation

Latin characters: lower case

a	shear span
b_{eff}	effective width
b_s	length of the extent on the concrete surface of the spalled cover
c	concrete cover
c_d	design value of the concrete cover
c_p	coefficient reducing the flexural plastic resistance to account for the presence of the axial force in the reinforcement
c_s	clear spacing of the reinforcement
$c_{s,lim}$	limit spacing of the reinforcement when group effect is governing
d_{dg}	maximum aggregate size parameter
d_g	maximum aggregate size
f_b	maximum average bond stress
f_c	concrete cylinder compressive strength
f_{c3}	tri-axial compressive strength
f_{ck}	characteristic value of the concrete compressive strength
f_{ct}	concrete tensile strength
$f_{ct,eff}$	concrete effective tensile strength
f_R	bond index
f_y	yield strength of reinforcement
f_{yk}	characteristic value of the yield strength of the reinforcement
h_R	height of the ribs
$h_{R,max}$	maximum height of the ribs
k_1 to k_4	factors of the model
k_b	coefficient accounting for the influence of cracking parallel to the reinforcement
l_b	bond length
l_{CD}	distance between point C and concrete surface
l_{DE}	distance between concrete surface and position of the LVDTs
l_{tail}	tail length
l_M	distance from the point B to the plastic hinge in the tail region
l_V	distance of the force V_{max} applied
n_b	number of bars interacting in the group effect
p	deviation forces
p_{avg}	average deviation forces
p_{curved}	out-of-plane forces in the curved region

p_{tail}	out-of-plane forces in the tail region
$p_\perp$	pressure perpendicular to the free surface
$p_\parallel$	pressure parallel to the free surface
s	curvilinear abscissa of a bar
s_R	spacing between ribs
u	out-of-plane displacement
u_{max}	maximum out-of-plane displacement
w	in-plane crack opening
x	coordinate in-plane in the x-direction
y	coordinate in-plane in the y-direction

Latin characters: upper case

A_c	area of the concrete cross section
F_{max}	maximum force applied
F	force applied
F_{sR}	anchorage capacity
$F_{s,curved}$	contribution of the curved region to the anchorage capacity
$F_{s,tail}$	contribution of the tail region to the anchorage capacity
$F_{s,M}$	contribution of the lever effect to the anchorage capacity
M	bending moment
M_{clamp}	bending moment at clamped end of the tail
M_{max}	maximum bending moment in the tail region
M_{R0}	bending plastic resistance
M_y	moment for first yielding in a section
N_B, N_C	force at point B and point C
P	prestressing force
R_M	reaction force due to the uplift forces
V	shear force
V_{max}	maximum shear force in the tail region

Greek characters: lower case

α	bending angle
β_{tgt}	target reliability index
δ_C	displacement of the point E measured in the direction of the bar
δ_E	displacement of the point E measured in the direction of the bar with respect to the concrete surface
ε	bar strain
ε_y	yield strain of a bar

γ	angle of the spalling crack
γ_R	partial safety factor for the anchorage strength model
η_{cp}	coefficient accounting for casting effects on bond conditions
η_{ct}	brittleness factor of concrete in tension
η_{is}	strength reduction factor to account for casting position effect
η_l	number of lugs per rib
λ	coefficient denoting the part of the bar perimeter associated to each component $p_\perp$ and $p_\parallel$
μ	friction coefficient
θ	angle between the compressive struts and the bar axis
ρ_w	shear reinforcement ratio
σ_b	transversal stresses due the bond forces
σ_c	compressive stress
σ_s	stress in the reinforcement
σ_{sR}	anchorage strength calculated with the model
σ_{sRd}	design anchorage strength
$\sigma_{sR,exp}$	maximum experimental stress in the reinforcement at the point C
$\sigma_{sR,group}$	design anchorage strength accounting for group effect
$\sigma_{sR,EC}$	anchorage strength calculated according to EN 1992:1-1:2004 (Eurocode 2 [Eur04])
σ_V	transversal stresses due the uplift forces
τ_b	bond stress
τ_{curved}	average bond stress in the curved region
$\tau_{curved,friction}$	average friction bond stress in the curved region
τ_{inner}	average bond stress in the inner region
τ_{tail}	average bond stress in the tail region
$\tau_{tail,spall}$	average bond stress for failures induced by spalling in the tail region
$\tau_{tail,friction}$	average friction bond stress in the tail region
ξ	angular coordinate
ψ	angle at which the crack develops

Greek characters: upper case

Δ_c	reduction of concrete cover for design

Others

$\varnothing$	bar diameter
$\varnothing_l$	longitudinal bar diameter within the bend
$\varnothing_{mand}$	mandrel diameter (= inner diameter after bending of the bar)

Chapter 4

Influence of amount of shear reinforcement and its post-yield response on the shear resistance of reinforced concrete members

This chapter is the pre-print version of the article mentioned below, submitted in Structural Concrete Journal in April 2022. The authors of the article are Frédéric Monney (PhD Candidate), Prof. Miguel Fernández Ruiz (thesis co-director) and Prof. Aurelio Muttoni (thesis director). The provisional reference is the following:

Monney F., Fernández Ruiz M., Muttoni A., *Influence of amount of shear reinforcement and its post-yield response on the shear resistance of reinforced concrete members*, Structural Concrete. [submitted for review, April 2022]

The work presented in this publication was performed by Frédéric Monney under the supervision of Prof. Miguel Fernández Ruiz and Prof. Aurelio Muttoni who provided constant and valuable feedbacks, proofreadings and revisions of the manuscript.

The main contributions of Frédéric Monney to this article and chapter are the following:

- Comprehensive literature review including research and design codes on shear beams with low amount of shear reinforcement.

- Preparation, casting and testing of 10 beams with variable shear reinforcement ratio, ductility class of the shear reinforcement and shear anchorage detail.

- Detailed measurements of the shape and the kinematics of cracks, using Digital Image Correlation.

- Detailed measurements of the strains of the stirrups and flexural reinforcement with Fibre-Optical measurements.

- Post-processing of the experimental data.

- Interpretation, analysis and discussion of the tests results.

- Calculation of the Shear Transfer Actions.

- Evaluation of the shear design equation of the actual [Eur04] and the new generation [Eur21] of Eurocode 2 in case of low amount of shear reinforcement.

- Elaboration of the figures and tables included in the article.

- Writing of the manuscript of the article.

Abstract

The minimum amount of shear reinforcement to be provided in reinforced concrete members has been a topic of debate and research for decades without reaching a consensus. Defining such values is however instrumental to build in an economic manner and to safely ensure the applicability of the models used for design or assessment.

This chapter presents the results of an investigation addressed at the activation and contribution of shear reinforcement to the resistance, particularly when low amounts are arranged. The research comprises an experimental part, where ten tests are performed on full-scale beams with varying amounts of shear reinforcement and different mechanical properties of the reinforcement. The tests were instrumented with refined measurement techniques such as Digital Image Correlation and Fibre Optic Measurements, allowing for a detailed tracking of the strains in the concrete and the reinforcement. The results of the programme clearly show that the transition from strain localization with a single shear crack to distributed cracking is influenced by both the ratio of shear reinforcement and its post-yield response. The results are confirmed by the analysis of a comprehensive database of 236 specimens collected from the literature, where the influence of the different parameters is analysed.

Finally, it is discussed how such findings can be implemented into codes of practice, explaining the recent changes introduced in prEN 1992-1-1:2021 (draft for the 2nd generation of Eurocode 2) and *fib* MC2020.

Keywords: beams; tests; shear reinforcement; minimum shear reinforcement; shear transfer actions; detailing rules; crack kinematics; stirrup rupture

4.1 Introduction and role of the minimum shear reinforcement

Since the early applications of reinforced concrete, shear reinforcement has been used in a wide variety of structures for building, bridges and other civil engineering works (Figure 4.1a and b). The first applications of shear reinforcement can be traced to the patents by Hennebique [Hen92, Hen93] and Coignet [Coi92] and was soon acknowledged as an efficient manner to increase the shear resistance. Following its practical application, a number of efforts were performed to better understand its mechanical response and to provide tools for its design, as those of Ritter [Rit99] based on a truss analogy. Such approach was later continued and extended by other scholars [Mör08, Kup69] and led to a number of consistent methods for shear design based on limit analysis [Nie78, Thü79] accounting for the distributed nature of shear cracking in case a sufficient amount of shear reinforcement is provided (Figure 4.1e).
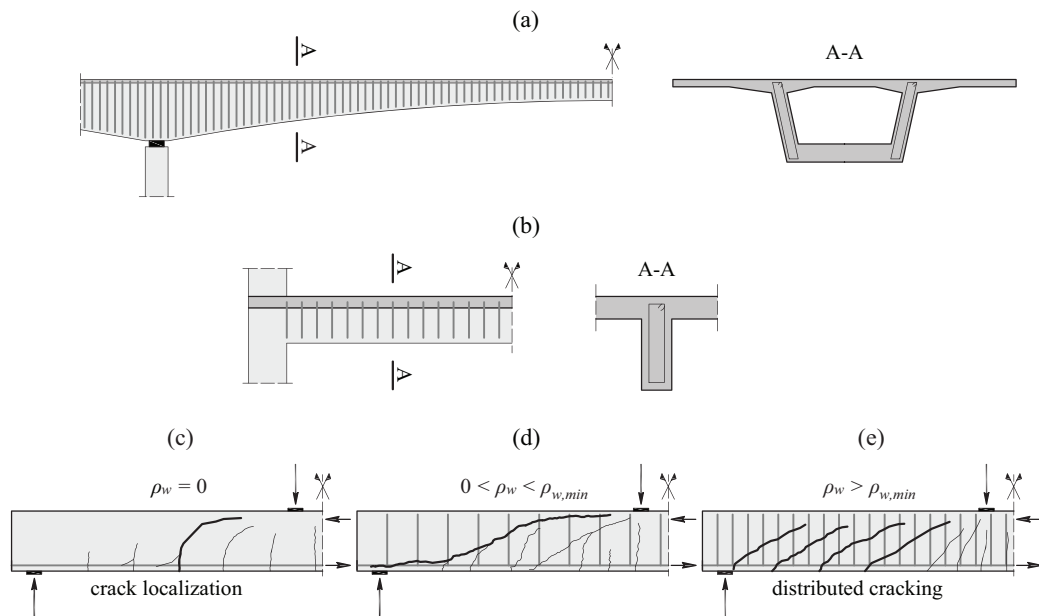

Figure 4.1:   Applications of shear reinforcement in (a) bridges; and (b) buildings. Influence of the amount of the shear reinforcement on the cracking patterns: (c) beam without shear reinforcement; (d) beam with low amount of shear reinforcement; and (e) with larger amount of shear reinforcement.

115

However, not all structural members contain shear reinforcement (as slabs or secondary elements [Eur04]). Such members are characterized by a brittle failure in shear due to the localization of the strains in a Critical Shear Crack (CSC) [Mut08, Fer15, Cav15] (Figure 4.1c). Limit analysis is thus not applicable and the strength and deformation capacity can be severely reduced. The required amount of shear reinforcement to consider a member as shear-reinforced has been traditionally defined in the following manner:

$$\rho_w = \frac{A_{sw}}{b_w \cdot s} \geq \rho_{w,min} \tag{4.1}$$

Where A_{sw} is the area of shear reinforcement unit, b_w is the width of the shear resisting cross section and s is the spacing of the shear reinforcement. The minimum amount of shear reinforcement ($\rho_{w,min}$) has been entitled with several roles:

- to ensure the limits of applicability of design models for members with shear reinforcement;

- to ensure sufficient robustness (avoid sudden brittle collapse after diagonal cracking);

- to ensure the development of distributed cracking (avoidance of crack localization);

- to cover several effects neglected in the design (transversal bending, imposed deformations, etc.).

Defining a suitable value for the minimum amount of shear reinforcement is instrumental for the economy of new structures, but also for the assessment of existing ones. The latter is relevant due to the fact that the minimum shear reinforcement ratio defined in former codes was very low (or even non-existent in older standards).

Although limited, several research efforts have been performed in the past to better understand the response of members with low amounts of shear reinforcement (Figure 4.1d, transition between responses governed by crack localization, Figure 4.1c, and distributed cracking, Figure 4.1e). The associated experimental programmes, [Ang99, Ang01, Hub16, Aut21, Cam13, Cla05, Mon21a, Piy02, Pla69, Rup13, Sør74, Teo02, Tue19, Yoo96, Tom02, Lee08, Joh90, Lim15] have acknowledged the role of several mechanical and geometrical parameters. Some of these parameters are related to the response of members without shear reinforcement (such as aggregate size [Tay63, Cam13], size of the member [Ang99, Aut21, Hub16, Tom02], strain effect [Lee08, Tom02] or influence of concrete compressive strength [Ang01, Cla05, Yoo96, Joh90]) while others refer to the arrangement and properties of the shear reinforcement [Aut21, Hub16] and its activation under different conditions [Rup13, Teo02, Mon21a].

For design, Eq. (4.1) has been traditionally adopted as a limit to consider if the approaches developed for members with shear reinforcement may be applied ($\rho_w \geq \rho_{w,\min}$) or if, conversely, models for members without shear reinforcement shall be used ($\rho_w < \rho_{w,\min}$). Some refined approaches have nevertheless been proposed in an effort to have tailored methods describing the transition from one regime to the other. They refer in many cases to models considering the shape and kinematics of the critical shear crack leading to failure where the contribution of the web reinforcement is accounted for [Cav17a, Tun20]. Such approach has been observed to be in agreement with experimental measurements [Mon21a] and is consistent with the Modified Truss Analogy (MTA) or truss with a concrete contribution, see Figure 4.2a.
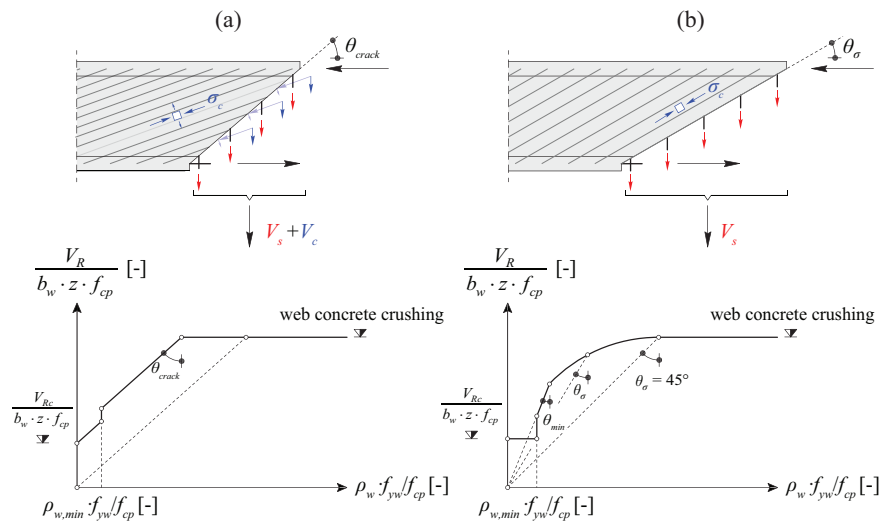
Figure 4.2:   Shear design: (a) Modified Truss Analogy (MTA, formulation adapted from ACI 318-19 [ACI19]); and (b) Variable Truss Angle (VTA, formulation adapted from EN 1992-1-1:2004 [Eur04]).

In the MTA, the shear strength (V_R) results from the contribution of the shear transfer actions related to concrete (V_c) and the contribution of the stirrups (V_s), but limited to the crushing capacity of the web (see Figure 4.2a where z refers to the inner level arm, f_{yw} refers to the yield strength of the stirrups and f_{cp}, to the equivalent concrete plastic strength [Fer07]). As it can be noted, the free-body investigated in the MTA is determined at the critical shear crack angle (θ_{crack}), which is not coincident with the average inclination of the compression field in the web (θ_σ). A refined approach based on a MTA is the Modified Compression Field Theory [Vec86, Ben06], which considers also the potential sliding along cracks (disengagement of aggregate interlock [Fer21]). An alternative approach to the MTA are the Variable Truss Angle (VTA) models [Gro76, Nie78, Thü79, Nie11], based on the limit analysis. In the VTA approach, the inclination of the compression field (θ_σ in Figure 4.2b) is directly selected by the designer to determine the required amount of shear reinforcement. Such inclination shall nevertheless remain within two limits. The upper limit corresponds to a value $\theta_\sigma = 45°$ (see Figure 4.2b), when crushing of the web without stirrup yielding governs (as for the MTA). The lower limit (θ_{min} in Figure 4.2b) is adopted to avoid excessive shear cracking in the web that may

reduce the strength of the compression field beyond the assumed compression softening values. In addition, for very low amounts of shear reinforcement, the shear resistance corresponding to a member without shear reinforcement may govern (refer to the value V_{Rc} in Figure 4.2b). It can be noted that MTA and VTA are both theoretically sound models and lead to similar results provided that the effect of cracking on the strength of the compression field is accounted for in a consistent manner.

With respect to the values adopted for $\rho_{w,\min}$ in different codes and design recommendations, several instances are plotted in Figure 4.3c [Eur04, FIB13, ACI19, AAS20, CSA14, SIA13]. All these codes depict a similar format, where the amount of shear reinforcement is a function of the compressive concrete strength and the yield strength of the shear reinforcement:

$$\rho_{w,\min} = \lambda \frac{\sqrt{f_c}}{f_{yw}} \tag{4.2}$$

where the material strengths are expressed in [MPa]. Such expression is based on the comparison of the concrete tensile strength (associated to the square root of the concrete compressive strength) with the reinforcement yield strength in a similar manner as the minimum reinforcement ratio in a member in pure tension, where the coefficient λ accounts for the particularities of the stress and strain state in the shear carrying area of the member and has been typically been determined in an empirical manner. All codes provide comparable values (with λ varying between 0.062 and 0.091), refer to Figure 4.3c. The influence of other relevant parameters, as previously discussed (size and strain effect, shear reinforcement response…) is however disregarded.

A comparison of the performance of the current version of Eurocode 2 (EN 1992-1-1:2004 [Eur04]) to a database of 236 beams for a wide range of shear reinforcement amounts is shown in Figure 4.3a (details of the formulation used are given in Appendix 4.A). The database is compiled from [Ang99, Aut21, Tue19, Bre63, Cam13, Cla05, Hub16, Piy02, Rup13, Vec04, Yoo96, Yos00, Teo02, Bac80, Kau96, Kuc08, Pla69, Sør74, De15, Fer08, Leo63, Moo14, Sag11] and comprises different loading conditions, different ductility classes of the shear reinforcement and different cross section types. Also, it includes both prestressed and non-prestressed members. On average, the results are safe, but with a relatively high scatter close to the minimum amount of shear reinforcement. This result seems logical, as the transition between both regimes allows activating the shear reinforcement while localization of strains still occurs. More refined models for the analysis of structural concrete accounting explicitly for strain compatibility (as the Elastic-Plastic Stress Fields method (EPSF) [Fer07, Mut15]), show better results on average and with a lower scatter, see Figure 4.3b. However, also for such refined methods, a significantly larger scatter is found close to the minimum amount of shear reinforcement confirming that this region is more sensitive to the localization of strains and deformation capacity.
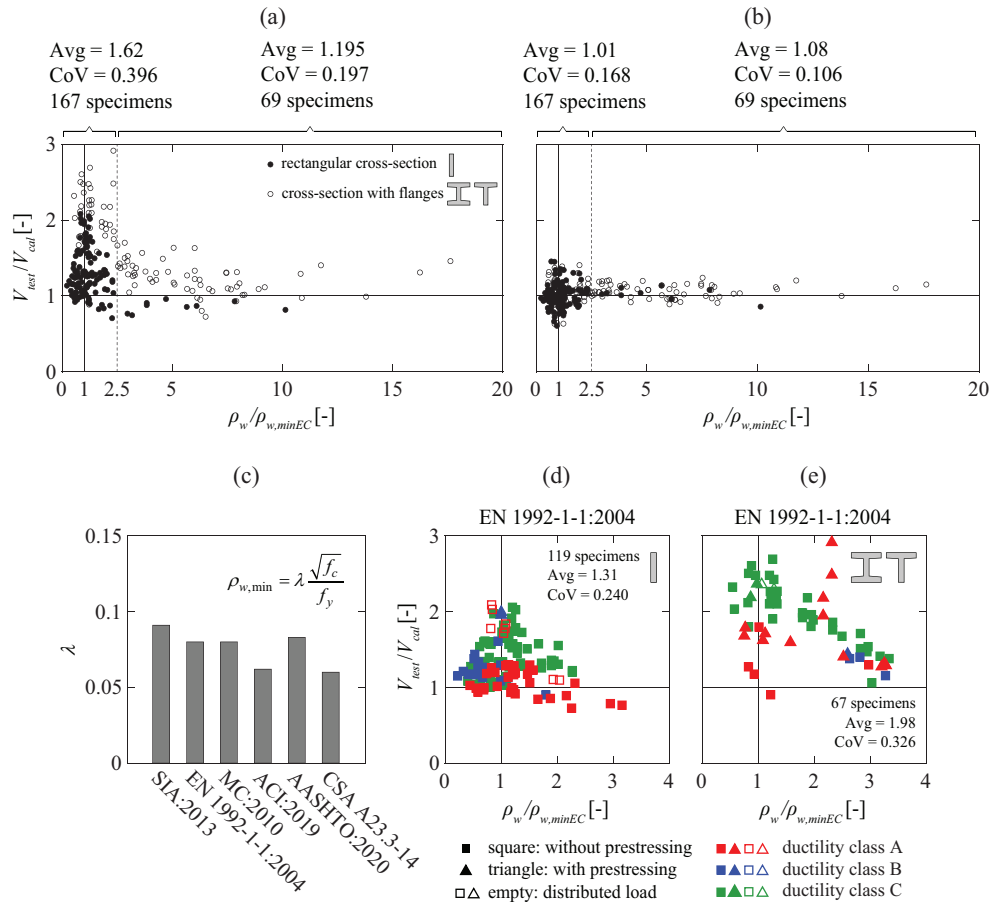
Figure 4.3:   Response of beams as a function of the amount of shear reinforcement. Comparison of measured-to-predicted shear strength V_{test}/V_{cal} according to: (a) EN 1992:1-1:2004 [Eur04, Mut15]; and (b) Elastic-Plastic Stress Fields method (EPSF) [Fer07]; (c) code recomendations for minimum shear reinforcement; and detail of comparison of measured-to-predicted shear strength V_{test}/V_{cal} according to EN 1992:1-1:2004 [Eur04] with low shear reinforcement ratio for: (d) specimens with rectangular cross section; and (e) specimens with flanges.

Some aspects can also be noted when the amount of shear reinforcement is close to $\rho_{w,\text{min}}$. A detailed view of this region ($0 < \rho_w \leq 4 \cdot \rho_{w,\text{min}}$), comparing the results of the current version of Eurocode 2 with the same test database used in Figures 4.3a-b, is presented in Figure 4.3d for rectangular cross-sections and in Figure 4.3e for flanged sections. It can be observed that, when the shear reinforcement has a relatively brittle post-yield response (corresponding to ductility class A according to EC2:2004 [Eur04], with a strain at maximum load 2.5 % $\leq \varepsilon_u <$ 5 % and a rupture-to-yield strength $1.05 \leq f_t/f_y <$ 1.08), it exhibits a lower performance than for reinforcement with larger ductility after yielding (as for ductility classes B (5 % $\leq \varepsilon_u <$ 7.5 % and $1.08 \leq f_t/f_y <$ 1.15) or C (7.5 % $\leq \varepsilon_u$ and $1.15 \leq f_t/f_y <$ 1.35) according to EC2:2004 [Eur04]).

This fact is even observed for amounts of shear reinforcement clearly above the minimum (Figures 4.3d-e).

In an effort to improve current knowledge on this topic and to lead to more consistent recommendations for shear design, this chapter presents a detailed investigation on the response of beams with low amounts of shear reinforcement. The results of a comprehensive testing programme performed on 10 beams with varying ratios of shear reinforcement ratio and shear reinforcement properties (ductility classes A and C according to [Eur04]) are presented. The tests were instrumented with advanced measurement techniques, such as Digital Image Correlation (to track the concrete displacement field) and Fibre-Optic Measurements (addressed at the strains of the stirrups and the flexural reinforcement). Based on these measurements, detailed analyses are performed on the role of the various potential shear-transfer actions. On that basis, and considering the results of the database previously introduced (Figure 4.3d-e), a number of changes are justified to enhance the performance of the design provisions of current Eurocode 2 (EN 1992-1-1:2004 [Eur04]) and *fib* MC2010 [FIB13]. These changes have currently been implemented on the drafts for the 2nd generation of Eurocode 2 (prEN 1992-1-1:2021) and of *fib* MC2020.

4.2   Experimental programme, series SM00

The experimental programme consisted of two series of tests (SM00 and SM10) conducted at the Structural Concrete Laboratory of Ecole Polytechnique Fédérale de Lausanne (Switzerland). They had some differences and will be described in different sections: SM00 in this section and SM10 in the following one.

4.2.1   Specimens

Series SM00 was composed of four simply supported beams tested in three-point bending, with a rectangular cross section ($b_w \times h = 250 \times 600$ mm). Figures 4.4a and c present the geometry of the specimens (details are given in Table 4.1). Two parameters were investigated: (i) the ductility class of the shear reinforcement (A and C); and (ii) the anchorage of the links.

The shear reinforcement ratio was $\rho_w = 0.113$ % consisting of one-leg links diameter 6 mm with a spacing of 100 mm. Two types of anchorages were considered, headed bars to ensure an efficient anchorage (specimens SM01 and SM02) and links with short bends (SM03 and SM04). The headed bars (Figure 4.4b) consisted of a glued steel head, whose performance was tested and verified in direct tension tests. For the links, the geometry shown in Figure 4.4b was used.

The flexural reinforcement ratio was $\rho = 1.34$ % consisting of 3 bars diameter 28 mm with an effective depth of $d = 550$ mm. The compression reinforcement consisted of 2 bars diameter 16 mm. At each extremity of the specimen, 4 stirrups diameter 10 mm were added to avoid failure at the end regions. The shear span of all specimens was $a = 1800$ mm ($a/d = 3.27$, see Figure 4.4c). It can be noted that, in order to save material, one extremity of the specimens was connected to a steel girder (Figure 4.4c). Such connection was performed outside of the region of study and introduced no disturbances within the test region.
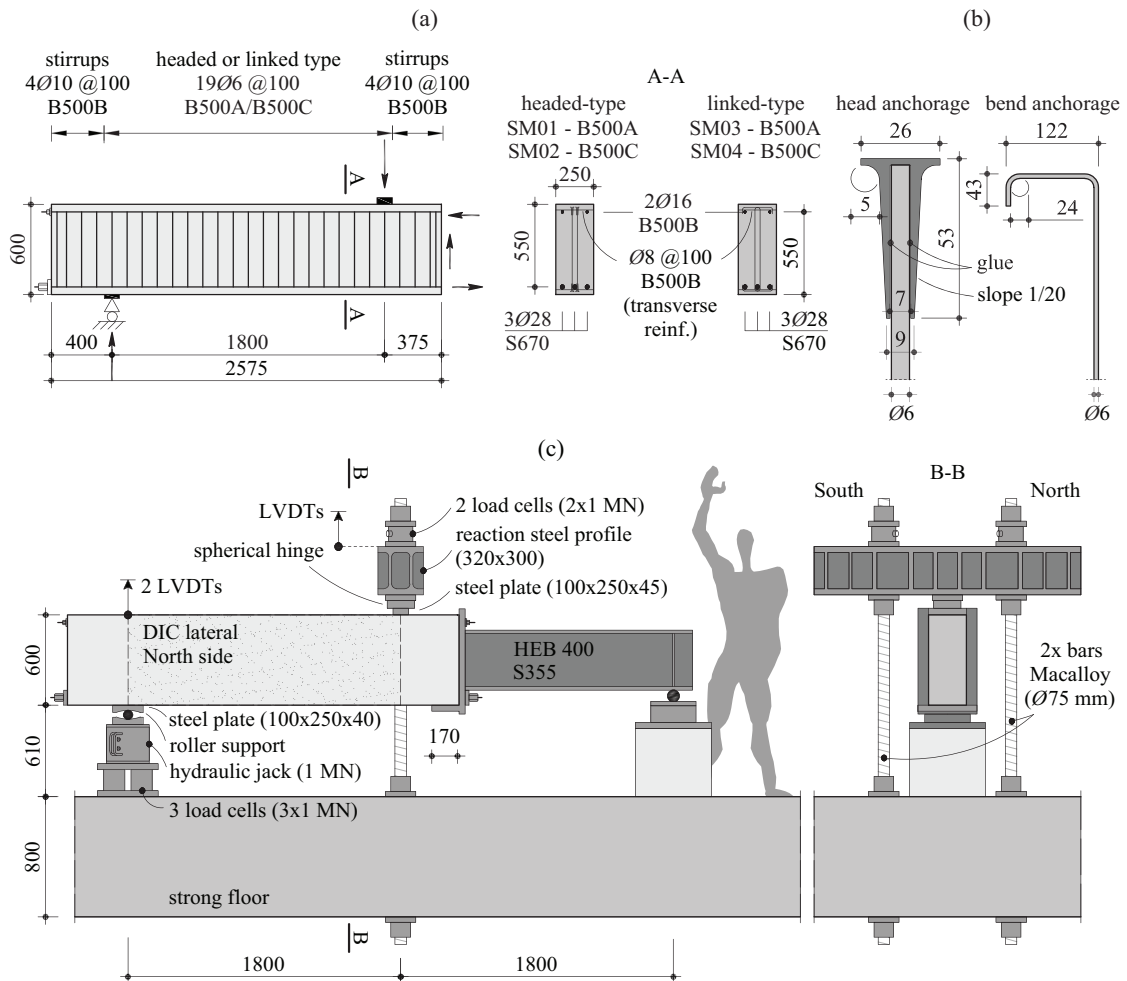

Figure 4.4:   Series SM00: (a) geometry of specimens with reinforcement layouts; (b) shear anchorage detail; and (c) test set-up.

Table 4.1: Main parameters and experimental results of series SM00 (for definition of parameters, refer to section Notation).

Specimen	Shear reinf. anchorage	Shear reinf. ductility class[1]	ρ_w [%]	f_c [MPa]	f_{ct} [MPa]	f_{yw} [MPa]	f_{tw} [MPa]	ε_{uw} [%]	V_{max}[2] [kN]	τ_{max}[3] [MPa]
SM01	Head	A	0.113	40.4	2.1	556	577	2.8	235	1.71
SM02	Head	C	0.113	40.5	2.1	516	608	7.5	286	2.08
SM03	Bend	A	0.113	40.6	2.2	556	577	2.8	235	1.71
SM04	Bend	C	0.113	40.6	2.2	516	608	7.5	269	1.96

[1] according to [Eur04]

[2] measured shear strength without self-weight

[3] $\tau_{max} = V_{max}/(b_w \cdot d)$

4.2.2 Material properties

All specimens were cast from one batch of normal strength concrete (water-to-cement ratio equal to 0.65 and a cement content equal to 308 kg/m³) and a maximum aggregate size of 16 mm (crushed aggregates). The compressive strength f_c measured on cylinders ($h \times \varnothing = 320 \times 160$ mm) at the time of testing was 41 MPa on average. Direct tension tests on cylinders 320×160 mm were also performed (see details in Table 4.1).

The shear reinforcement consisted of different steel types (Figure 4.5a and Table 4.1):

- B500A: 6-mm diameter bars of nominal ductility class A [Eur04]. The reinforcement was cold-worked with no clear yield plateau, exhibiting a nominal yield strength (0.2 % residual strain) equal to 556 MPa and a tensile strength of 577 MPa. The strain at maximum load was 2.8 % and was defined according to [Eur04] following the procedure given in EN ISO 15630-1 [ISO19]. It can be noted that the mechanical properties were complying with those of a ductility class A reinforcement according to EN 1992-1-1:2004 [Eur04] in terms of strain at maximum load, but not with respect to the ratio f_{tw}/f_{yw} which was lower ($f_{tw}/f_{yw} = 1.04$) than the required limit ($1.05 \leq f_t/f_y < 1.08$).

- B500C: 6-mm diameter bars of nominal ductility class C [Eur04]. The reinforcement was also cold-worked with a nominal yield strength equal to 516 MPa and a tensile strength of 608 MPa. The strain at maximum load was 7.5 %. This reinforcement complies with the requirements for a ductility class C according to EN 1992-1-1:2004 [Eur04].

The flexural reinforcement consisted of 28-mm diameter of water tempered high strength steel (Figure 4.5c). The compression reinforcement consisted of a 16-mm diameter hot rolled bars with a well-defined yield plateau (yield strength equal to 553 MPa and a tensile strength equal to 661 MPa).
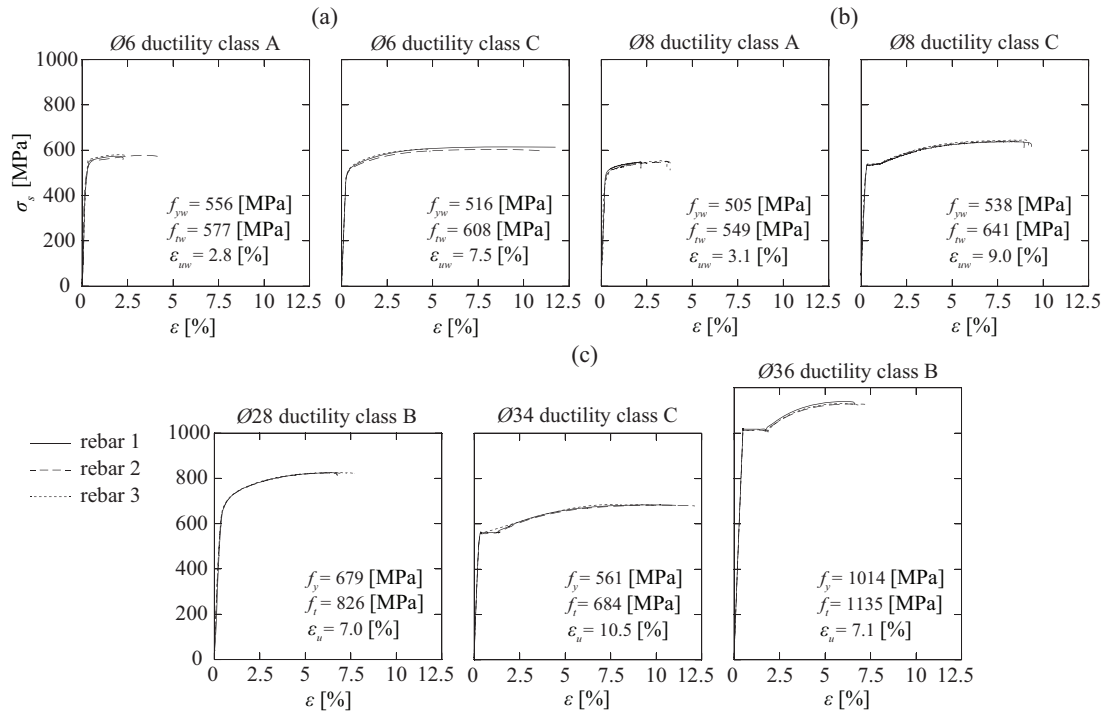
Figure 4.5:   Stress-strain curves for: (a) shear reinforcement bars of series SM00; (b) shear reinforcement bars of series SM10; and (c) flexural reinforcement bars of series SM00 and SM10.

4.2.3   Loading

A concentrated load was applied at the left roller support (free horizontal movements and rotations) by means of a hydraulic jack. The load was in equilibrium with the forces developing in the right roller support (free rotations) and a reaction frame at mid-span (connected to the strong floor by means of two threaded bars with a spherical hinge). The bearing plate at the load was 200x250x40 mm and 100x250x45 mm at mid-span. The load was applied at a loading rate of 25-45 kN/min. The effect of the self-weight of the beam on the left support was 8 kN and the effect of the weight of the set-up on the left support was 3.5 kN.

4.2.4 Measurements

Five load cells of 1 MN capacity were used. Three load cells were located directly under the hydraulic jack to measure the support reaction (Figure 4.4c). Two load cells were also arranged at mid-span. The deflection of the beam was measured using three LVDTs (Figure 4.4c, two on the top side of the beams and one at the reaction frame).

In addition, Digital Image Correlation (DIC) measurements were performed on the concrete lateral surface, refer to Figure 4.4c. They allowed tracking the cracking pattern and the displacement field. Two digital cameras SVS hr29050 (29 megapixels) were used for the DIC. The speckles painted on the surface had a size of 2 mm. The image acquisition rate of the cameras was 0.2 Hz at first loading stages, increased to 1 Hz near to failure. VIC3D software was used to analyse the images [Cor10]. Pictures were taken before running the tests (at displacement equal to zero, with self-weight) and a measured noise (average between the maximal and minimal displacement values) was around 1/50 of a pixel of the in-plane displacements.

4.3 Experimental programme, series SM10

The main objective of the second series was to vary the amount and the mechanical properties (ductility class) of the shear reinforcement.

4.3.1 Specimens

Six tests were performed on three beams. All specimens had constant length (7800 mm) and height (700 mm), but variable width (800, 600 and 500 mm). Figure 4.6a-b show the geometry of the specimens and the load arrangement (details are given in Table 4.2). First, a shear span of length $a = 2600$ mm was tested until failure. Then, the beam was removed and positioned again in order to test the other shear span (2600 mm). As the effective depth of the beams was $d = 650$ mm, the nominal shear span-to-effective depth ratio in the tested regions (a/d) was equal to 4.

In the test region, the shear reinforcement consisted of two-legs closed stirrups diameter 8 mm with a spacing of 200 mm. Depending on the width, the shear reinforcement ratio was thus $\rho_w = 0.063$ % ($b_w = 800$ mm), 0.084 % ($b_w = 600$ mm) and 0.101 % ($b_w = 500$ mm). The flexural reinforcement ratio in the shear spans (2600 mm) was $\rho = 1.5$ % for specimens SM11-SM12 with $b_w = 800$ mm (6 high-strength bars diameter 36 mm and 2 bars diameter 34 mm), $\rho = 1.51$ % for specimens SM13-SM14 with $b_w = 600$ mm (4 high-strength bars diameter 36 mm and 2 bars diameter 34 mm) and $\rho = 1.52$ % for specimens SM15-SM16 with $b_w = 500$ mm

(3 high-strength bars diameter 36 mm and 2 bars diameter 34 mm). The compression reinforcement was composed of 8, 6 or 5 bars diameter 20 mm for b_w = 800, 600 or 500 mm, respectively. In addition, two stirrups diameter 14 mm (spacing of 150 mm) were added in the central part of the beam (2200 mm) to avoid shear failures in that region which was not studied. In this central region, the flexural reinforcement was modified, replacing the 2 bars diameter 34 mm by 4 bars diameter 26 mm which were spliced with a welded connection, see Figure 4.6a (this detail was adopted due to the limitation on the length of the bars for installation of Fibre-Optic Measurements).
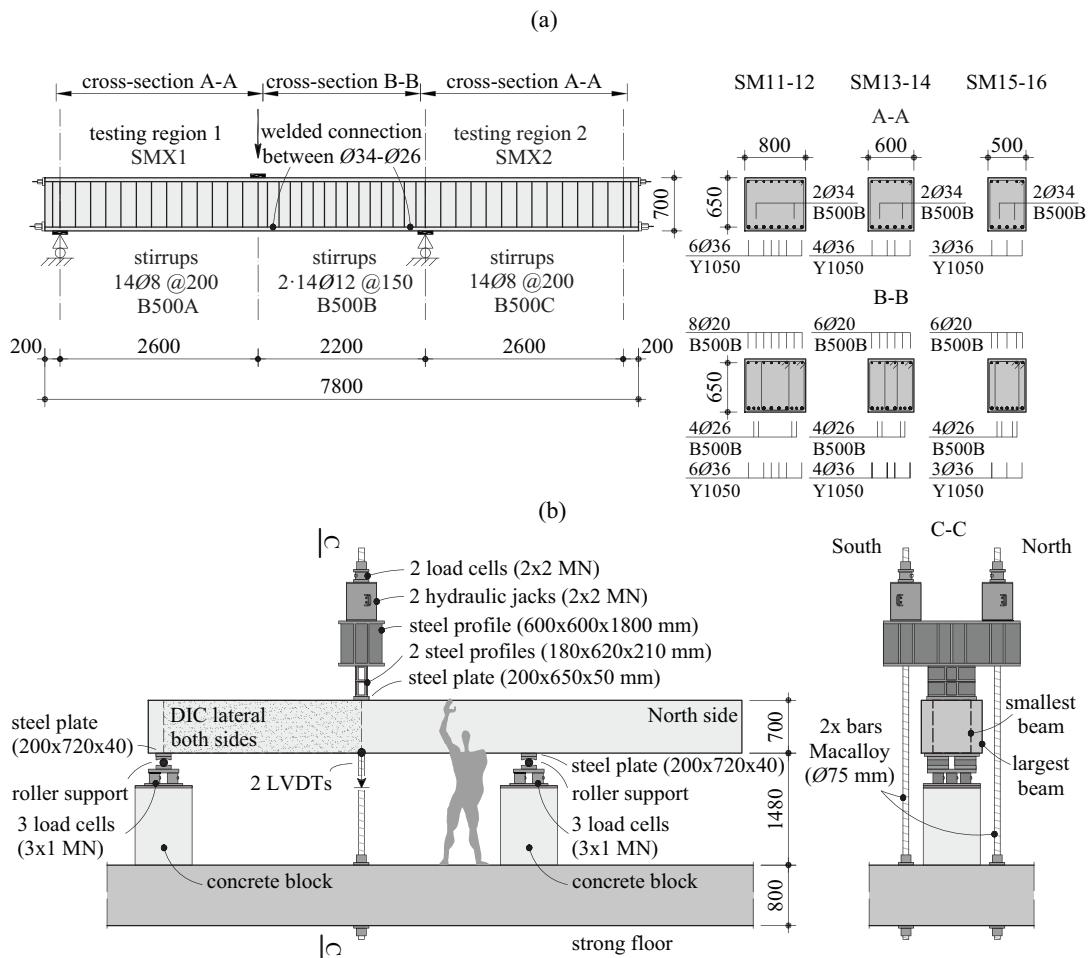
(a)

(b)

Figure 4.6: Series SM10: (a) geometry of specimens with reinforcement layouts; and (b) test set-up.

Table 4.2:   Main parameters and experimental results of series SM10 (for definition of parameters, refer to section Notation).

Specimen	Shear reinf. ductility class[1]	b_w [mm]	ρ_w [%]	f_c [MPa]	f_{ct} [MPa]	f_{yw} [MPa]	f_{tw} [MPa]	ε_{uw} [%]	V_{max}[2] [kN]	τ_{max}[3] [MPa]
SM11	A	800	0.063	50.7	3.2	505	549	3.1	603	1.16
SM12	C	800	0.063	50.6	3.2	538	641	9.0	610	1.17
SM13	A	600	0.084	50.4	3.2	505	549	3.1	540	1.38
SM14	C	600	0.084	50.4	3.1	538	641	9.0	639	1.64
SM15	A	500	0.101	50.2	3.1	505	549	3.1	454	1.40
SM16	C	500	0.101	50.0	3.1	538	641	9.0	515	1.58

[1] according to [Eur04]

[2] measured shear strength without the self-weight

[3] $\tau_{max} = V_{max}/(b_w \cdot d)$

4.3.2   Material properties

All specimens were cast from one batch of normal strength concrete (water-to-cement ratio equal to 0.5 and a cement content equal to 300 kg/m^3) and a maximum aggregate size of 16 mm (crushed aggregate). The compressive strength f_c measured on cylinders ($h \times \varnothing = 320 \times 160$ mm) at the time of testing was 50 MPa on average. Direct tension tests on cylinders 320×160 mm were also performed (for details on the values, refer to Table 4.2).

The shear reinforcement (stirrups) consist of two types of steel (Figure 4.5b and Table 4.2):

- B500A: 8-mm diameter bars of nominal ductility class A [Eur04]. The reinforcement was cold-worked with the mean yield strength equal to 505 MPa and a mean tensile strength of 549 MPa. The strain at maximum load was 3.1 % and was defined according to [Eur04] following the procedure given in EN ISO 15630-1 [ISO19]. Such reinforcement corresponds to a ductility class A according to EN 1992-1-1:2004 [Eur04] in terms of strain at maximum load, although it has a larger f_{tw}/f_{yw} than required.

- B500C: 8-mm diameter bars of nominal ductility class C [Eur04]. The reinforcement was hot-rolled steel with well-defined yield plateau and a mean yield strength equal to 538 MPa and a mean tensile strength of 641 MPa. The strain at maximum load was 9.0 %. This reinforcement fully complies thus with the requirements for a ductility class C according to EN 1992-1-1:2004 [Eur04].

To determine the yield and tensile strengths, tests on 8-mm diameter bars with a groove have been conducted (same groove as the one used to install FOM in instrumented bars, leading to a reduced area of 2 % with respect to a conventional bar, see section 4.3.4). The given yield and tensile strengths have been calculated by dividing the measured forces by the nominal value of the effective cross-sectional area (50.3 mm^2, without considering the groove). The flexural reinforcement in the testing region consisted of hot-rolled high strength steel with a well-defined yield plateau (for details on the values, refer to Figure 4.5c). With respect to the other reinforcements, the following material properties were measured:

- 26-mm diameter bars (flexural reinforcement in the central region): hot-rolled steel with f_y = 583 MPa and f_t = 688 MPa.

- 20-mm diameter bars (compression reinforcement): hot-rolled steel with f_y = 587 MPa and f_t = 725 MPa.

4.3.3   Loading

The test set-up is shown in Figure 4.6. The load was introduced by means of two hydraulic jacks placed on a transverse box-shaped steel profile. The jacks were anchored to the strong floor by a set of threaded bars. The loading plate under the steel profiles had dimensions equal to 200x650x50 mm. Two bearing plates with dimensions of 200x720x40 mm were arranged over the roller support allowing horizontal longitudinal displacement and rotations.

The load was applied at a rate of 10 kN/min. The effect of the self-weight of the beam at the left support was 25.1 kN for the beam with b_w = 800 mm, 18.5 kN for the beam with b_w = 600 mm and 15.6 kN for the beam with b_w = 500 mm. The reaction at that same support due to the weight of the load set-up was 9.6 kN.

4.3.4   Measurements

Three load cells of 1 MN were used for each bearing support and two load cells of 2 MN were arranged over the hydraulic jacks (Figure 4.6b). Two LVDTs were used to measure the deflection of the beams at the location of the applied load (Figure 4.6b). As for the previous series, DIC measurements were also performed to track the cracking pattern and displacement field of the tests. The same devices and procedure for DIC was followed except that the DIC measurements were performed on both lateral surfaces (North and South sides). The image acquisition rate of all cameras was 0.2 Hz at first loading stages, increased to 1 Hz before failure.

In addition to previous measurement devices, Fibre-Optical Measurement (FOM) based on Rayleigh scattering was also performed on selected stirrups and flexural reinforcement. The results have been post-processed using the software Odisi-B version by Luna Innovations [Lun13]. This technique allows obtaining measurement of the strain profiles along the bars with

a high frequency and a low spatial resolution [Bra19, Bad21] (a gage pitch of 0.65 mm was chosen). FOM was used for the stirrups ST2 to ST13 and for the bar Ø34 of the flexural reinforcement (Figure 4.7a). For stirrups ST5, ST8 and ST11, two fibres were glued (refer to blue and red lines in Figure 4.7b) to allow tracking the tension elongation and potential dowelling of the bars. For stirrups ST2-ST4, ST6-ST7, ST9-ST10 and ST12-ST13, only one fibre was glued (blue line in Figure 4.7c). With respect to the flexural reinforcement, one fibre was glued at each side (Figure 4.7d) to measure the tensile strains and the flexure associated to dowelling action.

The fibre used for FOM was a 125-µm polyimide optical fibre installed into grooves of 1 mm depth for the stirrups and 2 mm depth for the flexural reinforcement (see Figure 4.7e [Can20, Mat20, Mon21]). More details on the technique (installation of fibres, acquisition and processing of data) can be consulted in [Can20].
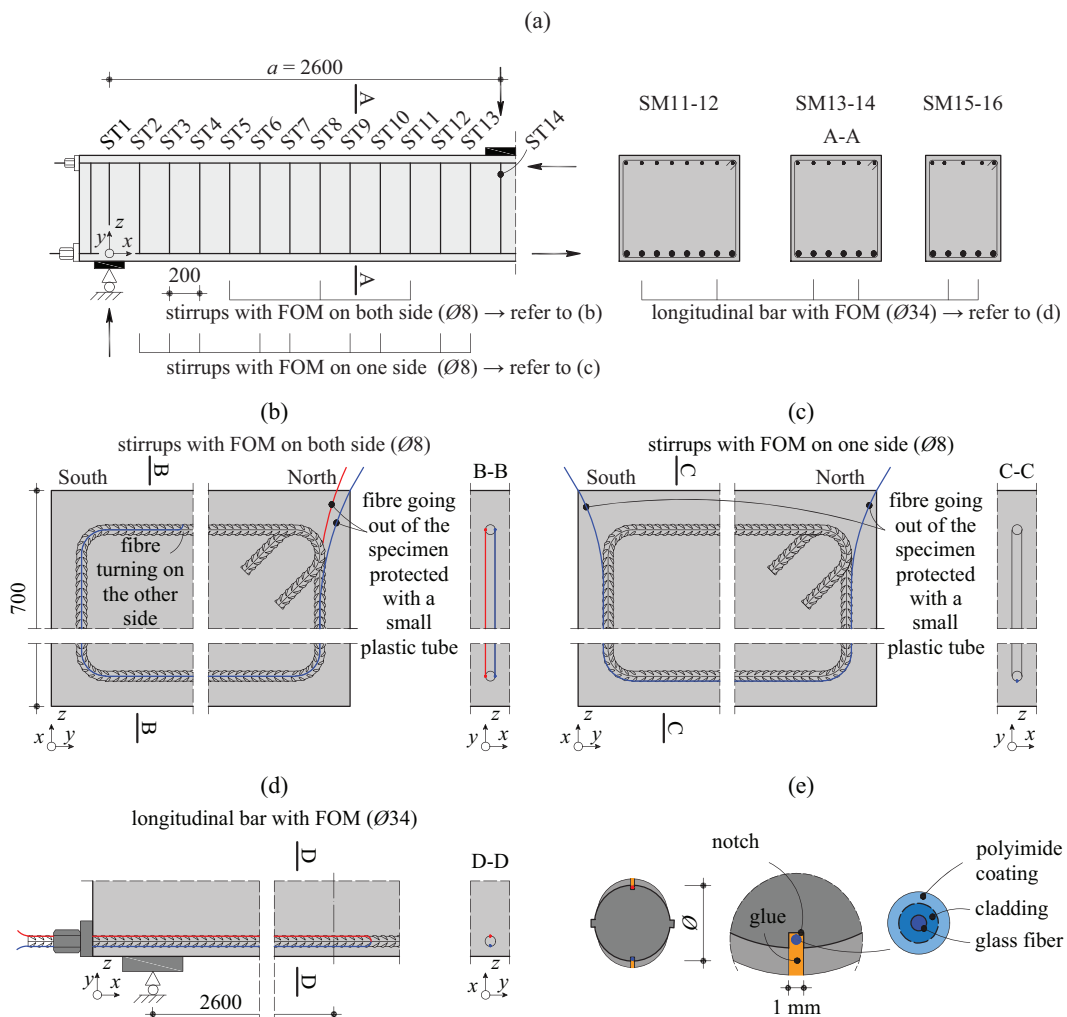

Figure 4.7: Fibre-Optical Measurement: (a) instrumented bars; (b) positions on the stirrups with two fibres; (c) position on the stirrups with one fibre; (d) position on the flexural reinforcement; and (e) detail of installation.

4.4   Experimental results

4.4.1   Shear resistance

All specimens failed in shear experiencing a brittle failure and without significant residual strength. The maximum shear force recorded (V_{max}) is listed in Tables 4.1 and 4.2 for the two series. The load-deflection curves are shown for the two series in Figure 4.8a (series SM00) and b (series SM10) in terms of average shear stress ($\tau = V/(b_w \cdot d)$). Also, Figure 4.8c depicts the shear resistance ($\tau_{max} = V_{max}/(b_w \cdot d)$) for the different tests as a function of the shear reinforcement ratio and of the ductility class. The following observations can be made:

- An increase of the shear reinforcement led to an increase of the shear strength and displacement δ at the peak load.

- For the series SM00, the type of shear anchorages (heads or bends) did not show any significant influence.

- Specimens with shear reinforcement of ductility class C failed at larger levels of load than the corresponding specimens with ductility class A reinforcement (about 10-15 % strength increase) when the shear reinforcement ratio was larger or equal than 0.084 %. No influence of the ductility class for specimens with a shear reinforcement ratio of 0.064 % was observed.

- For series SM10, the development of a diagonal crack had an influence on the load-deflection relationship. For specimens with a shear reinforcement ratio equal to $\rho_w = 0.064$ %, a sudden drop of the load was observed when the diagonal crack formed. The specimen could be reloaded after that, but failed at approximately the same level of load (Figure 4.8b). For specimens with larger shear reinforcement ratios (0.084 % and 0.101 %), the formation of the diagonal crack is also clearly visible in the load-deflection relationship which shows a change of slope (due to the larger shear deformations after diagonal cracking [Can22]). However, these specimens did not experience a sudden drop of the applied load and could be loaded at significantly larger levels of load (similar observations have also been made by Autrup et al. [Aut21]).
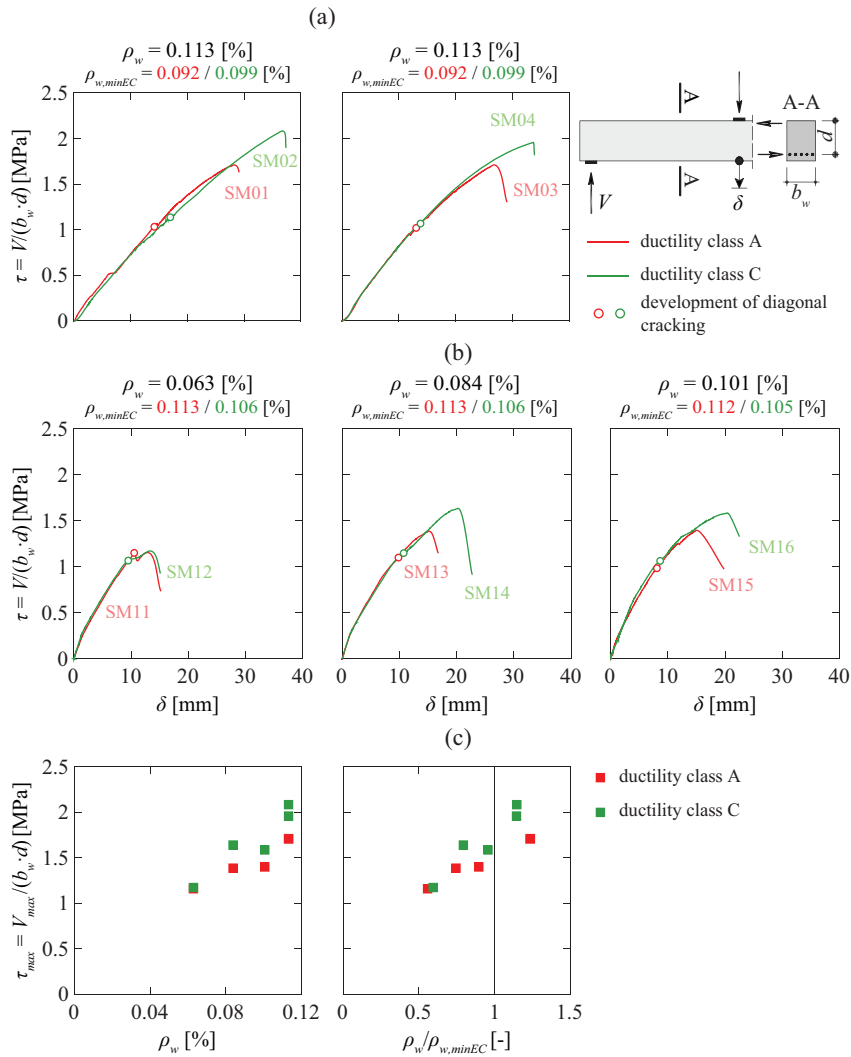
Figure 4.8:   Load-deformation curves for: (a) series SM00; and (b) series SM10. (c) Maximum shear capacity in function of the shear reinforcement ratio.

4.4.2   Cracking pattern

Figure 4.9 shows the cracking pattern recorded by DIC at selected load steps for specimens with $\rho_w = 0.063$ % (lower than the minimum shear reinforcement ratio according to EC2:2004 [Eur04]) and for $\rho_w = 0.101$ % (close to the minimum shear reinforcement ratio according to EC2:2004, Figure 4.3c). The selected load steps presented in Figure 4.9 correspond to: i) the load at which flexural cracks start developing in a sub-horizontal manner [Cav17] (indicated with green bullets); ii) the complete development of the Critical Shear Crack (CSC) (red bullets); and iii) failure (blue bullets). For beams SM15 and SM16, additional intermediate load steps are also presented (orange and magenta bullets).

For specimens with $\rho_w = 0.063$ %, the development of the CSC is followed by a rapid opening, which leads to a localization of strains and to failure of the member (CSC developing at approximately 95 % and 100 % of the maximal load, see Figure 4.9). For specimens with $\rho_w = 0.101$ %, several shear cracks were observed at failure. The first diagonal crack develops at the same absolute load level as for members with $\rho_w = 0.063$ %, but corresponds in this case only to 70 % and 80 % of the failure load (Figure 4.9). The development of multiple diagonal cracks was particularly marked for the specimen with ductility class C shear reinforcement (refer to specimens SM16 in Figure 4.9). Details on the cracking pattern at failure of the other specimens are given in Appendix 4.B.
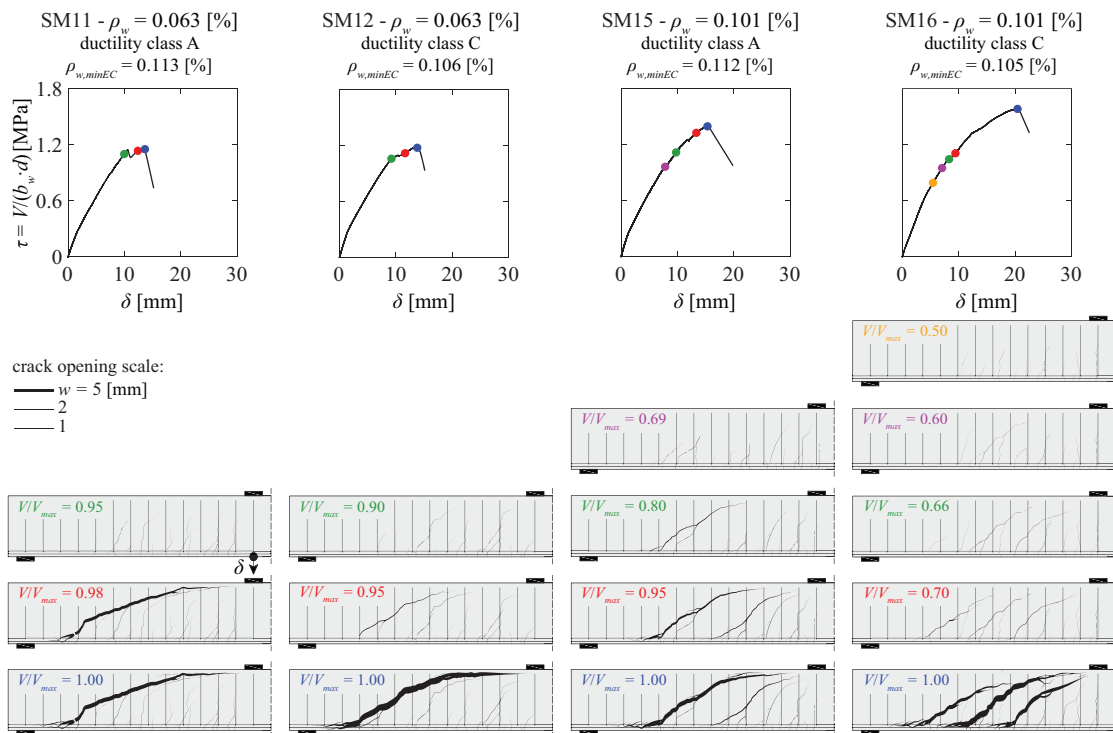
Figure 4.9:   Development of the cracking pattern during loading.

4.4.3   Crack kinematics

Figure 4.10 shows the crack kinematics obtained by means of DIC measurements for the same selected specimens presented before (see Appendix 4.C for other specimens). The kinematics is presented for the most relevant cracks (including the CSC) in terms of relative displacement vectors between points located on both sides of the cracks at different load step (varying from 70 % to 100 % of the peak load). For specimen SM12, the last measurement corresponds to the post-peak phase (at a load level equal to 98 % of the maximum load). As it can be noted, just before failure, the crack opening is relatively constant in all cases. The relative displacement between crack lips is in addition almost vertical, with a relative displacement which decreases

approximatively linearly in the sub-horizontal branch (due to a rotation around the crack tip [Fer15]), consistently with previous observations for members with [Rup13] or without shear reinforcement [Cav15].

For the tests with $\rho_w = 0.063$ %, the crack kinematics is similar despite the different ductility class. For these specimens, the development of the CSC opening occurs mostly just before failure (between 95 and 100 % of the peak load), leading to crack openings of about 5 mm just before failure. For the tests with $\rho_w = 0.101$ %, the development of the CSC is more progressive during the loading process and accompanied by secondary cracking (Figure 4.10). The crack opening remains below values of 2-3 mm up to 95 % of the maximum load, increasing thereafter rapidly and reaching approximately 5 mm at failure. In addition, the tests with $\rho_w = 0.101$ % showed a relative similar response between the two ductility classes of the reinforcement (A for SM15 and C for SM16).
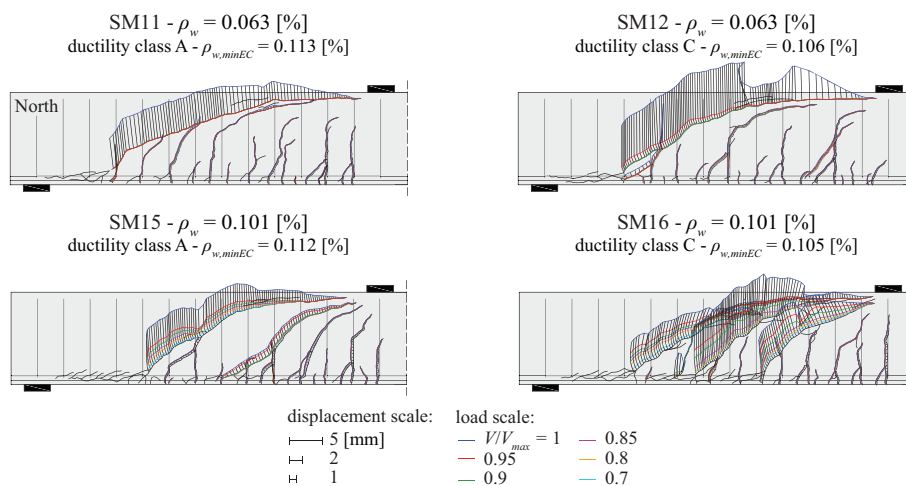
Figure 4.10: Crack kinematics for different shear reinforcement ratio and ductility class.

Figure 4.11 shows the evolution during the loading process of the crack opening (w), the sliding (Δ) and the angle ψ between the displacement vector and the vector perpendicular to the crack at mid-depth of the CSC. The crack opening w starts developing at approximately 50 % of the peak load in all cases (if the CSC was not fully developed, this measurement refers to the flexural crack at that location). The crack opening develops in a progressive manner thereafter. The crack slip Δ and angle ψ show a different trend. The crack slip starts developing later, at approximately 60 % of the peak load for $\rho_w \geq 0.084$ % and just before the failure load for $\rho_w = 0.063$ %, followed by a sudden propagation. It is thus strongly influenced by the amount of shear reinforcement. The relative angle ψ follows this trend.
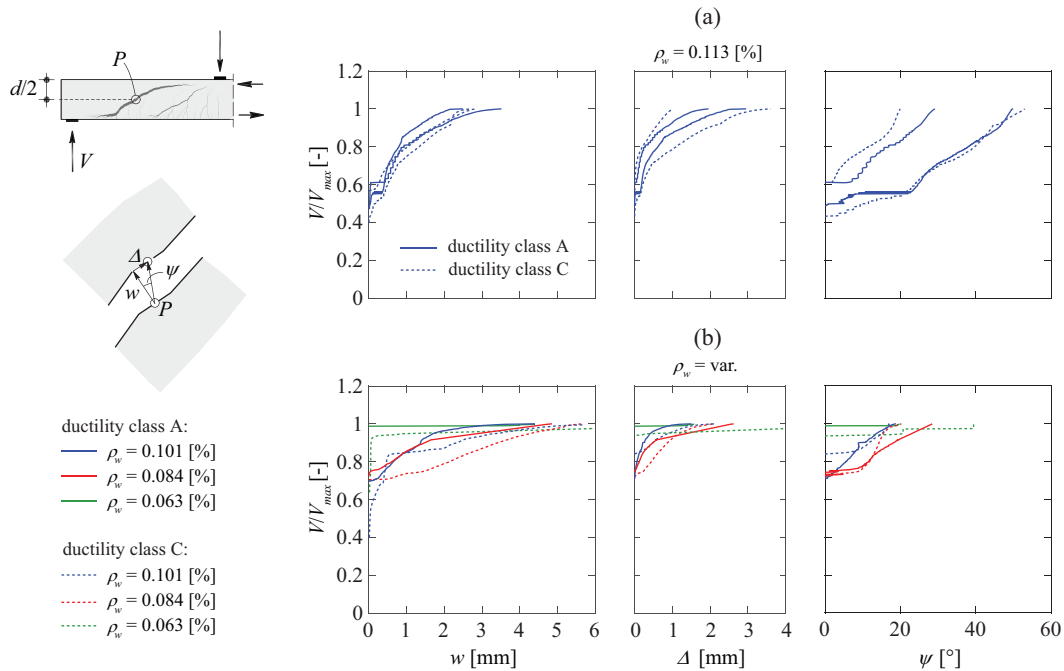
Figure 4.11:   Crack opening w, sliding Δ and angle ψ between Δ and w at position P for:
(a) series SM00; and (b) series SM10.

4.4.4   Stirrups and flexural strain profiles

Figure 4.12 shows the strains in the stirrups and in the flexural reinforcement measured by means of FOM for the same selected specimens (details for other specimens are given in Appendix 4.D). It shall be commented that the fibre was capable of measuring up to strains of approximately 1-1.5 % whereas the signal was lost for larger strains. The following observations of the FOM measurement can be made for the stirrups:

- all stirrups intercepted by the inclined branch of the CSC exhibited levels of strain at yielding or larger (red lines in Figure 4.12). In the case of $\rho_w = 0.101$ %, stirrups crossed by others cracks reached also the yield strength.

- The yielded region of stirrups extends over a length of about 6 to $10 \cdot \varnothing_w$. An approximately linear increase of strain is observed in the region where the bar is in the elastic domain indicating an almost constant bond stress (blue lines in Figure 4.12).

- for $\rho_w = 0.063$ %, the strain starts increasing significantly at approximately 90 % of the peak load, consistently with the development of the shear crack (see Figures 4.10 and 4.11). In the case of $\rho_w = 0.101$ %, the strains start developing at neatly lower load levels (approximately 80 % of the peak load).

- ▪ Near the flexural compression zone (where the CSC is sub-horizontal), the stirrups are not fully activated because the delamination crack partially develops above the stirrups. In the lower part of the beam, where the delamination crack develops along the tensile reinforcement, the stirrups reached the yield strength due to the dowel effect of the longitudinal bars.

With respect to the flexural reinforcement, it remained elastic and the strains on the top side of the bars were not the same as those on the bottom, indicating bending of the bar (associated to dowel effect). The specimens with $\rho_w = 0.063$ % showed that the activation of the dowel action occurred only close to the peak load, while for specimens with $\rho_w = 0.101$ %, it developed in a more progressive manner.
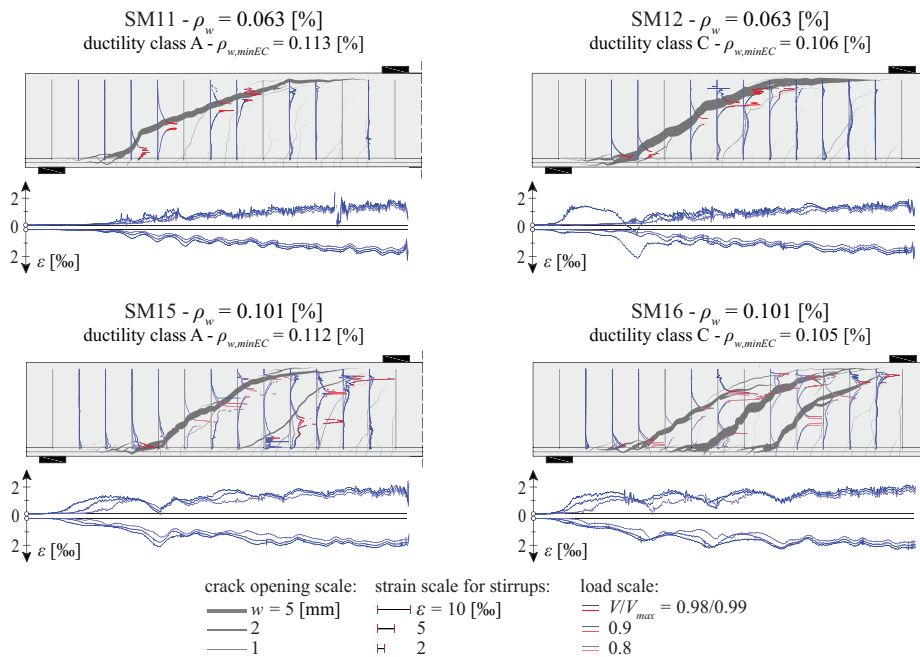
Figure 4.12:   Stirrups and flexural strain profiles for specimen SM11, SM12, SM15 and SM16 at different load steps (80, 90 and 100% of the maximal load). Note: red refers to yielding of the reinforcement, blue to its elastic domain.

4.5   Analysis of the shear transfer actions

As shown in different works [Cam13, Fer15, Cav17, Hub16, Tas20, Mon21a, Kos22], the shear strength can be estimated as the sum of the contribution of the various potential shear-transfer actions (STA, Figure 4.13b). The investigation of each STA is performed considering the free body defined by the CSC (refer crack presented in Figure 4.9). In the following, the methodology proposed by Cavagnis et al. [Cav17] will be applied. This approach considers the actual measured shape and kinematics of the CSC (Figure 4.13a) and applies suitable material

constitutive laws to determine their contribution to the total shear resistance. The various STA are briefly recalled in the following sections, highlighting the parameters that are refined or adapted with respect to [Cav17].
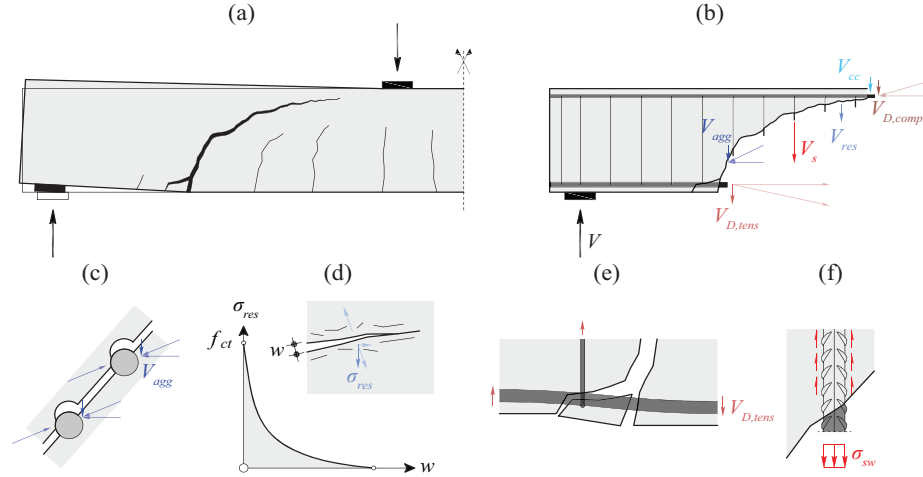
Figure 4.13:   Definition of the shear-transfer actions (STA): (a) CSC shape and kinematics at failure; (b) free-body with shear contributions; (c) aggregate interlock; (d) concrete residual tensile strength; (e) dowelling action of the longitudinal bars; and (f) axial force and bond in the shear reinforcement.

4.5.1   Aggregate interlock (V_{agg})

Aggregate interlock allows for the transfer of stresses through the crack due to the mechanical engagement of its rough lips (Figure 4.13c). Several approaches have been proposed in the literature to calculate the stresses based on crack kinematics (opening and sliding) such as the models of Walraven [Wal80] or Cavagnis et al. [Cav18]. The latter has a convenient analytical formulation, showing good results for crack openings in the range of 0.5-1 mm. In the case of beams with low shear reinforcement, the crack openings at failure are about 4-6 mm (Figure 4.10), which may lead to very low stresses when such formulae used. For this reason, the model proposed by Fernández Ruiz [Fer21], based on limit analysis and considering material damage conditions to describe the transfer of forces through a discontinuity line, will be used in the following. According to this model, the interface stresses can be calculated as:

$$\tau_{agg} = \frac{1}{2} f_{cp} \cdot \cos\left(\frac{\pi}{2} - \psi + \xi \right)$$
$$\sigma_{agg} = -\frac{1}{2} f_{cp} \cdot \left(1 - \sin\left(\frac{\pi}{2} - \psi + \xi \right) \right)$$

(4.3)

Where $\tan(\pi/2 - \psi) = w/\Delta$ (valid for $\pi/2 \geq \pi/2 - \psi + \xi \geq \varphi$) is the angle of the crack displacement with respect to the crack plane and φ is the friction angle of concrete ($\varphi = 37°$). The dilatancy

angle ξ takes into consideration the evolution of the cinematic during loading of the CSC as well as the associated deterioration at the lips of the crack. A suitable value for beams in shear was proposed by Fernández Ruiz [Fer21] as $\xi = 17°$ and will be used hereafter. The parameter f_{cp} is the equivalent plastic strength ($f_{cp} = f_c \cdot \eta_{fc} \cdot \eta_w$), where η_{fc} refers to the brittleness factor [FIB13, Moc20] and η_w is the concentrated crack opening factor defined as [Fer21]:

$$\eta_{fc} = \left(\frac{30}{f_c}\right)^{1/3} \leq 1$$
$$\eta_w = \frac{1}{1 + 100\dfrac{w}{d_{dg}}}$$
(4.4)

The parameter d_{dg} accounts for the maximum aggregate size (d_g) [Eur21, Cav18], and can be calculated as $d_{dg} = \min(40\text{ mm}, \quad 16\text{ mm} + d_g)$ for $f_c \leq 60$ MPa and $d_{dg} = \min(40\text{ mm}, 16\text{ mm} + d_g \cdot (60/f_c)^4)$ for $f_c > 60$ MPa. The aggregate interlock force V_{agg} is obtained by integration of the stresses along the CSC in the vertical direction.

4.5.2 Concrete residual tensile strength (V_{res})

The contribution of the Fracture Process Zone (FPZ, [Hil83]) is quantified consistently with the approach of Cavagnis et al. [Cav17], by considering the residual concrete tensile strength according to the equation of Hordijk [Hor92] (Figure 4.13d).

4.5.3 Dowelling action (V_D)

The dowelling action refers to the capacity of the flexural reinforcement to transfer shear forces due to a shearing displacement in the bar originated by the kinematics of the CSC (Figure 4.13e). For members without shear reinforcement, this action relies on the tensile strength of concrete [Cav17]. For members with shear reinforcement, the stirrups enhance the dowelling capacity [Cam13]. In this chapter, two approaches are used to calculate the dowel effect:

- Series SM10 (tension reinforcement). Based on the strain measurements performed by FOM (Figure 4.12 and Appendix 4.D), it is possible to directly estimate the internal forces in the reinforcement (bending moments and shear forces, refer to Appendix 4.E) consistently with the methodology detailed in Chapter 2 and in [Can20].

- Series SM00 and compression reinforcement of series SM10. Since no FOM have been conducted for these bars, the dowelling contribution is determined based on the deflected shape of the bars. Such analysis is performed based on the DIC readings consistently with the methodology detailed in [Cav17].

4.5.4   Compression chord (V_{cc})

In this chapter, the shear stresses in the compression zone at the tip of the shear crack are quantified on the basis of the concrete strains measures using DICs according to the approach proposed by Cavagnis et al. [Cav17].

4.5.5   Shear reinforcement (V_s)

The activation of the shear reinforcements is related to the opening of the inclined cracks intersecting them (Figure 4.13f). The strain profiles presented in Figure 4.12 show that, at failure, stirrups intersected by the CSC were at yielding or in the strain-hardening phase.

Details of the activation of the stirrups at different load levels are given in Figure 4.14, providing for each stirrup the following load levels: i) first activation (square); ii) yielding strain (circle); and iii) strain equal to 10 ‰ (triangle; it has to be noted that the FOM technique allows measuring the reinforcement elongation up to a strain of 10-15 ‰). In the Figure 4.14, empty markers refer to stirrups which are activated by the dowelling action of the flexural reinforcement. For the beam with the lowest shear reinforcement ratio ($\rho_w = 0.063$ %), all three points (activation, yielding and 10 ‰ strain) were attained almost at the same level of load (between 90 to 100 % of V_{max}). On the contrary, beams with larger shear reinforcement ratios showed that the first activation occurred at around 60 % of the failure load, followed by yielding and larger strains for larger loads. Only few stirrups intersected by the CSC and located close to the crack tip did not reach the 10 ‰ strain before failure. This response was observed independently of the ductility class A (red) or C (refer to green markers in Figure 4.14). Based on these observations, the stress of each stirrups is calculated considering a bi-linear law (linear elastic until f_{yw} and a linear stress-strain relationship until a strain of 10 ‰). When the strain exceeds 10 ‰, the stress in the stirrup is assumed to correspond to the tensile strength of the steel f_{tw} (maximum error of 3 % for ductility class A and 14 % for ductility class C). Dowelling of the vertical stirrups intercepted by the shear crack was in addition neglected accounting for the large strains at failure (cross section at yielding). For series SM10, the same consideration for the stress at failure in the stirrups (average between yield and tensile strengths) is adopted by analogy.

It can be noted that the influence on the failure load of the tensile strength of the reinforcement (f_{tw}) is also confirmed by the results presented by Autrup et al. [Aut21] who showed that beams with shear reinforcement of different ductility class, but comparable tensile strength, exhibited a similar shear resistance. This was not the case in the present programme, where the tensile strength associated to the different ductility classes was different (larger for ductility class C), so that the shear resistance was also different (larger for members with ductility class C reinforcement).

It has to be noted that the stirrups activated by the dowelling of the flexural reinforcement are not considered in the shear reinforcement contribution, but their contribution is included in this study within the dowelling action of the flexural reinforcement (dowel action calculated at the intersection of the CSC with the tensile reinforcement, see free-body diagram in Figure 4.13b).
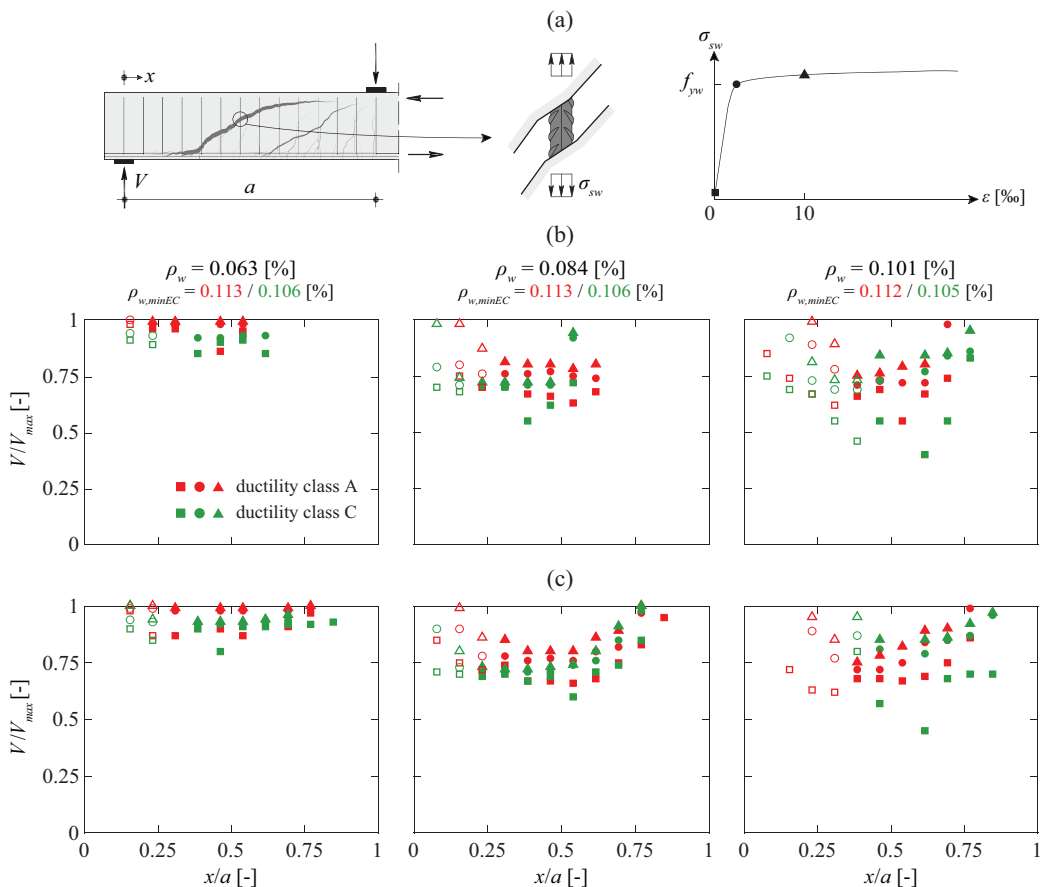

Figure 4.14: Activation of stirrups along the beam for series SM10: (a) definitions; (b) North face; and (d) South face (empty markers refer to stirrups activated by the dowelling action of the flexural reinforcement; square markers: first activation; circle markers: strain at yielding; and triangle markers: strain equal to 10 ‰).

4.5.6 Main results and governing shear transfer actions

Figure 4.15 shows the calculated contribution of each STA at peak load normalized by the square root of f_c [Cav17] to account for slightly different concrete compressive strengths. For series SM10, the analysis of the different STAs (V_{agg}, V_{res}, V_{cc}, V_s, $V_{D,comp}$ and $V_{D,tens}$) has been performed at each side of the beam and an average value is adopted. The comparison shows consistent results with low scatter (average value of the measured-to-calculated resistance ratio of each STA equal to 1.02 with a Coefficient of Variation of 5.9 %). The following observations can be made:

- the amount of shear carried by aggregate interlock V_{agg} is influenced by the location, the shape and the kinematics of the CSC. An increase of the shear reinforcement ratio leads to a slightly larger absolute contribution of V_{agg} due to the steeper shape of the crack (refer to Figures 4.9 and 4.B.1). However, its relative significance with respect to the total shear resistance remains roughly constant (about 15 % on average) for increasing shear reinforcement ratios.

- the amount of the shear carried by the residual tensile stress V_{res} is very limited, contributing to less than 3 % on average.

- the shear force carried by the compression chord V_{cc} is influenced by the location of the crack tip, the shape and the cinematics of the CSC as well as the depth of the compression zone at crack tip. For most of the beams, the sub-horizontal branch of the CSC is long (refer to Figures 4.9 and 4.B.1) leading to limited depths of the compression zone at crack tip and a relatively small contribution of this action (about 5 % on average).

- the shear reinforcement provided the highest contribution to the resistance. Beams with ductility class C showed larger contributions than those of ductility class A. This is to a large extent due to the difference on the tensile strength f_{tw} as explained previously.

- the contribution of the dowelling action of the tensile flexural reinforcement $V_{D,tens}$ is highly influenced by the shape of the crack. When shear reinforcement ratio is increased, the term $V_{D,tens}$ decreased. This is due to the change in the location of the CSC, shifting it farther away from the support (for delamination cracks reaching the support plate, a larger shear force can be carried by the longitudinal bars at the tip of the delamination crack).

- the contribution of the dowelling action of the compression reinforcement $V_{D,comp}$ was relatively small, due to the size of the reinforcement (diameter 16 or 20 mm) and the location of the CSC. On average, this contribution was about 2 % of the total shear force.
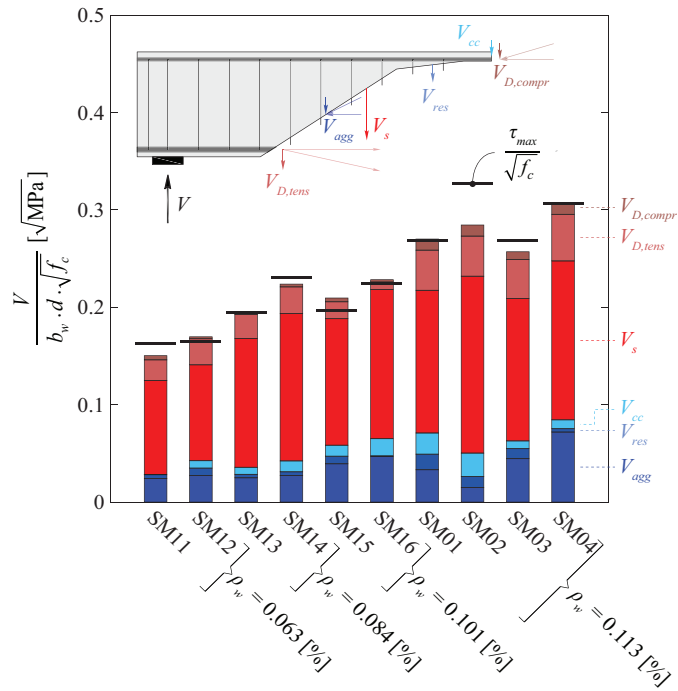
Figure 4.15:   Amount of calculated shear carried by each shear-transfer action (STA) at peak load compared to the experimental shear strength τ_{max}.

4.5.7   Evolution of the STA during loading

Figure 4.16 shows the evolution the STAs during the loading process for the same set of selected specimens presented in Figures 4.9, 4.10 and 4.12 (SM11, SM12, SM15 and SM16). The comparison between measured and calculated strengths shows consistent results at the different load levels investigated once the CSC develops. The contribution of each STA evolves during the loading process, with the stirrup contribution increasing its significance for larger levels of load (and thus, larger openings of the CSC). This contribution, as well as the contribution of $V_{D,tens}$ associated to the development of the delamination crack, are activated just before failure for the tests with the lowest shear reinforcement ratio ($\rho_w = 0.063$ %, SM11 and SM12).

For beams with larger ratios, ($\rho_w = 0.101$ %, SM15 and SM16), the contribution of the stirrups is mostly activated between 50 % and 70 % of V_{max}, when the stirrups start to yield just thereafter. Further increase of the contribution is related to the strain hardening of the shear reinforcement and further progression of the CSC (sub-horizontal branch). Contrary than for beams with low amounts of shear reinforcement, the contribution of $V_{D,tens}$ developed at around $0.6 \cdot V_{max}$ (development of the delamination crack) and remained relatively constant thereafter. The contribution due to aggregate interlock, V_{agg}, increased, once the CSC formed during the loading process, but diminished just before failure.
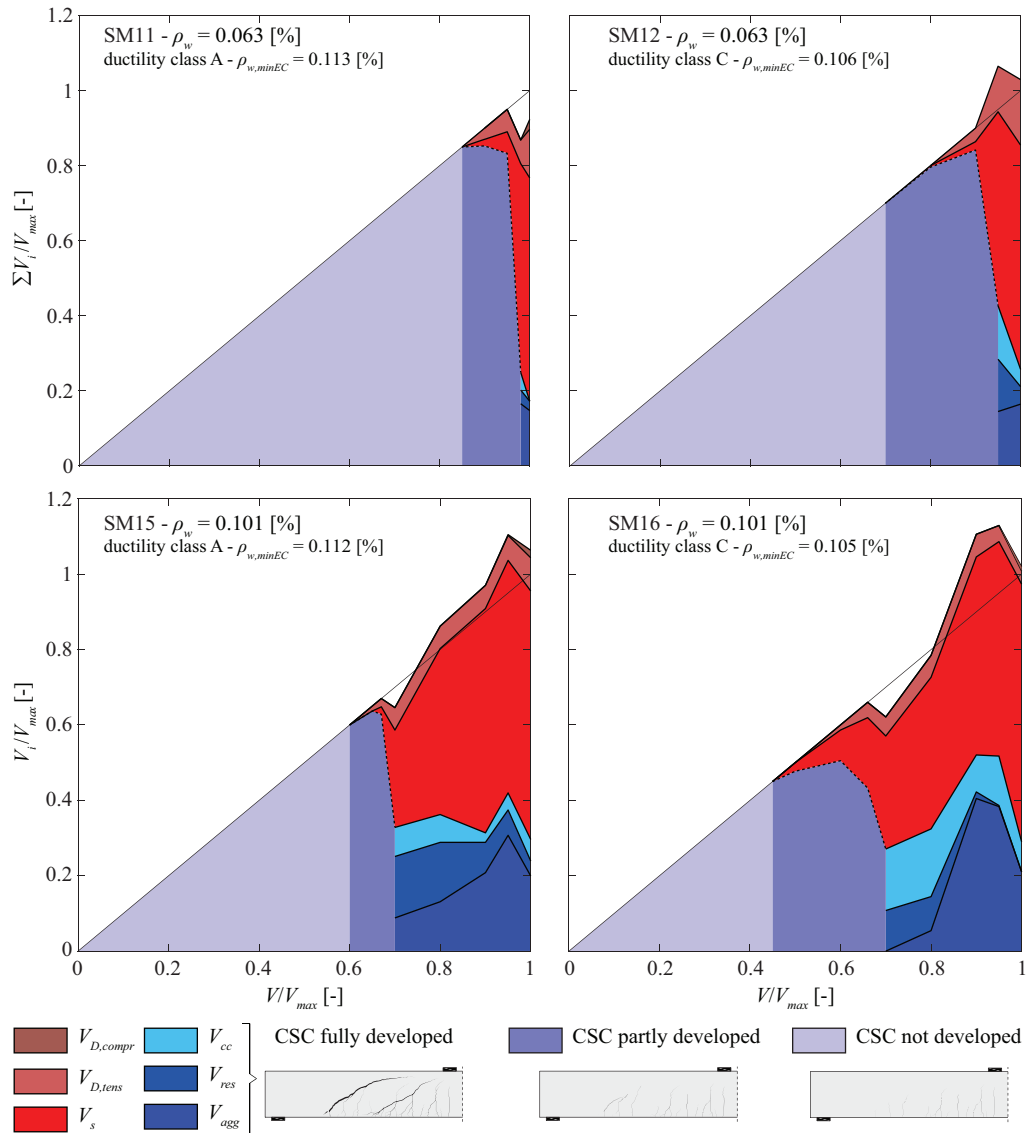
Figure 4.16:   Shear-transfer actions (STA) calculated at different step load.

4.6   Distribution of shear stresses across the member

In the previous section, the experimental results have been analysed in terms of the concrete and reinforcement contributions calculated for a free-body delimited by the CSC. This is in fact, the manner in which the phenomenon is dealt in the shear models based on the Modified Truss Analogy (MTA). In order to get an insight on the adequacy of models based on a Variable Truss Angle (VTA, smeared compression field developing in the web), this section presents a discussion on the distribution of the shear stresses in the elements.

To that aim, the approach of Cavagnis et al. [Cav17] to calculate the principal stresses in the compression chord will be extended. The principal stress directions are assumed to be parallel to the principal strain directions [FIB21] and computed on their basis [Fer07b] using the stress-strain relationship shown in Figure 4.17a (considering the pre- and post-peak behaviour). This analysis considers both cases where the concrete is uncracked (using a biaxial failure criterion based on the Kupfer's failure surface [Kup69], see Figure 4.17b) and when it is cracked. For the latter, the tensile concrete strength is neglected and the effective compressive strength $f_{c,eff}$ is reduced by the compression-softening law proposed by Vecchio et al. [Vec86] (refer to Cavagnis et al. [Cav17] for details). Close to the cracks (at distance lower than the aggregate size), the reduction of the compressive strength is however calculated according to Eq. (4.4) (valid for discontinuities). By considering such stress state, the associated shear stresses can be calculated at any location as shown in Figure 4.17c.
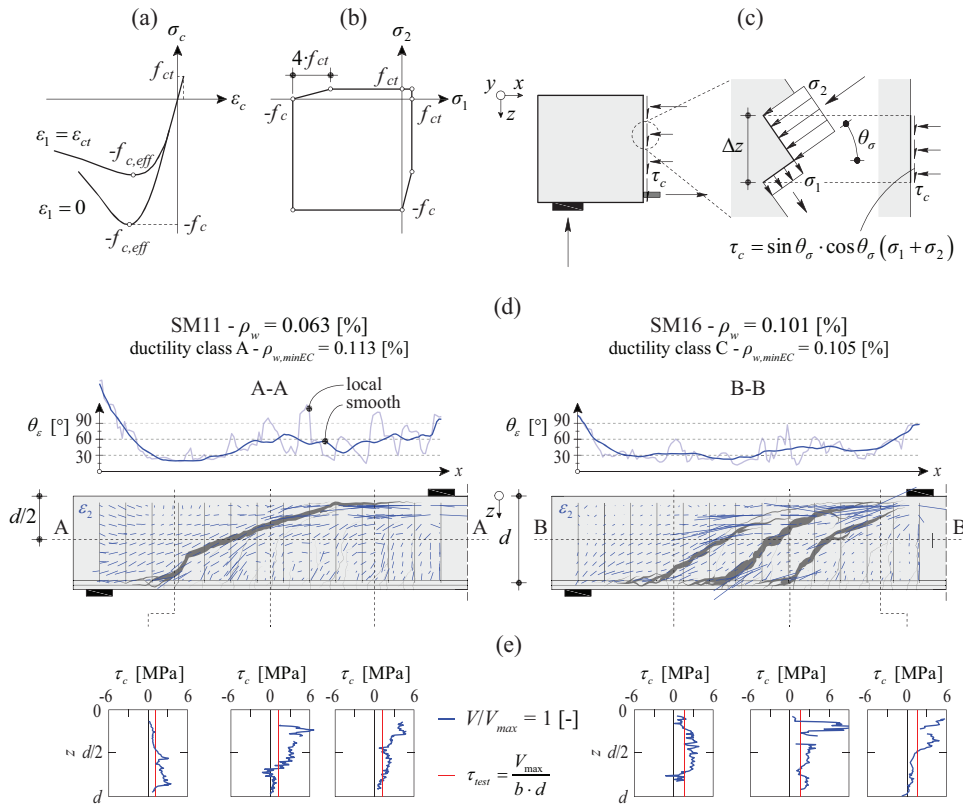
Figure 4.17:   (a) Adopted stress-strain relation for concrete [Fer07b]; (b) adopted failure surface [Nie11] based on the Kupfer's failure surface [Kup69]; (c) calculation of the de concrete shear stresses; (d) principal compression strain as well as strain angle along the beam; and (e) concrete shear stresses at different cross section.

The resulting principal angle of the compression field θ_ε at mid-depth and the principal compressive strain direction ε_2 at failure are shown in Figure 4.17d for two representative beams: SM11 with low shear reinforcement of ductility class A and SM16 with larger shear reinforcement and ductility class C. As it can be noted, the angle θ_ε is fairly constant, with a value close to 30°, except close to the load-introduction regions (where fan-shaped fields develop [Val20]).

With respect to the shear stress (τ_c), several cross sections are shown in Figure 4.17e (the calculated values are shown in blue and the average stress determined from the acting shear force is shown in red). For the specimen with larger shear reinforcement ratio (Figure 4.17e right), the plots show a relatively uniform distribution of the calculated shear stresses, except close to the load introduction (where they concentrate on the compression chord region). This result shows the consistency of the VTA approach for this case. For the specimen with lower shear reinforcement ratio (Figure 4.17e left), however, the distribution of the shear stresses is significantly less uniform. In this case, the shear stresses concentrate near to the compression chord close to the load introduction and to the tension chord close to the support. This indicates a potential direct strut action [Dru61, Mut08] and is less consistent with the assumptions of the VTA.

4.7   Design implications

The previous findings show that the ductility class of the shear reinforcement (characterizing its post-yield response) influences the shear resistance. This is to a large extent due to the increase of the stress in the reinforcement during its strain-hardening phase. It has also been observed that low amounts of shear reinforcement are not sufficient to control shear cracking, leading to strain localization (and thus disabling the development of a smeared compression field in the web). As already shown in Figures 4.3d-e, VTA models, as the one of current Eurocode 2 (EN 1992-1-1:2004 [Eur04]) can lead to unsafe predictions for shear reinforcement of ductility class A, but can also be excessively conservative when the shear reinforcement ratio is close to the minimum value required for crack control. These deficiencies require some modifications of the VTA models to suitably account for the post-yield response of the shear reinforcement. The authors will introduce in the following a number of proposals to fix these issues, that have enriched the discussions of the current draft for the 2nd generation of Eurocode 2 (prEN 1992-1-1:2021 [Eur21] and *fib* MC2020, see description in Appendix 4.A) and have been eventually included in it.

The first modification to be introduced accounts for the unsafe estimates of strength for low ductility classes of the reinforcement. In VTA models, the compression field can rotate freely between certain boundaries due to yielding of the shear reinforcement (for instance $2.5 \geq \cot\theta \geq 1$ according to EN 1992-1-1:2004 [Eur04]). As shown in this work, failures in members with fairly low amounts of shear reinforcement can however be originated by rupture of the stirrups in tension, potentially limiting the rotation of the compression field [Sig11]. This fact can be considered for design purposes by setting a more severe limit for shear reinforcement of ductility class A. For instance, in prEN 1992-1-1:2021, this condition has been introduced by reducing $\cot\theta_{min}$ (governing the extent where the shear reinforcement equilibrates the compression field) by 20 % (see details in Appendix 4.A). The results of this consideration are shown in Figure 4.18 for the simplified formulation of prEN 1992-1-1:2021 (Level-of-Approximation I (LoA I) hereafter, see Appendix 4.A), where the red line (with a flatter slope) corresponds to the reduction of 20 % in the value of $\cot\theta_{min}$. As it can be noted, this modification allows considering in a suitable manner the reduction of the compression field rotation and thus of the shear resistance observed in tests.
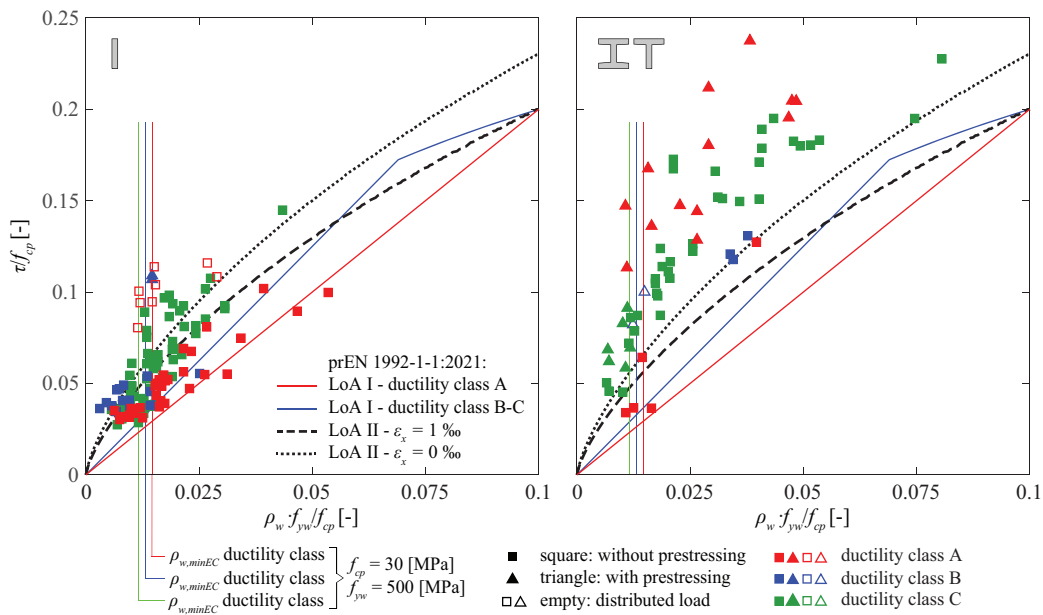
Figure 4.18:   Comparison of measured-to-predicted shear capacity according to prEN 1992-1-1:2021 [Eur21] for LoA I and II in case of low shear reinforcement ratio (rectangular section: $z = 0.9 \cdot d$; section with flange: z is the distance between the center of gravity of the flexural reinforcement and the center of gravity of the compression flange).

With respect to the improvement of accuracy of VTA models, particularly close to minimum amounts of shear reinforcement, this can be performed by considering a more suitable estimate of the state of strains and thus of the opening of the resulting cracks [Fer07, Rup13]. To that aim, the refined procedure of MC2010 [Sig13] can be used to evaluate the state of strains as a function of the level of strain in the flexural reinforcement at crushing of the compression field. The procedure implemented in prEN 1992-1-1:2021 for this purpose is detailed in Appendix 4.A (referred as LoA II hereafter). The results of this analysis allow reaching larger levels of rotation of the compression field, particularly for low amounts of shear reinforcement. In order to consider the potentially brittle rupture of stirrups before the full rotation of the compression field takes place, prEN 1992-1-1:2021 considers this method to be only applicable to shear reinforcement of ductility classes B or C. The results of this approach can also be seen in Figure 4.18, where the LoA II model, represented with black line is approximating in a closer manner the experimental results of ductility classes B and C.
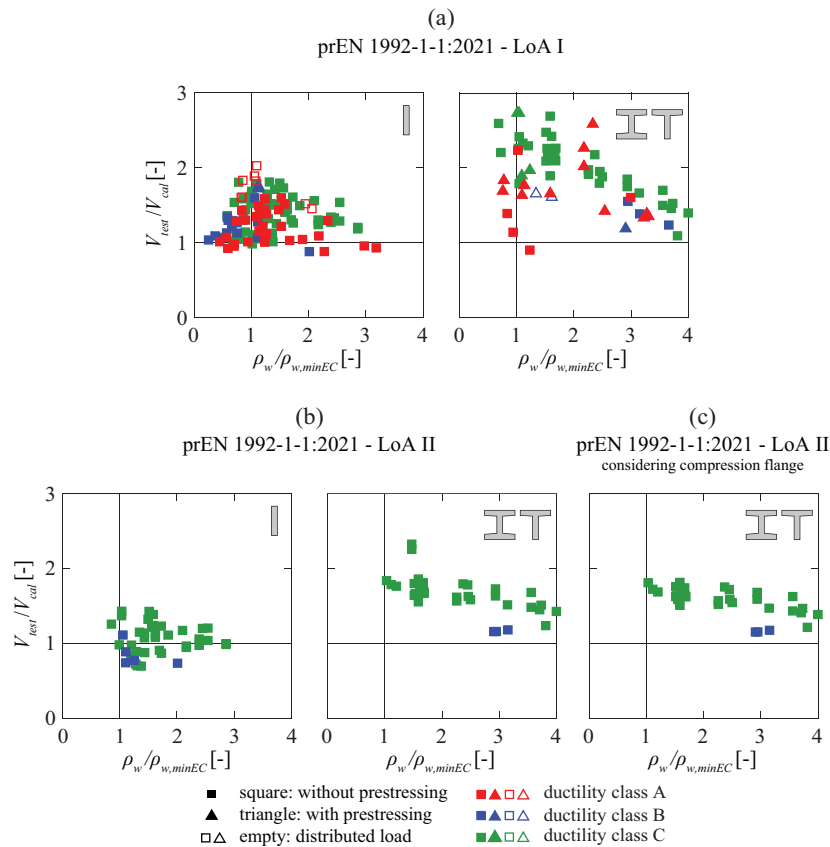
Figure 4.19:   Comparison of measured-to-predicted shear strength V_{test}/V_{cal} according to prEN 1992-1-1:2021 [Eur21] in case of low shear reinforcement ratio for: (a) LoA I; and (b) LoA II; and (c) LoA II considering compression flange (rectangular section: $z = 0.9 \cdot d$; section with flange: z is the distance between the center of gravity of the flexural reinforcement and the center of gravity of the compression flange).

Figure 4.19 and Table 4.3 compare the VTA model of prEN 1992-1-1:2021 incorporating the previous modifications with the same database as the one used for analysis of the performance of current Eurocode 2 (EN 1992-1-1:2004, in Figure 4.3d-e). The results for LoA I (Figure 4.19a) show that the resistance of ductility class A tests is suitably predicted, reducing the scatter and correcting the relatively unsafe predictions observed in EN 1992-1-1:2004 for ductility class A reinforcement. With respect to LoA II (Figure 4.19b), the predictions are much closer to the experimental results, providing consistent agreement for the whole range of shear reinforcement ratios available. The prEN 1992-1-1:2021 allows also to take into consideration the compression flange by shifting of the control section for LoA II (Figure 4.19c). The predictions are slightly closer to the experimental results showing the beneficial effect of the compression flange.

Table 4.3 shows the mean values (Avg) and the coefficient of variation (CoV) of measured-to-predicted shear resistances V_{test}/V_{cal} ratios according to prEN 1992-1-1:2021 [Eur21] for 186 tests (as Figure 4.3d-e) with small shear reinforcement ratios $\rho_w/\rho_{w,min}$ between 0 and 4. As expected, LoA II (considering the influence of the compression flange when applicable) depicts the best predictions. The comparison shows also that the ductility class A has, in general, lower mean values and larger CoVs of the measured-to-predicted shear resistance ratios. With respect to class B reinforcement, the mean of measured-to-calculated shear resistance ratios is relatively low for rectangular cross sections when using LoA II. This can however be partly attributed to the fact that for some of the tests investigated with class B reinforcement, the ratio f_{tw}/f_{yw} was close to its lower limit ($f_{tw}/f_{yw} = 1.08$) and the beams exhibited a response similar to those of class A reinforcement. For ductility class C, no particular issues were observed.

Table 4.3: Average (Avg) and Coefficient of Variation (CoV) of measured-to-predicted shear strength V_{test}/V_{cal} according to prEN 1992-1-1:2021 [Eur21] (186 tests with $\rho_w/\rho_{w,min}$ between 0 and 4).

Method	Cross-section	All tests Avg / CoV	Ductility class		
			A	B	C
LoA I	∏	1.35 / 0.193	1.32 / 0.224	1.25 / 0.193	1.39 / 0.167
	⊥⊤	1.95 / 0.284	1.74 / 0.305	1.39 / 0.022	2.06 / 0.261
LoA II	∏	0.96 / 0.224	(0.79 / 0.140)	0.85 / 0.187	1.07 / 0.184
	⊥⊤	1.56 / 0.175	(1.27 / 0.162)	1.17 / 0.011	1.66 / 0.133
LoA II considering compression flange	∏	-	-	-	-
	⊥⊤	1.49 / 0.145	-	1.16 / 0.011	1.57 / 0.096

Figure 4.20 provides the same results as Figure 4.19, but without considering the effect of the ductility classes. It shows that the 20 % reduction of $\cot\theta_{min}$ for steel with ductility class A is justified in the case of LoA I (unsafe results). Figure 4.20b shows also that use of the refined model LoA II for ductility class A reinforcement would lead to unsafe results.
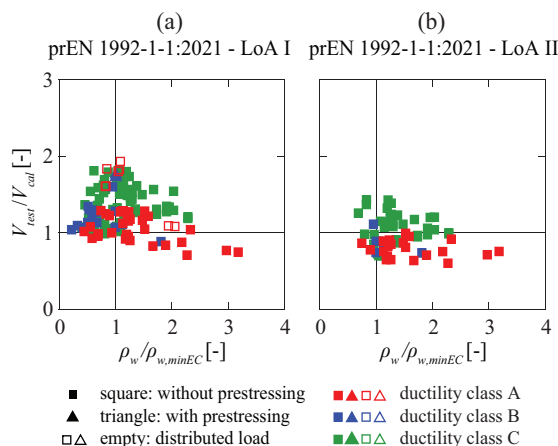
Figure 4.20: Comparison of measured-to-predicted shear strength V_{test}/V_{cal} of rectangular section according to prEN 1992-1-1:2021 [Eur21] without considering the ductility class in case of low shear reinforcement ratio for: (a) LoA I; and (b) LoA II.

4.8   Conclusion

This chapter presents the results of an experimental programme addressed at the response of members with low shear reinforcement ratios and investigating the influence of the ductility class of the shear reinforcement. The main conclusions are listed below:

1. The experimental results presented in this chapter as well as the detailed analyses performed in this chapter show that not only the amount of shear reinforcement, but also the post-yield properties of the shear reinforcement (tensile strength and strain at maximum load), influence the shear resistance of a member.

2. Low amounts of shear reinforcement are not capable of preventing crack localization. In this case, a Critical Shear Crack (CSC) develops and opens suddenly, leading to failure in shear and breaking the stirrups in tension.

3. For larger amounts of shear reinforcement, crack localization can be prevented. Several shear cracks develop in this case, allowing for more distributed deformations. The compression field develops in this case in a more uniform manner, in close agreement to the Variable Truss Angle (VTA) models. Even in these cases, for moderate amounts of shear reinforcement, shear cracks develop significant openings at failure. This implies that the reinforcement can be strained at its hardening phase or even fail by tension rupture.

4. Consistently with the previous conclusion, it is found that the tensile strength of the reinforcement is a key parameter governing the strength of members with low amounts of shear reinforcement. This conclusion is supported by the experimental results of this chapter, as well as others from the literature.

5. The capacity to rotate the compression field due to plastic deformations of stirrups in VTA approaches can be limited by rupture of the stirrups. The latter depends on the strain at rupture and the tensile strength. Both parameters can be considered by means of the ductility class of the reinforcement (as defined for instance by EN 1992-1-1:2004).

6. Design based on VTA models for members with sufficient shear reinforcement can be consistently performed provided that some restrictions are accounted for brittle shear reinforcement (for instance ductility class A according to EN 1992-1-1:2021). These restrictions consider a limitation on the minimum inclination that can be developed by the compression field. In addition, its accuracy can be enhanced when a suitable estimate of the state of strains in the web is considered.

Appendix 4.A: Shear verification based on EN 1992-1-1:2004 and prEN 1992-1-1:2021 for beam with shear reinforcement

EN 1992-1-1:2004 [Eur04]

The shear stress resistance is calculated as:

$$\tau_R = \rho_w \cdot f_{yw} \cdot \cot\theta_\sigma \leq \alpha_{cw} \cdot v_1 \cdot \frac{f_c}{2} \tag{4.A.1}$$

where ρ_w is the shear reinforcement ratio, f_{yw} is the yielding of the shear reinforcement f_c is the concrete compressive strength. The parameter $\cot\theta_\sigma$ is the inclination of the compression field in the web and is calculated as:

$$2.5 \geq \cot\theta_\sigma = \sqrt{\frac{\alpha_{cw} \cdot v_1 \cdot f_c}{\rho_w \cdot f_{yw}} - 1} \geq 1 \tag{4.A.2}$$

Where v_1 is the strength reduction factor for concrete cracked in shear:

$$v_1 = 0.6\left(1 - \frac{f_c}{250}\right) \qquad (f_c \text{ in [MPa]}) \tag{4.A.3}$$

The parameter α_{cw} is a coefficient taking account of the state of stress in the compression chord:

$$
\begin{aligned}
\alpha_{cw} &= 1 && \text{for non-presstressed structures} \\
\alpha_{cw} &= 1 + \frac{\sigma_{cp}}{f_c} && \text{for } 0 < \sigma_{cp} \leq 0.25 f_c \\
\alpha_{cw} &= 1.25 && \text{for } 0.25 f_c < \sigma_{cp} \leq 0.5 f_c \\
\alpha_{cw} &= 2.5\left(1 - \frac{\sigma_{cp}}{f_c}\right) && \text{for } 0.5 f_c < \sigma_{cp} < f_c
\end{aligned} \tag{4.A.4}
$$

Where σ_{cp} is the mean compressive stress, measured positive, in the concrete due to the axial force. The shear resistance is finally calculated as the minimum of the resistance for a member with and without shear reinforcement.

prEN 1992-1-1:2021 [Eur21]

The shear stress resistance is calculated as:

$$\tau_R = \rho_w \cdot f_{yw} \cdot \cot\theta_\sigma \leq v \cdot \frac{f_{cp}}{2} \tag{4.A. (5)}$$

where ρ_w is the shear reinforcement ratio, f_{yw} is the yielding of the shear reinforcement, f_{cp} is the concrete plastic compressive strength (= $\eta_{fc} \cdot f_c$) and η_{fc} is the brittleness factor of concrete (given in to Eq. 4.4). The parameter $\cot\theta_\sigma$ is the inclination of the compression field in the web and is calculated as:

$$\cot\theta_{\min} \geq \cot\theta_{\sigma} = \sqrt{\frac{\nu \cdot f_{cp}}{\rho_w \cdot f_{yw}} - 1} \geq 1 \tag{4.A.6}$$

Where ν is the strength reduction factor for concrete cracked in shear. For a simple design (named LoA I in this chapter), a value of $\nu = 0.5$ may be adopted with a minimal inclination of the compression field in case of shear reinforcement of ductility class B or C:

$\cot\theta_{\min} = 2.5$ for ordinary reinforced members without axial force

$\cot\theta_{\min} = 3.0$ for members subjected to significant axial compressive force
(average axial compressive stress $\geq$ |3 MPa|). Interpolated values between
2.5 and 3.0 may be adopted for intermediate cases. $\tag{4.A.7}$

$\cot\theta_{\min} = 2.5 - 0.1 \cdot \dfrac{N}{|V|} \geq 1$ for members subjected to axial tension

Where N is the normal force and V is the shear force. For shear reinforcement ductility class A, $\cot\theta_{min}$ shall be reduced by 20 %.

For a more refined assessment of the shear strength (named LoA II in this chapter), angles of the compression field lower than θ_{min} may be adopted provided that the shear reinforcement is of ductility class B or C and that the strength reduction factor is calculated according to:

$$\nu = \frac{1}{1 + 110 \cdot \left(\varepsilon_x + \left(\varepsilon_x + 0.001\right) \cdot \cot^2\theta_c\right)} \leq 1 \tag{4.A.8}$$

where ε_x is the average strain of the bottom and top chords calculated at a cross section not closer than $0.5 \cdot z \cdot \cot\theta_{\sigma}$ from a support or a concentred load. For shear reinforcement ductility class A, LoA II is not allowed. As for LoA I, the shear resistance is not less than the one for a member without shear reinforcement. The value of $\rho_{w,minEC}$ may be reduced by 10 % for ductility class B and 20 % for ductility class C.

Appendix 4.B: Cracking pattern at failure

Detailed cracking patterns for all tests are shown in Figure 4.B.1.
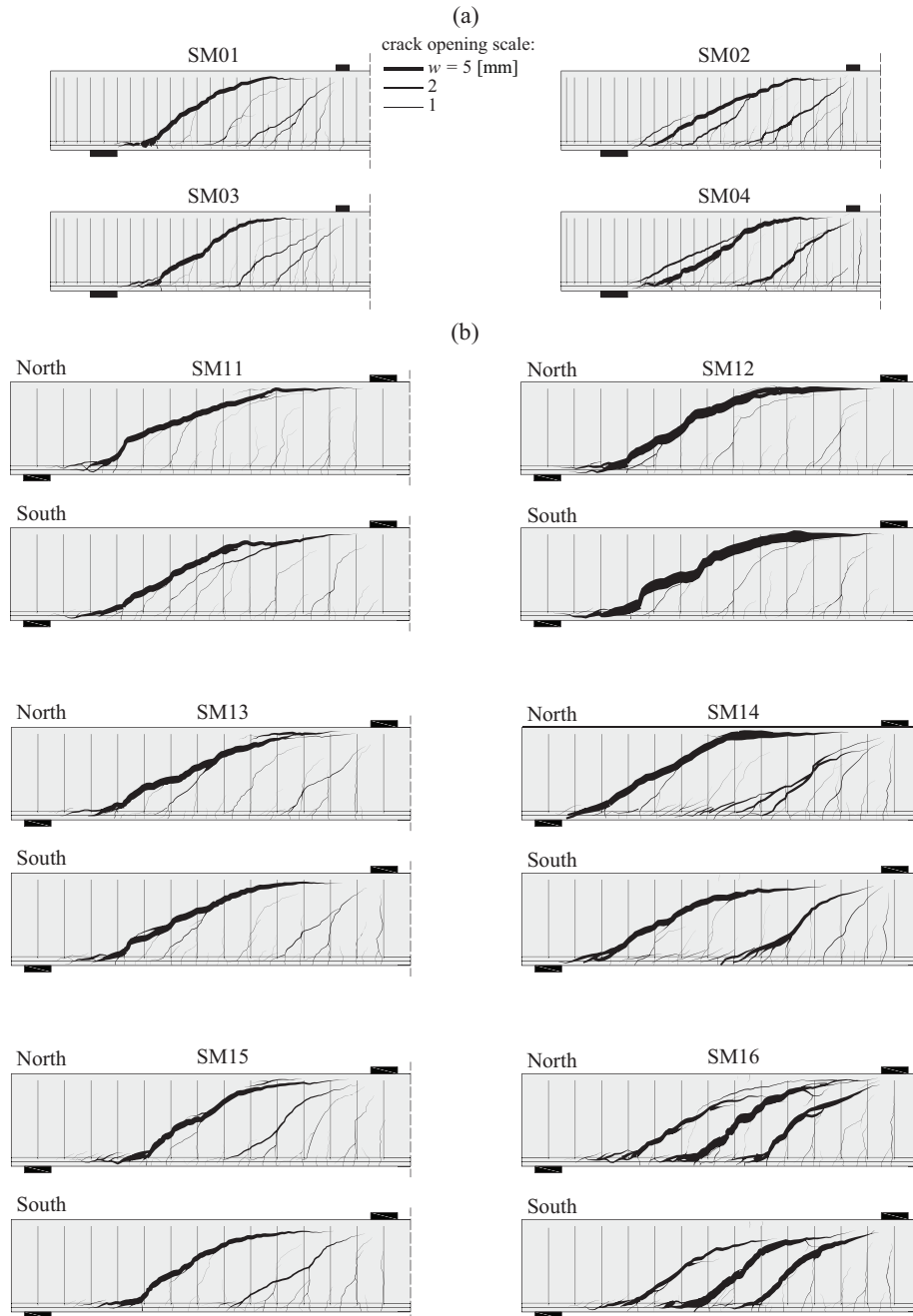
Figure 4.B.1:   Cracking pattern: (a) series SM00; and (b) series SM10.

Appendix 4.C: Crack kinematics

Details on the kinematics of the cracks for all tests are shown in Figure 4.C.1.
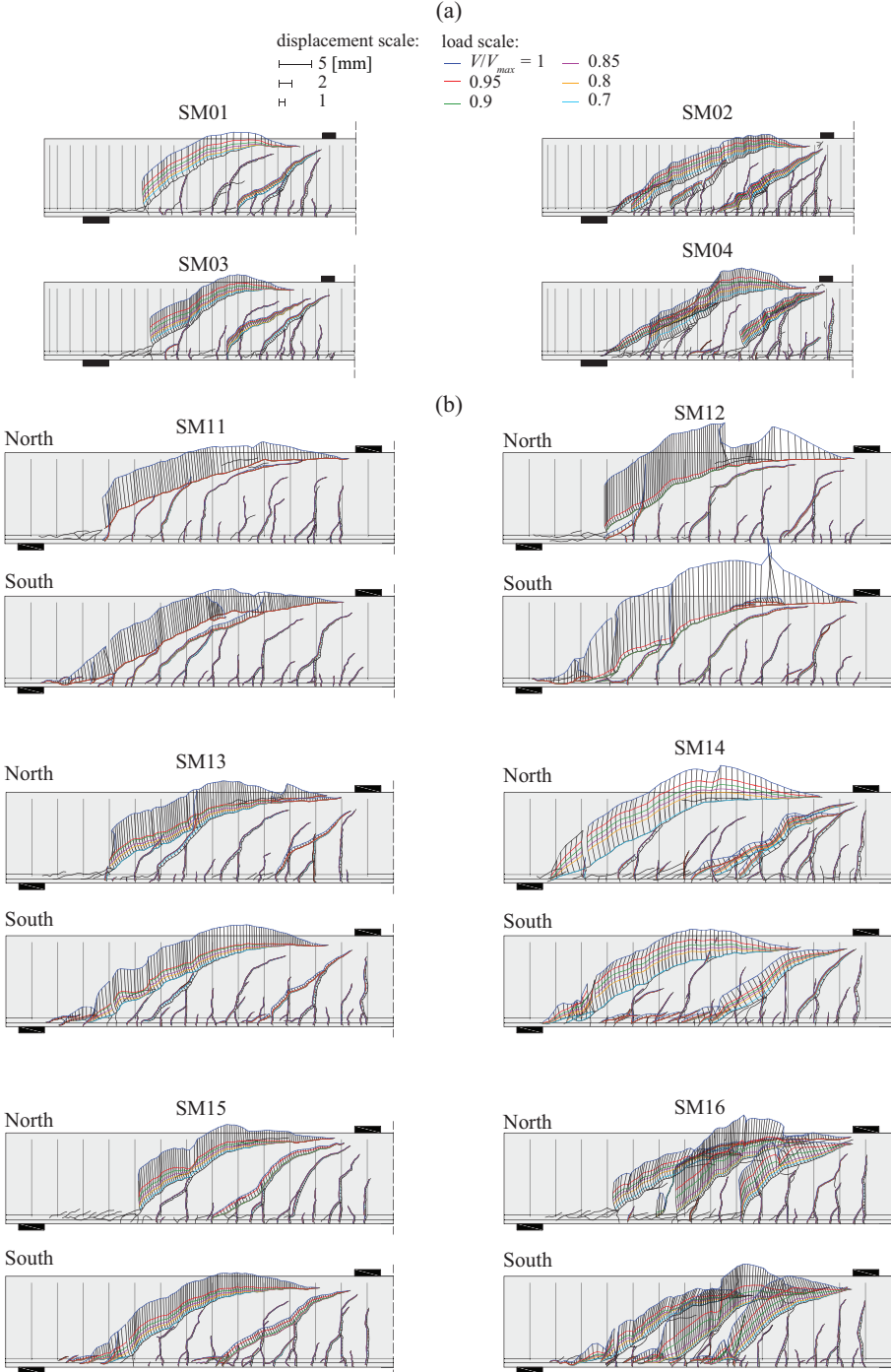
Figure 4.C.1:   Crack kinematics for: (a) series SM00; and (b) series SM10.

Appendix 4.D: Stirrups and flexural strain profiles

Strains in the stirrups and flexural reinforcement are shown in Figure 4.D.1 for series SM10.
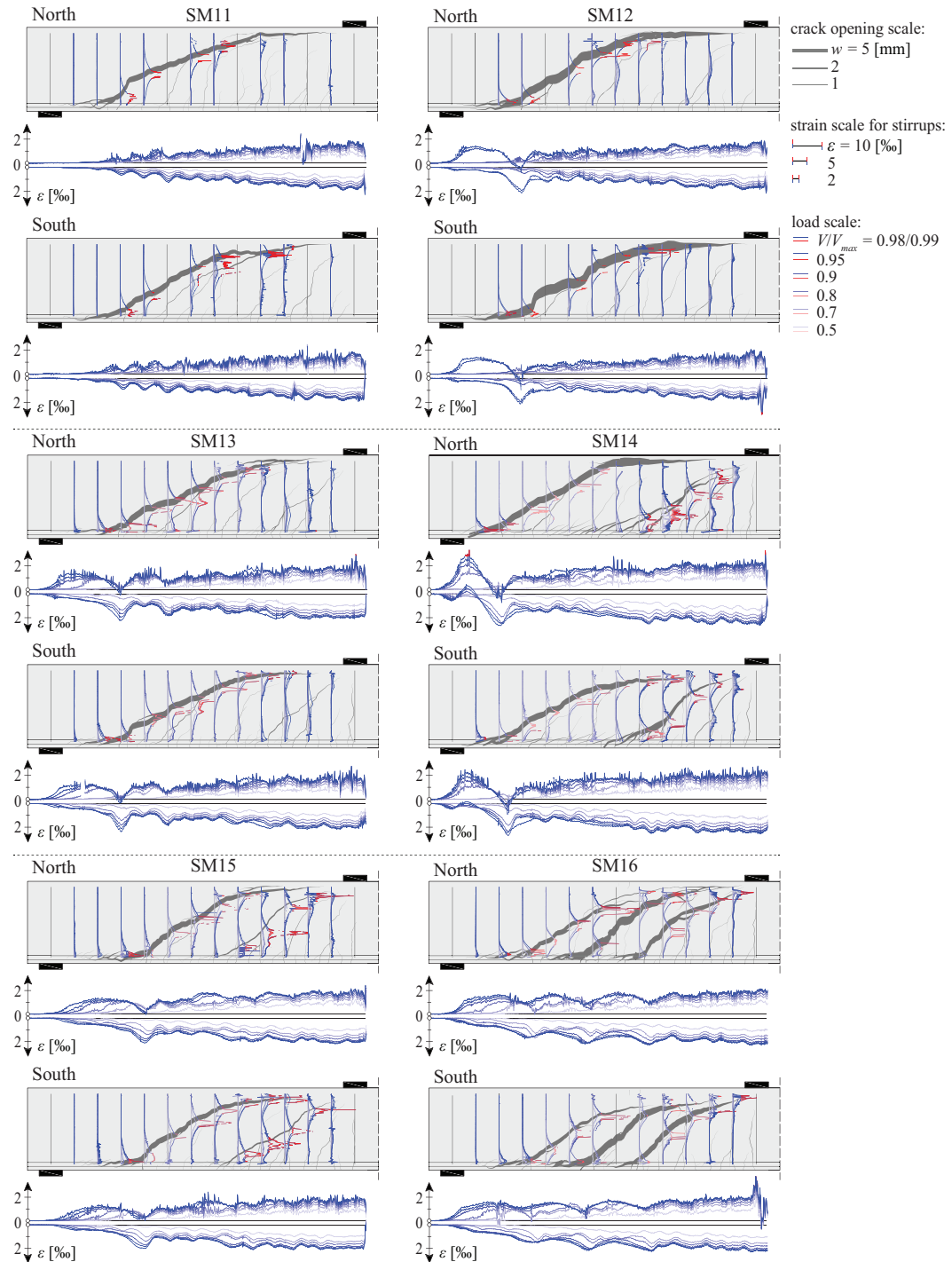
Figure 4.D.1:   Stirrups and flexural strain profiles for series SM10 at different load steps
(50, 70, 80, 90, 95 and 100 % of the maximal load).

153

Appendix 4.E: Dowelling action of the flexural reinforcement

Dowelling forces calculated for the flexural reinforcement are shown in Figure 4.E.1 for series SM10.
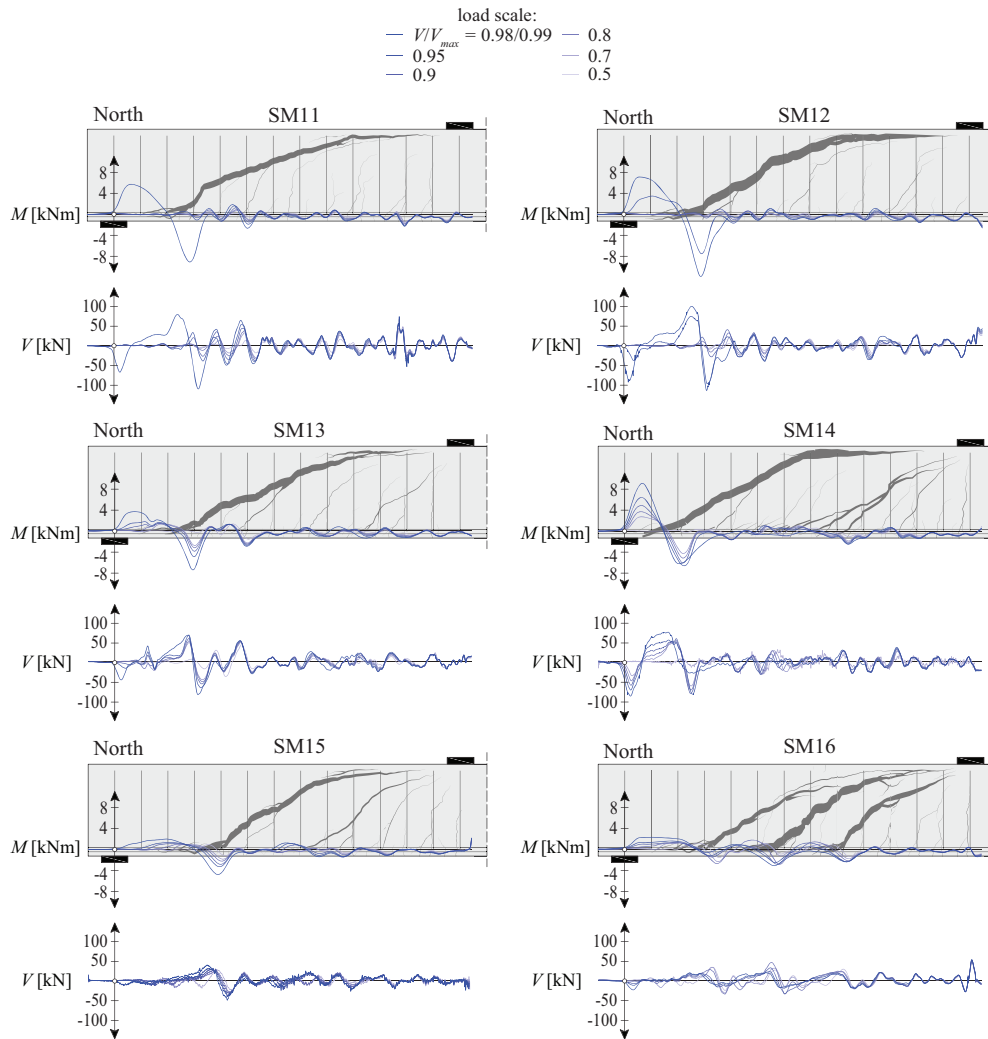
Figure 4.E.1:   Bending moment and shear force of the flexural reinforcement for series SM10 at different load steps (50, 70, 80, 90, 95 and 100 % of the maximal load).

Notation

Latin characters: lower case

a	shear span
b_w	beam width
d	effective flexural depth
d_g	maximum aggregate size
d_{dg}	parameter accounting for roughness of surface
h	beam height
f_c	concrete cylinder compressive strength
f_{cp}	equivalent concrete plastic strength
f_{ct}	concrete tensile strength
$f_{c,eff}$	effective compressive strength
f_t	maximum stress of reinforcement during hardening phase
f_{tw}	maximum stress of shear reinforcement during hardening phase
f_y	yield strength of reinforcement
f_{yw}	yield strength of shear reinforcement
s	shear reinforcement spacing
x,y,z	coordinates
w	crack opening
z	inner level arm

Latin characters: upper case

A_{sw}	area of shear reinforcement unit
N	normal force
M	bending moment
P	position
V	shear force
V_{agg}	shear force carried by aggregate interlock action
V_c	shear force carried by the concrete
V_{cc}	shear force carried by inclined compression chord
V_{cal}	calculated shear strength
$V_{D,compr}$	shear force carried by dowelling action of the compression reinforcement
$V_{D,tens}$	shear force carried by dowelling action of the tensile reinforcement
V_{max}	maximum measured shear force
V_R	shear strength

V_{Rc}	shear strength of members without shear reinforcement
V_{res}	shear force carried by the residual tensile strength of concrete
V_s	shear force carried by the shear reinforcement
V_{test}	measured shear strength

Greek characters: lower case

α_{cw}	coefficient taking account of the state of stress in the compression chord
δ	displacement of the beam
ε	bar strain
ε_1	principal tensile strain
ε_2	principal compressive strain
ε_c	concrete strain
ε_{ct}	tensile strain at concrete cracking
ε_u	bar strain at maximum load
ε_{uw}	bar strain at maximum load of shear reinforcement
ε_x	average strain of the bottom and top chords
η_{fc}	brittleness factor
η_w	crack opening factor
φ	friction angle of concrete
λ	minimum shear reinforcement ratio coefficient
ν	strength reduction factor for cracked concrete in shear according to Eurocode 2 (prEN 1992-1-1:2021)
ν_1	strength reduction factor for cracked concrete in shear according to Eurocode 2 (EN 1992-1-1:2004)
θ_{crack}	critical shear crack angle
θ_{min}	minimum angle with respect to beam axis of the compression field in the web
θ_ε	angle with respect to beam axis of principal compressive strain
θ_σ	angle with respect to beam axis of the principal compressive stress
ρ	flexural reinforcement ratio
ρ_w	shear reinforcement ratio
$\rho_{w,min}$	minimum shear reinforcement ratio
$\rho_{w,minEC}$	minimum shear reinforcement ratio according to Eurocode 2
σ_1	principal tensile stress
σ_2	principal compressive stress
σ_{agg}	aggregate interlock normal stress
σ_c	concrete stress
σ_{cp}	mean compressive stress in the concrete due to the axial force

σ_s	stress in the reinforcement
σ_{sw}	stress in the shear reinforcement
τ	shear stress
τ_{agg}	aggregate interlock shear stress
τ_c	shear stress of concrete
τ_{max}	maximum shear stress
τ_R	shear stress resistance
ξ	dilatancy angle ($= \pi/2 - \psi$)
ψ	angle of the crack displacement ($= \Delta/w$) with respect to the crack plane

Greek characters: upper case

Δ	crack sliding

Others

$\varnothing$	bar diameter or cylinder diameter
MTA	Modified Truss Analogy
VTA	Variable Truss Angle
EPSF	Elastic-Plastic Stress Fields
LoA	Level of Approximation

Chapter 5

Conclusions and Outlook

This chapter summarises the conclusions of this thesis. In addition, an outlook on the research which could be addressed in future works to advance the state-of-the-art is included.

5.1   Conclusions

Many of the detailing rules used nowadays have been formulated several decades ago based on empirical observations or are accepted as rules of good practice without a clear scientific background. These rules, however, play an important role in the economy of structures and particularly in the assessment of the resistance of existing structures. In this context, the aim of this thesis was to provide state-of-the-art detailing rules for design and verification of concrete structures.

The investigation focused on the following detailing rules: bending of reinforcement, anchorage of shear reinforcement and minimum amount of shear reinforcement. This thesis compiles several scientific papers, each one focusing on different aspects of the research. The results of this work have allowed to understand clearly the parameters influencing the spalling resistance of bent reinforcement, the anchorage resistance of bends and hooks and the influence of the steel proprieties on the shear resistance.

From a practical perspective, the results of this thesis provide new design and verification models and provisions for the detailing rules investigated. Some of them are incorporated in the 2nd generation of Eurocode 2 (prEN 1992-1-1:2021), as for example the design equation for bent reinforcement and the modification of the shear design model accounting for the ductility class of the shear reinforcement.

In the following, the main conclusions of this work are listed by chapter.

Chapter 2: *Design against splitting failures in reinforced concrete due to concentrated forces and minimum bend diameter of reinforcement*

1. Concentrated forces due to bent reinforcement close to the concrete edge can lead to spalling failures. The spalling resistance is increased for specimens with larger concrete cover, mandrel diameter and distance between bends. On the other hand, an increase of the bending angle leads to a decrease of the resistance. The experimental programme showed also that the casting direction had no marked influence on the spalling resistance.

2. Spalling failures governing the strength of bent reinforcement are related to the penetration of a concrete wedge developing inside the bend, associated to the development of a crack in the plane of the bend. This wedge is confined by the tensile forces developing out-of-plane in the spalling region and can thus resist stresses larger than the uniaxial concrete compressive strength.

3. A simple mechanical model was developed to design bent reinforcement based on a failure mechanism for spalling failures. The model is based on the equilibrium conditions of deviation forces and the strength of the confined wedge-shaped concrete volume.

4. Bending with large mandrel diameters can easily be replaced by a series of bends using a constant smaller mandrel diameter with smaller bending angles, separating the various bends by short straight segments. This solution has to potential to simplify the manufacturing processes of reinforcement.

Chapter 3: *Anchorage of shear reinforcement in beams and slabs*

1. Three failure modes potentially govern the strength of bend anchorage: (i) spalling of the concrete cover, (ii) pull-out (bond) failure and (iii) reinforcement yielding. The governing failure mode depends on the concrete cover, the opening of the transverse crack and the detailing of the region.

2. A simple mechanical model for the design of bends and hooks accounting for these three failure modes was developed. The model is based on equilibrium conditions and considers the bond, frictional and transversal forces that develop in the detail. The model also considers the location of the anchorage in the beam, accounting for favourable zones (compression chord) or unfavourable zones (tension chords potentially cracked in the transversal direction).

3. Regarding the stress demand of the shear reinforcement of a beam, it is reasonable to assume that the yield strength can be attained at the end of the curved region of bends and hooks.

Chapter 4: *Influence of amount of shear reinforcement and its post-yield response on the shear resistance of reinforced concrete members*

1. The amount of shear reinforcement but also its post-yield properties (tensile strength and strain at maximum load) govern the shear resistance of members when low amounts of shear reinforcement are provided. Beams with shear reinforcement with a better ductility class have a larger shear resistance than corresponding beams with a lower ductility class.

2. Variable Truss Angle (VTA) models for shear design, as the one of current Eurocode 2 (EN 1992-1-1:2004, chapter 6.2.3) can lead to unsafe predictions for shear reinforcement with ductility class A. This is due to the brittle rupture of stirrups before the full rotation of the compression field can take place. In this context, more severe limits for shear reinforcement of ductility class A are proposed for design based on VTA to account for the post-yield response of the shear reinforcement. For instance, in the 2nd generation of Eurocode 2 (prEN 1992-1-1:2021) for Level of Approximation I, this was introduced by reducing $\cot\theta_{min}$ (governing the extent where the shear reinforcement equilibrates the compression field) by 20 %. The analysis of a comprehensive database of 236 specimens collected from the literature confirmed the validity of these modifications.

5.2 Outlook and future works

Some questions related to the topics studied in this research remain open. In the following, some of these future research lines are outlined:

Chapter 2: *Design against splitting failures in reinforced concrete due to concentrated forces and minimum bend diameter of reinforcement*

1. Additional bent reinforcement tests should be carried out with systematic use of Fibre-Optical Measurements on the steel reinforcement in order to better understand the response of bent bars during spalling.

2. Spalling failure of bent reinforcement was investigated in the case of a casting direction perpendicular to the bending plane. Additional tests should be conducted with the bending plane parallel to the casting direction to understand if settlement of fresh concrete and the associated increased porosity due to bleeding could lead to a reduction of the strength of the confined wedge, and thus of its spalling resistance.

3. A theoretical investigation should be performed to validate the factor accounting for the shape of the confined wedge as well as the confinement factors.

4. A mechanical model should be developed giving the complete load-penetration response of the bent reinforcement allowing this response to be implemented in Finite Element (FE) models.

5. An extension of the mechanical model should be performed to other type of concentrated forces parallel and close to the concrete surface by adapting the surface of the confined and confining areas.

6. Spalling failure of bent reinforcement was investigated in the case of static loading. Additional tests should be conducted in case of cyclic loading to understand if progressive damage is developing and how this effect influences the spalling resistance.

Chapter 3: *Anchorage of shear reinforcement in beams and slabs*

1. Additional pull-out tests should be carried out with larger mandrel and bar diameters to validate the mechanical model. For example, pull-out tests with a mandrel diameter of seven times the bar diameter could be interesting because this is the requirement limit for a bar diameter larger than 16 mm according to Eurocode 2 [Eur04, Eur21]. Additional pull-out tests and theoretical considerations should also be performed to evaluate more in detail the influence of the longitudinal bar within the bend on the bond and spalling resistance.

2. Systematic pull-out tests should be carried out to understand and evaluate the influence of the shape, size, location and orientation of the ribs (bond index) on the bond and spalling resistance.

3. In the present experimental programme, the contribution of the straight region (inner) of the bend anchorage has been disregarded since the bond was disabled by means of a PVC tube. In a future experimental programme it could be interesting to evaluate the interaction and the deformation compatibility between this region and the other two (curved and tail region). In this regard, pull-out tests should be performed to evaluate the influence of the length of the inner region on the anchorage capacity.

4. Even if some considerations on group effect has been developed, further experimental investigations should be carried out on this topic to understand and evaluate its influence. Pull-out tests should be performed to evaluate the influence of group effect on bond and spalling resistance, including bars close to one another with variable clear distance as well as two bars facing each other with variable lap splice length of the tail.

5. Theoretical and experimental investigations are advised to validate the location of the uplift forces and the value of the friction coefficient in the mechanical model.

6. Development of a mechanical model giving the full load-penetration response of the bend and hook anchorage accounting for bond and spalling failure modes allowing the response to be implemented in FE models.

7. A new experimental programme of beam tests with various shear reinforcement anchorage should be performed to evaluate in detail the anchorage demand. Tracking the strain profile during loading would give valuable information.

8. In case of box-girder bridges, the presence of the deck slab induces transversal bending moments in the webs depending on their flexural stiffness (frame effect). Consequently, tensile forces are carried also by the stirrups. This effect has an influence on the anchorage demand in stirrups and it would be interesting to study this case in an experimental programme and theoretical (numerical) approach.

9. Anchorage of bend and hook anchorages were investigated in the case of static loading. Additional tests should be conducted in case of cyclic loading.

Chapter 4: *Influence of amount of shear reinforcement and its post-yield response on the shear resistance of reinforced concrete members*

1. A research on beam with flanges in case of low shear reinforcement ratio should be performed to improve the proposed design equation. Indeed, as presented, the prediction of the Eurocode 2 for Level of Approximation I and II are relatively far for beams with flanges leading to excessively safe results. This research should be completed with an experimental programme with varying flange geometries.

2. Further investigations on the contribution of the dowelling action of the tensile reinforcement should be performed in case of beams with low amount of shear reinforcement to improve the approach of Eurocode 2. This is particularly relevant with respect to the development of delamination cracks allowing to increase the number of stirrups activated.

3. Based on the Shear Transfer Action (STA), a mechanical model for beams with low amounts of shear reinforcement should be developed (as the one of Cavagnis et al. [Cav17a] or Tung et al. [Tun20]). This new mechanical model should take into account the shape, the kinematics of the Critical Shear Crack (CSC) and the post-yield response (ductility class) of the shear reinforcement. This model should provide a more consistent value of the minimum shear reinforcement that avoid strain localisation.

4. A value for the minimum shear reinforcement should be defined for more refined calculations based on Variable Truss Angle model (VTA) as, for example, the Elastic-Plastic Stress Fields method (EPSF). Indeed, close to the minimum shear reinforcement ratio, some tests predictions give unsafe results. A check of strain steel in the shear reinforcement should also be added to such model to limit the shear resistance.

Bibliography

[AAS20]   **AASHTO**, *AASHTO LRFD Bridge Design Specifications*, 9th Edition, Washington D.C., USA, 2020.

[Abr13]   **Abrams D. A.**, *Tests of Bond between Concrete and Steel*, University of Illinois Bulletin, 71, 238 p., USA, 1913.

[ACI19]   **ACI Committee 318**, *Building Code Requirements for Structural Concrete (ACI 318-19) and Commentary*, American Concrete Institute, 624 p., Farmington Hills, USA, 2019.

[Aja18]   **Ajaam A., Yasso S., Darwin D., O'Reilly M., Sperry J.**, *Anchorage Strength of Closely Spaced Hooked Bars*, ACI Structural Journal, p. 1143-1152, 2018.

[Ang99]   **Angelakos D.**, The Influence of Concrete Strength and Longitudinal Reinforcement Ratio on the Shear Strength of Large-Size Reinforced Concrete Beams With and Without Transverse Reinforcement, MSc thesis, Department of Civil Engineering, University of Toronto, 181 pp., 1999.

[Ang01]   **Angelakos D., Bentz E. C., Collins M. P.**, *Effect of Concrete Strength and Minimum Stirrups on Shear Strength of Large Members*, ACI Structural Journal, Vol. 98, pp. 290-300, USA, 2001.

[ASC98]   **ASCE-ACI Committee 445**, *Recent Approaches to Shear Design of Structural Concrete*, ASCE Journal of Structural Engineering, 124, pp. 1375-1417, USA, 1998.

[Aut21]   **Autrup F., Joergensen H. B., Hoang L. C.**, *Experimental Investigation of the Shear Capacity of RC Beams with Very Small Amounts of Shear Reinforcement*, fib Symposium 2021: Concrete Structures: New Trens for Eco-Efficiency and Performance, 1668 p., Lisbon, Portugal, 2021.

[Bac89]   **Bach C.**, *Elastizität und Festigkeit*, Springer Berlin Heidelberg, pp. 311ff, Berlin, Germany, German, 1889.

[Bac11]   **Bach C., Graf O.**, *Versuche mit Eisenbeton-balken zur Bestimmung des Einflusses der Hakenform der Eiseneinlagen*, Deutscher Ausschuss für Eisenbeton, Heft 9, pp. 1-79, Germany, German, 1911.

[Bac11a]   **Bach C., Graf O.**, *Versuche mit Eisenbeton-balken zur Ermittlung der Widerstandsfähigkeit verschiedener Bewehrung gegen Schubkräfte*, Deutscher Ausschuss für Eisenbeton, Heft 10, German, 1911.

[Bac80]   **Bach F., Nielsen M. P., Braestrup M. W.**, *Shear Tests on Reinforced Concrete T-Beams - Series V, U, X, B and S*, Structural Research Laboratory, Technical University of Denmark, Report No 120, 87 p., Copenhagen, Denmark, 1980.

[Bad21]   **Bado M. F., Casas J.-R., Kaklauskas G.**, Distributed Sensing (DOFS) in Reinforced Concrete members for reinforcement strain monitoring, crack detection and bond-slip calculation, Engineering Structures, Vol. 226, 111385, 13 p., 2021.

[Bal72]   **Balint P. S., Taylor H. P. J.**, *Reinforcement detailing of frame corner joints with particular reference to opening corners*, Cement and Concrete Association, 16 pp., London, England, 1972.

[Baz84]   **Bazant Z. P., Kim J.-K.**, *Size Effect in Shear Failure of Longitudinally Reinforced Beams*, Structural Journal, Vol. 81, No. 5, pp. 456-468, 1984.

[Ben06]   **Bentz E. C., Vecchio F. J., Collins M. P.**, *Simplified Modified Compression Field Theory for Calculating Shear Strength of Reinforced Concrete Elements*, ACI Structural Journal, Vol.103, No 4, pp. 614-624, 2006.

[Ber66]   **Bernardi B., Sagelsdorff R.**, *Die Krümmung abgebogener Armierungsstähle*, Schweizerische Bauzeitung, Vol. 84, pp. 884-892, Germany, German, 1966.

[Beu02]   **Beutel R., Hegger J.**, *The effect of anchorage on the effectiveness of the shear reinforcement in the punching zone*, Cement and Concrete Composites, 11 p., 2002.

[Bov04]   **Boverket**, *Boverkets handbok om betongkonstruktioner BBK 04 (Swedish Building Code - Regulations for Concrete Structures BBK 04)*, Boverket, Byggavdelningen, 271 p., Karlskrona, Sweden, Swedish, 2004.

[Bra16]   **Brantschen F., Faria D. M. V., Fernández Ruiz M., Muttoni A.**, *Bond Behaviour of Straight, Hooked, U-Shaped and Headed Bars in Cracked Concrete*, Structural Concrete, 17 No. 5, pp. 799-810, 2016.

[Bra19]   **Brault A., Hoult N. A.**, *Distributed Reinforcement Strains: Measurement and Application*, ACI Structural Journal, Vol. 116, No. 4, pp. 115-127, 2019.

[Bre63]   **Bresler B., Scordelis A. C.**, *Shear Strength of Reinforced Concrete Beams*, ACI Journal, V. 60, No. 1, pp. 51-74, 1963.

[Cam13]   **Campana S., Fernández Ruiz M., Anastasi A., Muttoni A.**, *Analysis of shear-transfer actions on one-way RC members based on measured cracking pattern and failure kinematics*, Magazine of Concrete Research, Vol. 56, No. 6, pp. 386-404, UK, 2013.

[Can20]   **Cantone R., Fernández Ruiz M., Muttoni A.**, *A detailed view on the rebar–to–concrete interaction based on refined measurement techniques*, Engineering Structures, 226, 19 p., 2020.

[Can22]   **Cantone R., Setiawan A., Fernández Ruiz M., Muttoni A.**, *Characterization of shear deformations in reinforced concrete members without shear reinforcement*, Engineering Structures, Vol. 257, 113910, 16 p., 2022.

[Cav17]   **Cavagnis F., Fernández Ruiz M., Muttoni A.**, An analysis of the shear-transfer actions in reinforced concrete members without transverse reinforcement based on refined experimental measurements, Structural concrete, Vol. 19, pp. 49-64, 2017.

[Cav17a]   **Cavagnis F.**, Shear in reinforced concrete without transverse reinforcement: from refined experimental measurements to mechanical models, EPFL PhD Thesis, n° 8216, 223 p., Lausanne, Switzerland, 2017.

[Cav15]   **Cavagnis F., Fernández Ruiz M., Muttoni A.**, Shear failures in reinforced concrete members without transverse reinforcement: An analysis of the critical shear crack development on the basis of test results, Engineering structures, Vol. 103, pp. 157-173, UK, 2015.

[Cav18]   **Cavagnis F., Fernández Ruiz M., Muttoni A.**, A mechanical model for failures in shear of members without transverse reinforcement based on development of a critical shear crack, Engineering structures, Elsevier, Vol. 157, pp. 300-315, 2018.

[CEB93]   **CEB**, *CEB-FIP Model Code 1990*, Comité Euro-International du Béton (CEB), 460 p., London, UK, 1993.

[Cha87]   **Chana P. S.**, *Investigation of the mechanism of shear failure of reinforced concrete beams*, Magazine of Concrete Research, Vol. 39, No. 141, pp. 196-204, London, UK, 1987.

[Cla05]   **Cladera A., Mari A. R.**, *Experimental study on high-strength concrete beams failing in shear*, Engineering Structures, Vol. 27, pp. 1519-1527, 2005.

[Coi92]   **Coignet E.**, Nouveau système de construction avec poutrelles droites ou courbes et plate-bandes en maçonnerie et fer combinés, French patent, No 226 634, 1892.

[Con07]   **Considère A.**, *Le glissement des armatures*, Le Ciment, (This publication reports the study by A. Considers, expressed in the meeting of 27.04.1907 at the meeting of the French and Belgian members of the l'Association internationale des matériaux de constructions), 12e Année, No. 7, pp. 102-106, Paris, 1907.

[Cor10]   **Correlated Solutions**, *Vic-3D 2010, Reference Manual*, 108 p., 2010.

[Cos16]   **Costa R., Providência P., Dias A.**, *Anchorage Models for Reinforced Concrete Beam-Column Joints under Quasi-Static Loading*, ACI Structural Journal, V. 113, No. 3, pp. 503-514, 2016.

[Cra65]   **Cranston W. B.**, *Tests on reinforced concrete frames*, Cement and Concrete Association, Vol. 1, 38 p., London, England, 1965.

[CSA14]   **CSA** , *CSA Standard A23.3-14: Design of concrete structures*, Canadian Standard Association, Ottawa, Canada, 2014.

[Dao13]   **Daoud A., Maurel O., Laborderie C.**, *2D mesoscopic modelling of bar–concrete bond*, Engineering Structures, Vol. 49, pp. 696-706, 2013.

[Dar98]   **Darwin D., Idun E. K., Zuo J., Tholen M. L.**, *Reliability-Based Strength Reduction Factor for Bond*, Structural Journal, Vol. 95, No. 4, pp. 434-443, 1998.

[De15]   **De Wilder K., Lava P., Debruyne D., Wang Y., De Roeck G., Vandewalle L.**, *Stress Field Based Truss Model for Shear-Critical Prestressed Concrete Beams*, The Institution of Structural Engineers, Vol. 3, pp. 28–42, London, UK, 2015.

[Dra75]   **Dragosavic M., Van Den Beukel A., Gijsbers F. B. J.**, *Loop connections between precast concrete components loaded in bending*, Heron, Vol. 20, no. 3, 36 p., Netherlands, 1975.

[Dru61]   **Drucker D. C.**, *On Structural Concrete and the Theorems of Limit Analysis*, IABSE International Association for Bridge and Structural Engineering, Report No.21, Zürich, Switzerland, 1961.

[Eur21]   **Eurocode 2**, *Design of concrete structures - Part 1-1: General rules, rules for buildings, bridges and civil engineering structures*, Stable version of the draft of the 2nd generation of prEN 1992-1-1:2021, European Committee for Standardization (CEN), Brussels, Belgium, 2021.

[Eur04]   **Eurocode 2**, *Design of concrete structures-Part 1-1: General rules and rules for buildings*, European Committee for Standardization (CEN), 225 p., Brussels, Belgium, 2004.

[Fen68]   **Fenwick R. C., Paulay T.**, *Mechanisms of shear resistance of concrete beams*, Journal of the Structural Division, Proceedings of the ASCE, Vol. 94, No. ST10, pp. 2325-2350, Reston, USA, 1968.

[Fer21]   **Fernández Ruiz M.**, *The influence of the kinematics of rough surface engagement on the transfer of forces in cracked concrete*, Engineering Structures, 231, 17 p., 2021.

[Fer08]   **Fernández Ruiz M., Muttoni A.**, *Shear strength of thin-webbed post-tensioned beams*, ACI Structural Journal, Vol.105, No 3, pp. 308-317, USA, 2008.

[Fer07]   **Fernández Ruiz M., Muttoni A.**, *On Development of Suitable Stress Fields for Structural Concrete*, ACI Structural Journal, Vol.104, No4, pp. 495-502, Farmington Hills, USA, 2007.

[Fer07a]   **Fernández Ruiz M., Muttoni A., Gambarova P.**, *A re-evaluation of test data on bond in R/C by means of FEM modeling*, Studi e ricerche, Starrylink, pub., V. 27, pp. 113-134, Brescia, Italy, 2007.

[Fer07b]   **Fernández Ruiz M., Muttoni A., Gambarova P.**, *Relationship between nonlinear creep and cracking of concrete under uniaxial compression*, Journal of Advanced Concrete Technology, Vol. 5, No 3, pp. 383-393, Japan, 2007.

[Fer15]   **Fernández Ruiz M., Muttoni A., Sagaseta J.**, Shear strength of concrete members without transverse reinforcement: A mechanical approach to consistently account for size and strain effects, Engineering structures, Vol. 99, pp. 360-372, UK, 2015.

[Fer10]   **Fernández Ruiz M., Plumey S., Muttoni A.**, *Interaction between Bond and Deviation Forces in Spalling Failures of Arch-Shaped Members without Transverse Reinforcement*, ACI Structural Journal, V. 107, pp. 346-354, USA, 2010.

[FIB11]   **FIB**, *fib Model Code 2010, Final Draft*, Special Activity Group 5, 653 p., Lausanne, Switzerland, 2011.

[FIB21]   **FIB**, *Design and assessment with strut-and-tie models and stress fields: from simple calculations to detailed numerical analysis*, Fédération Internationale du Béton - fib Bulletin n°100, 235 p., Lausanne, Switzerland, 2021.

[FIB13]   **FIB**, *fib Model Code for Concrete Structures 2010*, fib, First Edition, UK, 2013.

[FIB00]   **FIB**, *Bond of reinforcement in concrete*, fib bulletin, Fédération Internationale du Béton - fib Bulletin n°10; state-of-art report prepared by Task Group Bond models, 10, 427 p., Lausanne, Switzerland, 2000.

[For19]   **Forest S. B.**, *Anchorage of Single Leg Stirrups in Reinforced Concrete Slabs and Walls*, Master thesis, Graduate Department of Civil Engineering, University of Toronto, 240 p., Toronto, 2019.

[Gra33]   **Graf O.**, *Versuche über die Widerstandsfähigkeit des Betons an den Abbiegestellen der schief abgebogenen Eisen in Eisenbetonbalken*, Deutscher Ausschuss für Eisenbeton, Heft 73, pp. 17-28, Germany, German, 1933.

[Gra40]   **Graf O.**, *Versuche über die Widerstandsfähigkeit des Betons an den Abbiegestellen der schief abgebogenen Eisen in Eisenbetonbalken*, Deutscher Ausschuss für Eisenbeton, Heft 94, pp. 1-12, Germany, German, 1940.

[Gra40a]   **Graf O., Weil Gustav**, *Vershuche mit verdrillten Bewehrungsstählen*, Deutscher Ausschuss für Eisenbeton, Heft 94, pp. 13-56, Germany, German, 1940.

[Gra99]   **Grassl P.**, *Splicing of Reinforcement Loops in Beams: Experiments and Non-linear FiniteElement Analyses*, Chalmers University of technology, Master thesis 99:4, 82 p., Göteborg, Sweden, 1999.

[Gro76]   **Grob J., Thürlimann B.**, *Ultimate Strength and Design of Reinforced Concrete Beams Under Bending and Shear*, IABSE, No. 36, pp. 105-120, 1976.

[Hae17]   **Haefliger S., Mata Falcón J, Kaufmann W.**, *Application of distributed optical measurements to structural concrete experiments*, Fourth Conference on Smart Monitoring, Assessment and Rehabilitation of Civil Structures (SMAR 2017), pp. 159, Zurich, Switzerland, 2017.

[Hay13]   **Hayashi D., Nagai K.**, *Investigating the anchorage performance of RC by using three-dimensional discrete analysis*, Engineering Computations, Vol. 30, No. 6, pp. 815-824, 2013.

[Heg04]   **Hegger J., Sherif A., Roeser W.**, *Nonlinear finite element analysis of reinforced concrete beam-column connections*, ACI Structural Journal, Vol. 101, No. 5, pp. 604-614, 2004.

[Hen93]   **Hennebique F.**, *Combinaison particulière du métal et du ciment en vue de la création de poutraisons très légères et de haute résistance*, French patent (Patent of addition to the previous patent of 1892), No 223 546, 1893.

[Hen92]   **Hennebique F.**, Combinaison particulière du métal et du ciment en vue de la création de poutraisons très légères et de haute résistance, French patent, No 223 546, 1892.

[Hil83]   **Hillerborg A.**, *Analysis of a single crack*, Fracture mechanics of concrete, edited by F.H.Wittmann, Elsevier science Publishers B.V., pp. 223-249, Amsterdam, Netherlands, 1983.

[Hor92]   **Hordijk D. A.**, *Tensile and tensile fatigue behaviour of concrete; experiments, modelling and analyses*, Heron, 37/1, Delft, Netherlands, 1992.

[Hri69]   **Hribar J. A., Vasko R. C.**, *End Anchorage of High Strength Steel Reinforcing Bars*, ACI Journal, Vol. 66, No. 11, pp. 875-883, 1969.

[Hub16]   **Huber P., Huber T., Kollegger J.**, *Investigation of the shear behavior of RC beams on the basis of measured crack kinematics*, Engineering Structures, Vol. 113, pp. 41-58, 2016.

[Hwa17]   **Hwang H.-J., Park H.-G., Yi W.-J.**, *Development Length of Standard Hooked Bar Based on Non-Uniform Bond Stress Distribution*, ACI Structural Journal, Vol. 114, No. 6, pp. 1637-1648, 2017.

[Hya77]   **Hyatt T.**, An account of some experiments with Portland-cement-concrete combined with iron, as a building material, with reference to economy of metal in construction, and for security against fire in the making of roofs, floors, and walking surfaces, Printed for private circulation, at the Chiswick Press, 28 p., London, 1877.

[Ino11]   **Inoue Y., Nagai K.**, *Numerical Simulation of Fracture Pattern and Bond Performance of Anchorage in Reinforced Concrete*, ProcediaEng., Proc., 12th East Asia-Pacific Conf. on Structural Engineeringand Construction— EASEC12, Vol. 14, pp. 1165-1173, 2011.

[ISO19]   **ISO**, EN ISO 15630-1 Steel for the reinforcement and prestressing of concrete - Test methods - Part 1 : reinforcing bars, wire rod and wire, European Commitee For Standardization CEN, 36 p., 2019.

[Jir79]   **Jirsa J. O., Lutz A. L., Gergely P.**, *Rationale for Suggested Development, Splice, and Standard Hook Provisions for Deformed Bars in Tension*, Concrete International, Vol. 1, No. 7, pp. 47-61, 1979.

[Joe13]   **Joergensen H. B., Hoang L. C.**, *Tests and limit analysis of loop connections between precast concrete elements loaded in tension*, Engineering structures, 52, pp. 558-569, 2013.

[Joh00]   **Johansson M.**, *Structural behaviour in concrete frame corners if civil defence shelters (non-linear finite element analyses and experiments)*, Phd Thesis Department of Structural Engineering, Chalmers University of technology, Publication 00:2, 242 pp., Göteborg, Sweden, 2000.

[Joh01]   **Johansson M.**, *Reinforcement detailing in concrete frame corners*, ACI Structural Journal, Vol. 98, No. 1, pp. 105-115, 2001.

[Joh81]   **Johnson L. A., Jirsa J. O.**, *The Influence of Short Embedment and Close Spacing on the Strength of Hooked Bar Anchorages*, PMFSEL Report No.81-2, Department of Civil Engineering-Structures Research Laboratory, University of Texas, Austin, Texas, 93 p., 1981.

[Joh90]   **Johnson M. K., Ramirez J. A.**, *Minimum Shear Reinforcement in Beams with Higher Strength Concrete*, ACI Structural Journal, 87, pp. 376-382, Farmington Hills, USA, 1990.

[Kan64]   **Kani G. N. J.**, *The riddle of shear failure and its solution*, ACI Journal, Vol. 61, No. 4, pp. 441-467, Detroit, USA, 1964.

[Kau96]   **Kaufmann W., Marti P.**, *Versuche an Stahlbetonträgern unter Normal- und Querkraft*, Institut für Baustatik und Konstruktion, ETHZ, No 226, 141 p., Zürich, Switzerland, German, 1996.

[Kem68]   **Kemp E. L., Brezny F. S., Unterspan J. A.**, *Effect of Rust and Scale on the Bond Characteristics of Deformed Reinforcing Bars*, ACI Journal, Vol. 65, No. 9, pp. 743-756, 1968.

[Koe92]   **Koenen M., Wayss G. A.**, *Perfectionnement apportés aux massifs de maçonnerie au point de vue de leur résistance à la traction*, Austro-Hungarian patent, No 219 011, 1892.

[Kor72]   **Kordina K., Fuchs G.**, *Untersuchungen an übergreifungs-vollstössen mit hakenförmig-gebogenen rippenstählen*, Ernst & Sohn, Institut für Baustoffkunde und Stahlbetonbau der Technischen Universität Braunschweig, Schriftenreihe des DafStb, H. 226, pp. 57-81, Berlin, Germany, German, 1972.

[Kos22]   **Koscak J., Damjanovic D., Bartolac M., Duvnjak I.**, Shear behavior of RC beams without transverse reinforcement: An analysis of crack kinematics and transfer mechanisms based on stereophotogrammetric measurements, Engineering Structures, Vol. 255, No. 113886, 2022.

[Kuc08]   **Kuchma D., Kim K. S., Nagle T. J., Sun S., Hawkins N. M.**, *Shear Tests on High-Strength Prestressed Bulb-Tee Girders: Strengths and Key Observations*, ACI Structural Journal, Vol. 105, No. 3, pp. 358-367, Farmington Hills, USA, 2008.

[Kup69]   **Kupfer H., Hilsdorf H., Rüsch H.**, *Behavior of Concrete under Biaxial Stresses*, Journal of the American Concrete Institute, Proceedings, Vol. 66, No. 8, pp. 656-666, Detroit, USA, 1969.

[Lag16]   **Lagier F., Massicotte B., Charron J.-P.**, *3D Nonlinear Finite-Element Modeling of Lap Splices in UHPFRC* , Journal of Structural Engineering, Vol. 142, No. 11, 04016087, 2016.

[Lee08]   **Lee J.-Y., Kim U.-Y.**, Effect of Longitudinal Tensile Reinforcement Ratio and Shear Span-Depth Ratio on Minimum Shear Reinforcement in Beams, Structural Journal, Vol. 105, No. 2, pp. 134-144, 2008.

[Leo63]   **Leonhardt F., Walther R.**, *Schubversuche an Plattenbalken mit unterschiedlicher Schubbewehrung*, Deutscher Ausschuss für Stahlbeton, Wilhelm Ernst & Sohn, Vol. 156, 84 p., Berlin, Germany, German, 1963.

[Leo65]   **Leonhardt F., Walther R.**, *Geschweisste Bewehrungsmatten als Bügelbewehrung - Schubversuche an Plattenbalken und Verankerungsversuche*, Bautechnik, Band 42, Heft 10, pp. 329-341, Germany, German, 1965.

[Leo73]   **Leonhardt F., Walther R., Dieterle H.**, *Versuche zur Ermittlung der Tragfähigkeit von Zugschlaufenstössen*, Deutscher Ausschuss für Stahlbeton, Heft 226, pp. 1-22, Germany, German, 1973.

[Leq18]   **Lequesne R. D., O'Reilly M., Darwin D., Lepage A., Al-Sabawy A., Guillen E., Spradling D.**, *Use of Headed Bars as Shear Reinforcement*, Structural Engineering and Engineering Materials, SM Report No. 126, University of Kansas Center for Research, 244 p., Kansas, 2018.

[Lim15]   **Lima de Resende T., da Conceição Domingues Shehata L., Abd El Malik Shehata I.**, *Shear strength of self-compacting concrete beams with small stirrups ratios*, Structural Concrete, Vol. 19, No. 1, pp. 3-10, 2015.

[Lun13]   **Luna Technologies Inc.**, *Optical Backscatter Reflectometer 4600 User Guide*, Luna Technologies, 227 p., Blacksburg, VA, 2013.

[Lun05]   **Lundgren K.**, *Bond between ribbed bars and concrete. Part 1: Modified model*, Magazine of Concrete Research, Vol. 57, No. 7, pp. 371-382, 2005.

173

[Lun15]   **Lundgren K., Gylltoft K.**, *A model for the bond between concrete and reinforcement* , Magazine of Concrete Research, Vol. 62, No. 1, pp. 53-63, 2015.

[Luo94]   **Luo Y. H., Durrani A. J., Bai S., Yuan J.**, *Study of reinforcing detail of tension bars in frame corner connections*, ACI Structural Journal, Vol. 91, No. 4, pp. 486-496, Detroit, USA, 1994.

[Lur15]   **Lura P., Plizzari G., Riva P.**, *3D finite-element modelling of splitting crack propagation*, Magazine of Concrete Research, Vol. 54, No. 6, pp. 481-493, 2015.

[Mar51]   **Marcus H.**, *Load Carrying Capacity of Dowels at Transverse Pavement Joints*, ACI Structural Journal, Vol. 48, No.10, pp. 169-184, 1951.

[Mar75]   **Marques J. L. G., Jirsa J. O.**, *A Study of Hooked Bar Anchorages in Beam-Column Joints*, ACI Journal, Vol. 72., No. 5, pp. 198-209, 1975.

[Mar98]   **Marti P., Alvarez M., Kaufmann W., Sigrist V.**, *Tension chord model for structural concrete*, Structural Engineering International, IABSE, Vol. 8, No. 4, pp. 287-298, USA, 1998.

[Mat20]   **Mata Falcón J, Haefliger S., Lee M., Galkovski T., Gehri N.**, *Combined application of distributed fibre optical and digital image correlation measurements to structural concrete experiments*, Engineering Structures, Volume 225, Page: 111309, Amsterdam, 2020.

[Med18]   **Medziti M., Zwicky D.**, Ancrages sous traction transervale d'étriers dans le béton armé - développement d'un modèle de dimensionnement (EN: Anchorages of stirrups under transverse tension in concrete - development of a design model), De l'institut des Technologies de l'Environnement Construit (iTEC) à la Haute École d'Ingénierie et d'Architecture de Fribourg (HEIA-FR), Fribourg, Switzerland, 2018.

[Mes08]   **Mesnager A.**, *Les jonctions de barres tendues dans les poutres en béton armé*, Annales des Ponts et Chaussées, 78 année, 8e Série, Tome XXXII, No 2, pp. 109-140, Paris, 1908.

[Min71]   **Minor J.**, *Study of Bent Bar Anchorages in Concrete*, PhD Thesis, Faculty of Civil Engineering, Rice University, 135 p., Houston, USA, 1971.

[Min75]   **Minor J., Jirsa J. O.**, *Behavior of Bent Bar Anchorages*, ACI Journal, Vol. 72, No. 4, pp. 141-149, 1975.

[Moc21]   **Moccia F., Fernández Ruiz M., Metelli M., Muttoni A., Plizzari G.**, *Casting position effects on bond performance of reinforcement bars*, Structural Concrete, Wiley, 21 p., 2021.

[Moc21a]   **Moccia F., Fernández Ruiz M., Muttoni A.**, *Spalling of concrete cover induced by reinforcement* , Engineering Structures, 19 p., 2021.

[Moc20]   **Moccia F., Yu Q., Fernández Ruiz M., Muttoni A.**, *Concrete compressive strength: From material characterization to a structural value*, Structural Concrete, 21 p., 2020.

[Mon78]   **Monier J.**, *Applications à la construction de poutres, poutrelles pour ponts, passerelles*, French patent (patent of addition to the previous patent of 1877: "un système de traverses et supports en ciment et fer applicables aux voies, chemins ferrés et non ferrés"), No 120 989, 1878.

[Mon21]   **Monney F., Fernández Ruiz M., Muttoni A.**, *Design against splitting failures in reinforced concrete due to concentrated forces and minimum bend diameter of reinforcement*, Engineering Structures, Vol. 245, 112902, 2021.

[Mon22]   Monney F., Yu Q., Fernández Ruiz M., Muttoni A., Anchorage of shear reinforcement in beams and slabs, Engineering Structures.
           [accepted, May 2022]

[Mon21a]   **Monserrat López A., Fernández Ruiz M., Miguel Sosa P.**, *The influence of transverse reinforcement and yielding of flexural reinforcement on the shear-transfer* , Engineering Structures, 17 p., 2021.

[Moo14]   **Moore A.M.**, *Shear Behavior of Spliced Post-Tensioned Girders*, PhD Thesis Faculty of the Graduate School, The University of Texas at Austin, 250 p., Austin, USA, 2014.

[Mör08]   **Mörsch E.**, *Der Eisenbetonbau - Seine Theorie und Anwendung*, Verlang von Konrad Wittwer, 3. Auflage, 376 p., Stuttgart, Germany, German, 1908.

[Mör06]   **Mörsch E.**, *Der Eisenbetonbau - Seine Theorie und Anwendung*, Konrad Wittwer, 2nd Edition, 252 p., Stuttgart, Germany, German, 1906.

[Mut90]   **Muttoni A.**, *Die Anwendbarkeit der Plastizitätstheorie in der Bemessung von Stahlbeton*, Birkhäuser Verlag, Institut für Baustatik und Konstruktion ETH Zürich, No 176, 164 p., Basel, Switzerland, German, 1990.

[Mut08]   **Muttoni A., Fernández Ruiz M.**, *Shear strength of members without transverse reinforcement as function of critical shear crack width*, ACI Structural Journal, V. 105, No 2, pp. 163-172, Farmington Hills, USA, 2008.

[Mut15]   **Muttoni A., Fernández Ruiz M., Niketic F.**, *Design versus Assessment of Concrete Structures Using Stress Fields and Strut-and-Tie Models*, ACI Structural Journal, Vol.112, No 5, pp. 605-616, Farmington Hills, USA, 2015.

[Mut97]   **Muttoni A., Schwartz J., Thürlimann B.**, *Design of Concrete Structures with Stress Fields*, Birkhäuser Verlag, 143 p., Basel, Switzerland, 1997.

[Myl28]   **Mylrea T. D.**, *The Carrying Capacity of Semicircular Hooks*, ACI Journal, Proceedings, Vol. 24, pp. 240-272, 1928.

[Nie78]   **Nielsen M. P., Braestrup M. W., Bach F.**, *Rational Analysis of Shear in Reinforced Concrete Beams*, IABSE Colloquium Proceedings, P-15; Vol. 2, 16 p., Bergamo, Italy, 1978.

[Nie11]   **Nielsen M. P., Hoang L. C.**, *Limit Analysis and Concrete Plasticity*, CRC Press, 3rd edition, 788 p., Boca Raton, USA, 2011.

[Nil73]   **Nilsson I. H. E.**, *Reinforced concrete corners and joints subjected to bending moment*, The National Swedish Institute for Building Research (Stockholm), Division of Concrete Structures, Chalmers University of Technology, PhD Thesis, Document D7:1973, 249 p., Göteborg, Sweden, 1973.

[OFR10]   **OFROU**, *Directive ASTRA 12 004 Détails de construction de ponts*, Office fédéral de la Protection civile, Chapitre 3 : Extrémités de ponts, 42 p., Bern, Switzerland, 2010.

[Öst63]   **Östlund L.**, The influence of bending radius and concrete cover for deformed bars on the risk of splitting failure in RC structures (in Swedish: Inverkan av bockningsradier och täckande betongskikt hos kamstål på spjälkningsrisken för armerade betongkonstruktioner), The Royal Institute of Technology, Stockholm, Sweden, Swedish, 1963.

[Pin77]   **Pinc R. L., Watkins C. M., Jirsa J. O.**, *Strength of Hooked Bars Anchorages in Beam-Column Joints*, Report on a Research Project Sponsored by Reinforced Concrete Research Council, Project 33, Department of Civil Engineering-Structures Research Laboratory, University of Texas at Austin, 67 p., 1977.

[Piy02]   **Piyamahant S.**, *Shear Behavior of Reinforced Concrete Beams with a Small Amount Of Web Reinforcement*, Master Thesis, Department of Infrastructure System Engineering, Kochi University of Technology, Kochi, Japan, 2002.

[Pla69]   **Placas A.**, *Shear Strength of Reinforced Concrete Beams*, Imperial College of Science and Technology, PhD Thesis, 581 p., London, England, 1969.

[Pol19]   **Poldon J. J., Hoult N. A., Bentz E. C.**, *Distributed Sensing in Large Reinforced Concrete Shear Test*, ACI Structural Journal, 116(5), 235-245, 2019.

[Pol21]   **Poldon J. J., Hoult N. A., Bentz E. C.**, *Understanding Reinforcement Behavior Using Distributed Measurements of Shear Tests*, Structural Journal, Vol. 116, No. 3, pp. 255-266, 2021.

[Ram08]   **Ramirez J. A., Russell B. W.**, *Transfer, Development, and Splice Length for Standard Reinforcement in High-strength Concrete*, Washington, D.C.: Transportation Research Board, National Research Council, 122 p., Washington D.C., 2008.

[Reg80]   **Regan P. E.**, *Single-Legged stirrups as shear reinforcement in reinforced concrete flat slabs*, School of Environment, Polytechnic of Central London, The Building research establishment, 90 p., London, England, 1980.

[Reg04]   **Regan P. E., Kennedy Reid I. L.**, *Shear Strength of RC Beams with Defective Stirrup Anchorages*, Magazine of Concrete Research, Vol. 56, No. 3, pp. 159-166, 2004.

[Reh69]   **Rehm G.**, *Kriterien zur Beurteilung von Bewehrungsstäben mit hochwertigem Verbund*, Stahlbetonbau, Berichte aus Forschung und Praxis, Verlag Wilhelm Ernst & Sohn, pp. 79-96, Berlin, Germany, German, 1969.

[Reh79]   **Rehm G., Dieterle H., Eligehausen R.**, *Rationalisierung der Bewehrungstechnik im Stahlbetonbau - Das Tragverhalten verschiedener Verankerungselemente in Rissen*, Institut für Werkstoffe im Bauwesen, Universität Stuttgart, Stuttgart, Germany, German, 1979.

[Reh68]   **Rehm G., Martin H., Müller H.-H.**, *Ausziehversuche mit Betonstahlhaken*, Materialprüfungsanstalt für das Bauwesen, TU München, Bericht Nr. 1975, München, Germany, German, 1968.

[Ric28]   **Richart F. E., Brandtzaeg A., Brown R. L.**, *A Study of the Failure of Concrete under Combined Compressive Stresses*, Engineering Experiment Station, University of Illinois, Bulletin 185, 102 p., Illinois, USA, 1928.

[Rit99]   **Ritter W.**, *Die Bauweise Hennebique*, Schweizerische Bauzeitung, pp. 41-149, Zürich, Switzerland, German, 1899.

[Rup13]   **Rupf M., Fernández Ruiz M., Muttoni A.**, *Post-tensioned girders with low amounts of shear reinforcement: Shear strength and influence of flanges*, Engineering structures, Vol. 56, pp. 357-371, 2013.

[Sag11]   **Sagaseta J., Vollum R. L.**, *Influence of beam cross-section, loading arrangement and aggregate type on shear strength*, Magazine of Concrete Research, Vol.53, No 2, pp. 139-155, London, UK, 2011.

[Sag11a]   **Sagbas G., Vecchio F. J., Christopoulos C.**, *Computational Modeling of the Seismic Performance of Beam-Column Subassemblies*, Journal of Earthquake Engineering, Vol. 15, No. 4, pp. 640-663, 2011.

[Sal04]   **Salem H. M., Maekawa K.**, *Pre- and postyield finite element method simulation of bond of ribbed reinforcing bars*, ASCE Journal of Structural Engineering, Vol. 130, No. 4, pp. 671-680, USA, 2004.

[Sal13]   **Saliger R.**, *Schubwiderstand und Verbund in Eisenbetonbalken auf Grund von Versuch und Erfahrung*, Springer-Verlag Berlin and Heidelberg GmbH & Co. K, 68 p., Berlin, German, 1913.

[Sch87]   **Schlaich J., Schäfer K., Jennewein M.**, *Toward a Consistent Design of Structural Concrete*, PCI Journal, Vol.32, No 3, pp. 75-150, Chicago, USA, 1987.

[Sco94]   **Scott R. H., Feltham I., Whittle R. T.**, *Reinforced concrete beam-column connections and BS 8110*, The Structural Engineering, 72, No 4, pp. 55-60, London, England, 1994.

[Sha09]   **Sharma A., Genesio G., Reddy G. R., Eligehausen R.**, Nonlinear dynamic analysis using microplane model for concrete and bond slip model for prediction of behavior of nonseismically detailed RCC beam-column joints, Journal of Structural Engineering, Vol. 36, No. 4, pp. 250-257, 2009.

[Shi08]   **Shima H., Fukuju S.**, *Bond Stress Distribution along Bar Axis in Hook Anchorage of Deformed Reinforcing Bar*, 3rd ACF International Conference-ACF/VCA, pp. 654-660, 2008.

[SIA35]   **SIA**, SIA112 - Normes de la S.I.A. concernant le calcul, l'execution et l'entretien des constructions métalliques et des constructions en béton et en béton armé, Société Suisse des Ingénieurs et Architectes, 78 p., Suisse, 1935.

[SIA56]   **SIA**, *SIA 162 - Normes concernant les constructions en béton, en béton armé et en béton précontraint*, Société Suisse des Ingénieurs et Architectes, 48 p., Zürich, Switzerland, French - English, 1956.

[SIA93]   **SIA**, *SIA 162 : Ouvrages en béton - Edition de 1993*, SIA, 86 p., Zürich, Switzerland, 1993.

[SIA13]   **SIA**, *SIA 262:2013 - Structures en béton*, Société suisse des ingénieurs et des architectes, 102 p., Zurich, Switzerland, 2013.

[SIA03]   **SIA**, *SIA 262 - Construction en béton*, Société Suisse des Ingénieurs et des Architectes, 94 p., Zürich, Switzerland, 2003.

[SIA68]   **SIA**, *SIA 162 : Norme pour le calcul, la construction et l'exécution des ouvrages en béton, en béton armé et en béton précontraint*, Société Suisse des Ingénieurs et des Architectes, 84 p., Zürich, Switzerland, 1968.

[SIA03a]   **SIA 162**, *Provisorische Normen für Projektierung, Ausführung und kontrolle*, Schweizerischer Ingenieur und Architekten Verein, Zürich, Suisse, German, 1903.

[SIA09]   **SIA 162**, *Réglement sur les Constructions en béton armé*, Société Suisse des Ingénieurs et Architectes, 1909.

[Sig11]   **Sigrist V.**, *Generalized Stress Field Approach for Analysis of Beams in Shear*, ACI Structural Journal, Vol. 108, No. 4, pp. 479-487, Farmington Hills, USA, 2011.

[Sig13]   **Sigrist V., Bentz E. C., Fernández Ruiz M., Foster S. J., Muttoni A.**, *Background to the Model Code 2010 Shear Provisions - Part I: Beams and Slabs*, Structural Concrete, Vol. 14, No. 3, pp. 204-214, Berlin, Germany, 2013.

[Ske84]   **Skettrup E., Strabo J., Andersen N. H., Brondum-Nielsen T.**, *Concrete Frame Corners*, ACI Journal, Vol. 81, No. 6, pp. 587-593, Detroit, 1984.

[Sør74]   **Sørensen H. C.**, *Shear Tests on 12 Reinforced Concrete T-Beams*, Technical University of Denmark, No R60, 52 p., Lyngby, Denmark, 1974.

[Sor88]   **Soroushian P., Obaseki K., Nagi M., Rojas M.**, *Pullout Behavior of Hooked Bars in Exterior Beam-Column Connections*, ACI Structural Journal, Vol. 85, No. 3, pp. 269-276, 1988.

[Sor87]   **Soroushian P., Obaseki K., Rojas M.**, *Bearing Strength and Stiffness of Concrete Under Reinforcing Bars*, ACI Structural Journal, Vol. 84, No.3, pp. 179-184, 1987.

[Spe18]   Sperry J., Darwin D., O'Reilly M., Lepage A., Lequesne R. D., Matamoros A. B., Feldman L. R., Yasso S., Searle N., DeRubeis M., Ajaam A., *Conventional and High-Strength Steel Hooked Bars: Detailing Effects*, ACI Structural Journal, pp. 247-257, 2018.

[Spe17]   Sperry J., Yasso S., Searle N., DeRubeis M., Darwin D., O'Reilly M., Matamoros A. B., Feldman L. R., Lepage A., Lequesne R. D., Ajaam A., *Conventional and High-Strength Hooked Bars—Part 1: Anchorage Tests*, ACI Structural Journal, Vol. 114 (1), pp. 255-265, Anglais, 2017.

[Spe15]   Sperry J., Yasso S., Searle N., DeRubeis M., Darwin D., O'Reilly M., Matamoros A. B., Feldman L. R., Lepage A., Lequesne R. D., Ajaam A., *Anchorage of High-Strength Reinforcing Bars with Standard Hooks*, Structural Engineering and Engineering Materials, SM Report No. 111, University of Kansas Center for Research, Inc., Lawrence, 243 p., Kensas, 2015.

[Str81]   **Stroband J., Kolpa J. J.**, *The behaviour of reinforced concrete column-to-beam joints (part 2: corners subjected to positive moments)*, Stevin Laboratory, Department of Civil Engineering, Delft University of Technology, Report 5-81-5, 101 pp., 1981.

[Str83]   **Stroband J., Kolpa J. J.**, *The behaviour of reinforced concrete column-to-beam joints (part 1: corners subjected to negative moments)*, Stevin Laboratory, Department of Civil Engineering, Delft University of Technology, 105 pp., 1983.

[Stu90]   **Stucki D., Thürlimann B.**, *Versuche an Eckverbindungen aus Stahlbeton*, Institut für Baustatik und Konstruktion ETH Zürich, Nr. 8701-1, Switzerland, German, 1990.

[Swa69]   **Swann R. A.**, *Flexural strength of corners of reinforced concrete portal frames*, Cement and Concrete Association, 14 pp., London, England, 1969.

[Sys99]   **Système Hennebique**, *Le béton armé*, Organe des Concessionnaires et Agents du Système Hennebique, 2e année, No. 14, 14 p., 1899.

[Tas20]   **Tasevski D., Fernández Ruiz M., Muttoni A.**, *Influence of Load Duration on Shear Strength of Reinforced Concrete Members* , ACI Structural Journal, Vol 117 n° 2, pp. 157-169, 2020.

[Tay69]   **Taylor H. P. J.**, *Investigation of the Dowel Shear Forces Carried by the Tensile Steel in Reinforced Concrete Beams*, Cement and Concrete Association, Report No. TRA 431, 24 p., London, UK, 1969.

[Tay70]   **Taylor H. P. J.**, *Investigation of the forces carried across cracks in reinforced concrete beams in shear by interlock of aggregate*, Cement and Concrete Association, Technical Report No. 42-447, 22 p., London, UK, 1970.

[Tay76]   **Taylor H. P. J., Clarke J. L.**, *Some Detailing Problems in Concrete Frame Structures*, The Structural Engineer , Volume 54, Issue 1, pp. 19-32, 1976.

[Tay63]   **Taylor R., Brewer R. S.**, *The effect of the type of aggregate on the diagonal cracking of reinforced concrete beams*, Magazine of Concrete Research, Vol. 15, No. 44, 1963.

[Teo02]   **Teoh B. K., Mansur M. A., Wee T. H.**, *Behavior of High-Strength Concrete I-Beams with Low Shear Reinforcement*, ACI Structural Journal, V. 99, No. 3, pp. 299-307, 2002.

[Tep73]   **Tepfers R.**, *A theory of bond applied to overlapped tensile reinforcement splices for deformed bars*, Chalmers University, P-73:2, Division of Concrete structures, Chalmers University of Göteborg, 73 n°2, 328 p., Göteborg, Sweden, 1973.

[Thü79]   **Thürlimann B.**, *Plastic Analysis of Reinforced Concrete Beams*, IABSE Colloquium, Vol. 28, pp. 71-90, Copenhagen, Denmark, 1979.

[Tim69]   **Timm G.**, *Untersuchungen zur Verbindung von Stahlbetonplatten mit hakenförmiggebogenen Stäben*, Department of Civil Engineering, University of Karlsruhe, 81 p., Germany, German, 1969.

[Tom02]   **Tompos E. J., Frosch R. J.**, *Influence of Beam Size, Longitudinal Reinforcement, and Stirrup Effectiveness on Concrete Shear Strength*, ACI Structural Journal, V. 99, No. 5, pp. 559-567, 2002.

[Tue19]   **Tue N. V., Ehmann R., Betschoga C., Tung N. D.**, Effect of low amounts of shear reinforcement on the shear resistance of reinforced concrete beams with different M/V-combinations, Beton - und Stahlbetonbau, pp. 217-230, Berlin, Germany, German, 2019.

[Tun20]   **Tung N. D., Betschoga C., Tue N. V.**, Analysis of the crack development and shear transfer mechanisms of reinforced concrete beams with low amounts of shear reinforcement, Engineering Structures, Vol. 222, No. 111114, 20 p., 2020.

[Val20]   **Valeri P, Fernández Ruiz M., Muttoni A.**, *Modelling of Textile Reinforced Concrete in bending and shear with Elastic-Cracked Stress Fields*, Engineering Structures, 215, 14 p., 2020.

[Var11]   **Varney J. C., Brown M. D., Bayrak O., Poston R. W.**, *Effect of Stirrup Anchorage on Shear Strength of Reinforced Concrete Beams*, ACI Structural Journal, Vol. 108, pp. 469-478, Farmington Hills, USA, 2011.

[Vec86]   **Vecchio F. J., Collins M. P.**, *The modified compression-field theory for reinforced concrete elements subjected to shear*, ACI Structural Journal, Vol.83, No 2, pp. 219-231, USA, 1986.

[Vec04]   **Vecchio F. J., Shim W.**, *Experimental and Analytical Investigation of Classic Concrete Beam Tests*, ASCE Journal of Structural Engineering, Vol.130, pp. 460-469, USA, Anglais, 2004.

[Vel18]   **Vella J. P., Vollum R. L., Kotecha R.**, *Headed Bar Connections Between Precast Concrete Elements: Design Recommendations and Practical Applications*, Structures, Elsevier, V. 15, pp. 162-173, 2018.

[Wal80]   **Walraven J. C.**, *Aggregate interlock: a theoretical and experimental analysis*, PhD Thesis, Delft University of Technology, Faculty of Civil Engineering, 197 p., Delft, Netherlands, 1980.

[Wäs35]   **Wästlund G.**, *Om armering av vinkelformade betongkonstruktioner*, Betong, No. 1, pp. 22-35, Stockholm, Sweden, Swedish, 1935.

[Wäs34]   **Wästlund G.**, Untersuchungen über die Festigkeit von Beton bei Belastungen welche örtlich auf die Oberfläche sowie an Schleifen und abbiegungen von bewehrungseisen Wirken, The Royal Institute of Technology, PhD Thesis, 79 pp., Stockholm, Sweden, Swedish, 1934.

[Wäs36]   **Wästlund G.**, *Untersuchungen über die Bewehrung von winkelförmigen Eisenbetonkonstruktionen*, Beton & Eisen, Vol. 35, Heft 13, pp. 22-227, Germany, German, 1936.

[Win58]   **Winkler E.**, *Formänderung und Festigkeit gekrümmter Körper, insbesondere der Ringe*, Der Civilingenieur, Vol. 4, pp. 232-246, Germany, German, 1858.

[Yas21]   **Yasso S., Darwin D., O'Reilly M.**, *Effects of Concrete Tail Cover and Tail Kickout on Anchorage Strength of 90-Degree Hooks*, Structural Journal, Vol. 118, No. 6, pp. 227-236, 2021.

[Yoo96]   **Yoon Y.-S., Cook W. D., Mitchell D.**, *Minimum Shear Reinforcement in Normal, Medium,and High-Strength Concrete Beams*, ACI Structural Journal, Vol.93, No 5, pp. 576-584, USA, Anglais, 1996.

[Yos00]   **Yoshida Y.**, *Shear reinforcement for large lightly reinforced concrete members*, Master thesis, University of Toronto, 160 p., Toronto, Canada, 2000.

[Yu20]   **Yu Q., Muttoni A., Fernández Ruiz M.**, *Partial Safety Factor Format for the Resistance of Structural Concrete Considering Multiple Failure Modes*, Proceedings of the fib Symposium 2020, 2003-2010, Shanghai, China, 2020.

[Yu21]   **Yu Q., Valeri P, Fernández Ruiz M., Muttoni A.**, A consistent safety format and design approach for brittle systems and application to textile reinforced concrete structures, Engineering Structures, 249, 2021.

MONNEY Frédéric

frederic.monney@alumni.epfl.ch   +41 78 645 77 54
6 Rue du Beulet, 1203 Genève   Swiss nationality
28.05.1990   Married

Education

2017 - 2022   **PhD Candidate**
Doctoral thesis on both experimental and theoretical research focusing on detailing rules in reinforcement concrete bridges and structures, including:
 - Minimum bend diameter of reinforcement
 - Anchorage of shear reinforcement
 - Beams with low amount of shear reinforcement
Structural Concrete Laboratory (IBETON), Swiss Federal Institute of Technology (EPFL), Lausanne (CH)

2013 - 2016   **MSc in Civil Engineering**, specialisation in structural engineering
Swiss Federal Institute of Technology (EPFL), Lausanne (CH)

2008 - 2011   **BSc in Civil Engineering**, specialisation in structural engineering
University of Applied Sciences of Geneva (HEPIA)

2005 - 2008   **Technical Maturity in Civil Engineering**
High school in Geneva

Professional Experience

2017 - 2022   **PhD assistant in research and teaching**
Teaching assistant for: "Structures I and II", "Concrete structures", "Conceptual design of Bridges", "Concrete Bridges", "Concrete structures, selected topics", "Advanced design of concrete structures", "Structure and Architecture", "Stress field". Tutor/supervision of several semester and master projects (theoretical and practical).
Structural Concrete Laboratory (IBETON), Swiss Federal Institute of Technology (EPFL), Lausanne (CH)

2016 - 2017   **Structural engineer**
T ingénierie SA, Geneva (CH)

2016   **Teaching assistant in Civil Engineering**
University of Applied Sciences of Geneva (HEPIA)

2013 to 2015   **Structural engineer**
T ingénierie SA, Geneva (CH), internship, 1 month each year

2010   **Structural engineer**
Perreten & Milleret SA, Carouge (CH), internship, 1 month

Publications

2022	Monney F., Fernández Ruiz M., Muttoni A., *Influence of amount of shear reinforcement and its post-yield response on the shear resistance of reinforced concrete members*, Structural Concrete. [submitted for review, April 2022]
2022	Monney F., Yu Q., Fernández Ruiz M., Muttoni A., *Anchorage of shear reinforcement in beams and slabs*, Engineering Structures. [accepted, May 2022]
2021	Monney F., Fernández Ruiz M., Muttoni A., *Design against splitting failures in reinforced concrete due to concentrated forces and minimum bend diameter of reinforcement*, Engineering Structures, Vol. 245, 2021.
2021	Muttoni A., Fernández Ruiz M., Monney F., *Permissible mandrel diameters for bent bars*, Background document 11.3 to prEN 1992-1-1:2018, European Committee for Standardization (CEN), Brussels, Belgium, 2021.
2019	Muttoni A., Buchs P., Monney F., Mühlberg S., *Ponts en béton: Exemples de conception, dimensionnement et vérification (EN: Concrete Bridges: Examples of Design)*, MSc course Handout "Concrete Bridges", EPFL, 2019

Awards

2016	**Major of promotion MSc in Civil Engineering, EPFL**
	Award for the best grade of the MSc in Civil Engineering, EPFL *Association of Employers of Engineers and Architects of Vaud department*
	Award of the best Master thesis including prestressing, EPFL *Swiss Association of Prestressing Companies*

Associations

Committee	Maison de l'Architecture de Genève (Home of Architecture of Geneva)
Member	Société pour l'art de l'ingénieur (Society for the art of engineer)
Member	Alumni EPFL and HEPIA
Member	FC Veyrier sports (Football)

Languages

French	Native
English	Fluent
German	Basic

Computer skills

Office Suites	Latex	Illustrator	Matlab
SCIA	Cubus	Autocad	Jconc (elastic-plastic stress field)